EFFECTS OF FINES ON THE UNDRAINED BEHAVIOUR OF CHRISTCHURCH SANDY SOILS

A thesis presented in fulfillment of the requirements for the
Degree of Doctor of Philosophy
in the
Department of Civil and Natural Resources Engineering

Sean David Rees

University of Canterbury,
Christchurch, New Zealand
May 2010

Abstract

Liquefaction of sandy soil has been observed to cause significant damage to infrastructure during major earthquakes. Historical cases of liquefaction have typically occurred in sands containing some portion of fines particles, which are defined as 75μm or smaller in diameter. The effects of fines on the undrained behaviour of sand are not however fully understood, and this study therefore attempts to quantify these effects through the undrained testing of sand mixed with non-plastic fines sourced from Christchurch, New Zealand.

The experimental program carried out during this study consisted of undrained monotonic and cyclic triaxial tests performed on three different mixtures of sand and fines: the Fitzgerald Bridge mixture (FBM), and two Pinnacles Sand mixtures (PSM1 and PSM2). The fines content of each host sand was systematically varied up to a maximum of 30%, with all test specimens being reconstituted using moist tamping deposition.

The undrained test results from the FBM soils were interpreted using a range of different measures of initial state. When using void ratio and relative density, the addition of fines to the FBM sand caused more contractive behaviour for both monotonic and cyclic loadings. This resulted in lower strengths at the steady state of deformation, and lower liquefaction resistances. When the intergranular void ratio was used for the interpretation, the effect of additional fines was to cause less contractive response in the sand. The state parameter and state index were also used to interpret the undrained cyclic test results – these measures suggested that additional fines caused less contractive sand behaviour, the opposite to that observed when using the void ratio. This highlighted the dependency on the parameter chosen as a basis for the response comparison when determining the effects of fines, and pointed out a need to identify a measure that normalizes such effects.

Based on the FBM undrained test results and interpretations, the equivalent granular void ratio, e^*, was identified from the literature as a measure of initial state that normalizes the effects of fines on the undrained behaviour of sand up to a fines content of 30%. This is done through a parameter within the e^* definition termed the fines influence factor, b, which quantifies the effects of fines from a value of zero (no effect) to one (same effect as sand particles). The value of b was also determined to be different when interpreting the steady

state lines (b_{SSL}) and cyclic resistance curves (b_{CR}) respectively for a given mixture of sand and fines.

The steady state lines and cyclic resistance curves of the FBM soils and a number of other sand-fines mixtures sourced from the literature were subsequently interpreted using the equivalent granular void ratio concept, with b_{SSL} and b_{CR} values being back-calculated from the respective test data sets. Based on these interpretations, it was concluded that e^* was conceptually a useful parameter for characterizing and quantifying the effects of fines on the undrained behaviour of sand, assuming the fines influence factor value could be derived.

To allow prediction of the fines influence factor values, b_{SSL} and b_{CR} were correlated with material and depositional properties of the presented sand-fines mixtures. It was found that as the size of the fines particles relative to the sand particles became smaller, the values of b_{SSL} and b_{CR} reduced, indicating lower effect of fines. The same trend was also observed as the angularity of the sand particles increased. The depositional method was found to influence the value of b_{CR}, due to the sensitivity of cyclic loading to initial soil fabric. This led to b_{SSL} being used as a reference for the effect of fines, with specimens prepared by moist tamping having $b_{CR} > b_{SSL}$, and specimens prepared by slurry deposition having $b_{CR} < b_{SSL}$.

Finally the correlations of the fines influence factor values with material and depositional properties were used to define the simplified estimation method – a procedure capable of predicting the approximate steady state lines and cyclic resistance curves of a sand as the non-plastic fines content is increased up to 30%. The method was critically reviewed based on the undrained test results of the PSM1 and PSM2 soils. This review suggested the method could accurately predict undrained response curves as the fines content was raised, based on the PSM1 test results. It also however identified some key issues with the method, such as the inability to accurately predict the responses of highly non-uniform soils, a lack of consideration for the entire particle size distribution of a soil, and the fact the errors in the prediction of b_{SSL} carry through into the prediction of b_{CR}. Lastly some areas of further investigation relating to the method were highlighted, including the need to verify the method through testing of sandy soils sourced from outside the Christchurch area, and the need to correlate the value of b_{CR} with additional soil fabrics / depositional methods.

Acknowledgements

I would firstly like to thank my supervisors, Dr. Misko Cubrinovski and Dr. Elisabeth Bowman. Their advice, support and expertise have been invaluable to me throughout the course of this research, and have helped to make my time an enjoyable one. I also wish to thank Dr. Rolando Orense and Dr. Mitsutoshi Yoshimine who, along with Misko, gave their time to examine this thesis. I am very grateful for all their thoughtful feedback.

I would also like to acknowledge all technical assistance given to me by the laboratory and workshop technicians in both the Civil and Mechanical Engineering departments at the University of Canterbury. This in particular includes Siale Faitotonu from the Geomechanics Lab, and John Kooloos from the Transportation Lab.

The administrative staff within the Civil and Natural Resources Engineering department are thanked for all help with the organization of funding, travel, courses, and general day-to-day tasks that have occurred during my time at the University of Canterbury.

Financial support for this research was generously provided by the New Zealand Earthquake Commission (EQC) and the University of Canterbury. I am extremely thankful for this support, which helped make this study possible.

The soils tested in this study were kindly donated from site investigations carried out by local engineering practices. These were Tonkin and Taylor, who supplied the Fitzgerald Bridge sandy soils, and Aurecon, who donated the Pinnacles sandy soils. Their assistance with this study is greatly appreciated.

Finally I would like to thank all family, friends and fellow postgraduate students for their support throughout the course of my studies.

Contents

List of Figures

List of Tables

Symbols and Abbreviations

Symbols:

A_{2D}	=	Angularity measure
A_e	=	Adjusted specimen area
A_f	=	Angularity effect
a_{max}	=	Peak ground acceleration
b	=	Fines influence factor
Δb	=	Change in fines influence factor
b_{CR}	=	Cyclic resistance fines influence factor
b_{SSL}	=	Steady state fines influence factor
C_N	=	Overburden stress correction coefficient
CRR	=	Cyclic resistance ratio
$CRR_{6.0}$	=	CRR corresponding to a $M_w = 6.0$ earthquake
$CRR_{7.5}$	=	CRR corresponding to a $M_w = 7.5$ earthquake
CSR	=	Cyclic stress ratio
CSR_{15}	=	CSR on the cyclic resistance curve when $N_C = 15$
C_u	=	Uniformity coefficient of sandy soil
C_{uc}	=	Uniformity coefficient of sand
C_{uf}	=	Uniformity coefficient of fines
D_{10}	=	Diameter of which 10% of soil particles are smaller than
D_{50}	=	Diameter of which 50% of soil particles are smaller than
$d_{10,\ fines}$	=	Diameter of fines of which 10% of particles are smaller than
$d_{50,\ sand}$	=	Diameter of sand of which 50% of particles are smaller than
d	=	Distance from the benchmark response curve
d_{large}	=	Representative diameter of sand particles
d_{small}	=	Representative diameter of fines particles
D_r	=	Relative density
D_{r0}	=	Relative density on the steady state line when $p' = 0$kPa
e	=	Void ratio

e_0	=	Void ratio on the steady state line when p' = 0kPa
e_{100}	=	Void ratio on the steady state line when p' = 100kPa
e_g	=	Intergranular void ratio
e_{g0}	=	e_g on the steady state line when p' = 0kPa
e_{g100}	=	e_g on the steady state line when p' = 100kPa
$e_{gCSR=0.2}$	=	e_g on the cyclic resistance curve when CSR = 0.2
e^*	=	Equivalent granular void ratio
e^*_{100}	=	e^* on the steady state line when p' = 100kPa
$e^*_{100\text{-}cs}$	=	e^* on the steady state line when p' = 100kPa for clean sand
e^*_b	=	e^* on the benchmark response curve
$e^*_{CSR=0.2}$	=	e^* on the cyclic resistance curve when CSR = 0.2
$e^*_{CSR=0.2\text{-}cs}$	=	e^* on the cyclic resistance curve when CSR = 0.2 for clean sand
e_{max}	=	Maximum void ratio
e_{min}	=	Minimum void ratio
$(e_{max} - e_{min})$	=	Void ratio range
e_{ss}	=	Void ratio on the steady state line
F	=	Axial load
f_C	=	Fines content
f_{Cth}	=	Threshold fines content
Δh	=	Axial displacement
h_i	=	Initial specimen height
I_s	=	State index
MSE	=	Mean squared error
m_s	=	Mass of solid particles
m_w	=	Mass of water
M_w	=	Moment magnitude
N	=	SPT blowcount
N_1	=	SPT blowcount corrected for 100kPa overburden stress
$(N_1)_{60}$	=	Normalized SPT blowcount
$(N_1)_{60cs}$	=	Normalized SPT blowcount for clean sand
N_C	=	Number of load cycles required to reach cyclic liquefaction
p'	=	Mean effective stress
p'_i	=	Initial mean effective stress
p'_{ss}	=	Mean effective stress at the steady state of deformation

P_a	=	Atmospheric pressure
PI	=	Plasticity index
q	=	Deviator stress
q_{peak}	=	Peak deviator stress
q_{ss}	=	Deviator stress at the steady state of deformation
R	=	Roundness (particle shape)
R_d	=	Particle diameter ratio
r_d	=	Stress reduction coefficient
S	=	Sphericity (particle shape)
u	=	Pore water pressure
Δu	=	Excess pore water pressure
Δv	=	Volume change
V	=	Specimen volume
V_s	=	Volume of solid particles
V_v	=	Volume of voids
z	=	Depth below ground surface
ε_a	=	Axial strain
ρ	=	Particle regularity (when discussing particle shape)
ρ	=	Bulk density of soil
ρ_s	=	Mass density of solid particles
ρ_w	=	Mass density of water
σ	=	Total normal stress
σ'	=	Effective normal stress
σ_1	=	Major principal stress
σ_3	=	Minor principal stress
σ_{vo}	=	Total vertical overburden stress
σ'_{vo}	=	Effective vertical overburden stress
τ_{av}	=	Average cyclic shear stress
χ	=	Particle size disparity ratio
χ_e	=	Effective particle size disparity ratio
ψ	=	State parameter

Abbreviations:

A	=	Angular particle shape
CPT	=	Cone penetration test
CRC	=	Cyclic resistance curve
FBM	=	Fitzgerald bridge mixture
IL	=	Initial liquefaction
LRC	=	Liquefaction resistance curve
MSF	=	Magnitude scaling factor
NP	=	Non-plastic
PGA	=	Peak ground acceleration
PSD	=	Particle size distribution
PSM	=	Pinnacles sand mixture
R	=	Rounded particle shape
SA	=	Sub-angular particle shape
SEM	=	Scanning electron microscope
SPT	=	Standard penetration test
SR	=	Sub-rounded particle shape
SS	=	Steady state
SSL	=	Steady state line

1. Introduction

1.1. General Remarks

It is well understood that major seismic events can cause severe damage to infrastructure, buildings and lifelines. A significant part of such damage is often related to ground failures associated with liquefaction. Liquefaction is a phenomenon that occurs in saturated, sandy soils during earthquakes, which results in a loss of soil strength and bearing capacity. During 1964, large earthquakes in Alaska, USA and Niigata, Japan highlighted the need to better understand and design for liquefaction effects, due to the observed liquefaction-related damage such as that displayed in Figure 1-1. Subsequent events, including the 1989 Loma Prieta earthquake, and the 1995 Kobe earthquake, have continued to reinforce our understanding of the destructive potential of liquefaction.

Figure 1-1 Soil liquefaction causing failure of apartment building foundations during the 1964 Niigata, Japan earthquake (U.S. Geological Survey, 2009).

Interestingly, the majority of historical cases of liquefaction have occurred in sandy soils containing some portion of fines (Baziar and Dobry, 1995), which are typically classified

as soil particles with diameters ranging from 0.075mm to 0.002mm. However, whilst the undrained response of clean sands has been extensively investigated and documented, there still exists a limited understanding as to how the smaller fines particles affect the undrained response and liquefaction potential of sand. Some laboratory tests, performed using the triaxial shear apparatus, have suggested that the addition of fines to sand increases the flow potential of a sandy soil (Cubrinovski and Ishihara, 2000), whilst design charts such as those used in the simplified procedure (Seed and Idriss, 1971) suggest fines increase the cyclic liquefaction resistance of sandy soil. Given that liquefaction often occurs in sands with some amount of fines particles, it is important to properly understand how fines influence the undrained behaviour of sand.

The sandy soils underlying city of Christchurch, located in the South Island of New Zealand, have a significant potential to undergo liquefaction during a large earthquake. This is due to the large amount of near-surface soils containing sand and fines particles, a high water table saturating these soil deposits, and the relatively high seismic hazard of the city (Brown and Weeber, 1992). Figure 1-2 displays the location of Christchurch relative to the various active faults that contribute to this seismic hazard.

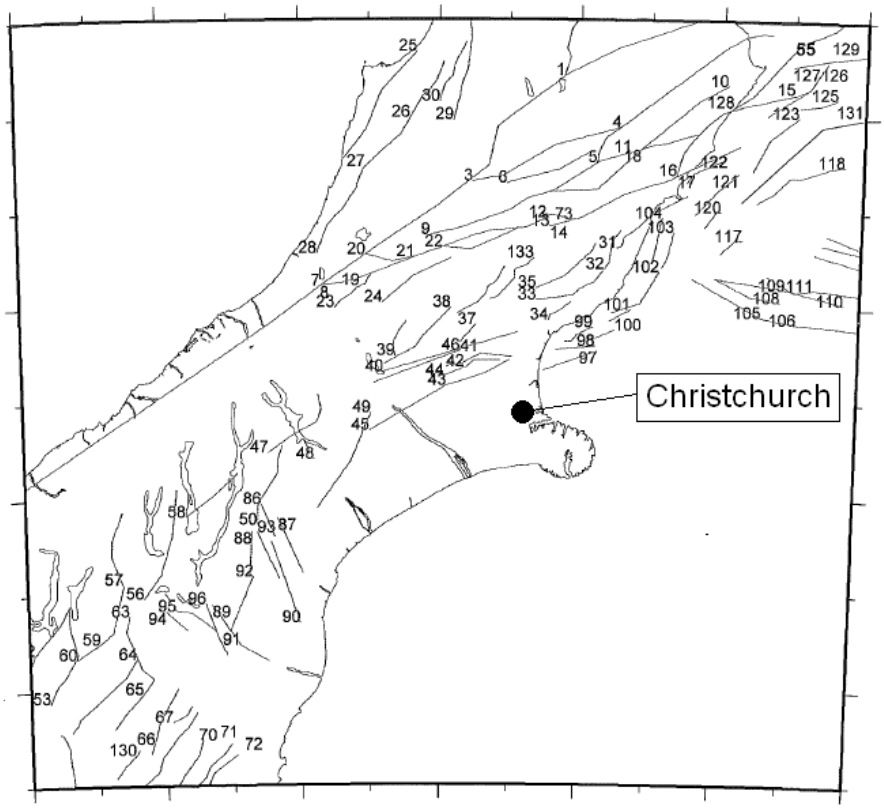

Figure 1-2 The South Island of New Zealand, showing the location of Christchurch and nearby active faults contributing to the seismic hazard (Stirling et al., 2008).

Although there exists this potential for liquefaction in Christchurch sandy soil deposits, very little laboratory testing has actually been performed on these soils. In general, site-specific investigations using in-situ testing methods such as the Standard Penetration Test (SPT) or Cone Penetration Test (CPT) have been preferred to estimate the liquefaction potential of Christchurch soil deposits. However, laboratory testing of fines-containing sandy soils can help to increase the knowledge about the liquefaction potential and undrained behaviour of the soil deposits underlying Christchurch.

1.2. Objectives and Scope of the Present Study

There are two main objectives of this study: (1) to assess and quantify the effects of fines on the undrained behaviour of sand, and (2) to develop concepts for the characterization of the undrained response and liquefaction potential of sand with fines, using sandy soils sourced from Christchurch.

As stated in Section 1.1, the first objective is highly relevant to engineering practice as many of the soils in which liquefaction has historically occurred have been sands containing some portion of fines (Chang et al., 1982). Regardless of this fact, there has still remained confusion as to whether the addition of fines to sand increases the potential for liquefaction, or decreases the potential for liquefaction. The source of this confusion is typically due to the different measures of state used for evaluating and comparing the effects of fines, which include the void ratio, relative density, state parameter, intergranular void ratio, and penetration resistance (SPT blowcount or cone resistance). For example, when comparing the liquefaction resistances of sandy soils with identical SPT N-values, sands with higher fines contents tend to show higher resistances. However, when using void ratio as the measure of state, sand with lower fines contents tend to display a higher resistance to liquefaction. As such, this study aims to systematically compare the undrained monotonic and cyclic behaviour of sands with varying fines contents using a range of state measures, to show that fines are consistent in their effect on these responses when using a consistent means of comparison. It also aims to identify a measure of soil state that quantifies this effect of fines on the undrained response of sand.

In terms of scope, this study only deals with non-plastic or low plasticity fines, and with fines contents below a threshold fines content of approximately 30%. High plasticity fines are not included in the study as they tend to produce a significant effect on the stress-strain

behaviour of fine-grained soils, altering the response from sand-like to clay-like as the plasticity index becomes greater than 7 (Boulanger and Idriss, 2006). Fines contents above 30% are not included in this study as the structure of sandy soil inherently changes once this threshold is exceeded, with the response becoming dominated by the fines particle contacts rather than the sand particle contacts (Thevanayagam and Mohan, 2000). The defined scope therefore ensures that only the effects of fines on sand-like behaviour are discussed and evaluated in this study.

The second objective aims to provide a framework for characterizing and evaluating the change in the undrained response of sands when fines are added to such soils. This includes an attempt to quantify the influence of material properties, such as particle size and angularity, on the effects of fines. It also aims to enable data gained from laboratory tests on sandy soils to help guide the assessment of liquefaction potential in the field.

The scope of this objective is currently limited to evaluating the effects of fines on the undrained behaviour of Christchurch soils, although the concepts developed aim to be applicable to sandy soil deposits in general. As stated in Section 1.1, Christchurch soil deposits are a relevant material to test for such a study as they contain significant amounts of sand and fines, and possess a high potential for liquefaction during large earthquakes. There is also a lack of laboratory test data available for these soils, meaning the results from this study will provide new information to the local geotechnical practice.

1.3. Organization of this Thesis

This thesis is comprised of eight chapters, including this chapter which provides an introduction to the topic of liquefaction, as well as the objectives and the scope of this study. The remaining chapters are summarized below:

Chapter 2 presents a background on topics relevant to this study and the undrained behaviour of sandy soils through a review of the literature. The liquefaction potential of Christchurch soils are firstly discussed by identifying the geological setting and seismic hazard of the city. The effects of fines on the undrained behaviour of sand are then discussed by presenting results from previous studies performed in the laboratory. This includes sections outlining the effects of fines have on the structure of sand, the monotonic and cyclic behaviour, and how the plasticity of fines can alter their effects. Lastly the liquefaction of silty

sand is discussed based on historic cases of liquefaction in the field, and the effect fines have when using in-situ parameters to compare the cyclic liquefaction resistances of sandy soils.

Chapter 3 describes the sandy soils and procedures used in the laboratory tests. The characteristics of the sandy soils are firstly presented, with particle size distributions, scanning electron microscope images, and other material properties being defined. The laboratory testing procedures, from specimen preparation to post-test calculations, are then described, along with the expressions used to interpret the test data.

Chapter 4 presents the results from the undrained monotonic and cyclic triaxial tests on four Fitzgerald Bridge Mixture (FBM) sandy soils. These results are interpreted using stress-strain and stress-path responses, the state concept framework for the monotonic tests, and cyclic resistance curves for the cyclic tests. The effect of fines content, ranging from f_C = 1 – 30%, on the undrained response is compared using four different initial state measures, namely the void ratio, e, relative density, D_r, state parameter, ψ, and state index, I_s. This is done to investigate if the effects of fines vary when different measures of state are used to compare the undrained behaviour.

Chapter 5 interprets the laboratory test data of the FBM soils, as well as a range of sandy soil data sourced from the literature, using the intergranular void ratio, e_g, and the equivalent granular void ratio, e^*. These parameters include the fines content of sand in their definitions in an attempt to better characterize the state of sandy soils. For this interpretation the steady state lines and cyclic resistance curves of the various sand and fines mixtures are used as the main reference for soil response. The aim of this chapter is to try and identify a measure of initial state that allows the effects of fines on the undrained behaviour of sand to be quantified.

Chapter 6 presents an examination of the fines influence factor, b, which is a parameter used for modeling and quantifying the effects of fines on the structure of sand. A definition of the factor is firstly given, followed by an assessment as to whether or not b can be considered a constant value for a given mixture of sand and fines. The differences between fines influence factor values relating to monotonic and cyclic loadings are then discussed, followed by a series of correlations of b with soil particles sizes, angularities, and fabrics. This is done to allow quantification of the effects of fines based on the material properties of both sand and

fines particles. Finally a simplified method is proposed to enable the estimation of the undrained response of sand with fines, in terms of steady state lines and cyclic resistance curves, using the response of the clean sand and the fines influence factor correlations. This is done to provide a framework for evaluating the change in sand behaviour as the fines content is altered.

Chapter 7 applies and critically reviews the simplified estimation method proposed in Chapter 6 using soil from a site investigation in Christchurch. Laboratory test results on two soils sourced from the Pinnacles site are discussed, with predictions being made about the steady state lines and cyclic resistances curves of the soils using the simplified estimation method. The aim of this chapter is to demonstrate how the framework for evaluating the effects of fines on the undrained behaviour of sand can be applied for use in laboratory studies, and to critically review the performance of this method.

Chapter 8 presents the conclusions made from this study. It highlights the main contributions the study has made to the knowledge of the undrained behaviour of sand and fines, along with the liquefaction resistances of sandy soils sourced from Christchurch. Finally recommendations are made for further research relating to the scope of this study.

2. Literature Review

2.1. Introduction

Liquefaction is a phenomenon that occurs in loose, saturated, sandy soil deposits, with the damage that it can cause being highlighted for the first time in 1964 during major earthquakes in Niigata, Japan and Alaska, USA respectively. Due to these events, liquefaction has been extensively studied in the field and laboratory, allowing the liquefaction potential and resistance of specific sites to be assessed using information based on soil properties and seismic hazard. This has led to a general consensus being formed about the undrained behaviour of clean sand, yet the effects of fines on such behaviour still remains a topic of disagreement.

As such, this literature review presents and discusses a number of studies that have investigated the effects of fines on the undrained behaviour of sand, from both laboratory and in-situ field perspectives. Section 2.3, which comprises the bulk of the review, focuses on the effects of fines observed in laboratory studies. This includes discussions as to how fines affect the internal structure of sand, their effect on behaviour at the steady state of deformation, and their effect on the liquefaction resistance of sand. The plasticity of fines is also reviewed to explain why the scope of this study is limited to the effects of non-plastic fines on the undrained behaviour of sand.

Section 2.4 provides a brief review of the effects of fines as quantified using in-situ field parameters, such as the SPT blowcount, and observations based on historic cases of liquefaction during earthquakes. The plasticity of fines and their effect on liquefaction resistance are also further addressed.

Firstly however, Section 2.2 discusses the potential for liquefaction of sandy soils underlying Christchurch, New Zealand, through a review of the geological setting, seismic hazard, and previous liquefaction studies. This is done to provide background on where the sandy soils tested during this study were sourced from, why they could potentially liquefy during an earthquake, and finally to show that they tend to consist of sand mixed with some amount of fines in-situ.

2.2. Liquefaction Potential of Christchurch Soils

The city of Christchurch is situated on the east coast of the South Island of New Zealand, which borders the Pacific and Indian-Australian tectonic plates. The near-surface soils underlying Christchurch consist of clean and silty sands, with a high water table saturating these soils. As such, the potential for liquefaction occurring in Christchurch soils during a major earthquake is high. This section discusses the geology and liquefaction potential of these soils, along with the seismic hazard posed to Christchurch.

2.2.1. Geology of Christchurch Soils

Christchurch is located on the eastern edge of the Canterbury Plains, which were formed through the deposition of materials carried by eastward-flowing rivers originating from the Southern Alps. The basement below the Canterbury Plains is comprised of Torlesse Supergroup rocks from the Permian to Jurassic age, whilst the Plains themselves are primarily comprised of gravels deposited during the last Tertiary and Quaternary periods (Brown and Weeber, 1992). A cross-section schematic of these deposits is presented in Figure 2-1.

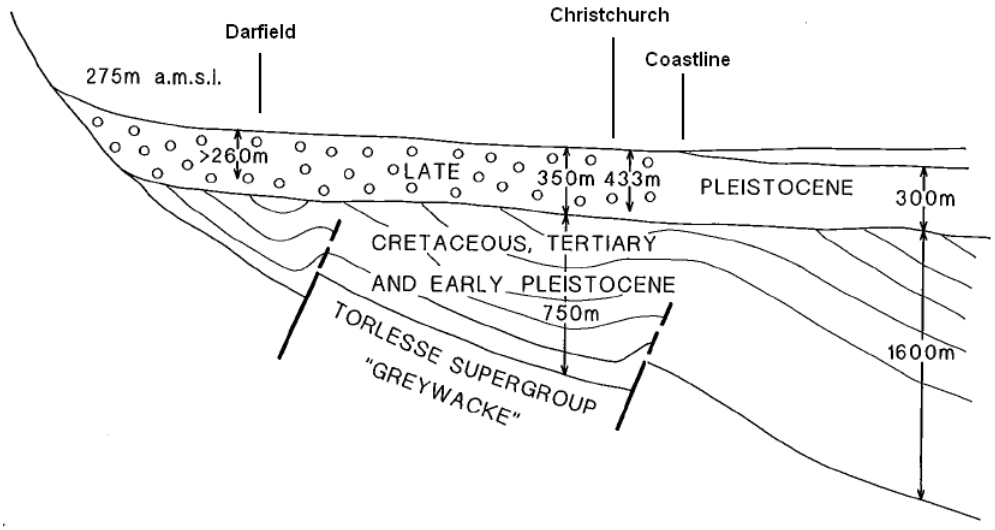

Figure 2-1 Schematic of a cross-section through the Canterbury Plains (Brown and Weeber, 1992).

The soil deposits directly underlying the city of Christchurch, which are significant to engineering works, include the Springston and Christchurch Formations. The composition of

each of these formations is described in the following, with their thicknesses displayed in Figure 2-2:

Springston Formation – this is a postglacial fluvial formation comprised of well sorted gravel, sand, and silt (Brown and Weeber, 1992). The formation reaches a maximum thickness of approximately 20m, and radiocarbon dating has suggested the near-surface sediments were deposited during the last 3000 years. It reaches to within 5km of the eastern coastline, where it becomes interspersed with the Christchurch Formation sediments.

Christchurch Formation – this is also a postglacial formation, created by beach, estuarine, lagoonal, dune, and coastal swamp deposits. Gravel, sand, silt, clay, shell and peat are all present sediments in this formation (Brown and Weeber, 1992). It outcrops up to 11km inland from the eastern coastline amongst the Springston Formation, and is up to 40m thick along the coastline itself.

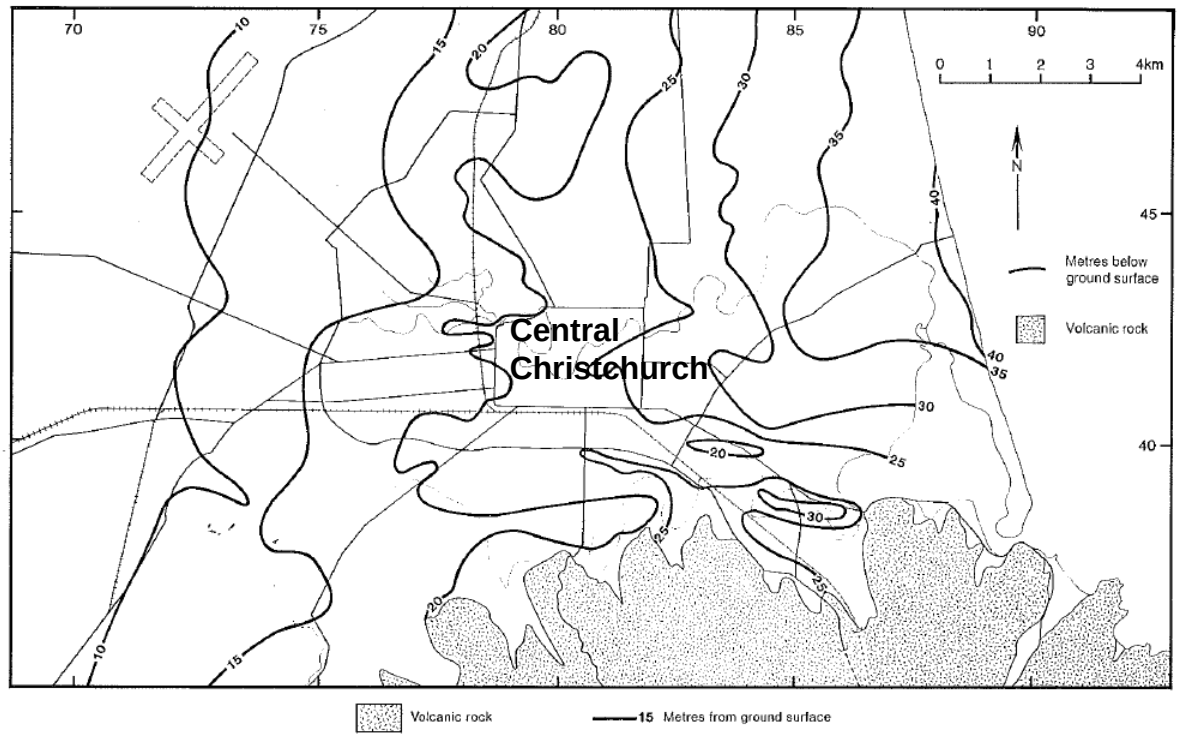

Figure 2-2 Thickness of the Springston and Christchurch formations (Brown and Weeber, 1992).

A series of gravel aquifers supply Christchurch with groundwater from the Southern Alps. Due to this, and the close proximity of the city to the ocean, the groundwater table

underlying Christchurch sits relatively near to the ground surface (Brown and Weeber, 1992). This geological feature increases the potential susceptibility of Christchurch soils to undergo liquefaction during major seismic events, as sandy soils are required to be saturated to liquefy. Figure 2-3 presents the approximate depth from the ground surface to the water table. Note that the 'wet area' displayed in Figure 2-3, where the water table is less than 1m from the ground surface, occurs in the central city and eastern suburbs.

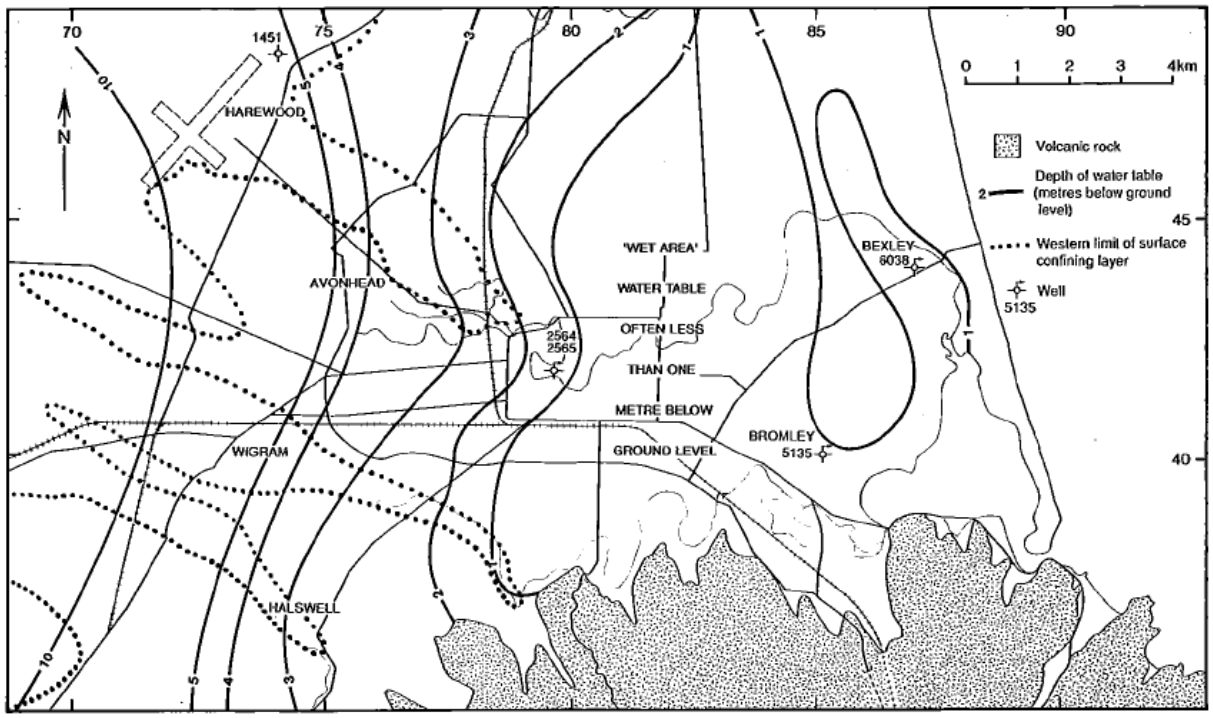

Figure 2-3 Depth to the water table below the ground surface (Brown and Weeber, 1992).

2.2.2. Seismic Hazard

New Zealand is located along the boundary between the Indian-Australian and Pacific tectonic plates, which presents a significant seismic hazard to the Canterbury region. The major active fault running through the South Island is the Alpine Fault, which has been shown to produce $M \geq 8$ earthquakes with recurrence intervals of a few hundred years (Stirling et al., 2008). This fault is located approximately 120km from Christchurch. There are however many other active faults spread throughout the Canterbury Plains which also present a significant hazard to Christchurch and the underlying soils: these include the Ashley, Awatere ($M \geq 7.5$), Hope ($M \geq 7$), Mt Grey, Pegasus Bay, Poulter ($M \geq 7$), and Porters Pass Faults (Brown and Weeber, 1992). Figure 2-4 displays the location of these faults relative to Christchurch.

At the latitude of the Canterbury region, the relative movement of the Indian-Australian and Pacific plates is approximately 40mm per year. The majority of this movement is accommodated by the Alpine Fault, where dextral slip rates of 15 – 35mm per year, and uplift rates of 17mm per year, have been recorded (Stirling et al., 2001). The strike-slip and reverse/thrust faults located nearer to Christchurch tend to have slip rates of less than 5mm per year.

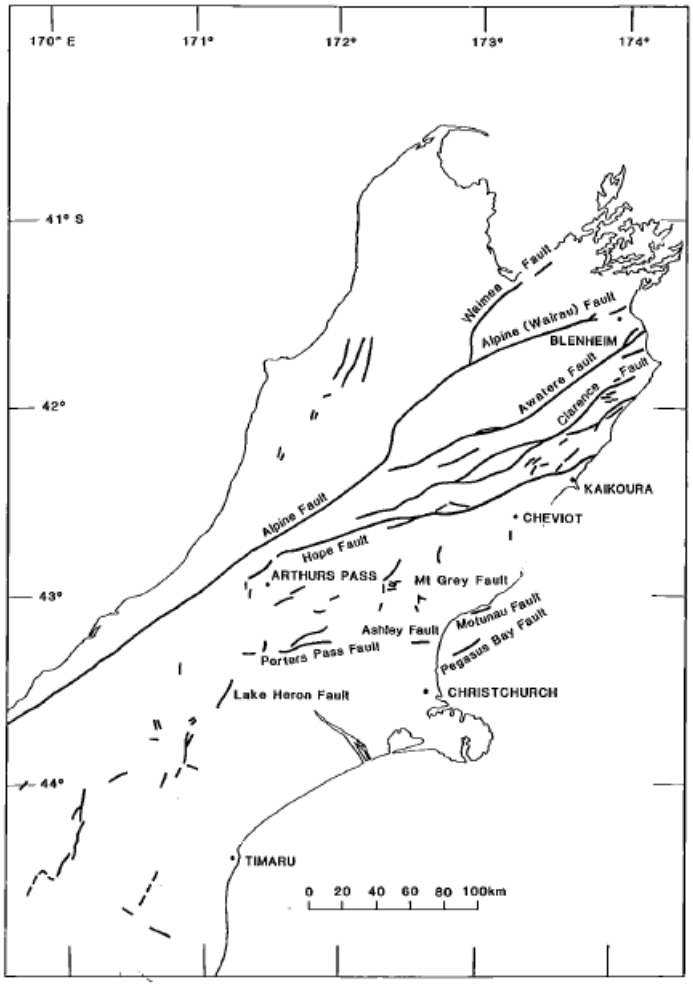

Figure 2-4 Active faults located near Christchurch (Brown and Weeber, 1992).

Information on historical seismicity in the Canterbury region has been documented for events occurring after 1840 using felt intensity data, whilst instrument recording has been in place since 1940 (Stirling et al., 2001). From 1946 to 1990 the largest Modified Mercalli earthquake intensity felt in Christchurch was MMVII, which occurred during a M5.4 earthquake located in Pegasus Bay in March 1987 (Brown and Weeber, 1992). There is also evidence that the New Brighton earthquake of June 1869 was consistent with a M5.75 quake

located 10km from the centre of Christchurch, causing MMVII – VIII intensities to be felt (Brown and Weeber, 1992). An illustration of the historical seismic events occurring near Christchurch since 1840 is presented in Figure 2-5 (Stirling et al., 2008). The numbered points correspond to shallow crustal earthquakes of $M \geq 6.5$, which are listed in the following:

1. M = 7.5 1848 Marlborough
2. M = 7.1 1888 North Canterbury
3. M = 6.9 1901 Cheviot
4. M = 7.8 1929 Buller
5. M = 7.1 1929 Arthur's Pass
6. M = 6.7 1968 Inangahua
7. M = 6.7 1994 Avoca

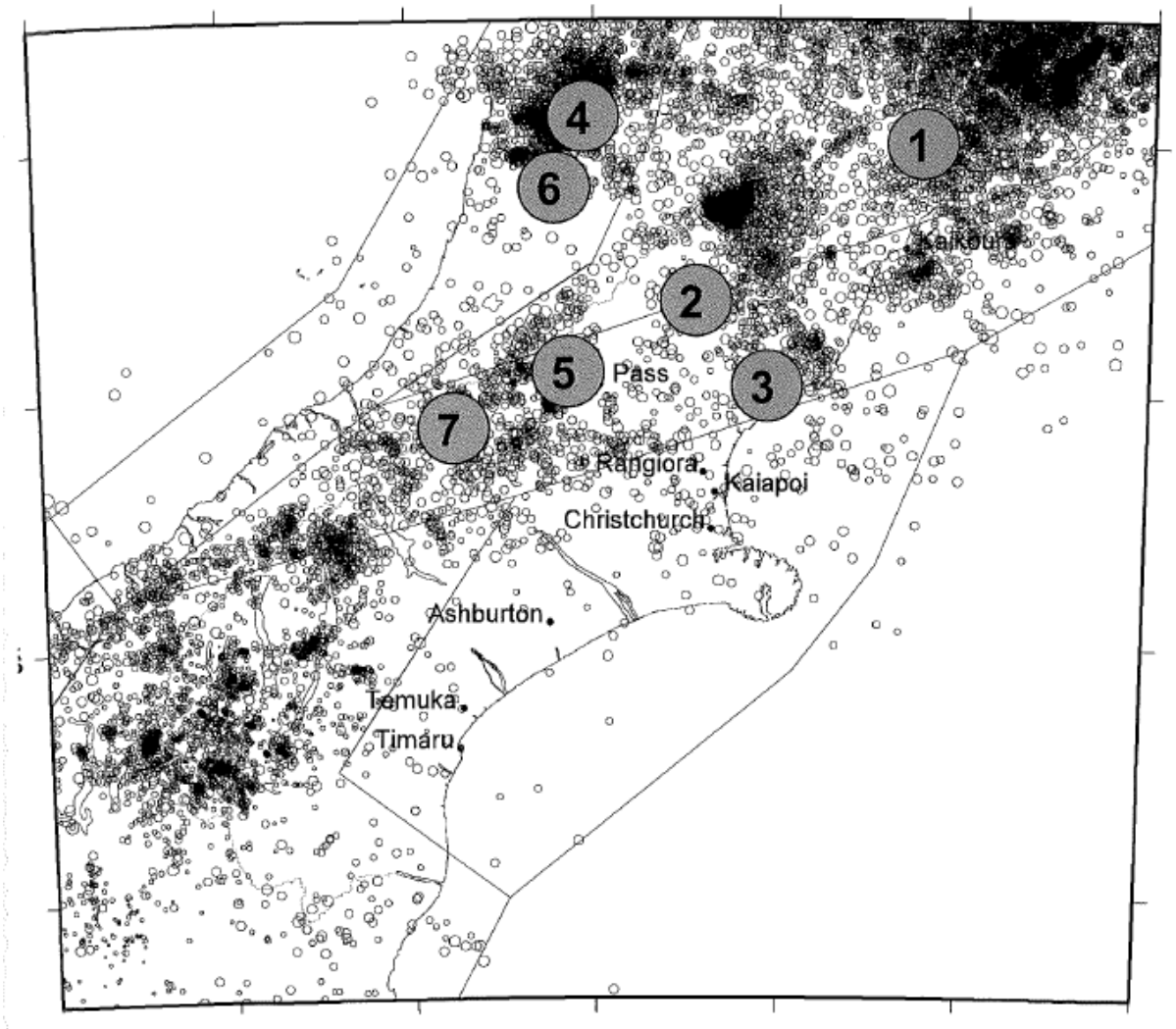

Figure 2-5 Historical seismic events near Christchurch since 1840 (Stirling et al., 2008).

A probabilistic seismic hazard assessment for the Canterbury region, including Christchurch, was performed to identify peak ground accelerations (PGA), spectral accelerations (SA), and Modified Mercalli (MM) intensities for various seismic return periods. The expected peak ground accelerations for the Canterbury region are displayed in Figure 2-6 for the 475 year return period, and the expected Modified Mercalli intensities for the 475 year return period are shown in Figure 2-7. Based on this probabalistic seismic hazard assessment and intermediate subsoil conditions, the expected peak ground accelerations for Christchurch are a PGA = 0.22g for a 200 year return period, and a PGA = 0.31g for a 475 year return period (Stirling et al., 2008). The expected Modified Mercalli intensities are MMVII-VIII for a return period between 150 – 475 years.

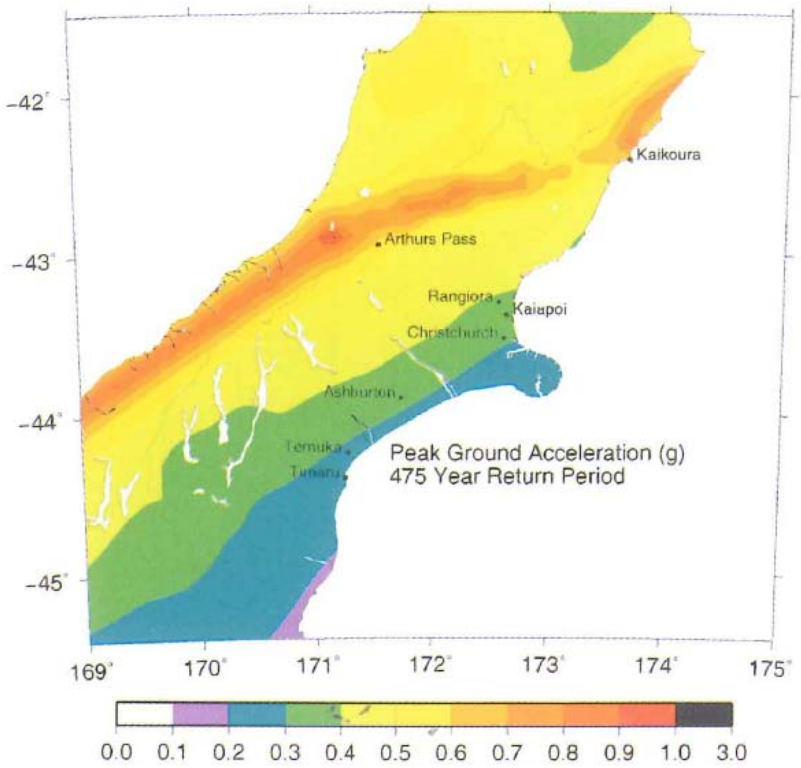

Figure 2-6 Expected peak ground accelerations in the Canterbury region for a 475 year return period (Stirling et al., 2008).

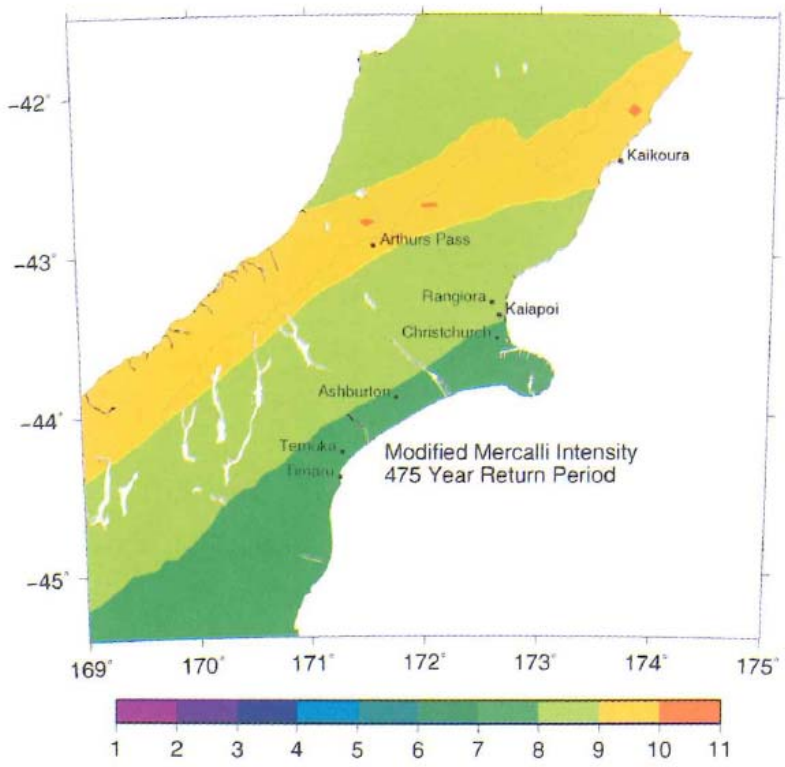

Figure 2-7 Expected Modified Mercalli intensities in the Canterbury region for a 475 year return period (Stirling et al., 2008).

2.2.3. Liquefaction Potential

The soils underlying Christchurch have a significant potential for undergoing liquefaction during a major seismic event. This is due to the deposited sands, silts and high water table as discussed in Section 2.2.1, the seismic hazard as discussed in Section 2.2.2, and the relatively young age (less than 9000 years old) of these deposits (Brown and Weeber, 1992). As such, a number of liquefaction studies have been previously performed to identify the liquefaction potential of sites around the Christchurch area (Christensen, 2001; Anderson and McMorran, 2003; URS New Zealand Ltd, 2006).

The most recent major published study is the "Christchurch Liquefaction Study – Stage IV" (Beca Carter Hollings & Ferner Ltd, 2004) report, performed for Environment Canterbury, the local regional council. Borelogs taken from various sources were used to assess the cyclic strength of the soil deposits underlying Christchurch, with SPT and CPT results most commonly being available. These parameters were then used in conjunction with the simplified procedure of Seed and Idriss (1971) to estimate the potential for liquefaction. Peak ground accelerations of PGA = 0.20g and PGA = 0.33g were used to determine the expected cyclic stress ratios for 150 and 475 year return periods respectively. Note that the

PGA values reported in Section 2.2.2 were presented after the completion of the 2004 liquefaction study. It should also be noted that liquefaction occurring beyond a depth of 5m below the ground surface was not considered, and is a major shortcoming of the study.

Two different water table scenarios were assessed to produce liquefaction potential maps for Christchurch: the first scenario considered the water table to be located as shown in Figure 2-3, whilst the second used average ground water levels from Environment Canterbury's Well Database to define the water table location. The first scenario was considered to be more conservative, and as such produced a greater area of expected liquefaction. This map is presented in Figure 2-8, with areas of high liquefaction potential around the central city and eastern suburbs being highlighted. Note that high liquefaction potential refers to "areas in which earthquake peak ground accelerations of greater than 0.12g, but less than 0.2g, for a Richter Magnitude 8 Alpine Fault earthquake, potentially cause some of the soils to liquefy" (Beca Carter Hollings & Ferner Ltd, 2004).

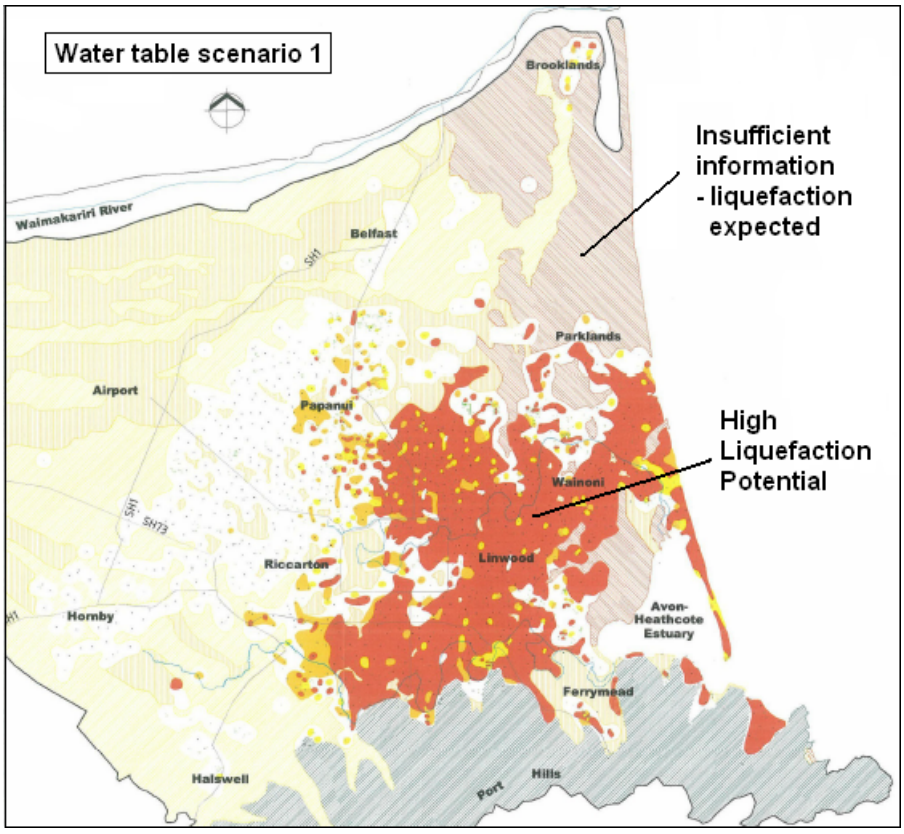

Figure 2-8 Liquefaction potential for Christchurch and surrounding suburbs based on the first water table scenario (Beca Carter Hollings & Ferner Ltd, 2004).

Investigations have also been carried out around Christchurch at key lifeline sites to assess liquefaction potential (Guilhem and Berrill, 1993). These investigations primarily took

place at water pumping stations, telephone exchanges and power supply substations. It was concluded that at least 75% of the investigated sites were susceptible to liquefaction, although complex site stratigraphy meant further investigations would be required to fully determine the likelihood of liquefaction occurring during a significant earthquake.

Historically however there has been very little observation of liquefaction actually occurring in Christchurch and the surrounding suburbs in the period following European settlement. The single instance of documented liquefaction was recorded in Kaiapoi, approximately 20km north of Christchurch, during the 1901 Cheviot earthquake (Brown and Weeber, 1992). According to newspaper reports, ejection of sand, lateral spreading and ground settlement all occurred during this earthquake (Berrill et al., 1994) at a series of sites around Kaiapoi, shown in Figure 2-9. Some liquefaction is also thought to have occurred at sites in Belfast, a suburb 6km closer to Christchurch, also during the 1901 Cheviot quake.

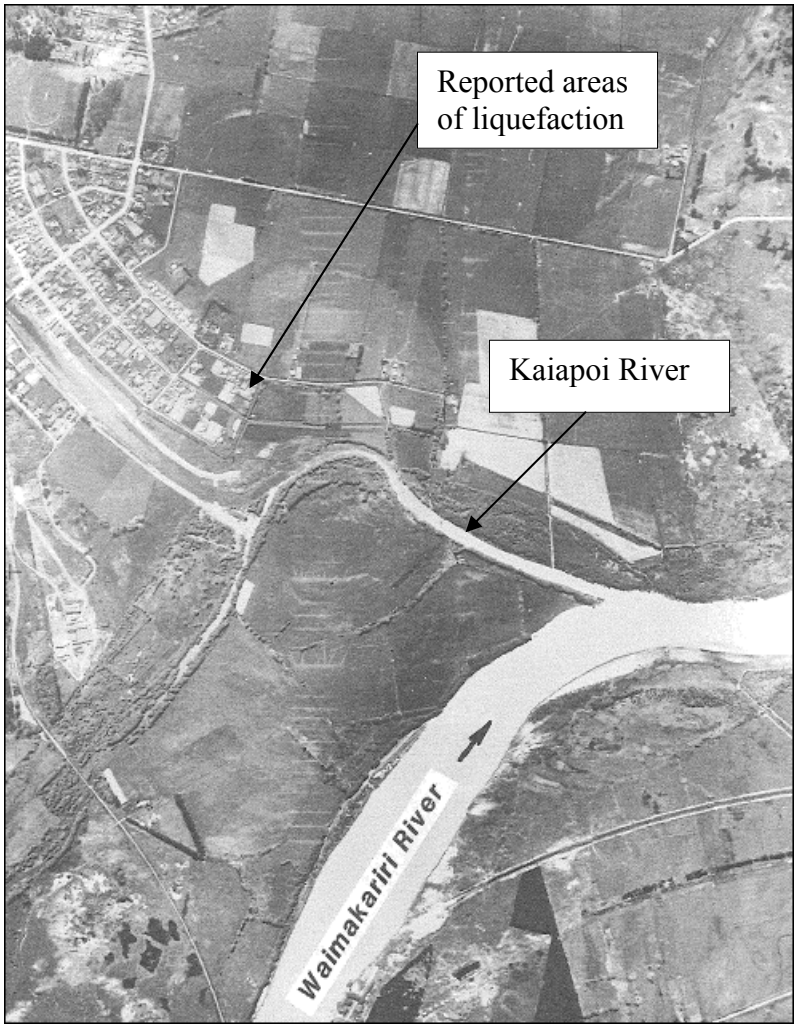

Figure 2-9 Aerial photograph of Kaiapoi in 1941 showing the locations of observed liquefaction effects (Berrill et al., 1994).

2.3. Effects of Fines in Laboratory Studies

A number of major studies that have investigated the effects of fines on the undrained behaviour of sand are presented and discussed in this section. These studies include both the monotonic testing of sandy soils, using axial compression, and the cyclic loading of test specimens. The review of these studies firstly focuses on how fines affect the structure of sand, as well as providing some discussion on the general effects of fines on the undrained behaviour of sand. Following this, priority is given to the monotonic undrained behaviour at the steady state of deformation, and the cyclic liquefaction resistances of sand with fines. Note that these two measures of undrained response are the primary focus in this study. Finally the different effects on the undrained behaviour coming from the plasticity of fines are also reviewed to explain why the scope of this study only extended to the undrained behaviour of sand mixed with non-plastic (or low plasticity) fines.

2.3.1. Effects of Fines on Sand Structure

It has been recognized that the addition of fines to sand affects the internal structure of sandy soil. As far back as 1956, Terzaghi suggested that silt particles added to sand could create a ‘metastable’ soil structure that would help to explain static liquefaction of submarine slopes (Yamamuro and Covert, 2001). Subsequent studies on sand with fines have also proposed such a structure as being plausible, including during the discussion of axially-compressed Nevada and Ottawa sands mixed with fines (Lade and Yamamuro, 1997; Yamamuro and Lade, 1997). These monotonic tests suggested that loosely-deposited sand with a small amount of fines added was much more compressible, particularly at low confining pressures, than clean sand itself. It was discussed that a metastable soil structure, such as that shown on the left in Figure 2-10, could be the cause of this increase in compressibility.

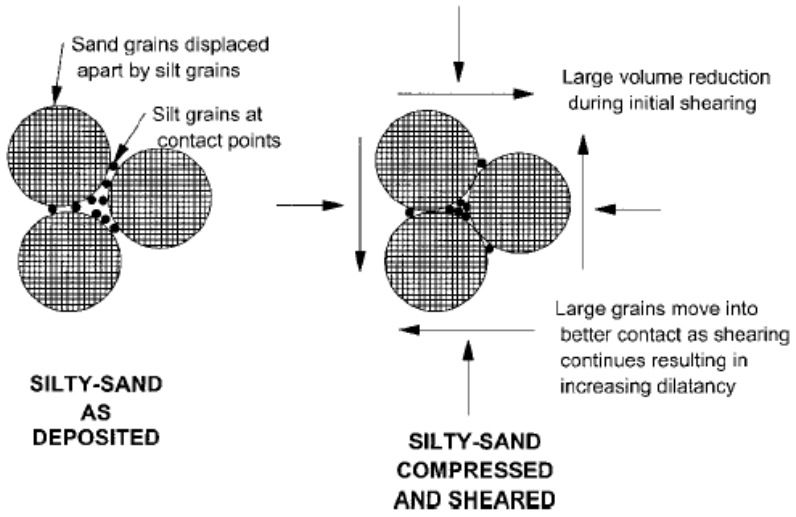

Figure 2-10 Schematic of loose sand and fines particles. The left diagram shows the soil pre-shear; the right diagram shows the soil post-shear (Yamamuro and Lade, 1997).

Other studies have focused on the relationship between the fines content of sand and the maximum and minimum void ratios, e_{max} and e_{min}. These void ratio limits relate to the loosest and densest soil structures respectively. Studies that have investigated these limits using typical sandy soils tested in the laboratory (gap-graded) such as Cambria sand have shown that the maximum and minimum void ratios tend to initially decrease as fines are added to sand, up to a fines content between f_C = 20% - 40% (Lade et al., 1998). Following this, the void ratio limits tend to increase again, as presented in Figure 2-11 for the Cambria sand mixed with Nevada fines.

The void ratio limits of natural sandy soils do not display such a noticeable drop in void ratio limit value as the fines content is raised from f_C = 0% → 30% (Cubrinovski and Ishihara, 2002). Instead, both e_{max} and e_{min} tend to increase as fines are added to sand, as observed for over 300 soils sourced from natural deposits in Japan. Note that this also leads to an increase in the void ratio range, $(e_{max} - e_{min})$, as displayed in the correlation in Figure 2-12 with fines content (Cubrinovski and Ishihara, 2002). It must however be noted that fines are not responsible alone for the change in void ratio limit values, and that grain-size properties, particle angularity etc also contribute to a variation in the void ratio limits of sandy soils. Despite this, the addition of fines to sand clearly has some affect on the extreme densities, which means the internal structure of the sand is also being affected.

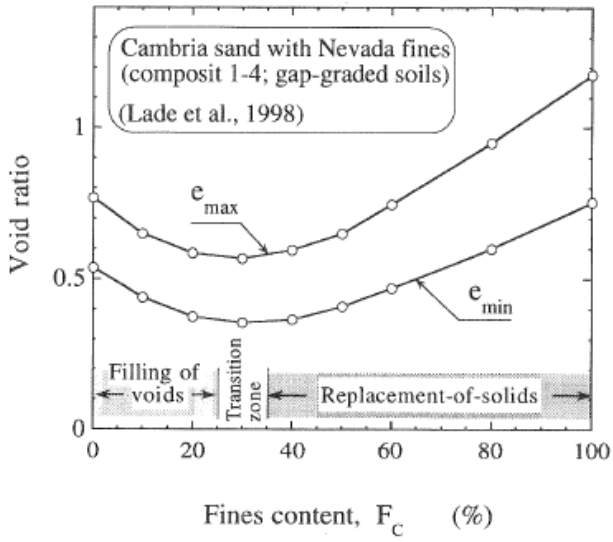

Figure 2-11 Maximum and minimum void ratios of Cambria sand mixed with Nevada fines (Cubrinovski and Ishihara, 2002).

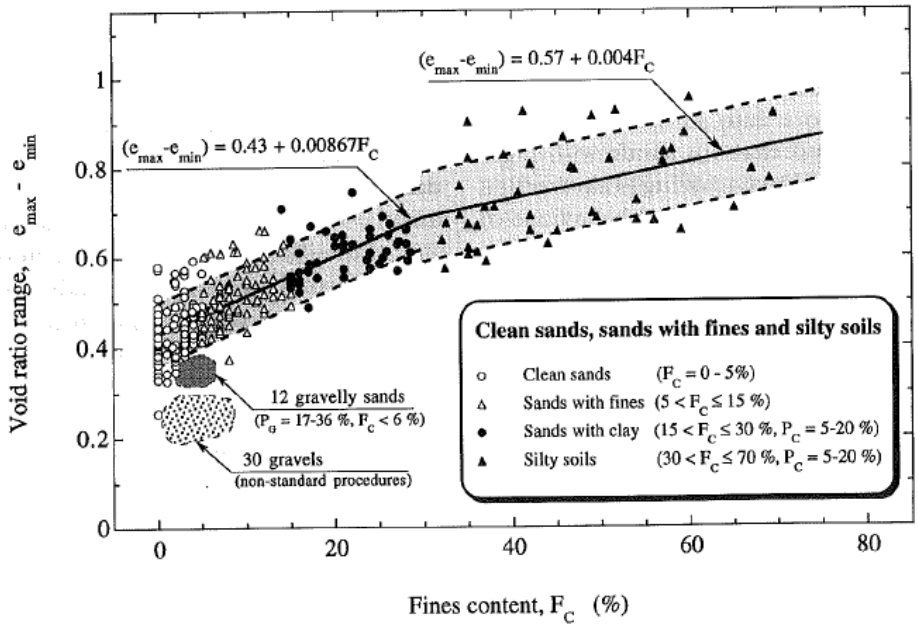

Figure 2-12 Variation in the void ratio range, $(e_{max} - e_{min})$, with fines content (Cubrinovski and Ishihara, 2002).

The internal structure of sand with fines has also been discussed in terms of the soil force-chain, and particle activity. It has been proposed that when a soil is loaded, forces are transferred and sustained through an internal force-chain that operates at different scale levels (Thevanayagam, 1998). Given that sand with fines contains a wide range of grain sizes, it is possible that smaller particles such as fines do not participate (or are inactive) in the soil force-chain during loading, as they can sit in void space created by the larger sand grains. This

concept of the internal structure of sand with fines has been used in a number of studies to compare the undrained response of sandy soils. Cyclic tests performed on Ottawa C-109 sand reported the state of the test specimens using the "void ratio of sand structure", which effectively assumed that the fines sat within the void space created by the sand and did not contribute to sustaining shear stress (Shen et al., 1977). This modification to the void ratio by only reporting the void ratio of the sand structure was termed the 'skeleton void ratio' (Kenny, 1977), and has since also been termed the granular void ratio and intergranular void ratio, e_g. This concept of neglecting the fines in the void ratio calculation is displayed by the phase diagram in Figure 2-13. Studies that have used this measure of state to compare the undrained behaviour of sand with fines are presented in the following sections that discuss response at the steady state of deformation and cyclic liquefaction.

Given that additional fines may cause a metastable sand structure, as shown in Figure 2-10, or sit within the sand void space, as suggested by the intergranular void ratio, a range of different cases can be defined for the internal structure of sand with fines. These cases are schematically presented in Figure 2-14, for (a) a coarse grain soil mix, (b) a fine grain soil mix, and (c) a layered soil mix (Thevanayagam et al., 2002). The coarse grain soil mix corresponds to cases where the sand particles primarily control the undrained response, as they make up the bulk of the soil force-chain. This can be split up further into three sub-cases: (i) the fines are fully confined within the sand void space, in which case the intergranular void ratio best describes the sandy soil state; (ii) the fines are confined and in partial contact with the sand grains, in which case the equivalent granular void ratio best describes the soil state; (iii) some fines are confined whilst others separate the sand grains, in which soil state is also best described using the equivalent granular void ratio. Note that cases (b) and (c) are outside of the scope of this study, as the effects of fines on the undrained behaviour of sand are the focus, rather than the effects of sand on the undrained response of fines.

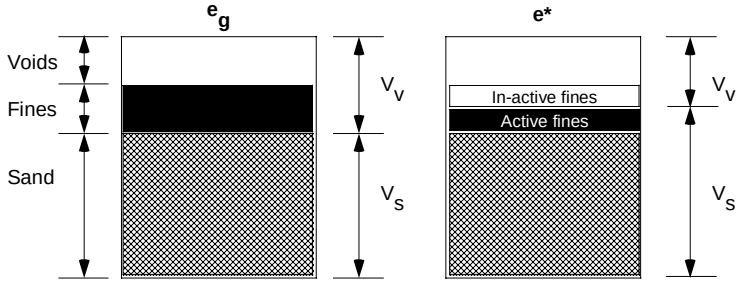

Figure 2-13 Phase diagrams showing the concept of the intergranular (e_g) and equivalent granular (e^*) void ratios.

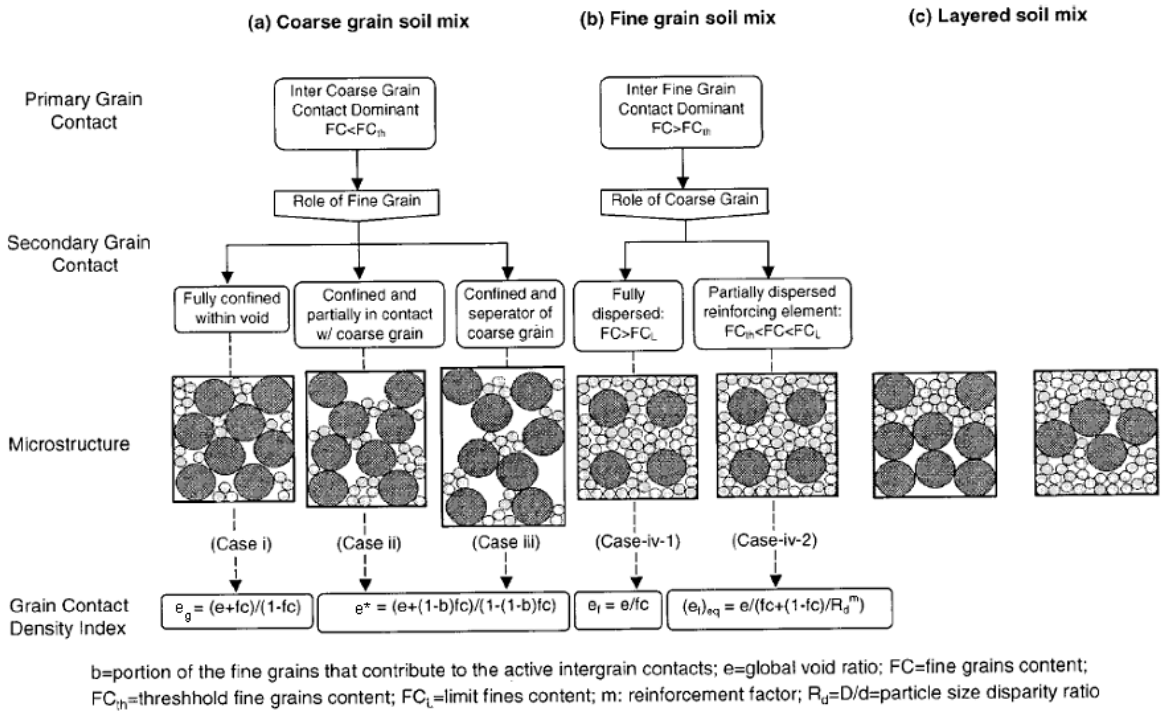

b=portion of the fine grains that contribute to the active intergrain contacts; e=global void ratio; FC=fine grains content; FC_{th}=threshhold fine grains content; FC_L=limit fines content; m: reinforcement factor; R_d=D/d=particle size disparity ratio

Figure 2-14 Classification of intergranular sand and fines mixtures (Thevanayagam et al., 2002).

The equivalent granular void ratio, as is best used to describe internal structure cases (ii) and (iii), allows for some participation of fines in the soil force-chain (Thevanayagam et al., 2000). This participation is due to the fines particles being in partial contact with, or separating, the sand grains. Due to such internal structures, the fines are likely to be active in transferring and sustaining stress during undrained loading. This participation is accounted for in the equivalent granular void ratio definition through the parameter *b*, termed the 'fines influence factor'. It is the portion of fines that contribute to the active intergrain contacts, or portion of fines that participate in the force-chain during loading (Thevanayagam et al., 2002). The concept of the equivalent granular void ratio, e^*, is shown in Figure 2-13 using a phase diagram. Note that this measure of state is unique as it quantifies soil state for a wide range of possible internal soil structures, unlike the void ratio (all fines are assumed to be active) and intergranular void ratio (all fines are assumed to be inactive).

Note in Figure 2-14 that cases (a) and (b) are divided through the use of the threshold fines content, f_{Cth}. This is the fines content that separates internal soil structures which are controlled by the sand grain contacts, and by the fines particle contacts respectively. The value of f_{Cth} has been observed to sit somewhere between f_C = 20 – 30% (Thevanayagam and Mohan, 2000), with f_{Cth} = 30% being used as a representative value in this study. Various

methods are also available to calculate f_{Cth} for a given mixture of sand and fines (Yang et al., 2006a).

2.3.2. Effects of Fines on General Undrained Behaviour of Sand

Early investigations into the behaviour of sand with fines did not always systematically vary the fines content. For example, silty sand sourced from the Koto and Katsushika wards in Tokyo were cyclically tested at differing fines contents: Takasago clean sand with f_C = 0%; Koto-A sandy silt at f_C = 58% and 100%; Koto-B silty sand at f_C = 15%; Suzaki silt at f_C = 100% (Ishihara et al., 1978). The slurry-reconstituted test specimens suggested that the Koto-B silty sand had lower liquefaction resistance than the Takasago clean sand, but that the Koto-A sandy silts and Suzaki silt had higher liquefaction resistances than the Takasago clean sand. Note that the majority of tests were performed at $e \approx 0.82 - 1.02$, although the Suzaki silt was tested at much higher void ratios ($e \approx 1.40 - 1.60$), and that the fines were plastic ($PI \approx 20$). Interestingly it was concluded that as the overconsolidation ratio of the sandy soil was increased, the addition of fines to sand produced a greater increase in the cyclic liquefaction resistance. This is presented in Figure 2-15.

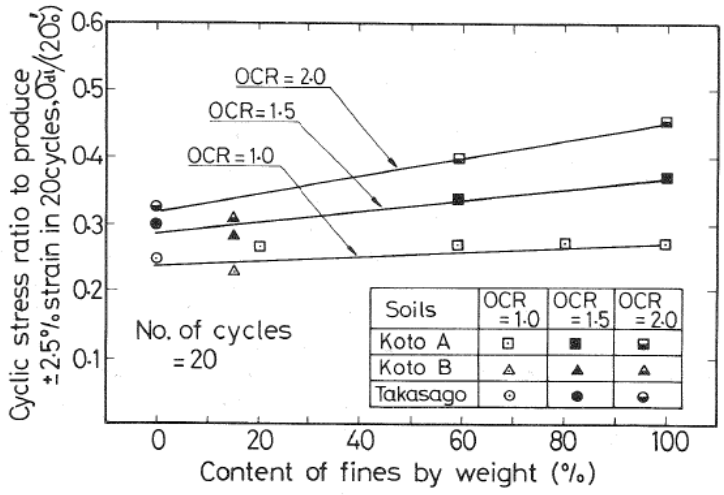

Figure 2-15 Effect of fines content and overconsolidation ratio on the liquefaction resistance of Tokyo silty sands and sandy silts (Ishihara et al., 1978).

Monotonic tests performed on Ottawa C-109 sand mixed with crushed non-plastic silica fines did use a systematical variation in the fines content. These tests suggested that the behaviour of the Ottawa sand became more dilative as the fines content was increased, with less strain-softening response being observed (Pitman et al., 1994). This is displayed in Figure

2-16, with the fines content changing from f_C = 0% → 40%. It must however be noted that the moist-tamped test specimens did not have similar void ratio values during testing, even though they were prepared to similar void ratios pre-saturation and consolidation. Instead, both the post-consolidation void ratio and relative density values increased as the fines content of the sand was raised. Thus, whilst the behaviour of the Ottawa C-109 sand did become more dilative as fines were added when using the pre-saturation void ratio as a measure for comparison, the same conclusion cannot be drawn if using the post-consolidation void ratio or relative density as the comparative measure. This highlights one of the key aspects when trying to determine the effect of fines on the undrained behaviour of sand – the measure used to compare state can alter the apparent effect of fines.

Axial compression tests conducted on Brenda 20/200 sand mixed with non-plastic fines also showed a similar trend in effect of fines to that of the Ottawa C-109 sand. The undrained response of slurry-prepared test specimens tended to show more dilation as the fines content was increased from f_C = 0% → 22.3%, with the relative density also increasing from D_r = 29% → 98% (Vaid, 1994) with an increase in fines content. Interestingly, the relative density of the sand fraction actually reduced as fines were added, from 29% to 0%. The stress-strain responses obtained from these tests are shown in Figure 2-17. They again reinforce the fact that the measure used to compare the state of a sandy soil can greatly affect the interpretation of the effects of fines on the undrained response.

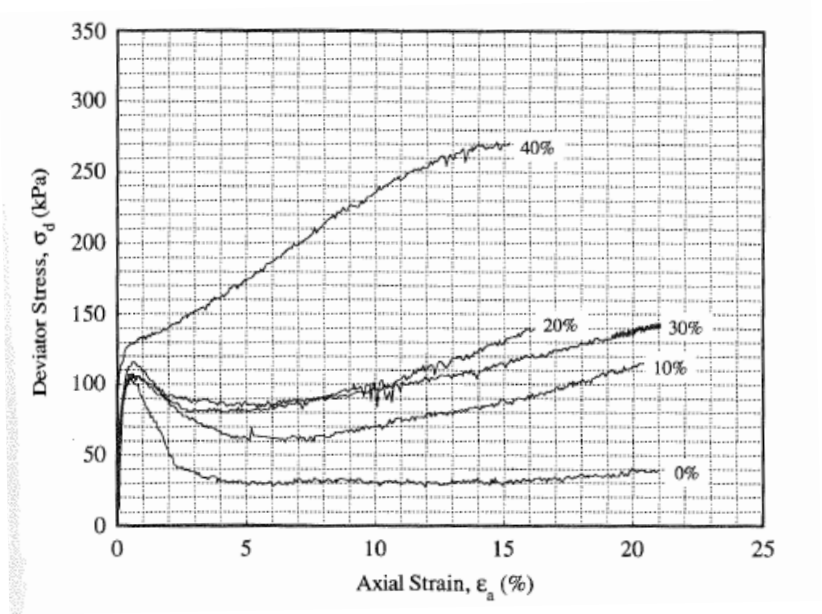

Figure 2-16 Stress-strain response of Ottawa C-109 sand mixed with varying amounts of crushed silica fines, prepared to similar pre-consolidation void ratios (Pitman et al., 1994).

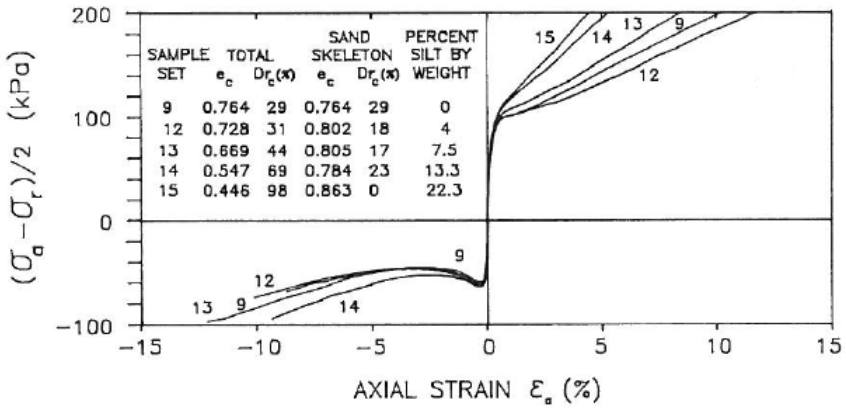

Figure 2-17 Stress-strain response of Brenda 20/200 sand mixed with non-plastic fines (Vaid, 1994).

Another study tested both Nevada and Ottawa sands mixed with non-plastic Nevada fines using strain-controlled axial compression. The stress-paths of the Nevada 50/200 sand with varying fines content are displayed in Figure 2-18, with the void ratio and relative density values also included. The trends observed in Figure 2-18 applied to all monotonic tests on the Nevada and Ottawa sands – the test specimens reached a lower peak stress and exhibited more contractive behaviour as the fines content of the sand was increased (Lade and Yamamuro, 1997). This occurred even though the density of the specimens, in terms of both void ratio and relative density, also increased as the fines content was raised. Note that the behaviour of the Nevada and Ottawa sand with fines was opposite to that seen for the Ottawa C-109 sand in Figure 2-16, and Brenda 20/200 sand in Figure 2-17.

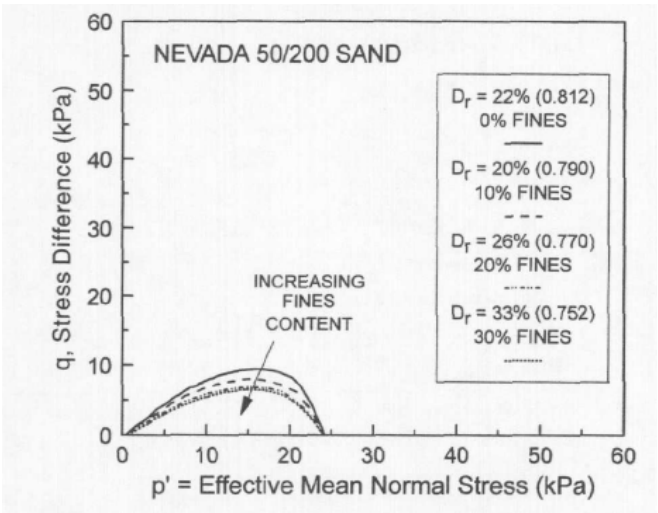

Figure 2-18 Stress-paths of Nevada 50/200 sand mixed with non-plastic Nevada fines (Lade and Yamamuro, 1997).

Cyclic strain-controlled tests performed on Ottawa C-190 sand mixed with non-plastic ground silica fines at constant void ratio values have shown that higher excess pore water pressures are built up during undrained loading as the fines content of sand is increased (Erten and Maher, 1995a). Figure 2-19 displays the normalized amounts of excess pore water pressure generated when moist-tamped sandy soil specimens were loaded to shear strains of 0.015% and 0.75% per cycle, for both 10 and 30 load cycles. As can be observed, small amounts of pore water pressure buildup occurred when the specimens were loaded at 0.015% shear strain per cycle, but initial cyclic liquefaction was reached after 30 cycles when applying 0.75% shear strain per load cycle. At this higher level of loading, increasingly higher pore water pressures had been generated by the end of the undrained loading as the fines content was increased from f_C = 0% → 30%. Note that no specimens were prepared with f_C > 30%, as similar void ratio values could not be obtained beyond this fines content (Erten and Maher, 1995a).

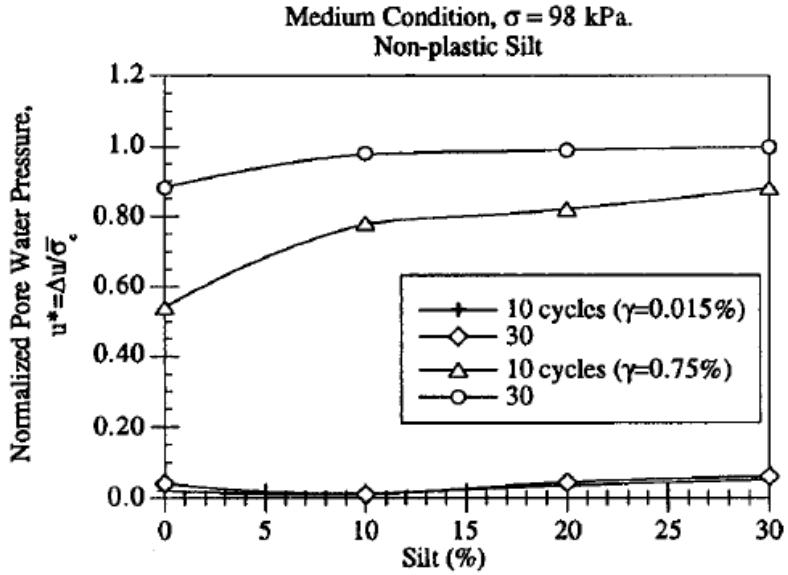

Figure 2-19 Excess pore water pressure buildup in Ottawa C-109 sand mixed with non-plastic ground silica fines (Erten and Maher, 1995a).

2.3.3. Effects of Fines on the Steady State of Deformation

Numerous studies that have investigated the effects of fines on the undrained monotonic behaviour of sand have discussed the soil response using the steady state line. In particular, the location of the steady state line of clean sand in the $e - p'$ plane has been compared with the location of the steady state line of silty sand, using different measures of state to make such comparisons.

The steady state of deformation, also known as critical state, is defined as the state at which a sandy soil deforms under constant shear stress, constant effective stress and constant volume (Casagrande, 1976; Castro and Poulos, 1977). The strength and mean effective stresses which occur at the steady state of deformation change as the density of sand is varied, enabling a 'steady state line' to be defined in $e - q - p'$ space. The projection of this line in the $e - p'$ plane is often presented to discuss the response of sand at the steady state of deformation. Initial states with densities lower than those of the steady state line tend to result in contractive soil response during monotonic loading, whilst initial states with densities higher than the steady state line tend to dilate during loading. Note however that the steady state line only provides an approximation for division between initial states that contract or dilate (Cubrinovski and Ishihara, 2000) – the initial dividing line (Ishihara, 1993) actually marks the boundary between contractive and dilative initial states.

The void ratio, e, has most commonly been used to describe the state of sand with fines at the steady state of deformation, although other measures such as relative density, intergranular void ratio, and equivalent granular void ratio have also been used. Monotonic tests performed on Ottawa C-109 sand mixed with Kaolinite fines (plastic) showed that as the fines content was increased up to f_C = 20%, the void ratio at the steady state of deformation moved to higher densities, or lower void ratio values (Pitman et al., 1994). This is displayed in Figure 2-20. Notice that as the fines content was increased beyond f_C = 20%, the void ratio at steady state moved to lower densities, with the f_C = 40% steady state point being located closer to the clean sand steady state line than the f_C = 10% point.

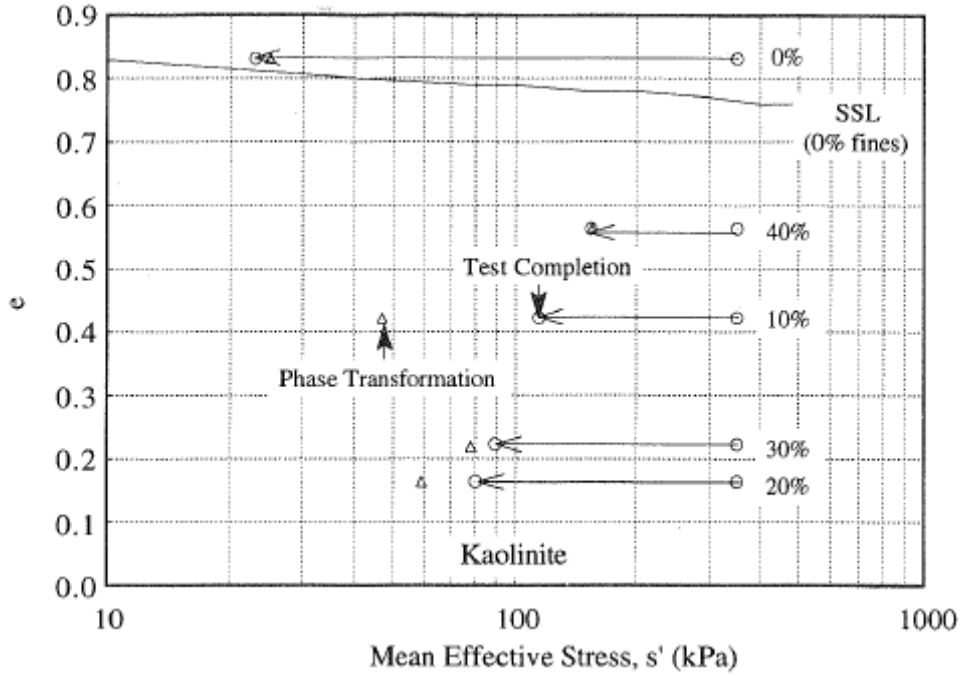

Figure 2-20 Steady state points of Ottawa C-109 sand mixed with Kaolinite fines (Pitman et al., 1994).

This trend of the steady state line moving to higher densities as the fines content was increased was also observed in a number of other studies. Axial compression tests performed on Toyoura sand mixed with Toyoura silt (non-plastic) showed the steady state line moving to lower void ratio values up to f_C = 30%, with the steady state line when f_C = 100% (pure silt) sitting between the f_C = 15% and f_C = 25% steady state lines (Zlatovic, 1994). Other studies that mixed non-plastic silt with clean sand (Thevanayagam, 1998; Thevanayagam et al., 2002; Naeini and Baziar, 2004; Yang et al., 2006b; Murthy et al., 2007; Papadopoulou and Tika, 2008) tended to show the steady state line sitting at higher densities up until a fines content of f_C = 30% - 40% was reached, at which point the steady state line located back at lower densities. This is displayed in Figure 2-21 for F55 Foundry sand mixed with non-plastic crushed silica fines from f_C = 0% → 100%.

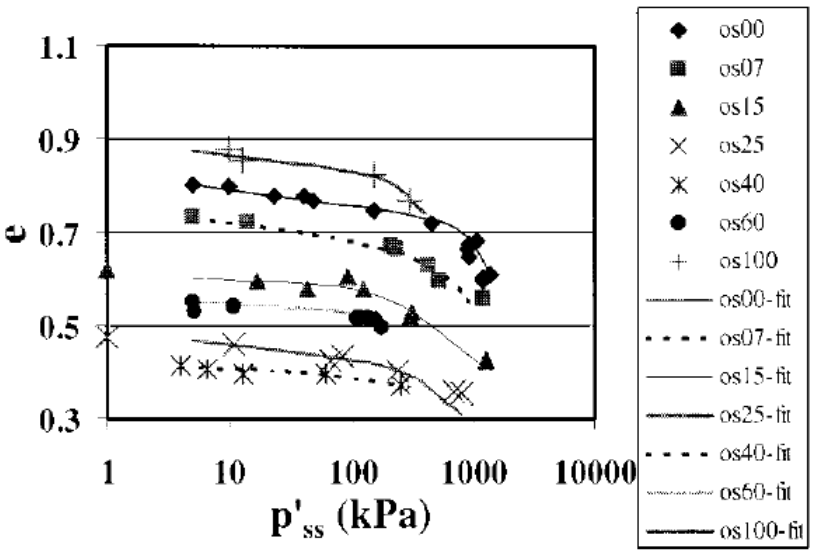

Figure 2-21 Steady state lines of F55 Foundry sand mixed with crushed silica fines (Thevanayagam et al., 2002).

Sand that has been mixed with plastic fines has also shown a similar trend as discussed above (Pitman et al., 1994; Thevanayagam, 1998; Huang et al., 2004), although there is a lack of steady state line data for sand with higher plastic fines contents. Steady state data from monotonic tests performed on Sydney sand mixed with low-plasticity fines (PI = 11) are presented in Figure 2-22, showing the steady state line locations moving from high void ratio values to lower void ratio values as the fines content is increased from f_C = 0% → 30%.

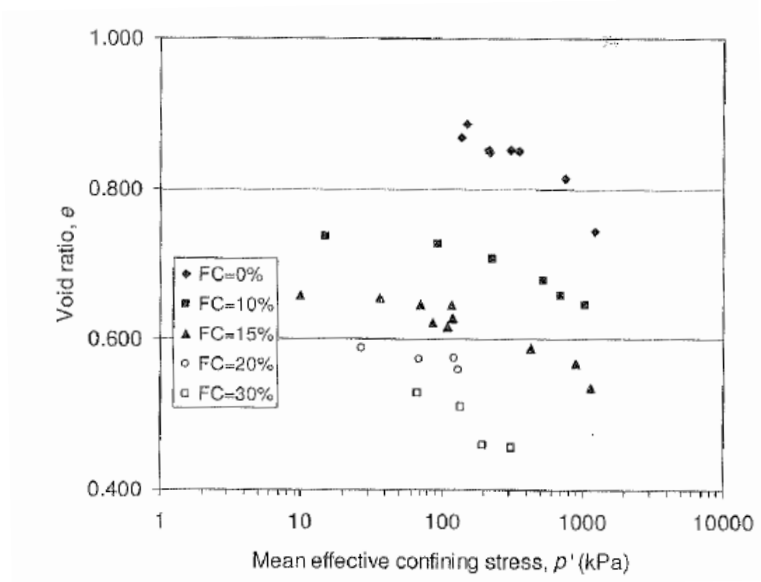

Figure 2-22 Steady state points of Sydney sand mixed with low-plasticity fines (Rahman and Lo, 2007).

Therefore in general, when using *e* to measure and compare soil state at the steady state of deformation, an increase in fines content tends to move the steady state line to higher densities, up to fines contents around 30% - the approximate threshold fines content. This trend also appears to occur when the maximum and minimum void ratio values are used to represent the changing fines content of sand. As discussed in Section 2.3.1, an increase in the fines content of sand has been shown to lead to an increase in the void ratio range, $(e_{max} - e_{min})$. Figure 2-23 presents the steady state lines representative of clean sand, where $(e_{max} - e_{min}) = 0.35$, and sand mixed with 20% fines, where $(e_{max} - e_{min}) = 0.60$. In this case relative density, calculated based on an empirical correlation with $(e_{max} - e_{min})$, is used as the measure of soil state, which allows the flow potential of initial soil states to be determined based on their location relative to the steady state line. From Figure 2-23, it appears that sandy soils with high void ratio range values, typical of sand with fines, have a greater potential for undergoing flow (strain-softening behaviour) during axial compression (Cubrinovski and Ishihara, 2000).

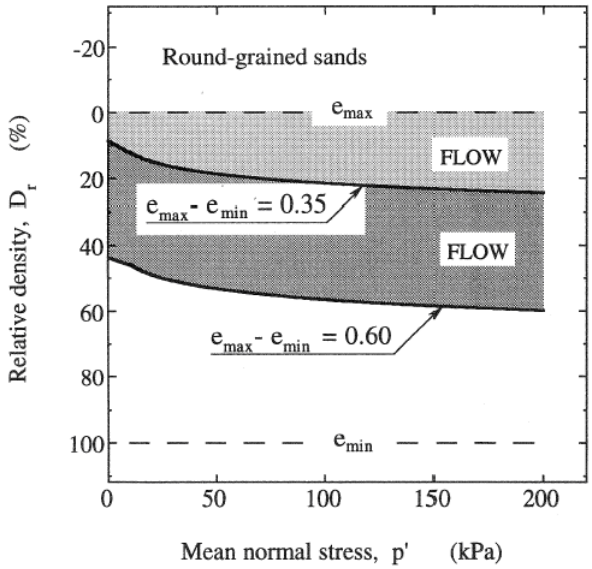

Figure 2-23 Steady state lines representative of a clean sand, $(e_{max} - e_{min}) = 0.35$, and a sand with 20% fines, $(e_{max} - e_{min}) = 0.60$ (Cubrinovski and Ishihara, 2000).

Interestingly, relative density has rarely been used to compare the steady state line location of sand with fines in the literature, as it has in Figure 2-23. However a number of studies have used the intergranular void ratio, and equivalent granular void ratio, as measures of state to compare the change in steady state line as the fines content of sand is raised. In the

majority of these studies (Thevanayagam, 1998; Thevanayagam et al., 2002; Papadopoulou and Tika, 2008) the steady state line has been shown to move to lower intergranular densities as the fines content was increased from f_C = 0% → 30%, as displayed in Figure 2-24 for the F55 Foundry sand. Note that this is opposite to the trend observed when the void ratio was used to compare the steady state line locations in Figure 2-22. However the monotonic tests performed on Ottawa C-109 sand mixed with plastic Kaolinite fines showed the steady state data points moving to higher intergranular void ratio values as the fines content was increased to 20%, which was the same trend as when the void ratio was used to compare state. This was most likely due to the extremely low void ratio values obtained when f_C = 20% (e = 0.16, e_g = 0.45). It was suggested that such high densities were obtainable due to the highly compressible nature of the Kaolinite fines, as well as the flat elongated shape of the fines observed in scanning electron microscope images (Pitman et al., 1994). These factors enabled the fines to fit within the void spaces created by the sand, thus allowing an extremely low void ratio value of the sandy soil to be reached. This in turn also allowed for high soil density in terms of intergranular void ratio.

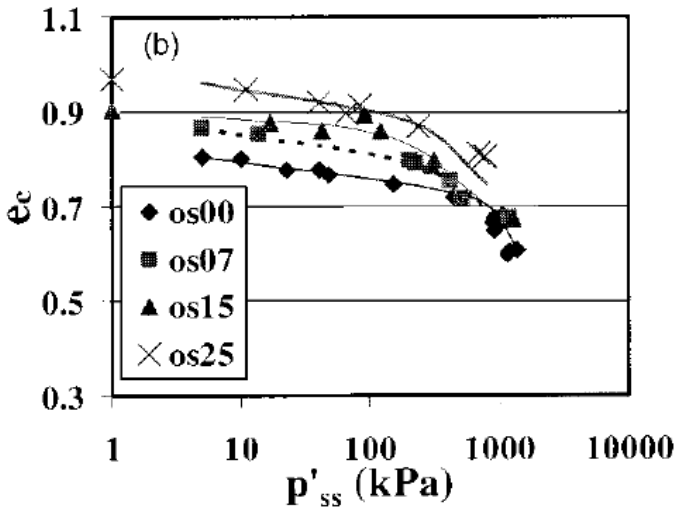

Figure 2-24 Steady state lines of F55 Foundry sand mixed with non-plastic fines using the intergranular void ratio as the measure of state (Thevanayagam et al., 2002).

The studies that used the equivalent granular void ratio to compare soil state showed that the steady state line can become largely independent of fines content, assuming the soil has not reached the threshold fines content. The monotonic tests performed on the F55 Foundry sand used a b = 0.25 in the equivalent granular void ratio definition to collapse all steady state lines with f_C = 0% - 25% onto a single curve, located about the clean sand data.

This data is presented in Figure 2-25. Similar results were also observed for Hokksund sand steady state lines with f_C = 0 – 30%, b = 0.25 (Yang et al., 2006b), and Sydney sand steady state lines with f_C = 0 – 30%, b = variable (Rahman and Lo, 2007).

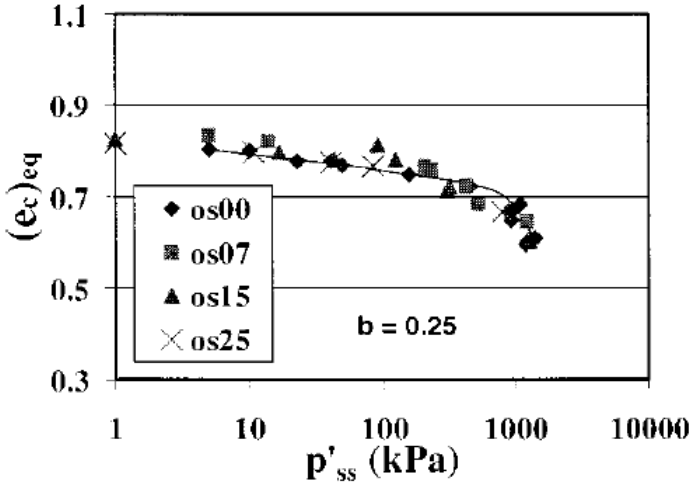

Figure 2-25 Steady state lines of F55 Foundry sand mixed with non-plastic fines using the equivalent granular void ratio as the measure of state (Thevanayagam et al., 2002).

2.3.4. Effects of Fines on Cyclic Liquefaction Resistance

Studies that have investigated the undrained cyclic behaviour of sand with fines have typically discussed the cyclic liquefaction resistance of such soils as the fines content is altered. The results from these studies have in cases been contradictory, with some studies reporting that the addition of fines to sand increases the liquefaction resistance, whilst others suggest additional fines decrease the liquefaction resistance. Note that in this section the number of cycles to reach liquefaction has been defined at the onset of initial liquefaction unless otherwise stated.

A number of studies have reported that the liquefaction resistance of sand decreases as the fines content is increased, when using the void ratio, e, to compare specimen state. Cyclic tests performed on Ottawa sands showed that, for a constant dry density, the liquefaction resistance decreased as fines were added to sand (Shen et al., 1977). This is displayed in Figure 2-26 by the liquefaction resistance curves of the Ottawa C-109 sand. It was also reported in that study that when a constant skeleton void ratio, e_s, of sand was considered, then additional fines tended to increase the liquefaction resistance of the Ottawa sands. This increase in resistance was however stated to be dependent on a number of factors, such as amount of fines, relative density of the sand structure, and number of load cycles.

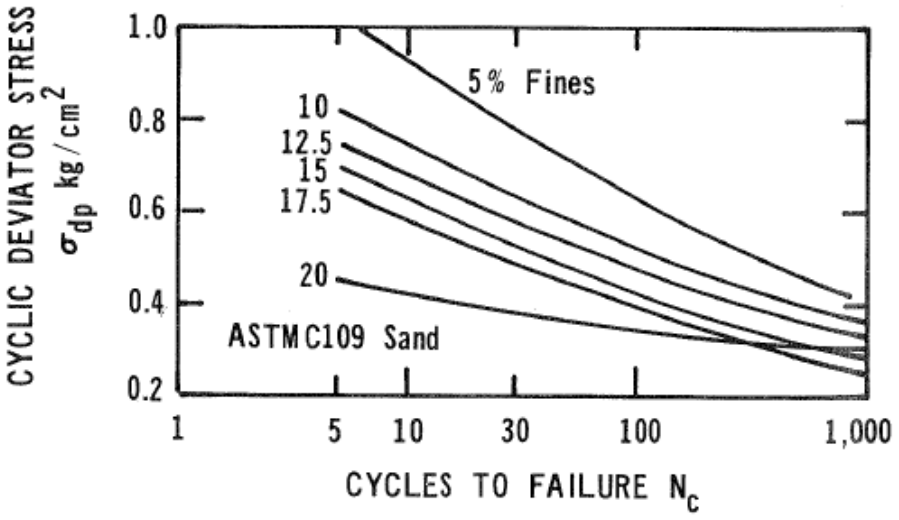

Figure 2-26 Liquefaction resistance curves of Ottawa C-109 sand (Shen et al., 1977).

Many other studies (Troncoso and Verdugo, 1985; Kuerbis et al., 1988; Finn et al., 1994; Vaid, 1994; Erten and Maher, 1995b; Thevanayagam et al., 2000; Polito and Martin II, 2001; Chien et al., 2002; Carraro et al., 2003; Xenaki and Athanasopoulos, 2003) have also shown that for a constant void ratio, sand specimens with higher fines contents display lower cyclic liquefaction resistance. Note that this trend was generally observed for fines content ranging from f_C = 0% - 30%, or below the threshold fines content.

A number of studies have also suggested that the liquefaction resistance of a sand increases as fines are added. Cyclic tests performed on sand from Clear Creek, Colorado showed a general increase in liquefaction resistance with the addition of fines when behaviour was compared at a constant void ratio corresponding to 50% relative density of the parent, or host, sand (Chang et al., 1982). This increase was however preceded by a drop in liquefaction resistance from f_C = 0% → 10%, with the liquefaction strength not moving above that of the clean sand until after f_C > 20% were reached.

Another study that tested undisturbed silty sand specimens concluded that an increased fines content led to an increase in cyclic liquefaction resistance (Dezfulian, 1984). The results from that study are presented in Figure 2-27 – note that liquefaction was considered to occur at 5% double amplitude axial strain in this study. As is shown the fines content varies greatly between the specimens, and it is difficult to clearly discern that additional fines increase the liquefaction resistance of the sand. It must also be noted that no information was given on the densities of these specimens, that the initial confining stresses were varied, and that some results were corrected based on fines content (the *CSR* of specimens with f_C < 20% were

increased by 5%; the *CSR* of specimens with f_C > 80% were reduced by 5%). These factors make the effects of fines on the liquefaction resistance problematic to determine.

Further cyclic tests performed on Ottawa 20-30 sand with low plasticity silt also suggested that, at a constant relative density, additional fines (f_C = 10% → 50%) acted to increase the liquefaction resistance of sand (Amini and Qi, 2000). The liquefaction strength curves derived from those tests are displayed in Figure 2-28. It was noted in that study that the void ratios and relative densities did vary from the target values (D_r = 34% - 44%), although it does not specify which specimens were affected by such variation. This again makes it difficult to accurately determine how additional fines affected the liquefaction resistance.

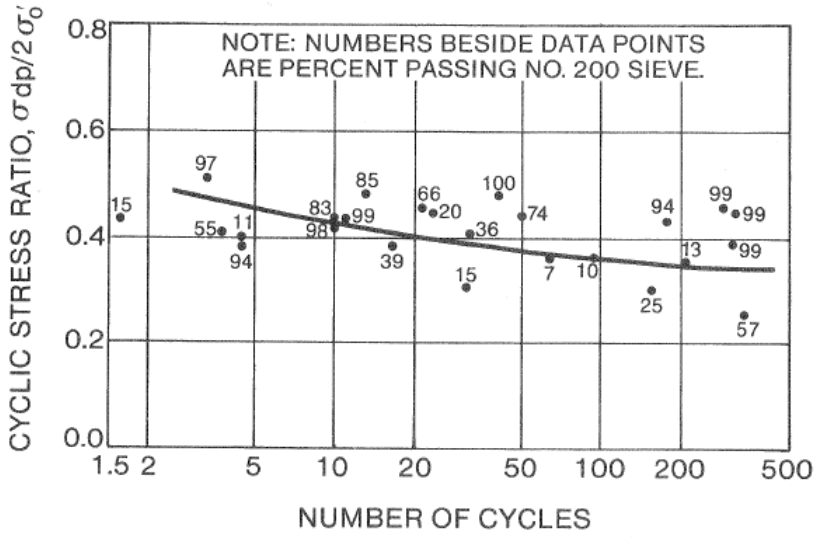

Figure 2-27 Liquefaction resistances of undisturbed silty sand specimens (Dezfulian, 1984).

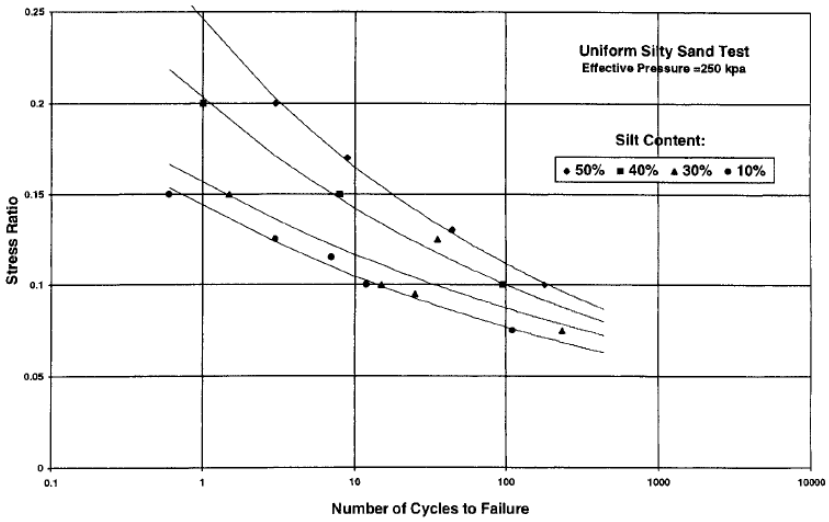

Figure 2-28 Liquefaction resistance curves of moist-tamped Ottawa 20-30 sand specimens (Amini and Qi, 2000).

It has also been shown that sand tested at a constant relative density has a higher cyclic liquefaction resistance than sand with fines. Cyclic tests conducted on Flint shot #4 sand mixed with non-plastic silt at $D_r \approx 50\% \pm 1.5\%$ showed that the liquefaction resistance reduced as fines were added up to $f_C = 20\% - 30\%$, before the resistance increased again as the fines content was raised to 100% (Singh, 1995). Note that the liquefaction resistance of the pure silt was still lower than that of the clean sand. The resistance curves from that study are presented in Figure 2-29.

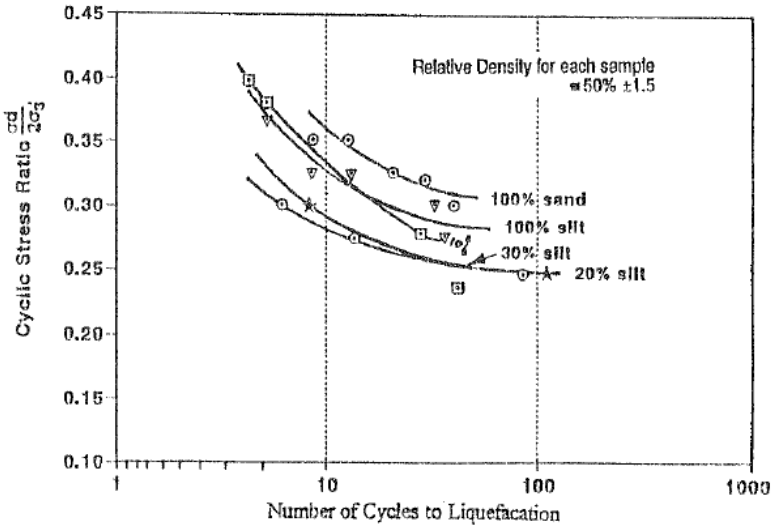

Figure 2-29 Liquefaction resistance curves of Flint shot #4 sand mixed with non-plastic fines (Singh, 1995).

As stated when discussing the Ottawa C-109 sand cyclic test results, the skeleton void ratio, or intergranular void ratio, has been used to compare the state of sand when assessing the effects of fines. A number of other studies that have also used this parameter to characterize sandy soil state when investigating cyclic liquefaction resistance (Kuerbis et al., 1988; Vaid, 1994; Thevanayagam et al., 2000; Carraro et al., 2003; Xenaki and Athanasopoulos, 2003; Hyodo et al., 2008) have shown that fines appear to increase such resistance, as they did for the Ottawa C-109 sand. Figure 2-30 displays the cyclic liquefaction resistance curves of silica sand mixed with Tottori silt (non-plastic) using the intergranular void ratio as the state measure, which shows the liquefaction resistance of the sand increasing as the fines content is raised. Note that liquefaction was considered to occur at 5% double amplitude axial strain for these tests.

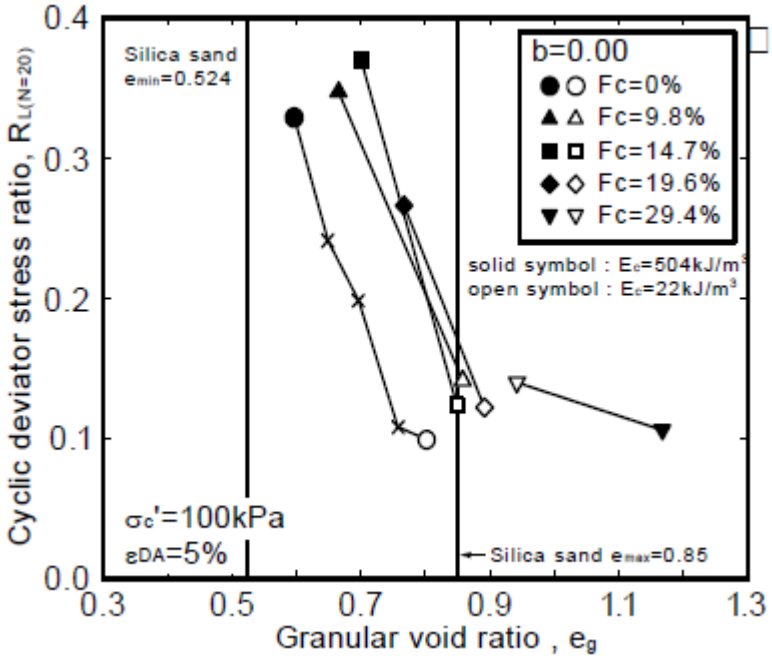

Figure 2-30 Cyclic liquefaction resistance curves of silica sand mixed with non-plastic silt (Hyodo et al., 2008).

Note that in Figure 2-30 the fines influence factor value, *b*, is stated to be equal to zero. This factor is used in the equivalent granular void ratio definition, which becomes equal to the intergranular void ratio value when $b = 0$, or when all fines are thought to sit in the void space created by the sand particles. A number of studies have also used the equivalent granular void ratio to compare the state of cyclically-tested sands – these studies show that, when using a unique value of *b*, the liquefaction resistance becomes largely independent of the fines content (Thevanayagam et al., 2000; Hyodo et al., 2008; Rahman et al., 2008). This is clearly shown in Figure 2-31, which presents the cyclic liquefaction resistance curves of Monterey sand mixed with non-plastic Yatesville silt using the equivalent granular void ratio as the measure of soil state. Note that the cyclic data used to produce Figure 2-31 was sourced from an earlier study (Polito and Martin II, 2001).

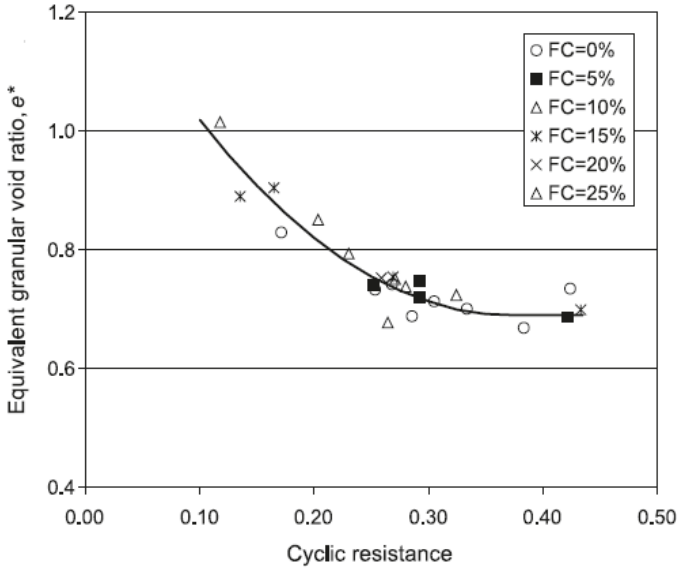

Figure 2-31 Cyclic liquefaction resistance curves of Monterey sand mixed with Yatesville silt (Rahman et al., 2008).

The liquefaction resistance of sand with fines becoming independent from the fines content when using the equivalent granular void ratio is useful as it allows the effects of fines to be quantified. This is done through the value of the fines influence factor, *b*, whereby low values correspond to small amounts of fines participating in the soil force-chain, whilst high values correspond to large amounts of fines contributing to the force-chain (Thevanayagam, 2007). Thus, the reporting of the fines influence factor value can potentially help to quickly quantify what effect fines are having on the undrained behaviour of sand.

2.3.5. Effects of Plasticity of Fines

It has been stated that as the plasticity of fine-grained soil increases to $PI \geq 7$, the stress-strain behaviour becomes more clay-like than sand-like (Boulanger and Idriss, 2006). As such, variation in the plasticity of fines has been shown to affect the undrained response of sand. The majority of studies investigating such effects suggest that an increase in plasticity of fines acts to increase the liquefaction resistance of sand. For example, a report discussing cyclic tests performed on Toyoura sand mixed with bentonite, low-plasticity mica powder, and non-plastic mine tailings stated an increase in cyclic stress ratio required to reach liquefaction in 20 load cycles with increasing plasticity index values (Ishihara and Koseki, 1989). This correlation is presented in Figure 2-32. Another study involved the cyclic loading of Chalk River sand mixed with both Little Jackfish silt (non-plastic) and New Liskeard clay ($PI \approx 50$) respectively. The liquefaction resistance curves obtained during that study are

presented in Figure 2-33, with curve 4 being that of clean sand. Curves 5, 6, 7, and 8 correspond to the sand and silt mixtures, whilst curves 1, 2, and 3 correspond to the sand and clay mixtures. Note that in general the sand and silt mixtures have lower cyclic liquefaction resistance than the clean sand, unlike the sand and clay mixtures which have higher resistances than that of the clean sand. These results again suggest that higher plasticity fines increase the liquefaction resistance of sand.

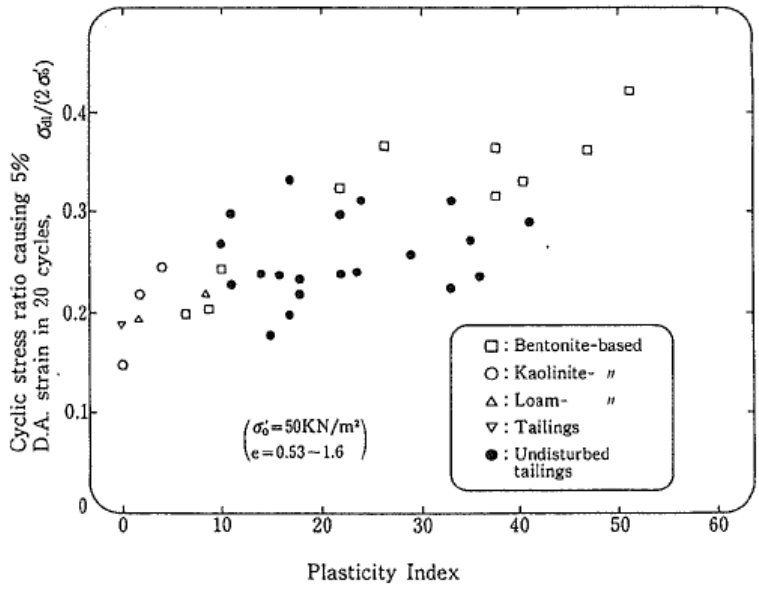

Figure 2-32 Correlation of cyclic stress ratio required to reach liquefaction after 20 load cycles with plasticity index (Ishihara and Koseki, 1989).

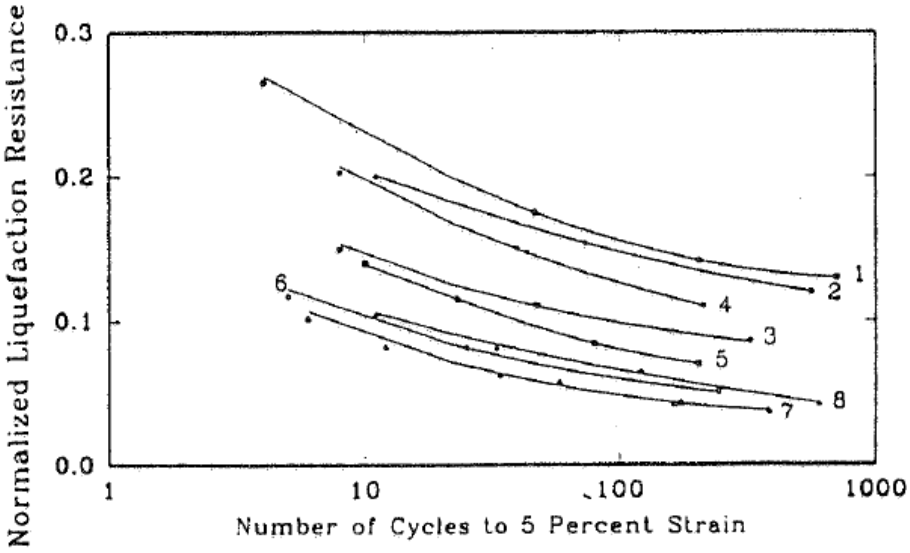

Figure 2-33 Liquefaction resistance curves of Chalk River clean sand (4) mixed with Little Jackfish silt (5, 6, 7, 8) and New Liskeard clay (1, 2, 3) (Law and Ling, 1992).

Other studies, such as tests performed on Ottawa sand mixed with non-plastic silica fines, and silty clay (*PI* = 10), have suggested that in both the cases the liquefaction resistance of the sand decreases with additional fines, but that this decrease is less pronounced as the plasticity of the fines is raised (Erten and Maher, 1995b).

When using the equivalent granular void ratio as a measure of state, some studies have proposed that the fines influence value for the steady state of deformation should be less than zero when plastic fines are mixed with clean sand (Ni et al., 2004). This was concluded based on the analysis of monotonic tests performed on Host sand with 10% kaolin fines (Thevanayagam and Mohan, 2000), and suggests that plastic fines weaken the strength of sand at steady state even more than non-plastic fines do. However, recent cyclic testing performed on silica sand mixed with Iwakuni clay, *PI* = 47.5 (Hyodo et al., 2006), has also shown that the fines influence factor may be positive when considering highly plastic fines. It was determined that such a mixture of sand and fines produced a value of b = 0.20 when considering the cyclic liquefaction resistance of the clayey sand mixtures (Ishikawa et al., 2007), as displayed in Figure 2-34. Given that the equivalent granular void ratio is a recent development in measuring the state of sandy soil, there still remains a gap in the knowledge as to how the plasticity of fines affects the fines influence factor, b.

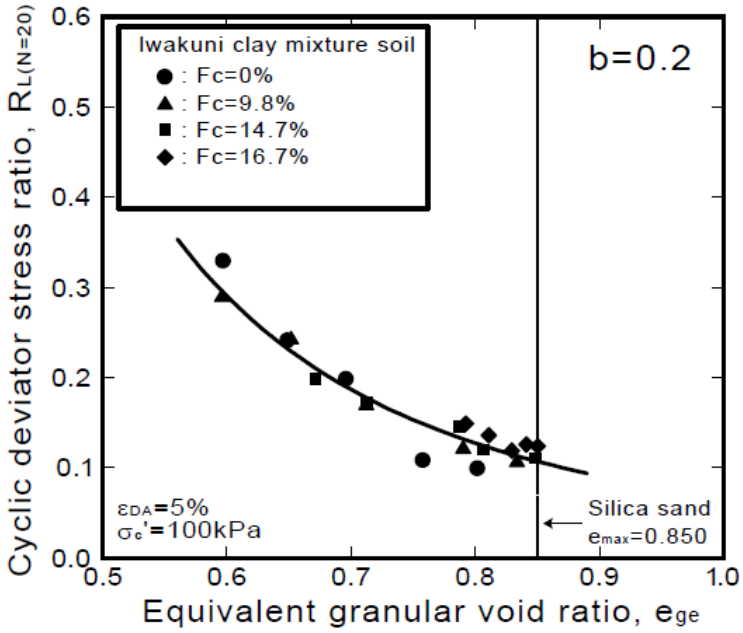

Figure 2-34 Cyclic liquefaction resistance data of silica sand mixed with Iwakuni clay (Ishikawa et al., 2007).

As discussed in this section, the plasticity of fines clearly produces some effect on the undrained behaviour of sand which is not yet fully understood and quantified. Due to this fact, the scope of this study is limited to quantifying the effects of non-plastic fines on the undrained behaviour of sand, rather than complicating the study by including another variable that must be accounted for.

2.4. Effects of Fines in Field Studies

Numerous studies have reported that liquefaction often occurs in silty sand deposits during earthquakes (Chang et al., 1982), based on historical cases of liquefaction. For example, a study which presented data for 20 historic cases of liquefaction (Baziar and Dobry, 1995) showed that sand with up to 80% fines was liquefiable – this corresponded to flow failure of Mochi-koshi tailings dams during the 1978 Izu-Oshima earthquake (M = 7.0). Another example included 1.6m of lateral spreading occurring in sand with f_C = 65% at San Fernando Juvenile Hall during the 1971 San Fernando earthquake, $M_w \approx 6.5$. Such case histories have confirmed that liquefaction in sand with fines is a reality in the field, and not purely confined to laboratory tests.

The simplified design procedure (Seed and Idriss, 1971) currently remains the most widely used method for determining the cyclic liquefaction resistance of a soil deposit in the field. Figure 2-35 presents the design chart that relates the normalized SPT blowcount of a soil layer, $(N_1)_{60}$, with the potential cyclic liquefaction resistance ratio of a soil layer. This chart is based on numerous case histories of earthquakes in soil deposits with available SPT data. Similar charts are also available using the CPT resistance or shear wave velocity as a field measure for the in-situ state of the soil.

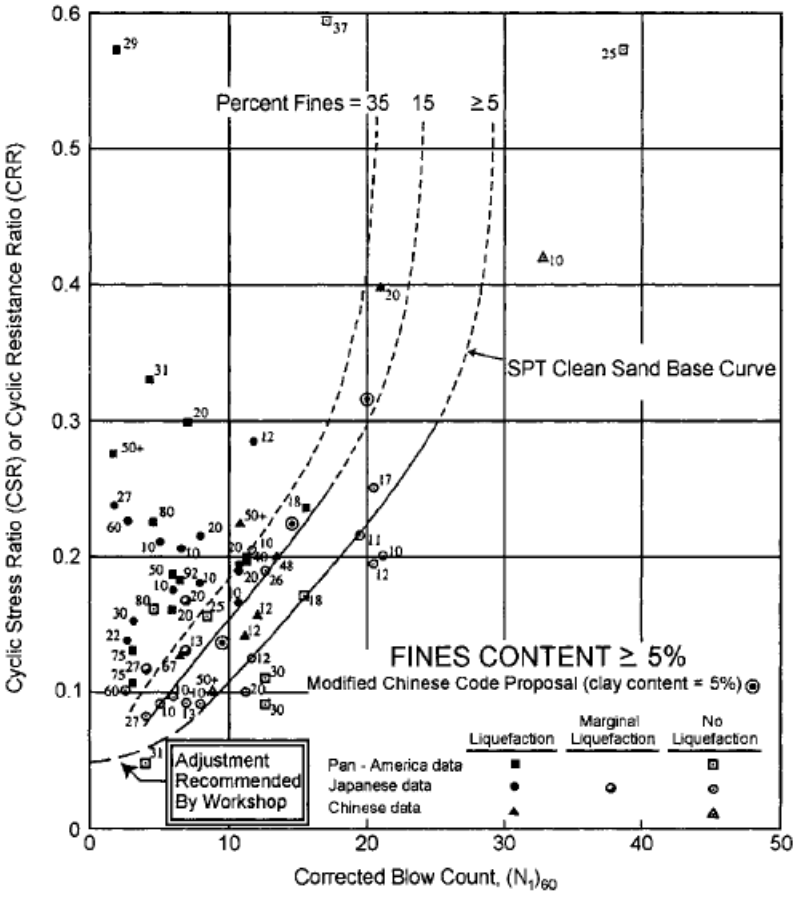

Figure 2-35 Chart used for determining the cyclic resistance ratio of a soil deposit based on the SPT blowcount (Youd and Idriss, 2001).

Note that for similar values of $(N_1)_{60}$ in Figure 2-35, sand with higher fines content appears to have a higher resistance to cyclic liquefaction (Seed et al., 1983). The same conclusion was also drawn when a number of liquefaction case histories from Japan were correlated with SPT blowcount data (Tokimatsu and Yoshimi, 1983). This has previously led to practicing engineers assuming that the addition of fines to sand has a beneficial impact on the liquefaction resistance (Law and Ling, 1992), however it has clearly been stated that this trend may simply be due to a decrease in penetration resistance with increase in fines content (Youd and Idriss, 2001). This again highlights how the choice of state measure used to characterize a sandy soil deposit can influence the apparent effect fines have on the undrained response of such soils.

The influence of plasticity on the effects of fines has also been discussed based on in-situ field data. It has been reported that sands with more than 20% clay particles are unlikely to liquefy during a large earthquake based on Japanese case histories (Tokimatsu and Yoshimi, 1983), assuming the plasticity index of the fines is not low. This was also backed up

by liquefaction data from China, which led to Seed and Idriss defining the 'Chinese criteria'. The criteria states that a soil can only liquefy if: (1) the clay content is < 15% by weight; (2) the liquid limit is < 35%; (3) the natural moisture content is > 0.9 times the liquid limit (Youd and Idriss, 2001). However, case histories such as apparent liquefaction of clayey silt at Moss Landing during the 1989 Loma Prieta earthquake (Boulanger et al., 1997) suggest that care should be taken when investigating the liquefaction potential of plastic fines. A recent study has proposed that the plasticity index can be used as an indicator of liquefaction susceptibility, but should not be used as an absolute criterion, and that the Chinese criteria should not be used in engineering practice (Bray and Sancio, 2006). Instead the study suggested that plasticity be used in conjunction with the water content and liquid limit (w_c/LL) of the soil, with plastic fine-grained soil at $w_c/LL < 0.8$ being unlikely to liquefy, whilst non-plastic fine-grained soil at $w_c/LL > 1.0$ being a prime candidate for liquefaction. Thus, there tends to be a general consensus that higher plasticity fines tend to decrease the liquefaction potential of a soil deposit, although there still remains debate as to the quantification of such effect.

3. Test Soils and Procedures

3.1. Introduction

A number of mixes of sand and fines were triaxially tested under undrained monotonic and cyclic loading conditions as part of this study. Fines were defined as particles smaller than 75μm. All tested soils were natural sands sourced from Christchurch, New Zealand. The fines content was varied throughout testing by adding different amounts of fines to clean sand in order to assess the effect of fines on the undrained sand response. All tested fines were found to be non-plastic.

Undrained triaxial tests were conducted in temperature controlled conditions within the Geomechanics laboratory at the University of Canterbury, carried out using an advanced stress-path triaxial apparatus. Moist tamping was used in the preparation of all triaxial test specimens.

This chapter outlines the testing concept, the tested soils and their properties, the testing procedures used to prepare and perform the undrained triaxial tests, and the equations used for interpreting the acquired data.

3.2. Testing Concept

The aim of the testing program was to investigate how fines affect the response of sand under undrained monotonic and cyclic loading conditions. To do this, the amount of fines added to clean sand was systematically varied. This process created sandy soils with the same sand and fines properties respectively, but differing fines contents. This allowed the effect of fines to be directly compared across a number of undrained triaxial tests.

Undrained monotonic tests were systematically performed on the sandy soils, targeting initial specimen states above and below the steady state line. These states were specifically targeted so that contractive and dilative specimen response could be observed. They also enabled the steady state line for each of the soils to be defined. The testing concept is presented in Figure 3-1, showing initial and steady states for two sandy soils with different fines contents.

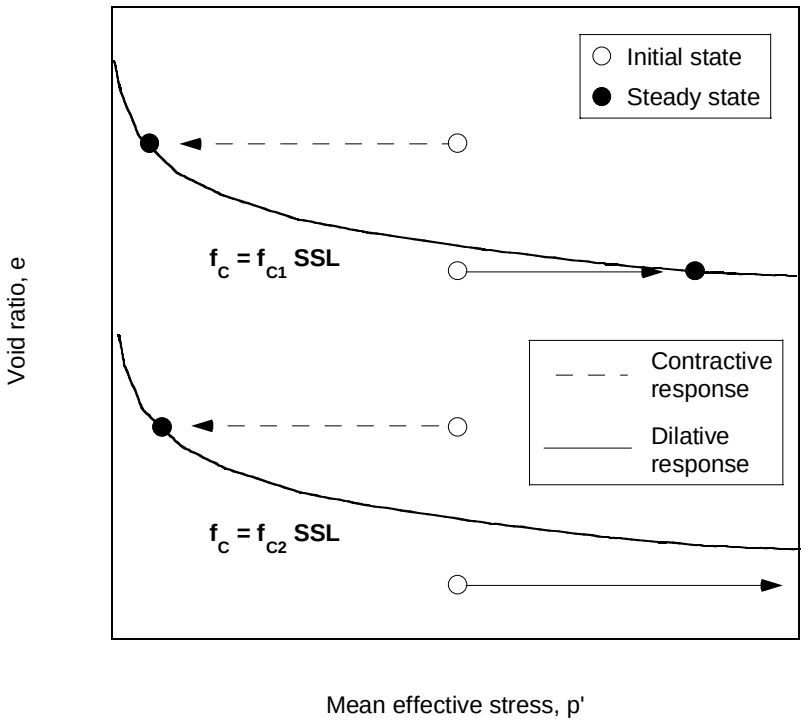

Figure 3-1 Schematic of the undrained monotonic testing concept. Steady state lines (SSL) correspond to the same clean sand with differing amounts of fines.

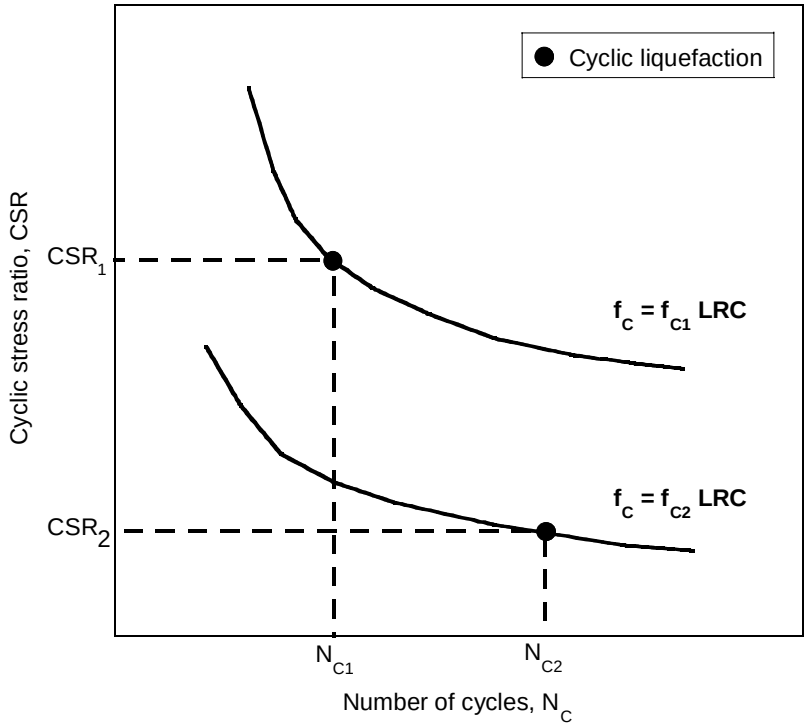

Figure 3-2 Schematic of the undrained cyclic testing concept. Liquefaction resistance curves (LRC) correspond to the same clean sand with differing fines contents at similar (~ identical) initial states.

Undrained cyclic tests were also systematically performed on the sandy soils. Multiple undrained cyclic tests were conducted on similar initial specimen states by varying the cyclic stress ratio. The number of cycles (N_C) required to reach liquefaction (double amplitude axial strain of 5%) were then used to define the liquefaction resistance curves (LRC) for a specific initial specimen state. The testing concept is presented in Figure 3-2 for two sandy soils with different fines content at similar initial states.

3.3. Tested Sandy Soils

The sandy soils tested in this study were natural sands sourced from Christchurch, New Zealand. This location has many silty sand deposits, a high water table and a significant earthquake hazard, making it an appropriate location to source sandy soils for the purpose of this study.

Sandy soils were obtained during three separate field investigations at different geographical locations. The location of each site is shown in Figure 3-3. The soils were named after their source locations – the Fitzgerald Bridge sands, sourced in 2006; the Ferrymead sands, also sourced in 2006; the Pinnacles sands, sourced in 2008. Each site investigation yielded a number of sandy soil samples taken from various depths that were individually assessed and combined to create soils of varying fines contents. The details and properties of these sandy soils are described in Sections 3.3.2 - 3.3.5.

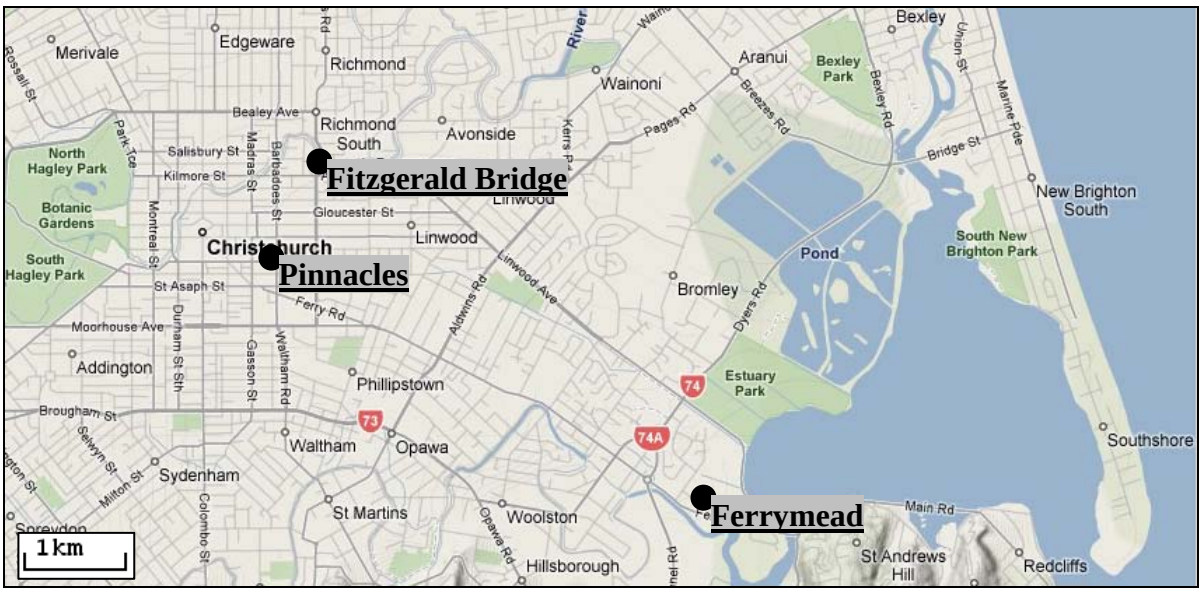

Figure 3-3 Site investigation locations in Christchurch of the sourced sandy soils (adapted from maps.google.co.nz).

3.3.1. Geological Characteristics of Christchurch

Christchurch is located on the eastern coast of the South Island of New Zealand. The underlying soil deposits most relevant to engineering works are the Springston and Christchurch formations, dating back to the last glacial and postglacial Quaternary periods respectively (Brown and Weeber, 1992). The Springston formation consists of alluvial gravels, sands and silts, and underlies Christchurch to within 5km of the eastern coastline. The Christchurch formation consists of marine sand and swap deposits, and outcrops up to 11km inland from the coastline amongst Springston formation deposits. Figure 3-4 displays the near-surface soils of the Christchurch area, with the Christchurch formation included in the postglacial marine deposits, and the Springston formation included in the quaternary fluvial deposits. The primary minerals found in Christchurch sands are quartz and feldspar, but also includes biotite, chlorite, calcite and magnetite (Brown and Weeber, 1992).

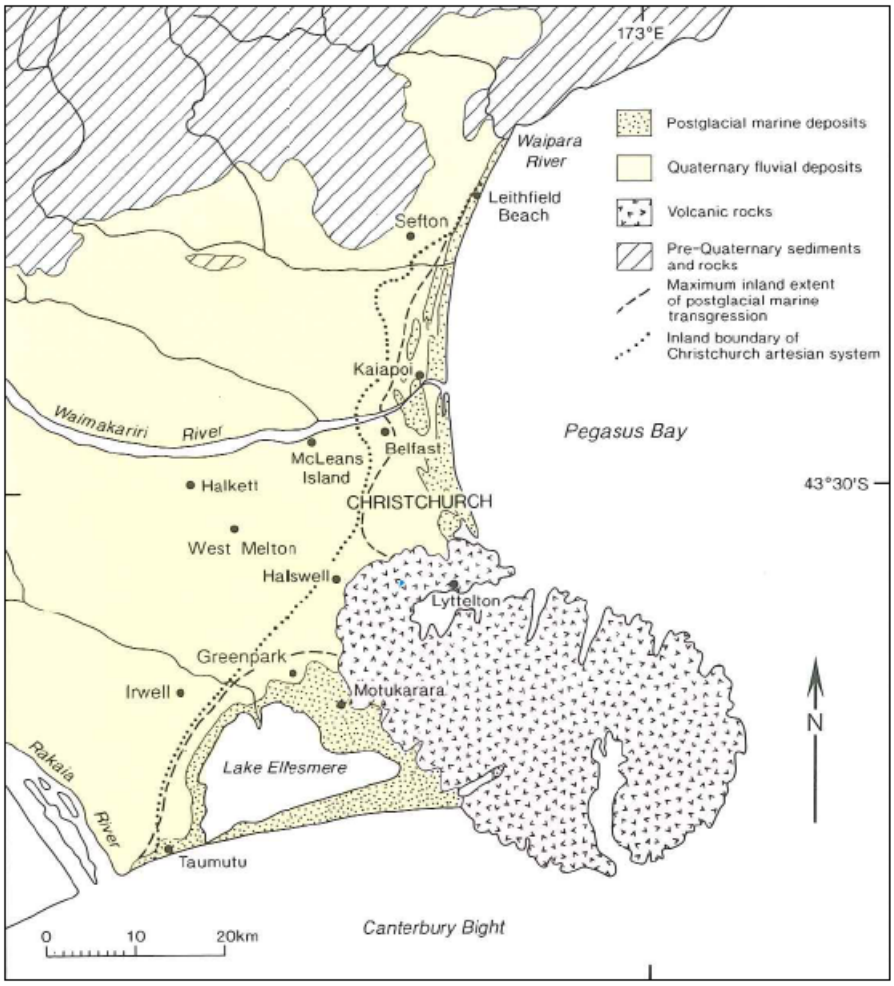

Figure 3-4 Location of Christchurch and the types of near-surface soils (Brown and Weeber, 1992).

The deposited fines within the Springston and Christchurch formations tend to be primarily comprised of silt-sized particles, with very few clay-sized particles being recorded (Brown and Weeber, 1992). As such, the fines generally display low-plasticity.

The groundwater table is located very near to the soil surface throughout the majority of Christchurch. It tends to sit 1m or less below the surface from the coastline to the central city, and up to 5m below the surface around the outer-western suburbs (Brown and Weeber, 1992). The high groundwater table means that most of the engineering structures are founded in saturated soils, which pose a liquefaction risk during seismic activity.

New Zealand sits on the boundary between the Pacific and Indian-Australian tectonic plates. Due to this location, Christchurch is situated near to a number of seismically active faults that represent a seismic hazard to the city. These faults include the Alpine, Hope, Porters Pass and Pegasus Bay Faults, amongst others (Brown and Weeber, 1992).

The combination of silty and sandy soil deposits, high water table, and seismic hazard means there is a reasonable risk of liquefaction occurring in Christchurch soil deposits during a large earthquake. This makes the undrained triaxial testing of Christchurch sandy soils practically very relevant, as well as being good soils to use to assess the effect of fines on the undrained response of sand.

3.3.2. Fitzgerald Bridge Mixtures (FBM)

The Fitzgerald Bridge site investigation was conducted as part of a remediation project for the Fitzgerald Avenue Bridge, which crosses the Avon River in central Christchurch. Soil profiles were adapted and simplified from the site borelogs, and are presented in Figure 3-5. Note there was considerable variability in the measured SPT resistance across the site.

Particle size distribution (PSD) tests were performed on the recovered soil samples (Standards Association of New Zealand, 1986). The PSD curves are presented in Figure 3-6 and Figure 3-7 for Borehole #4 and DT #2 respectively. Note that these original soils were classified as clean to silty sands, with fines contents ranging from f_C = 1 – 12%. It is apparent that the PSD curves were similar throughout the depth of the deposit.

Samples with similar PSD were selected to be mixed together, creating a homogeneous sandy soil mixture. The Borehole #4 soil samples from depths 4.8 – 5.8m, 7.0 – 7.8m, and 22.5m were not included. Mixing was carried out by carefully stirring small portions of the selected samples together until all soil was mixed. The resultant homogeneous sandy soil

mixture was found to have a fines content of 10%, and was named the Fitzgerald Bridge Mixture 10% (FBM-10). The moisture content was approximately 9% after mixing.

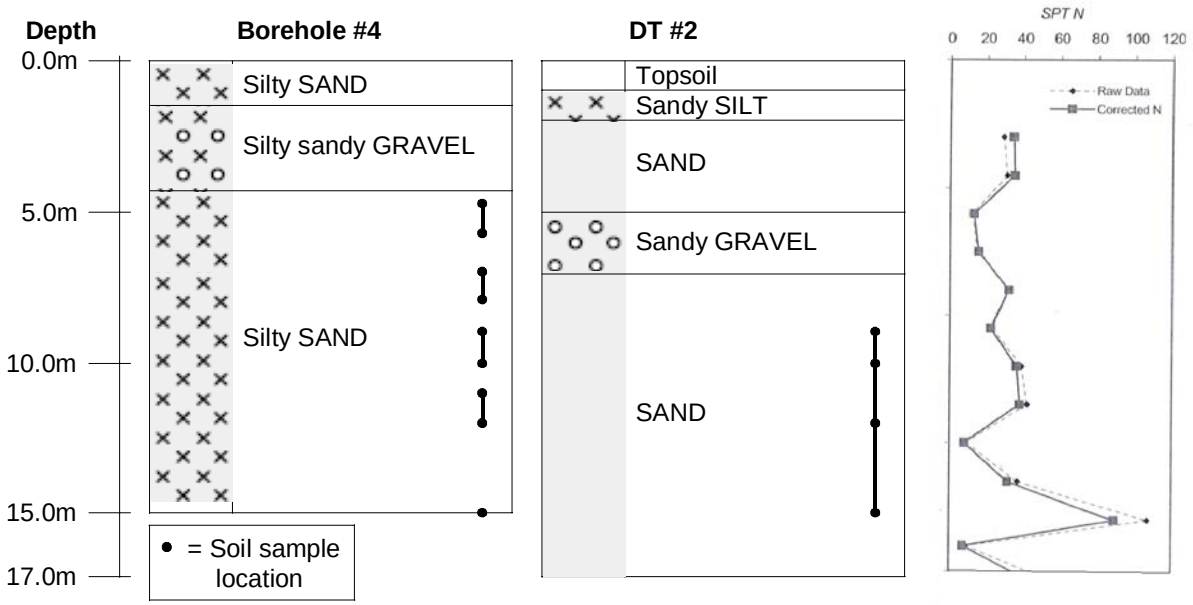

Figure 3-5 Fitzgerald Bridge site profile with SPT N-value profile near Borehole #4 (adapted from Tonkin & Taylor site investigation report, 2006).

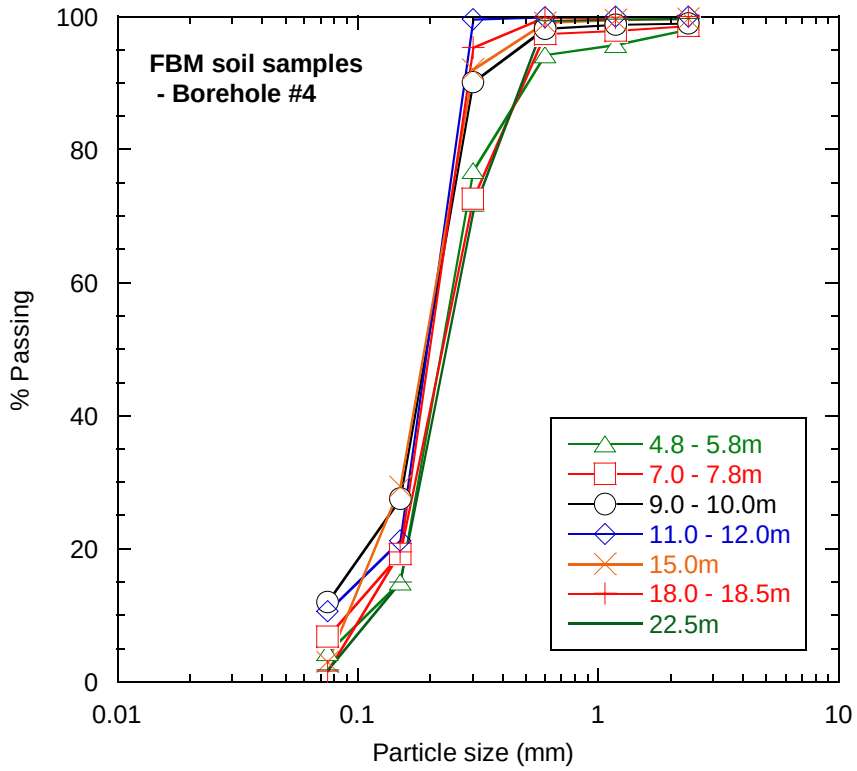

Figure 3-6 Particle size distributions of the Fitzgerald Bridge sandy soil samples recovered from Borehole #4.

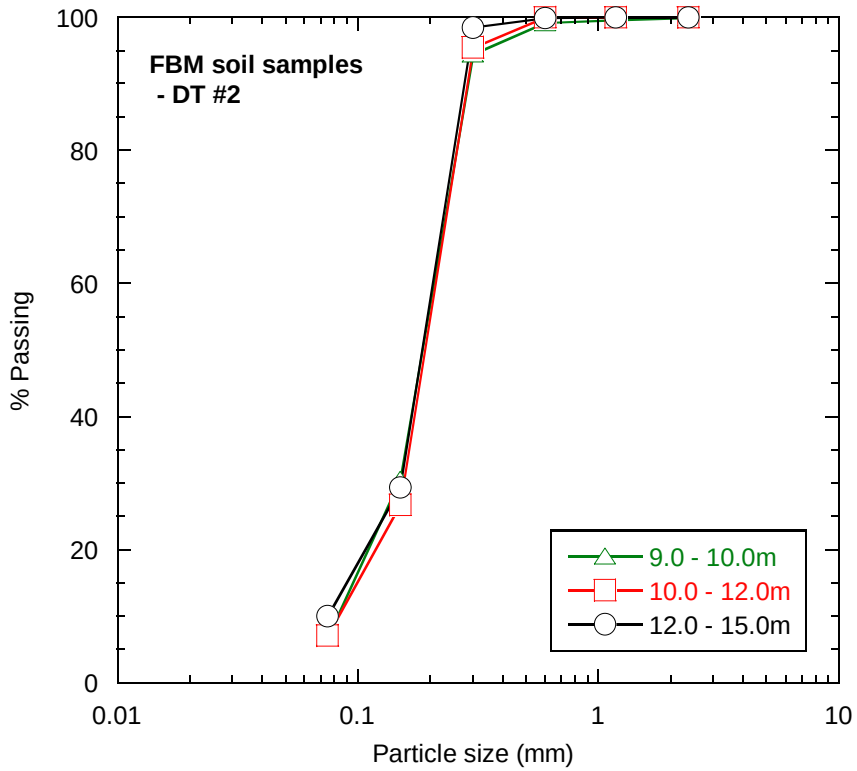

Figure 3-7 Particle size distributions of the Fitzgerald Bridge sandy soil samples recovered from DT #2.

FBM-10 was used for the first set of undrained triaxial tests. After each test the tested soil was dried at 104°C and gently ground using a mortar and rubber pestle to return the material to a homogeneous state, as settling occurred during oven drying. The grounding was carried out very carefully to avoid any significant loss of fines.

The FBM-10 sandy soil was separated into clean sand and fines components following the completion of the undrained monotonic and cyclic triaxial tests on this mixture. The separation was performed using dry sieving. Particle size distributions were then carried out on each of the soil components, using a sedimentation analysis (Standards Association of New Zealand, 1986) for the fines. The particle size distributions of the clean sand and fines are shown together in Figure 3-8.

Plasticity tests using Atterberg limits (Standards Association of New Zealand, 1986) were performed on the fines. They were determined to be non-plastic as the plastic limit could not be defined during testing. The fines were too silty, and separated before they could be rolled into the correct diameter required to calculate the plastic limit. This was not surprising given the general low plasticity of fines deposited in Christchurch soils.

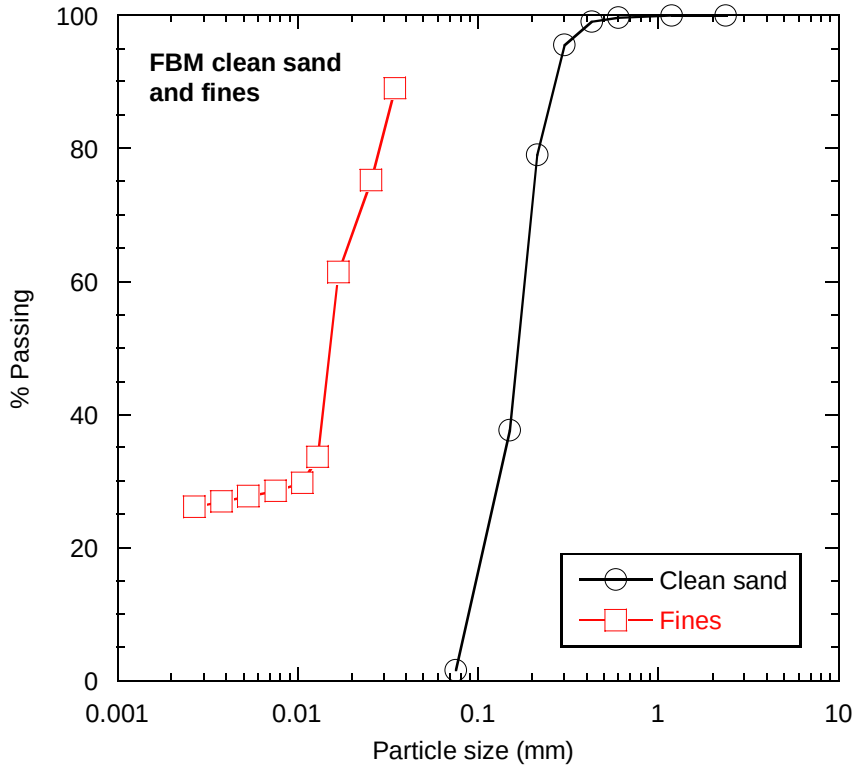

Figure 3-8 Particle size distributions of the Fitzgerald Bridge Mixture clean sand and fines components.

Three additional mixtures named FBM-1 (f_C = 1%), FBM-20 (f_C = 20%) and FBM-30 (f_C = 30%) were created by mixing different amounts of the FBM clean sand and fines together. These sandy soils, together with FBM-10, made up the four FBM soils used during the undrained monotonic and cyclic tests on soils sourced from the Fitzgerald Bridge site. The individual PSD of the four mixtures are presented in Figure 3-9.

The angularity of the clean sand particles was classified during the testing program by examining the particles with a magnifying glass. This determined the sand particles to be sub-angular to sub-rounded (SA – SR). Scanning electron microscope (SEM) images of the sand and fines were also taken in the University of Canterbury Mechanical Engineering laboratory after triaxial testing had been completed. Two of these images are displayed in Figure 3-10 and Figure 3-11, which are included to provide a visual record of the sand and fines particles, as well as to allow future assessment of particle angularity using quantitative numerical methods. Sand angularity and subsequent effects are specifically discussed in Chapter 6.

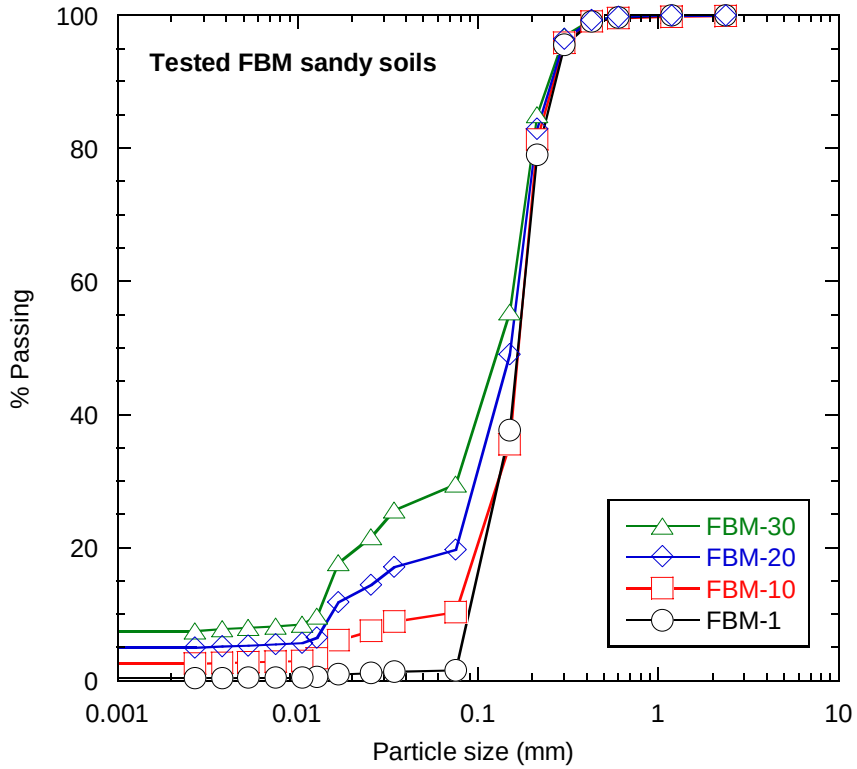

Figure 3-9 Particle size distributions of the tested Fitzgerald Bridge Mixtures of sand and fines.

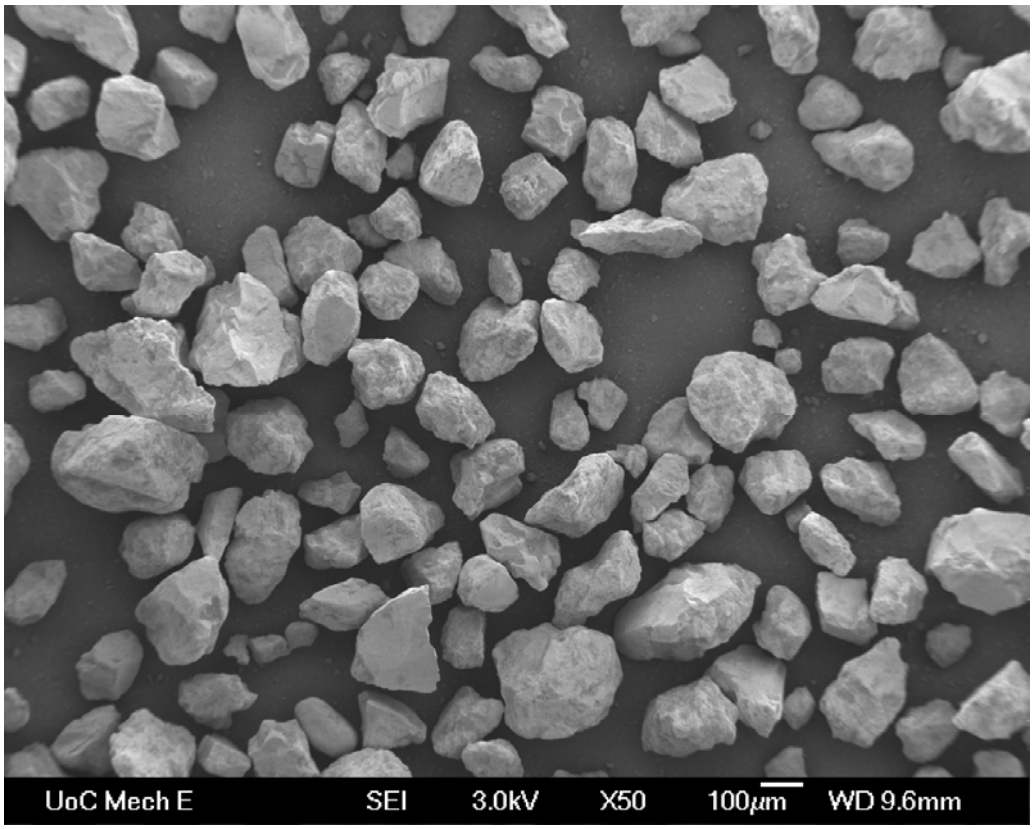

Figure 3-10 Scanning electron microscope (SEM) image of the FBM clean sand particles.

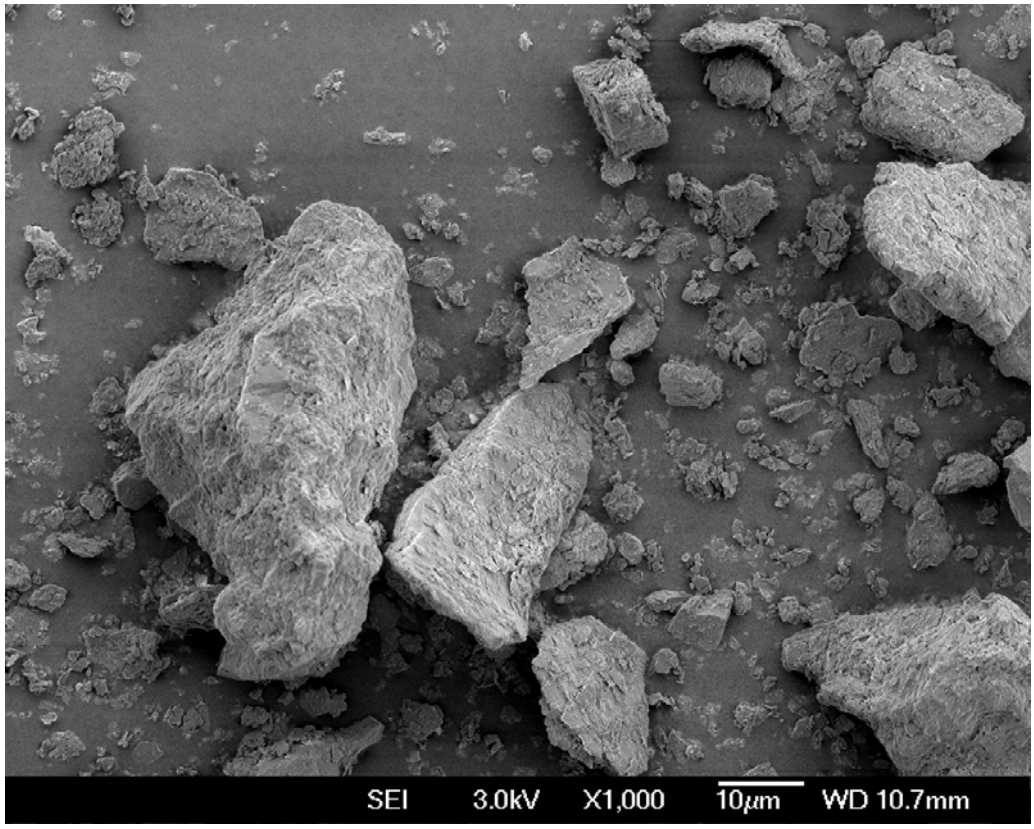

Figure 3-11 Scanning electron microscope (SEM) image of the FBM fines particles.

3.3.3. Pinnacles Sand Mixtures (PSM1 and PSM2)

The Pinnacles site investigation was conducted as part of a development along Lichfield Street in central Christchurch. Soil profiles adapted from the site borelogs are displayed in Figure 3-12 for Borehole #1 and #2.

All soil samples sourced from the Pinnacles site were dried at 104°C. PSD were then performed on the individual samples using dry sieving. The distributions of each soil sample are presented in Figure 3-13 and Figure 3-14 for Borehole #1 and Borehole #2 respectively. Note the original soils were classified as clean to silty sands, with fines contents ranging from f_C = 3 – 18%, except for one soil sample from Borehole #1 which had f_C = 30%.

Sandy soil samples from Borehole #1 and Borehole #2 were combined in two separate groups based on depth. Pinnacles Sand Mixture 1 (PSM1) contained soils from 12.5 – 16.0m depth; Pinnacles Sand Mixture 2 (PSM2) contained soils from 16.5 – 20.0m depth. The division of samples was based on the SPT N-values measured during the site investigation: PSM1 soils had low N-values below 10, whilst PSM2 soils had higher N-values, around 50. All samples were dry sieved before mixing, separating the sand and fines particles.

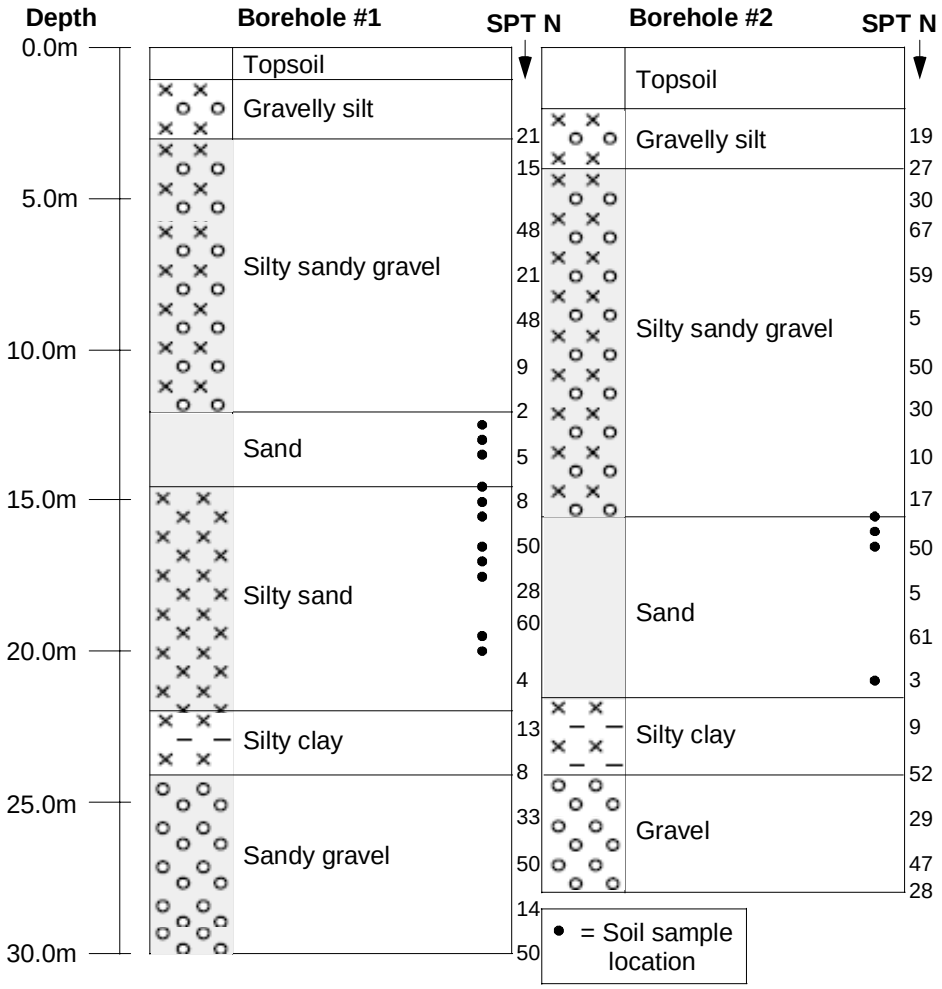

Figure 3-12 Schematic of the Pinnacles site profile – adapted from Connell Wagner site investigation report (2008).

Two clean sands, PSM1-0 and PSM2-0, were available for the first set of triaxial tests on the Pinnacles soils. The PSD for the PSM1 and PSM2 clean sands and fines are displayed in Figure 3-15. Note the similarity of the distributions between PSM1 and PSM2 soils.

After triaxially testing PSM1-0, two additional mixtures named PSM1-10 (f_C = 10%) and PSM1-20 (f_C = 20%) were created by mixing PSM1 and PSM2 fines with the PSM1 clean sand. Both sets of fines were used due to their PSD similarity, and together are named the Pinnacles Sand fines (PS fines). Plasticity tests also showed the fines to be non-plastic. These soil mixtures, along with PSM1-0, made up the three triaxially tested PSM1 soils. Their individual PSD are shown together in Figure 3-16.

Similarly, after triaxially testing PSM2-0, PSM2-10 (f_C = 10%) and PSM2-25 (f_C = 25%) were created by mixing Ferrymead fines, described in Section 3.3.4, with the PSM2 clean sand. Ferrymead fines were used for mixing in order to introduce fines with a distinctly

different particle size distribution compared to that of the PS fines. PSM2-0, PSM2-10 and PSM2-25 made up the three triaxially tested PSM2 soils, and their individual PSD are displayed together in Figure 3-17.

The angularities of PSM1 and PSM2 clean sand particles were classified during testing by examining the particles with a magnifying glass. The angularities were determined to be sub-angular to sub-rounded (SA – SR). SEM images were also taken of the sands and fines, which are shown in Figure 3-18, Figure 3-19, Figure 3-20 and Figure 3-21 respectively.

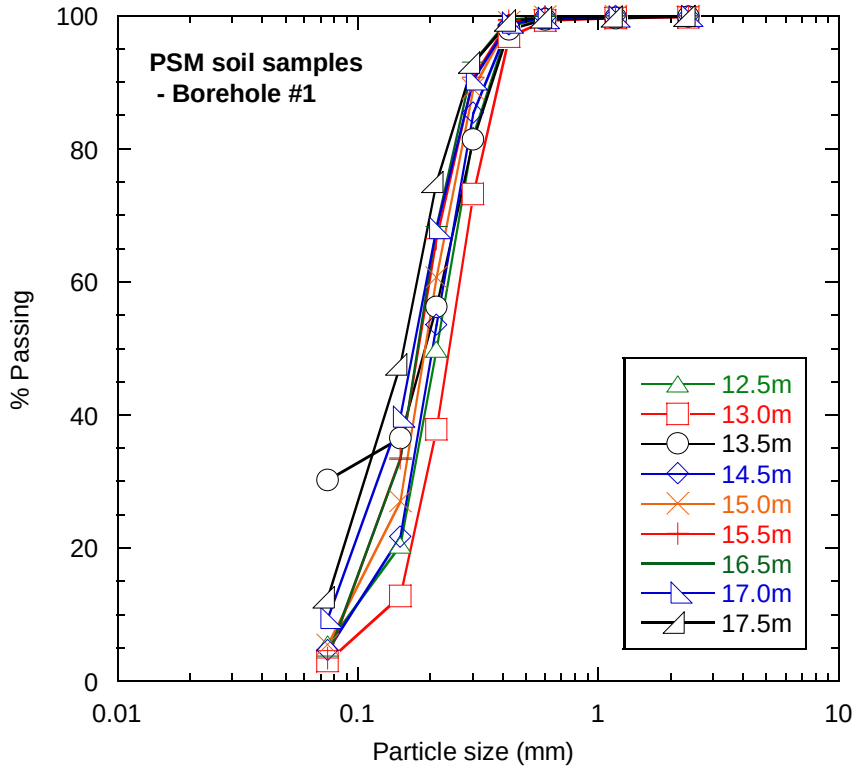

Figure 3-13 Particle size distributions of the Pinnacles sandy soil samples recovered from Borehole #1.

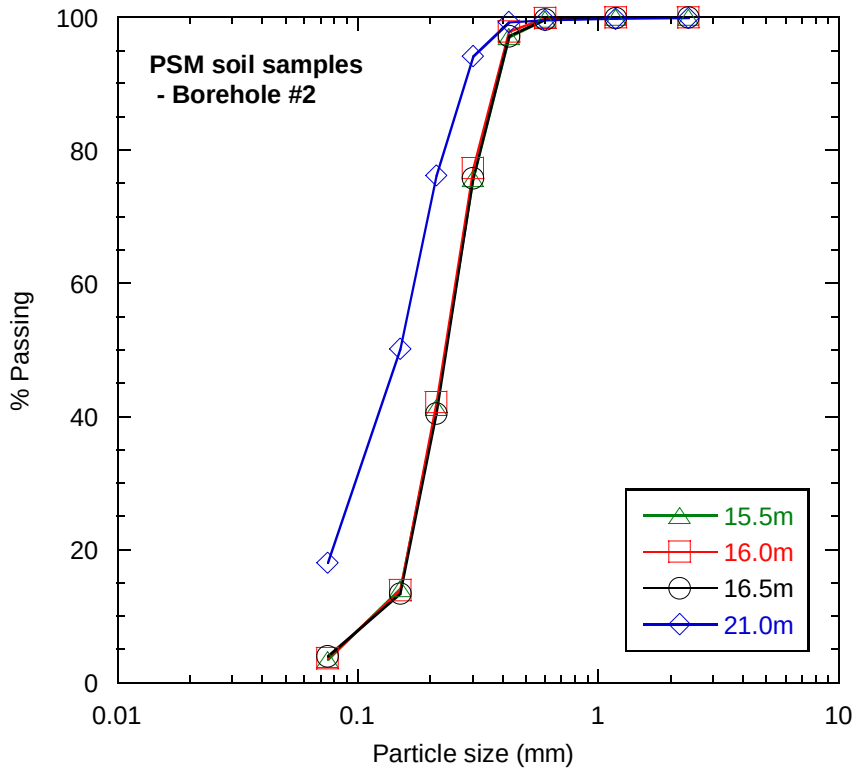

Figure 3-14 Particle size distributions of the Pinnacles sandy soil samples recovered from Borehole #2.

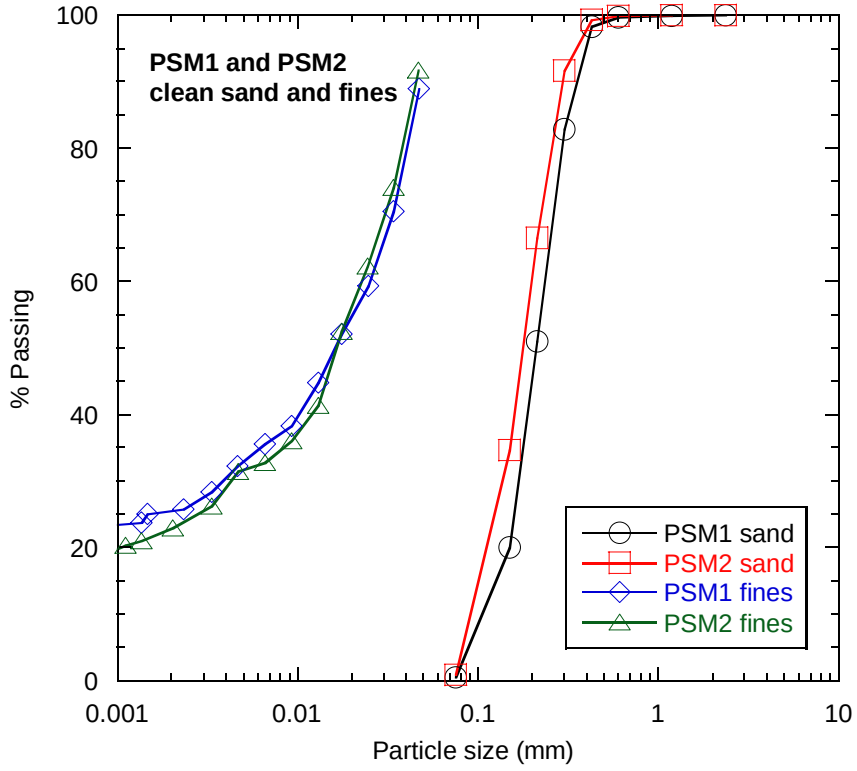

Figure 3-15 Particle size distributions of the Pinnacles Sand Mixtures clean sand and fines components.

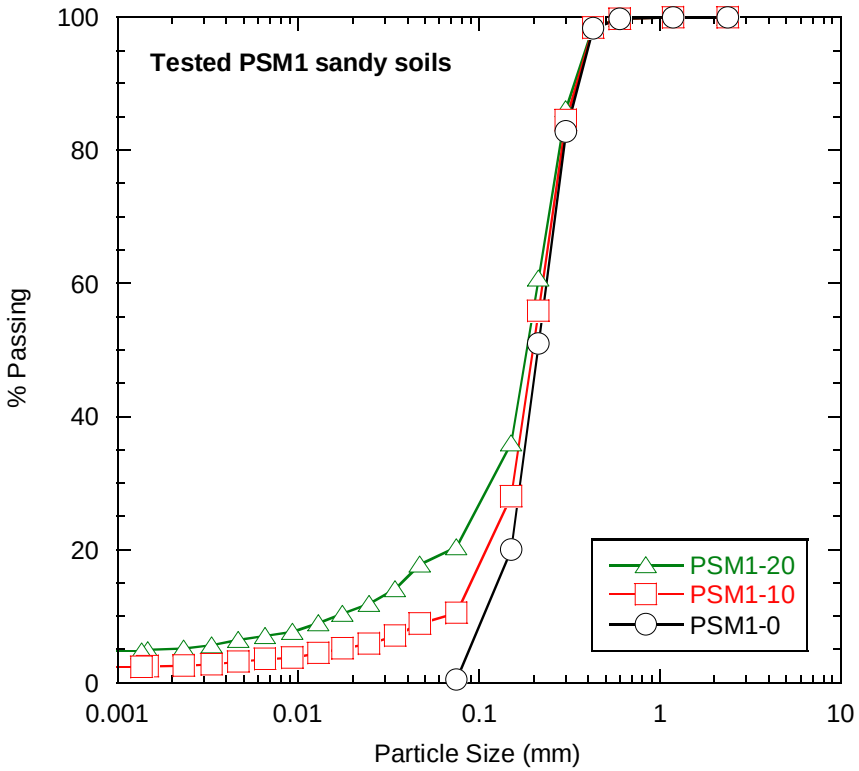

Figure 3-16 Particle size distributions of the tested PSM1 sandy soils.

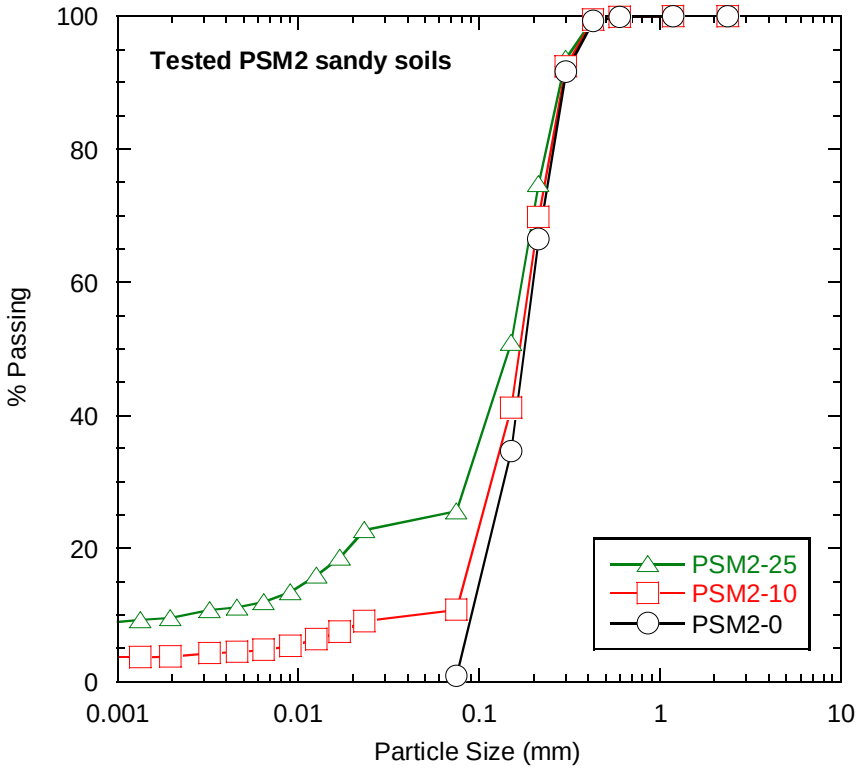

Figure 3-17 Particle size distributions of the tested PSM2 sandy soils.

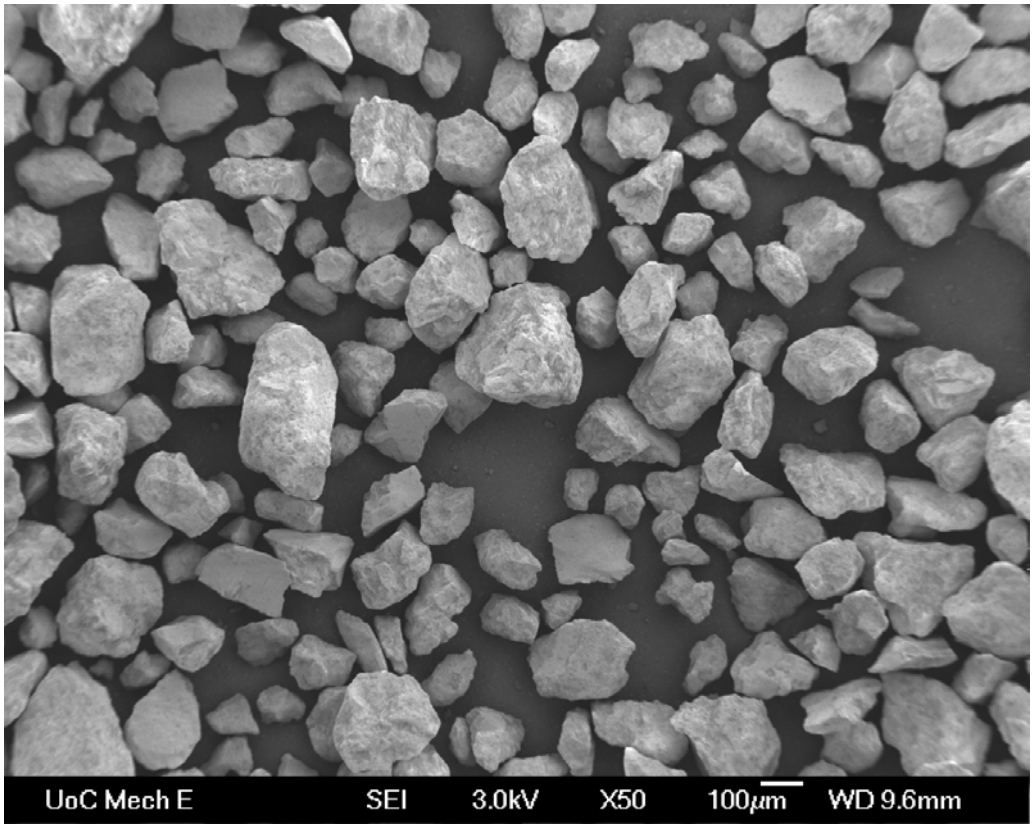

Figure 3-18 Scanning electron microscope (SEM) image of the PSM1 clean sand particles.

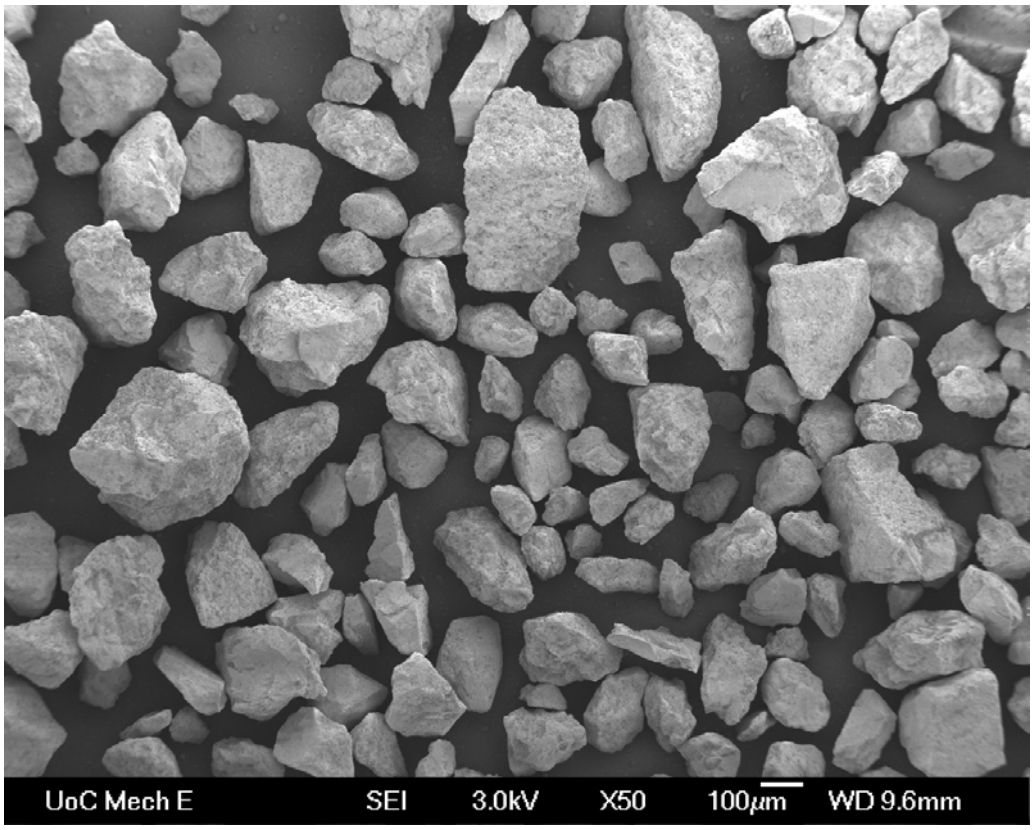

Figure 3-19 Scanning electron microscope (SEM) image of the PSM2 clean sand particles.

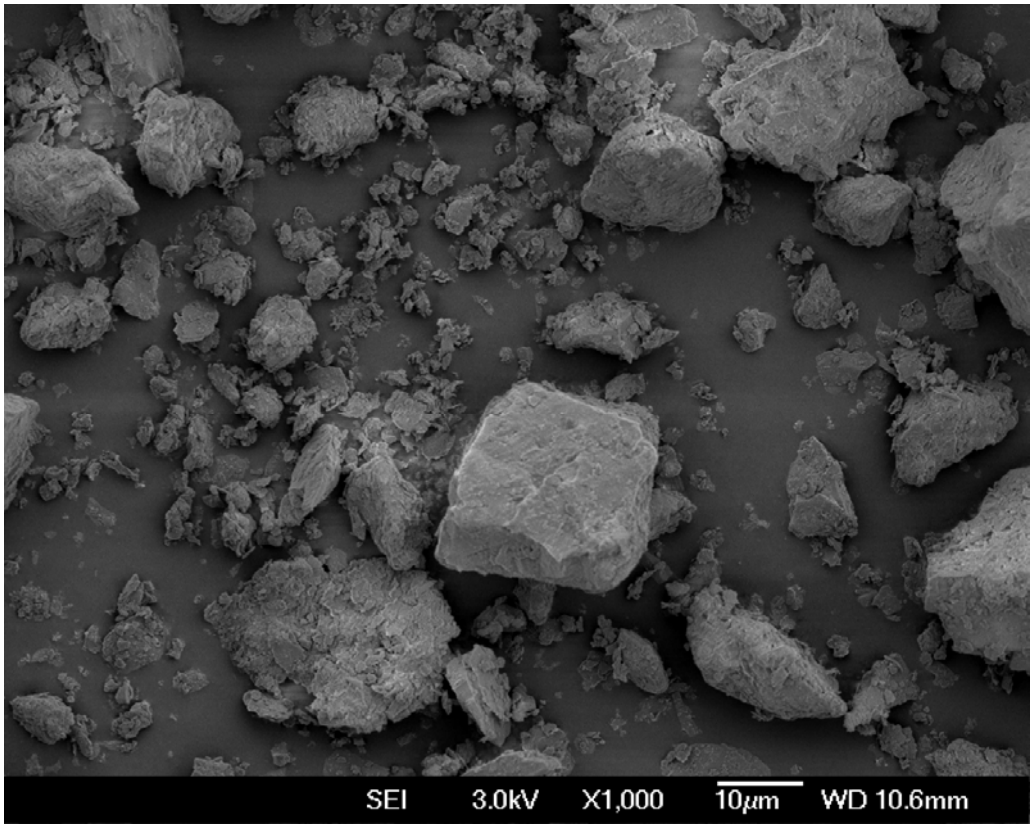

Figure 3-20 Scanning electron microscope (SEM) image of the PSM1 fines particles.

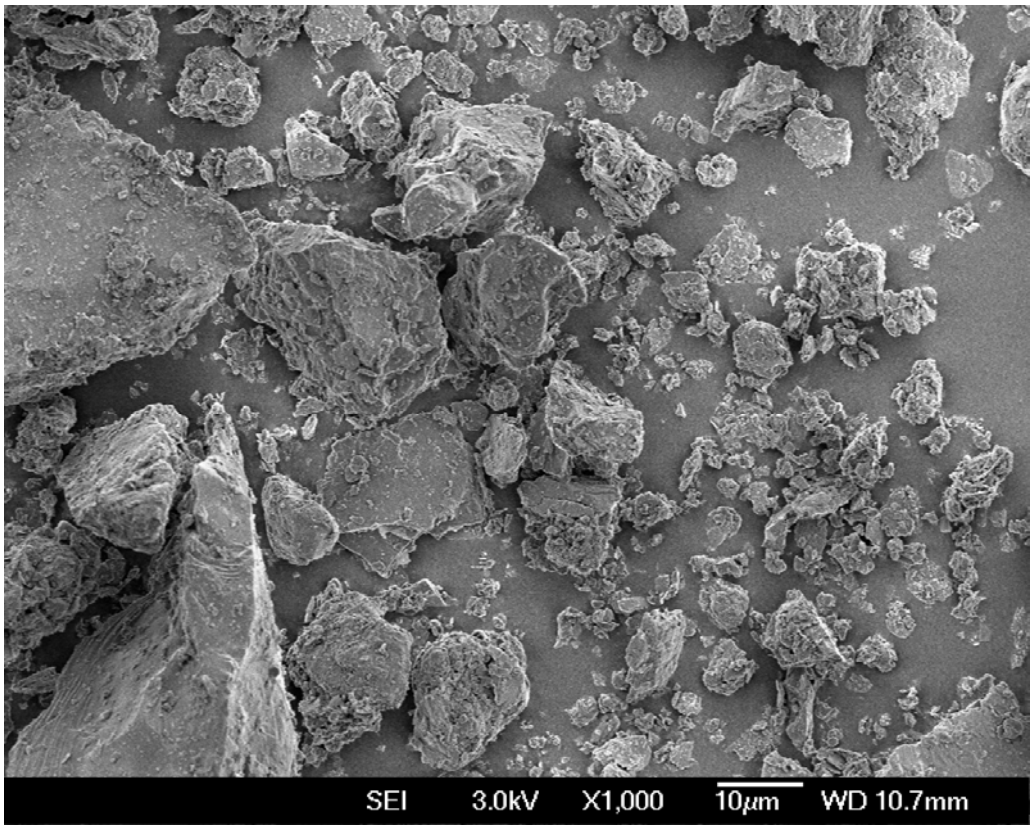

Figure 3-21 Scanning electron microscope (SEM) image of the PSM2 fines particles.

3.3.4. Ferrymead Fines

The Ferrymead site investigation was part of a site development in Ferrymead, a suburb south-east of central Christchurch, near the Port Hills and Estuary. The sand fraction of the Ferrymead soil samples was not used for testing, but a portion of the fines were added to the PSM2 clean sand, as discussed in Section 3.3.3. Plasticity tests determined the Ferrymead fines to be non-plastic.

Ferrymead soil samples were dried at 104°C. Dry sieving using a 75µm sieve was performed to separate the sand and fines particles. A sedimentation analysis was performed on the fines, and the resulting initial PSD was very similar to the Pinnacles fines. The fines were dry sieved a second time, removing the 37 - 75µm particle sizes. The adjusted fines, 37µm or smaller, were then mixed with the PSM2 clean sand as discussed in Section 3.3.3. The initial and adjusted Ferrymead fines particle size distributions are presented in Figure 3-22.

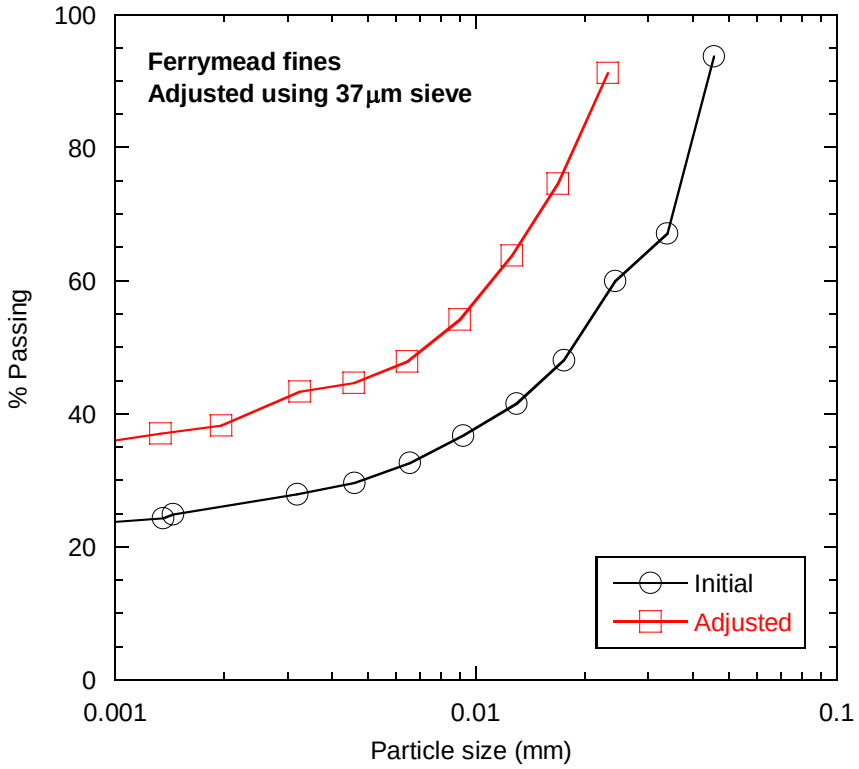

Figure 3-22 Initial and adjusted particle size distributions of the Ferrymead fines.

3.3.5. Soil Properties

The material properties for each of the tested sandy soils were determined based on the New Zealand Standard (Standards Association of New Zealand, 1986), with the British Standard (BSI, 2002) used as a guideline for determining the maximum and minimum void ratios e_{max} and e_{min}. The soil properties are reported in Table 3-1.

Table 3-1 Tested sandy soil properties.

Soil	f_C (%)	ρ_S (t/m^3)	D_{50} (mm)	D_{10} (mm)	C_u	Plasticity	e_{max}	e_{min}
FBM-1	1	2.65	0.168	0.089	2.0	-	0.907	0.628
FBM-10	10	-	-	-	2.4	-	0.945	0.597
FBM-20	20	-	-	-	11.0	-	0.895	0.511
FBM-30	30	-	-	-	12.2	-	0.860	0.527
FB fines	100	-	0.015	-	-	NP	-	-
PSM1-0	0	2.66	0.208	0.104	2.2	-	0.927	0.642
PSM1-10	10	-	-	-	2.9	-	0.861	0.505
PSM1-20	20	-	-	-	12.2	-	0.834	0.449
PS fines	100	-	0.016	-	-	NP	-	-
PSM2-0	0	2.66	0.175	0.091	2.2	-	0.941	0.637
PSM2-10	10	-	-	-	2.6	-	0.888	0.506
PSM2-25	25	-	-	-	68.8	-	0.941	0.420
F fines	100	-	0.009	-	-	NP	-	-

Note that all fines were found to be non-plastic (NP). D_{10} for the fines is not shown as this was not used in the interpretation of the test data, and was considered difficult to accurately define given the slope of the fines PSD at 10% passing.

The maximum void ratios e_{max} were determined following the British Standard. The minimum void ratios e_{min} were determined using a variation of the British Standard procedure. The primary variation was that the soils were compacted under dry conditions on a shake table, rather than saturated under water. The reason for this was to retain as much fines mass as possible, which was considered more likely in dry conditions. A limited amount of soil was recovered from the Christchurch site investigations, hence the need to limit the loss of fines.

3.4. Test Procedures

Undrained monotonic and cyclic triaxial tests were conducted on reconstituted specimens created from the FBM, PSM1, and PSM2 sandy soils. Details of the triaxial test

apparatus, sample preparation, testing procedures, and calculations used for data interpretation are described in the following sections.

3.4.1. Triaxial Test Apparatus

All triaxial testing was carried out in a temperature-controlled research room (20°C). The advanced stress-path GDS triaxial apparatus consisted of a Motorised Triaxial Cell with control box, two Advanced Digital Controllers for cell and back pressures, and an 8 Channel Serial Data Acquisition Pad. The cell and controllers were interfaced with a PC via a Measurement Computing PCI-GPIB card connection using IEEE488.2 communication. GDSLab v2 software was installed on the PC to allow testing control. The apparatus hardware is displayed in Figure 3-23.

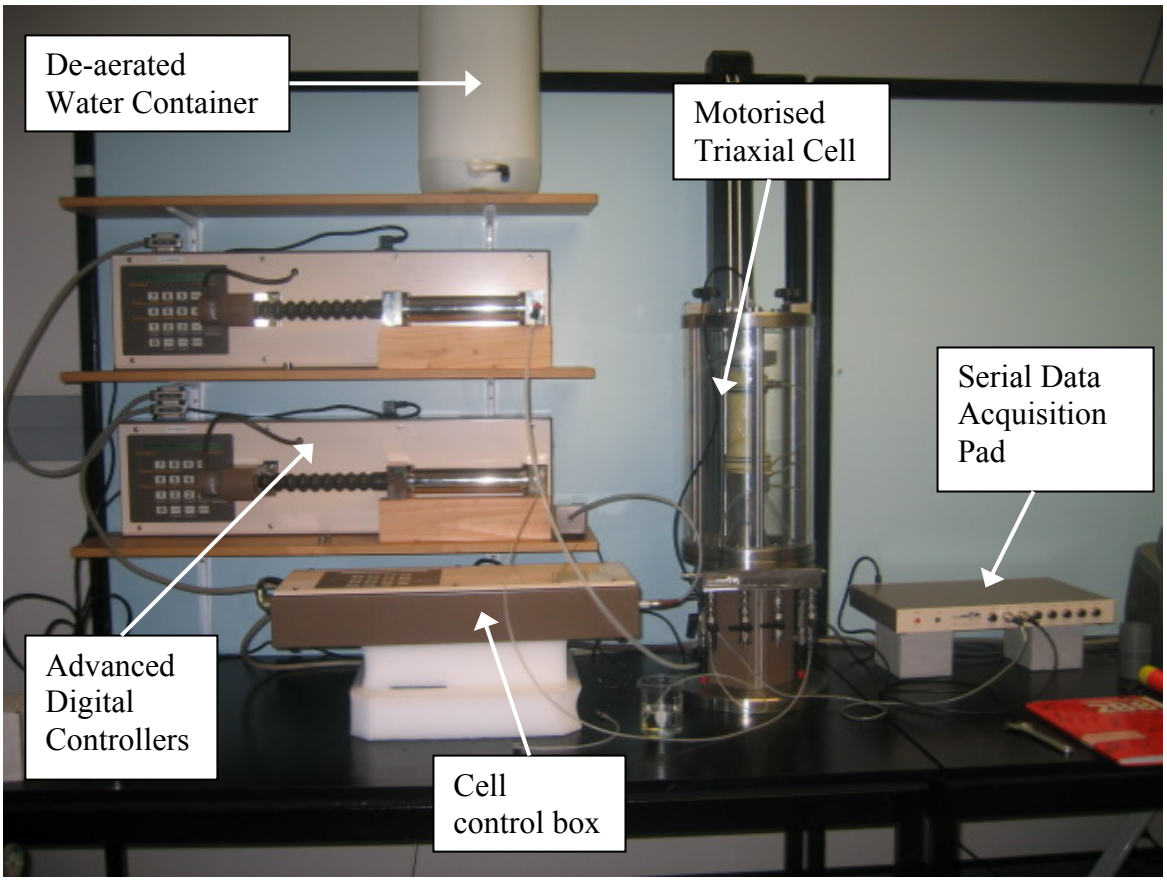

Figure 3-23 Triaxial apparatus setup in the temperature-controlled research room.

The **Motorised Triaxial Cell** was capable of testing specimens up to 50mm in diameter at a maximum cell pressure of 1700kPa and maximum axial load of 7kN (GDS Instruments Ltd, 2002b). The load cell used with the apparatus during this study had a maximum working

load of 2kN. Axial force was applied to the test specimens through a direct screw drive at the specimen pedestal base. Axial force was measured by a submersible load cell at the top of the triaxial cell. Axial displacements were measured from the stepper motor rotation controlling the screw drive, and an independent displacement transducer directly measuring ram movement.

The **Advanced Digital Controllers** were used to apply cell and back / pore water pressures to the test specimens, as well as record pressure and volume change. The controllers stored a quantity of de-aerated water in a pressure cylinder, which was pressurised by application of a moving piston (GDS Instruments Ltd, 2000). The maximum volume of de-aerated water the cylinders held was approximately 200000mm^3 (200mL). Pressure was recorded through an integrated solid state pressure transducer, and volume change measured in steps of the stepper motor that activated the piston.

The **Channel Serial Data Acquisition Pad** was used to collect data from the independent displacement transducer directly measuring axial ram movement, and an independent pore water pressure transducer directly measuring internal specimen pressures (pore water pressures). Data from the pad was transferred to the PC via RS232 serial communication, connecting into a PC Comm port (GDS Instruments Ltd, 2002a).

The **GDSLab v2** software allowed control of the triaxial cell and pressure controllers, as well as the acquisition of data from these sources (GDS Instruments Ltd, 2005). It was primarily used for data acquisition during the specimen setup and saturation phases of testing during this study. During consolidation and loading it was used for both apparatus control and data acquisition. It also enabled real-time monitoring of all data (including data from the serial data acquisition pad) during the loading stage, in both tabular and graphical formats.

3.4.2. Triaxial Test Measurements

The following lists and describes the various measurements made throughout specimen loading.

Axial Load, *F* was recorded by the submersible load cell within the triaxial cell. The specimen top-cap was directly attached to this load cell. The maximum load that was applied to the specimens during testing was 2kN.

Axial Displacement, *Δh* was recorded using the stepper motor rotation driving the axial displacement, and the independent displacement transducer measuring axial ram movement. It was this secondary transducer data that was used for all specimen test calculations. Also note

that no transducers were directly placed onto the specimens, hence only global axial displacement was recorded between the base pedestal and top-cap. This was considered acceptable as the primary interests of the research did not require local or small strain measurements.

Cell Pressure, σ_3 was recorded by the integrated solid state pressure transducer within the Advanced Digital Controller. No other measurements of cell pressure were required.

Back / Pore Water Pressure, u was recorded using the integrated solid state pressure transducer within the Advanced Digital Controller, and a secondary independent pore water pressure transducer measuring pore water pressure at the top-cap end of the specimen. All specimen test calculations were made using the data from the secondary transducer.

Volume Change, ΔV was recorded in terms of mm^3 within each of the Advanced Digital Controllers by measuring the stepper motor steps that activated the piston in the pressure cylinder. This measurement enabled the specimen volume change to be defined during the consolidation phase of the test preparation. As all loadings were conducted under undrained conditions, no volume change occurred during specimen loading.

3.4.3. Specimen Mould Setup

Enlarged end platens were used throughout testing to promote uniform radial specimen deformation and reduce specimen barreling at large strains (Tatsuoka and Haibara, 1985). Thus, the first step in mould preparation was to apply a thin layer of silicon grease to the surfaces of the removable steel pedestal and plastic top-cap. These were both 60mm diameter, with 10mm diameter porous stones at each center. Two layers of greased membrane segments, extending to 50mm diameter and cutaway to fit around the porous stones, were placed on each surface. The pedestal and top-cap with the greased membranes in place are displayed in Figure 3-24. Each layer of these lubricated end membrane segments was approximately 0.25mm thick, reducing the nominal specimen height between the pedestal and top-cap by 1.0mm, from 100mm → 99mm.

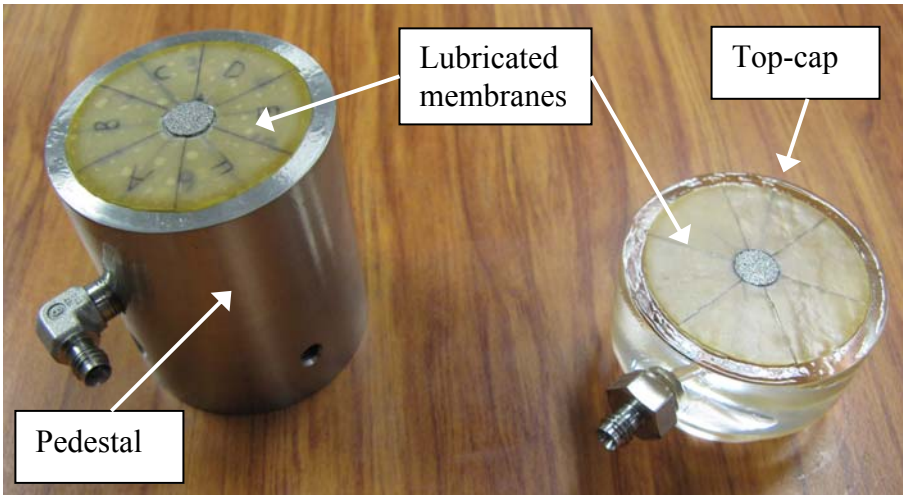

Figure 3-24 Pedestal and top-cap with lubricated end membranes in place.

Thin layers of silicon grease were placed around the sides of the pedestal and top-cap. This was done to prevent cell water from leaking into the specimen between the membrane and pedestal / top-cap sides. Following this, the membrane was placed around the outside of the pedestal. It extended 30mm below the edge of the pedestal surface, secured in place with two rubber O-rings and a thin strip of unused membrane to increase the water tightness of the specimen. The membrane is shown secured to the pedestal in Figure 3-25 (a).

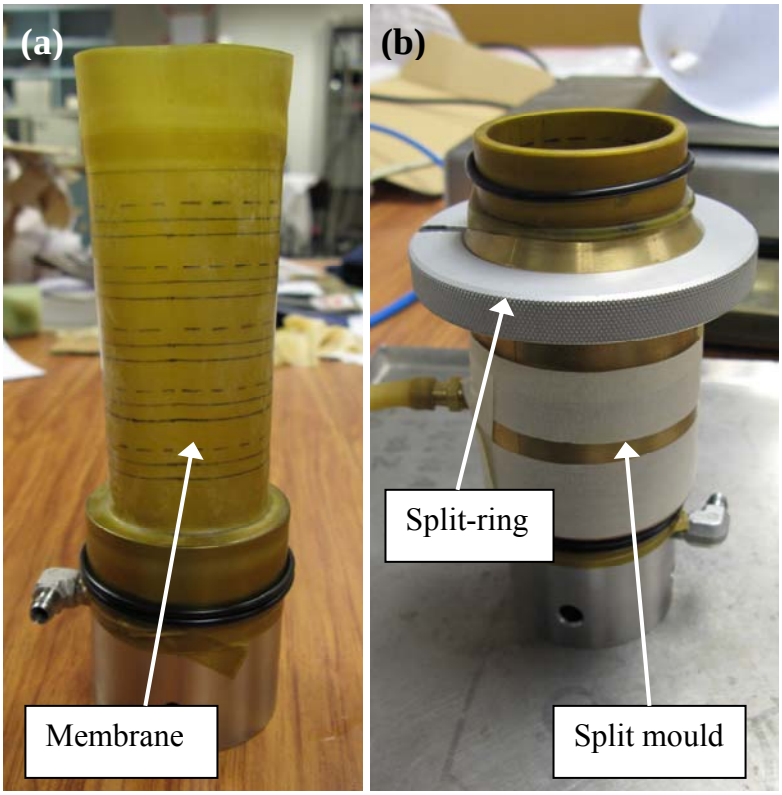

Figure 3-25 (a) Membrane secured to the pedestal, and (b) mould secured around the pedestal.

A metal split mould was placed around the pedestal, with an internal diameter approximately 50.5mm. The mould flared out around the base, allowing it to sit on the 60mm diameter pedestal surface. This meant that the membrane was held between the mould and pedestal around the pedestal surface and edge. The mould was secured in place with a metal split-ring, and two pieces of tape wrapped around the mould below the split-ring. A small amount of vacuum was applied to the internal mould space through a valve, holding the membrane against the mould wall during material deposition. This ensured a uniform specimen diameter with minimal inconsistencies along the surface. The membrane was folded down over the mould top and held in place with a single O-ring. The final stage of mould preparation is displayed in Figure 3-25 (b), with a schematic diagram shown in Figure 3-26.

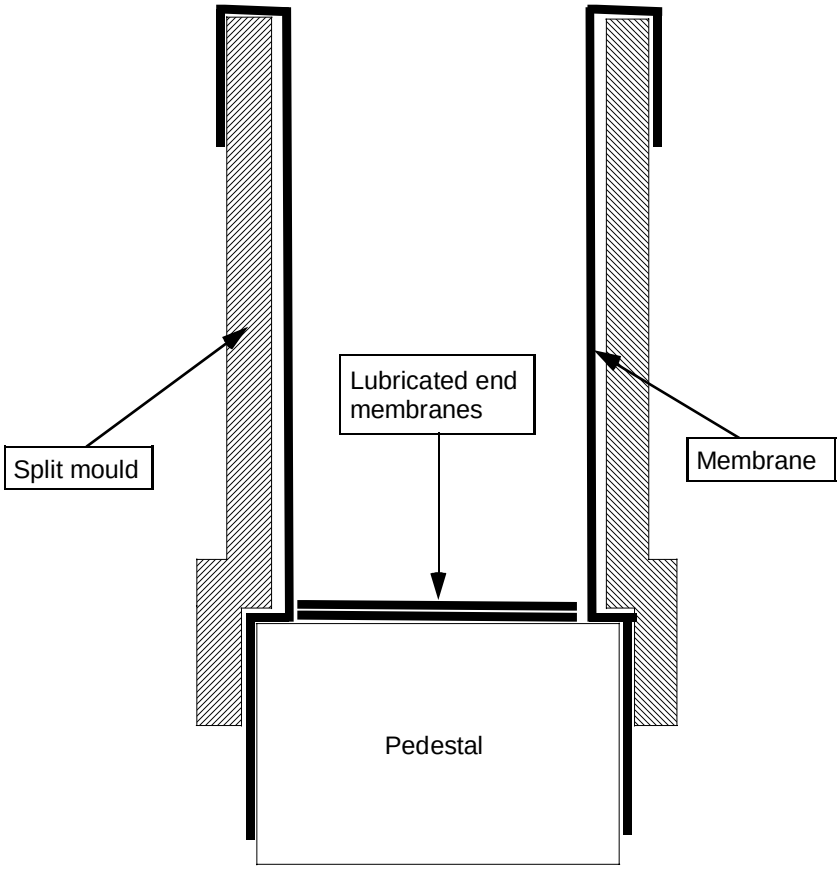

Figure 3-26 Schematic of mould setup before soil deposition.

3.4.4. Soil Preparation

Moist tamping was used to prepare all specimens during testing. The main advantage of moist tamping is the ability to create very loose specimens with high void ratios which allow the steady state line (SSL) to be identified at low confining stresses for sandy materials

(Zlatovic, 1994; Murthy et al., 2007). It also avoids segregation between the sand and fines particles (Ladd, 1978), and was found to give good control over the global specimen density.

The tested sandy soils required some initial preparation before depositing into the specimen mould setup. As all specimens were prepared using moist tamping, a small amount of water was required to be added to the test soil. This addition was carried out by firstly placing a measured quantity of soil in a plastic container with lid. A measured amount of de-aerated water was then mixed with the soil using a glass rod to bring the soil moisture content to approximately 9%. The lid was placed over the container and sealed within an airtight plastic bag. This was left for one hour before the soil deposition phase began. The time of one hour was chosen to provide a balance between allowing the moisture to penetrate the soil, and continuing with specimen setup.

3.4.5. Soil Deposition

The moist soil prepared for deposition was placed into the mould in six separate layers of equal mass. The layer mass was determined from the specimen target void ratio. Each layer was tamped with a plastic tamping cylinder 25mm in diameter, 203mm high and with a weight of 145g, shown in Figure 3-28 (a). 12 – 15 tamps were applied in a circular motion around the inside of the mould to the soil layer. These 12 – 15 tamps were repeated four times to complete a 'tamping cycle', each time starting from a different point around the mould and with alternating directions. Figure 3-27 shows a top-view schematic of the tamping cycle.

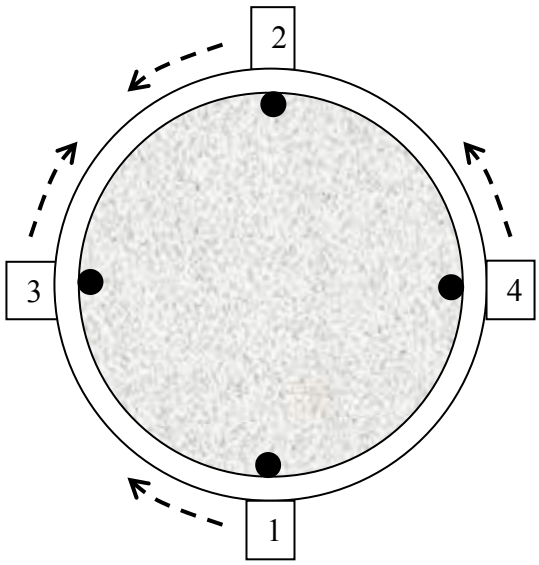

Figure 3-27 Tamping cycle schematic for each layer of soil deposition. The numbered points show the starting locations for each set of 12 – 15 tamps.

After each tamping cycle was completed, the depth of soil was checked relative to the top of the mould using a depth-marked stick. The stick was used to indicate how close the soil was to reaching the target depth, and therefore density, for the layer. Each layer was targeted to be of equal thickness, as each layer contained an equal mass of moist soil. Tamping cycles were repeated until the target depth was reached.

The surface of the deposited layer was lightly scored using a small screwdriver. A cross-hatch pattern with scores approximately 5mm apart and 1 – 2mm depth was applied. The scoring was an attempt to promote a better interface between the deposited layer and the base of the next layer. The top soil layer was gently tamped down so it was flush with the top of split mould, carefully avoiding any membrane punctures. The final top layer surface is shown in Figure 3-28 (b). Note that no scoring was applied to the top soil surface of the specimen.

No specific tests were performed on the moist tamped specimens to check their uniformity. Visual inspection of the specimens suggested looser soil deposition in between the deposited layers. This suggests the layer-surface scoring did not create a fully seamless transition in fabric from one layer to the next. However the bulk of the soil layers did appear to be reasonably uniform based on inspection during deposition, and following specimen saturation. Segregation of the sand and fines particles was also observed to be insignificant.

A wide range of specimen densities were achieved using the described moist tamping depositional method. Clean sand specimens had relative densities ranging from D_r = 0 – 60%, whilst silty sand specimens achieved relative densities from D_r = 20 – 80%. In general the actual specimen relative density following consolidation tended to be 0 – 5% lower than the targeted density. This density difference was reasonably consistent, allowing specimen densities to be targeted accurately. This enabled desired initial specimen states to be achieved, which in turn produced desired specimen response during loading, increasing the efficiency of the triaxial testing program.

Note that the undercompaction moist tamping method (Ladd, 1978) was not used for specimen preparation in this research. It was attempted during a phase of triaxial tests leading up to the main triaxial testing program, but was not used as it tended to produce specimens with more visual inconsistencies, and hence of poorer quality. This appeared to be due to a required smaller size of tamping rod when using the undercompaction method.

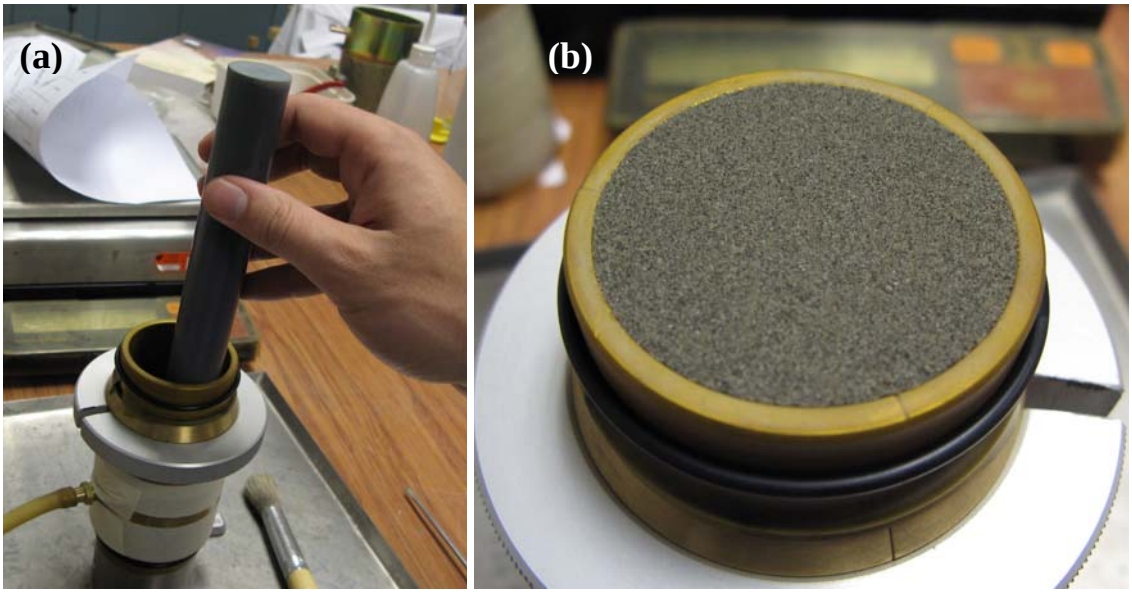

Figure 3-28 (a) Soil tamping using the plastic tamping rod, and (b) top soil layer flush with the top of the mould.

3.4.6. Specimen Docking in Triaxial Cell

The specimen was placed in the triaxial cell and secured to the loading ram at the cell base by locking the pedestal in place. This process did not introduce any additional stresses or deformations to the specimen. Two O-rings had been placed around the outside of the mould previous to this, allowing attachment of the membrane to the top-cap. With the specimen secured, the top-cap was connected to the submersible load cell at the top of the triaxial cell using a plastic sleeve. The split-ring was removed from around the specimen mould, and the specimen was raised up into contact with the top-cap. This was done slowly and in such a way that the lubricated end membranes on the surface of the top-cap slightly pushed on the specimen surface, obtaining full contact with the test material. The specimen is shown docking with the top-cap in Figure 3-29 (a).

Once docked, the membrane around the outside of the mould was rolled up over the top-cap and secured in place by the two O-rings sitting on the mould. An axial load of 0.0kN was then targeted on the Triaxial Cell controller box to ensure no axial loads were applied to the specimen before test loading. A vacuum of 20kPa was applied to the specimen, allowing the split mould to be removed. The diameter was carefully measured at five regular intervals up the specimen with vernier calipers, enabling an average specimen diameter (and initial area) to be determined. The triaxial cell was then assembled and secured, ready for filling with de-aerated water. The specimen is shown before the triaxial cell was assembled in Figure 3-29 (b).

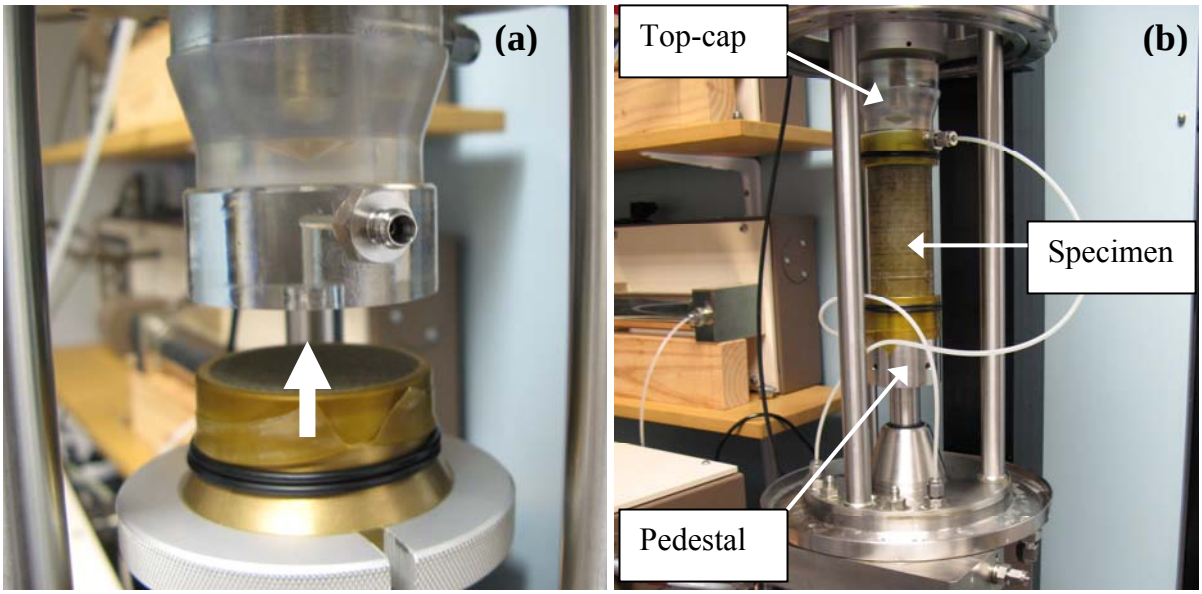

Figure 3-29 (a) Specimen docking with top-cap, and (b) specimen secured in triaxial cell before assembling the cell.

3.4.7. Water De-aeration

A Nold DeAerator Model 2100 from Geokon, Inc. was used for all water de-aeration during the laboratory testing program. A running time of around five minutes was suggested for most soils laboratory applications (Geokon, 2002), however the device was generally run for 10 minutes, as there were periods of waiting between de-aeration and triaxial cell filling – the triaxial cell required two batches of de-aerated water. All de-aerated water for the triaxial cell was transferred using a plastic airtight container with a tap at the base. All de-aerated water used to fill the digital controllers was transferred in open glass beakers.

3.4.8. CO_2 Percolation and Water Saturation

Once the triaxial cell had been filled with water and sealed, a cell pressure of 10 - 12kPa was applied to confine the specimen before removing the vacuum. This pressure was raised to 30kPa after the vacuum had been removed. Recording of axial deformations was begun before the initial application of cell pressure.

CO_2 was percolated up through the specimen using a pressure of approximately 2 – 3kPa. This expelled 3 - 4 CO_2 bubbles per second into a beaker of de-aerated water. The percolation was continued for a period of 30 minutes for low fines content soils, or up to two hours for the FBM-30 soil. The CO_2 percolation pushed out air trapped within the specimen

voids and replaced it with CO_2, which is more soluble in water. This helped to promote full specimen saturation during the water saturation phase.

Specimen saturation was carried out using the ramp function of the back pressure Advanced Digital Controller. This function pushed a specified amount of de-aerated water within the pressure cylinder into the specimen at a specified constant rate. The rate was varied depending on the specimen properties, specifically the fines content. Lower rates were used as the fines content increased, ensuring no fines washout during saturation. Rates varied from percolating 400mL of water in 14 hours (28.6mL / hr for clean sand specimens) to 400mL of water in 28 hours (14.3mL / hr for FBM-30 specimens). These were successful percolation rates for the tested soils, as no significant washout of fines was observed and Skempton's B-values were greater than 0.95. The specimen setup following saturation is schematically presented in Figure 3-30.

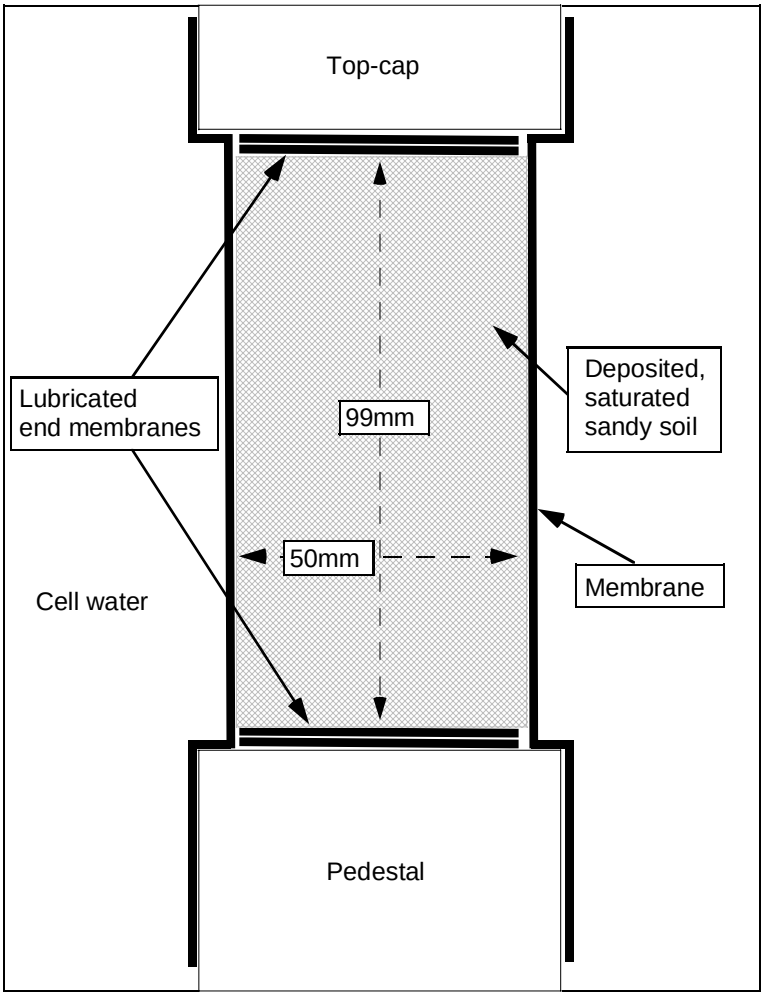

Figure 3-30 Schematic of specimen following saturation phase.

3.4.9. Consolidation

Specimen consolidation was performed following the saturation phase. Pressure ramps were used to incrementally bring the cell and back pressures to 200kPa and 100kPa respectively over the course of one hour, reaching a mean effective stress p' = 100kPa. A deviator stress of 0.0kPa was continuously targeted throughout the pressure ramps, enabling isotropic consolidation. All triaxial tests were performed at an initial stress of p' = 100kPa, except for a single undrained monotonic test on the FBM-10 soil where p' = 200kPa.

Specimens were left to consolidate under the final confining stress for a varying amount of time, dependent on the specimen material and density. Consolidation was considered complete when a volume change of less than 5mm^3 was observed over a period of 30 minutes. Saturation checks were then performed, calculating Skempton's B-value greater than 0.95. The typical pressures applied during the consolidation phase are displayed in Figure 3-31.

The final stage of preparation was to target a deviator stress q = 1kPa. This was an attempt to eliminate bedding issues between the specimen surface and top-cap. This did not cause any significant additional stresses or deformations to be applied to the specimen. It also appeared to be successful in eliminating potential bedding issues, as a positive change in load was simultaneously observed as initial strains were applied.

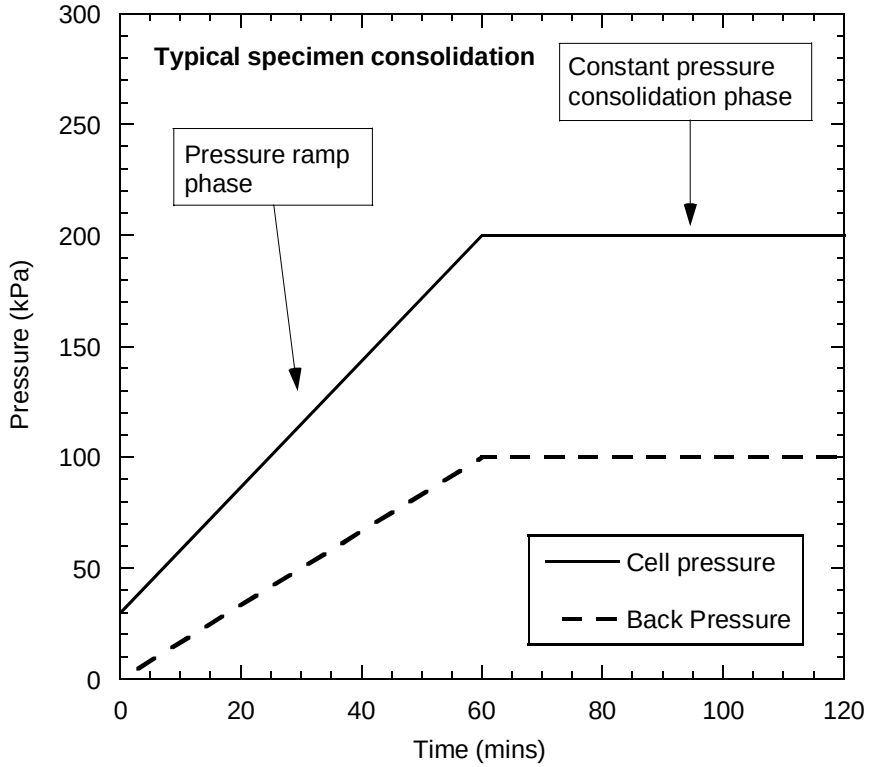

Figure 3-31 Typical cell and back pressures during specimen consolidation.

3.4.10. Undrained Monotonic Loading

Undrained monotonic loading was applied to the specimens using axial compression. All tests were strain-controlled, loading at a rate of 0.3mm / min, as is shown in Figure 3-32. This rate was chosen as it is commonly used in the laboratory during monotonic triaxial testing and has been shown to produce high quality data, as evidenced by Verdugo (1992) and Zlatovic (1994). The target strain of the specimens was 40% axial strain, as the primary interest of the undrained monotonic tests was to observe the steady state of deformation. Some specimens did not reach this strain level due to a number of factors. These include the maximum apparatus axial load being reached before steady state, irregular specimen deformations rendering the data unreliable, or the specimens undergoing complete flow liquefaction and reaching zero residual strength.

3.4.11. Undrained Cyclic Loading

Undrained cyclic loading was applied to the specimens in a stress-controlled manner at a loading rate of 2min / cycle, as shown in Figure 3-33. This loading rate was chosen based on the rate at which the triaxial apparatus could log data, with approximately 60 data points being obtained per cycle. The target cyclic stress ratio (*CSR*) was determined with the goal of obtaining the liquefaction strength curve for a given specimen density in 3 – 4 tests. The number of cycles required to achieve liquefaction (N_C) or 5% double amplitude axial strain was recorded. This is herein referred to as cyclic liquefaction. Initial liquefaction was also observed during loading, occurring when the excess pore pressures caused the mean effective stress to reduce to p' = 0kPa.

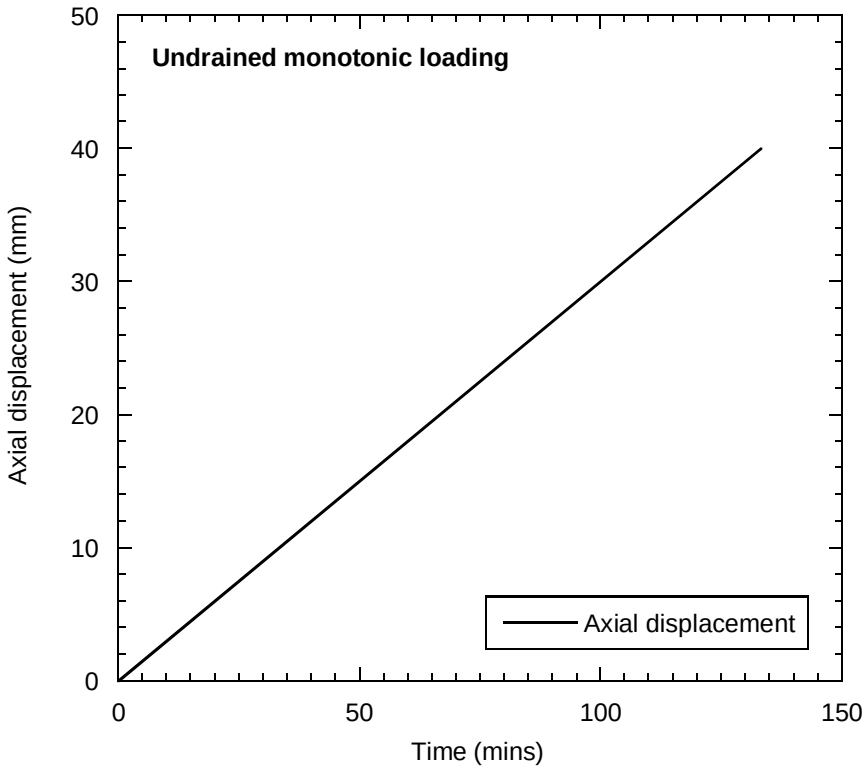

Figure 3-32 Strain-controlled undrained monotonic loading.

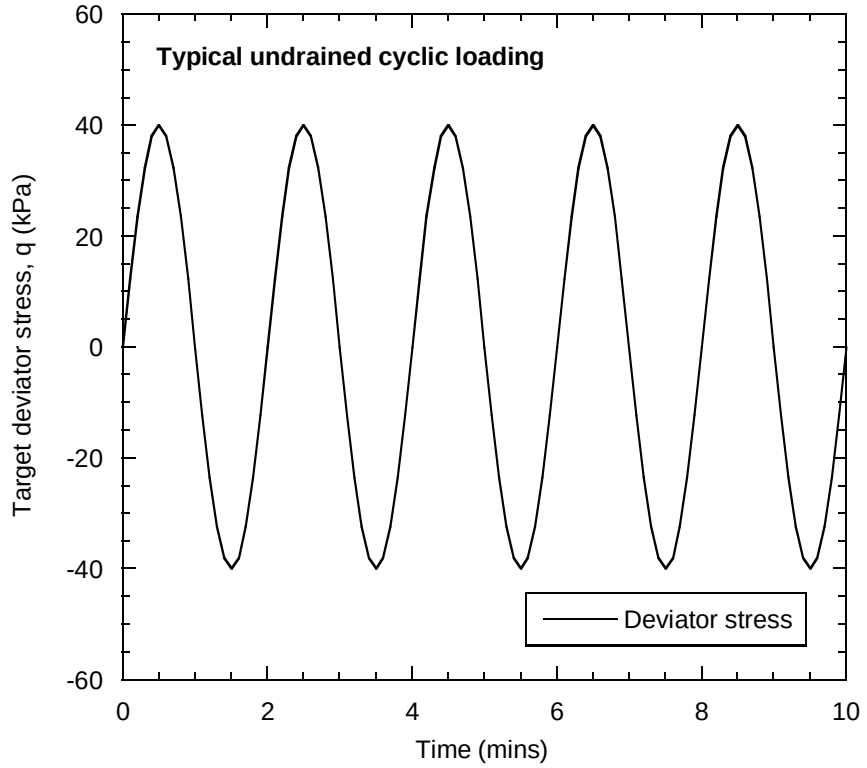

Figure 3-33 Typical stress-controlled undrained cyclic loading showing five cycles with a target cyclic stress ratio of $CSR = 0.2$.

3.4.12. Post-test Void Ratio Determination

A procedure was developed to determine the void ratio of the tested specimens after the loading had been completed. The procedure was similar to that described by Verdugo (1992). It was considered to produce void ratio values of higher accuracy than if using pre-test mass, height and diameter measurements of the specimen. The increased accuracy is due to the simplicity of only weighing materials, rather than also measuring dimensions.

The masses of the pedestal, top-cap, membrane etc were all recorded in the setup stages of testing. Following the completion of loading, the valve leading from the specimen to the back pressure controller was closed. This was done to ensure no water moved in or out of the specimen, retaining the same volume as during testing. Cell water was removed from the triaxial cell, and the cell was disassembled. This enabled the outside of the specimen membrane to be fully dried using paper towels. These soaked up any excess cell water sitting on the specimen, including around the top-cap, membrane, O-rings and pedestal. The drying process is shown in Figure 3-34 (a).

The specimen was then removed and placed in a steel bowl whilst the internal tubing was attached. After checking that the specimen membrane was fully dried, the internal tubes were removed, making sure no excess water from the tubing dropped in the bowl. This left the specimen, including pedestal, O-rings, membrane, thin membrane strip, top-cap, tested soil and specimen water in the steel bowl. The bowl was weighed at this point.

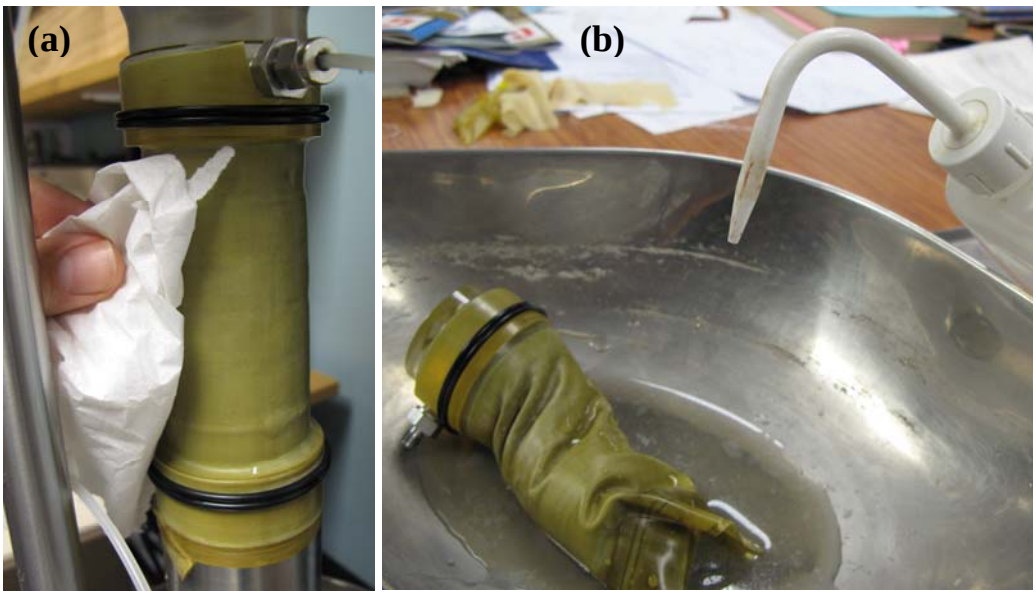

Figure 3-34 (a) Specimen being dried after testing, and (b) soil being rinsed into the steel bowl using a water bottle.

The next step was to carefully dismantle the specimen whilst it was still in the steel bowl. This involved using a water bottle to rinse all the tested soil into the bowl, shown in Figure 3-34 (b). The primary concern was to ensure that all the tested soil was retained, and to not leave significant amounts stuck to the membrane, top-cap etc.

The tested soil within the steel bowl was placed in an oven at 104°C to dry for at least 24 hours. Following this the bowl was weighed, allowing the mass of dry tested soil to be determined, and enabling a void ratio to be calculated based on the mass of dry tested soil (m_s) and water (m_w) in the specimen. All reported specimen void ratios for this research were derived using this method.

3.4.13. Potential Sources of Error

There are potentially a number of sources of error when testing sandy soils in a triaxial apparatus. These are addressed with respect to the tests carried out during this study.

Membrane Penetration – all tested soils were classified as fine sand (the maximum D_{50} = 0.208mm for PSM1-0). Due to this classification, the potential error in void ratio arising from membrane penetration effects was considered to be insignificant (Sladen and Handford, 1987).

Bedding Error – a procedure used to mitigate bedding errors between the specimen surface and top-cap is described in Section 3.4.9. Such errors are generally only important to the small-strain deformation of a specimen (Verdugo, 1992), which was not of interest for this study. Hence no further adjustments were made.

Void Ratio Calculation – a procedure used to determine the specimen void ratio post-test using the dry tested material mass (m_s) and water mass (m_w) is described in Section 3.4.12. This was considered to provide more accurate void ratio values than using pre-test specimen mass and dimensions. Specimen dimensions were considered to be less accurate as they changed throughout saturation and consolidation, even though axial deformations were recorded during these stages, and some soil moisture may have evaporated during deposition, increasing the error in the measured pre-test sand mass.

Specimen barreling – as discussed in Section 3.4.3, lubricated end membrane segments were placed on the enlarged end platens to promote uniform radial deformation and reduce specimen barreling. This was not entirely successful, as specimen barreling did occur, noticeably at larger axial strains. Such deformations are discussed further in Chapter 4.

As barreling could not be prevented, specimen response at high levels of axial strain was critically reviewed during data analysis. This involved discarding data that was recorded beyond acceptable levels of radial deformation.

3.4.14. Equations used for Test Data Interpretation

Test data from the undrained monotonic and cyclic tests was interpreted using a number of standard definitions and corrections. These are detailed in Equations (3-1) to (3-7):

Void Ratio, *e* - where V_v = volume of voids, V_s = volume of solid particles, m_w = mass of water, m_s = mass of solid particles, ρ_w = mass density of water, ρ_s = mass density of solid particles:

$$e = \frac{V_v}{V_s} = \frac{m_w}{\rho_w}\frac{\rho_s}{m_s} \tag{3-1}$$

Specimen Volume, *V* – assuming full specimen saturation:

$$V = V_s + V_v = \frac{m_s}{\rho_s} + \frac{m_v}{\rho_v} \tag{3-2}$$

Axial Strain, ε_a – where h_i = initial specimen height, Δh = axial displacement:

$$\varepsilon_a = \frac{\Delta h}{h_i} \qquad (+\Delta h = \text{compression}) \tag{3-3}$$

Adjusted Specimen Area, A_e – corrects for changes in the average specimen area as deformation is increased:

$$A_e = \frac{V}{h_i(1-\varepsilon_a)} \tag{3-4}$$

Deviator Stress, *q* – where F = applied axial load:

$$q = \frac{F}{A_e} \tag{3-5}$$

Mean Effective Stress, *p'* – where σ_3 = cell pressure, u = pore pressure:

$$p' = \frac{1}{3}(q + 3\sigma_3) - u \tag{3-6}$$

Cyclic stress ratio, *CSR*: – where σ'_{3i} = initial effective confining pressure

$$CSR = \frac{q}{2\sigma'_{3i}} \tag{3-7}$$

3.5. Test Information

Table 3-2 and Table 3-3 present the test information for the undrained monotonic and cyclic tests performed on the FBM, PSM1 and PSM2 sandy soils. Note that the density measures (e and D_r) corresponds to post-consolidation values, q_{ss} = deviator stress at steady state, p_{ss} = mean effective stress at steady state, N_C = number of load cycles required to reach cyclic liquefaction (5% double amplitude axial strain), SS = steady state, and IL = initial liquefaction.

Table 3-2 Undrained monotonic test information.

Test No.	Soil	e	D_r (%)	q_{ss} (kPa)	p'_{ss} (kPa)	Remark
M1	FBM-1	0.835	26	-	-	SS not reached
M2	FBM-1	0.882	9	238	198	
M3	FBM-1	0.888	7	172	141	
M4	FBM-1	0.863	16	-	-	SS not reached
M5	FBM-1	0.892	5	58	46	
M6	FBM-1	0.872	13	263	198	
M7	FBM-1	0.821	31	-	-	SS not reached
M8	FBM-1	0.873	12	262	209	
M9	FBM-1	0.907	0	2	2	
M10	FBM-10	0.821	36	85	65	
M11	FBM-10	0.854	26	18	14	
M12	FBM-10	0.863	24	7	6	
M13	FBM-10	0.828	34	48	37	
M14	FBM-10	0.847	28	32	25	
M15	FBM-10	0.806	40	189	155	
M16	FBM-10	0.814	38	180	142	
M17	FBM-10	0.780	47	244	200	
M18	FBM-10	0.744	58	-	-	SS not reached
M19	FBM-10	0.725	63	-	-	SS not reached
M20	FBM-10	0.829	33	77	65	p'_i = 200kPa
M21	FBM-10	0.691	73	-	-	SS not reached
M22	FBM-20	0.722	45	5	4	
M23	FBM-20	0.698	51	21	15	
M24	FBM-20	0.652	63	323*	230*	*SS at ε_a = 10%
M25	FBM-20	0.677	57	98*	69*	*SS at ε_a = 8%
M26	FBM-30	0.693	50	5	1	
M27	FBM-30	0.662	60	15	7	
M28	FBM-30	0.659	60	11	5	
M29	FBM-30	0.643	65	106*	71*	*SS at ε_a = 14%
M30	FBM-30	0.637	67	142*	93*	*SS at ε_a = 12%
M31	FBM-30	0.628	70	101	72	
M32	FBM-30	0.626	70	332*	240*	*SS at ε_a = 10%
M33	PSM1-0	0.885	15	230	185	

Test No.	Soil	e	D_r (%)	q_{ss} (kPa)	p'_{ss} (kPa)	Remark
M34	PSM1-0	0.933	-2	6	3	
M35	PSM1-0	0.911	6	36	26	
M36	PSM1-10	0.804	16	87	64	
M37	PSM1-10	0.796	18	125	92	
M38	PSM1-20	0.709	32	61	40	
M39	PSM1-20	0.694	36	82	66	
M40	PSM2-0	0.913	9	12	7	
M41	PSM2-0	0.886	18	216	163	
M42	PSM2-0	0.909	11	31	23	
M43	PSM2-10	0.774	30	98	73	
M44	PSM2-10	0.765	32	225	162	
M45	PSM2-25	0.587	68	126	87	
M46	PSM2-25	0.581	69	161	103	

Table 3-3 Undrained cyclic test information.

Test No.	Soil	e	D_r (%)	CSR	N_C	Remark
C1	FBM-1	0.892	5	0.270	1	
C2	FBM-1	0.890	6	0.209	2	
C3	FBM-1	0.889	7	0.170	4	IL = 5 cycles
C4	FBM-1	0.879	10	0.140	16	
C5	FBM-1	0.890	6	0.120	32	
C6	FBM-1	0.821	31	0.370	2	
C7	FBM-1	0.828	28	0.228	4	
C8	FBM-1	0.820	31	0.194	14	
C9	FBM-1	0.821	31	0.160	43	
C10	FBM-1	0.734	62	0.566	3	IL = 4 cycles
C11	FBM-1	0.740	60	0.475	5	
C12	FBM-1	0.735	62	0.334	6	IL = 7 cycles
C13	FBM-1	0.740	60	0.243	21	
C14	FBM-1	0.743	59	0.206	126	
C15	FBM-10	0.804	41	0.259	1.5	IL = 2 cycles
C16	FBM-10	0.818	36	0.225	2	IL = 3 cycles
C17	FBM-10	0.815	37	0.192	4	IL = 5 cycles
C18	FBM-10	0.805	40	0.150	16	
C19	FBM-10	0.823	35	0.121	39	IL = 40 cycles
C20	FBM-10	0.796	43	0.313	1.5	IL = 2 cycles
C21	FBM-10	0.791	44	0.257	2	IL = 3 cycles
C22	FBM-10	0.786	46	0.233	4	
C23	FBM-10	0.788	45	0.196	8	IL = 9 cycles
C24	FBM-10	0.785	46	0.151	29	
C25	FBM-10	0.746	57	0.436	2	IL = 2.5 cycles
C26	FBM-10	0.740	59	0.316	3	
C27	FBM-10	0.744	58	0.279	5	
C28	FBM-10	0.747	57	0.239	9	
C29	FBM-10	0.740	59	0.200	22	

Test No.	Soil	e	D_r (%)	CSR	N_C	Remark
C30	FBM-10	0.736	60	0.175	39	
C31	FBM-10	0.716	66	0.555	3	
C32	FBM-10	0.711	67	0.349	5	IL = 4 cycles
C33	FBM-10	0.710	68	0.284	8	
C34	FBM-10	0.711	67	0.218	21	
C35	FBM-10	0.707	68	0.180	75	
C36	FBM-20	0.668	59	0.357	2	IL = 3 cycles
C37	FBM-20	0.667	59	0.237	6	
C38	FBM-20	0.668	59	0.198	15	IL = 14 cycles
C39	FBM-20	0.670	59	0.159	40	IL = 39 cycles
C40	FBM-20	0.606	75	0.429	6	IL = 7 cycles
C41	FBM-20	0.603	76	0.288	14	
C42	FBM-20	0.604	76	0.216	37	IL = 36 cycles
C43	FBM-30	0.708	46	0.181	1.5	IL = 1 cycles
C44	FBM-30	0.702	47	0.148	5	
C45	FBM-30	0.713	44	0.100	20	
C46	FBM-30	0.692	51	0.253	2	
C47	FBM-30	0.693	50	0.195	5	
C48	FBM-30	0.693	50	0.150	14	
C49	FBM-30	0.693	50	0.121	28	IL = 27 cycles
C50	FBM-30	0.634	68	0.403	2	
C51	FBM-30	0.627	70	0.284	5	
C52	FBM-30	0.631	69	0.199	26	IL = 25 cycles
C53	FBM-30	0.626	70	0.176	37	IL = 35 cycles
C54	FBM-30	0.594	80	0.379	5	
C55	FBM-30	0.590	81	0.309	8	
C56	FBM-30	0.593	80	0.239	13	
C57	FBM-30	0.592	81	0.199	34	IL = 33 cycles
C58	PSM1-0	0.913	5	0.150	17	
C59	PSM1-0	0.898	10	0.121	71	
C60	PSM1-0	0.911	6	0.249	1.5	IL = 2 cycles
C61	PSM1-0	0.806	43	0.243	13	
C62	PSM1-0	0.810	41	0.368	4	
C63	PSM1-0	0.807	42	0.200	55	IL = 54 cycles
C64	PSM1-10	0.817	12	0.159	19	IL = 18 cycles
C65	PSM1-10	0.813	14	0.178	13	IL = 12 cycles
C66	PSM1-10	0.780	23	0.198	13	
C67	PSM1-10	0.783	22	0.176	25	
C68	PSM1-20	0.747	23	0.161	12	
C69	PSM1-20	0.734	26	0.141	28	
C70	PSM1-20	0.674	42	0.233	11	
C71	PSM1-20	0.666	44	0.219	16	
C72	PSM2-0	0.898	14	0.150	12	
C73	PSM2-0	0.900	14	0.214	2	
C74	PSM2-0	0.898	14	0.121	51	IL = 50 cycles
C75	PSM2-0	0.816	41	0.243	11	IL = 10 cycles
C76	PSM2-0	0.806	44	0.265	3.5	IL = 4 cycles

Test No.	**Soil**	***e***	**D_r (%)**	***CSR***	**N_C**	**Remark**
C77	PSM2-0	0.814	42	0.191	59	
C78	PSM2-10	0.796	24	0.141	30	
C79	PSM2-10	0.793	25	0.177	9	
C80	PSM2-10	0.715	45	0.246	51	IL = 50 cycles
C81	PSM2-10	0.718	45	0.284	7	IL = 8 cycles
C82	PSM2-25	0.625	61	0.159	75	IL = 74 cycles
C83	PSM2-25	0.622	61	0.239	9	
C84	PSM2-25	0.582	69	0.266	15	
C85	PSM2-25	0.578	70	0.288	12	

4. Undrained Behaviour of the FBM Soils

4.1. Introduction

The FBM sandy soils, as described in Chapter 3, were tested under undrained monotonic and cyclic loading conditions using a triaxial apparatus. The undrained monotonic tests were interpreted within the state concept framework, focusing on the effects of fines on the steady state line (SSL). The undrained cyclic tests were also assessed using a similar framework, evaluating the effects of fines on the liquefaction resistance curve (LRC) and cyclic resistance curve (CRC).

Four different parameters – void ratio, relative density, state parameter and state index – were used as a basis for characterizing the initial state of the sandy soil specimens. They were chosen to show how the effects of fines on the undrained behaviour of sand vary as the characterization parameter is changed. The parameters are detailed in the following:

Void ratio, *e* - where V_v = Volume of voids, V_s = Volume of solid particles:

$$e = \frac{V_v}{V_s} \tag{4-1}$$

Void ratio only characterizes state in terms of a density measurement. Also note that when using *e*, no distinction is made between sand and fines-sized soil particles.

Relative density, D_r – where e_{max} = maximum void ratio, e_{min} = minimum void ratio:

$$D_r = \frac{e_{\max} - e}{e_{\max} - e_{\min}} \times 100 \ (\%) \tag{4-2}$$

Relative density characterizes state in a similar manner to void ratio, except it includes information on the range of 'limiting' soil densities using the maximum and minimum void

ratios. It is also similar to the void ratio definition in that no distinction is made between sand and fines-sized particles.

State parameter, ψ – where e_{ss} = void ratio of the steady state line at the initial mean effective stress (p'_i):

$$\psi = e - e_{ss} \tag{4-3}$$

State parameter is different to void ratio and relative density in that it characterizes state by relating specimen density to a physical state of soil response, which is in this case the steady state of deformation. This means that the state parameter also accounts for the initial mean effective stress p'_i of the specimen when characterizing state. Note however that there is still no explicit distinction between sand and fines-sized particles in the state parameter definition.

State index, I_s – where e_0 = void ratio of the steady state line at zero mean effective stress ($p' = 0$):

$$I_s = \frac{e_0 - e}{e_0 - e_{ss}} \tag{4-4}$$

State index characterizes state in a similar way to the state parameter. It also provides information on states that will result in zero residual stress, or $p' = 0$kPa, under monotonic undrained loading.

This chapter presents the undrained monotonic and cyclic triaxial test data of the FBM sandy soils. Typical soil response observed in these tests is displayed, along with the steady state lines derived from the monotonic testing, and liquefaction resistance curves derived from the cyclic testing. The effects of fines on the steady state of deformation are discussed within the state concept framework using void ratio and relative density as state characterization parameters. The effects of fines on the liquefaction resistance curves and the cyclic resistance are discussed using void ratio, relative density, state parameter and state index as state

characterization parameters. The objective is to point out the differences in apparent effects of fines when using different measures of soil state.

4.1.1. State Concept for Undrained Monotonic Response

The state concept is used as the main framework for interpreting the undrained monotonic triaxial test data of the FBM sandy soils. This concept essentially provides a reference for expected undrained response based on initial state of the soil, in terms of density and initial mean effective stress *p'* relative to the reference state.

Figure 4-1 displays a schematic plot of three types of typical sand response, in terms of effective stress-path, when undergoing undrained monotonic loading. These are strain-softening (flow), strain-softening followed by strain-hardening (limited flow), and strain-hardening only. Flow response coincides with fully contractive behaviour, whilst limited flow coincides with contractive and dilative behaviour.

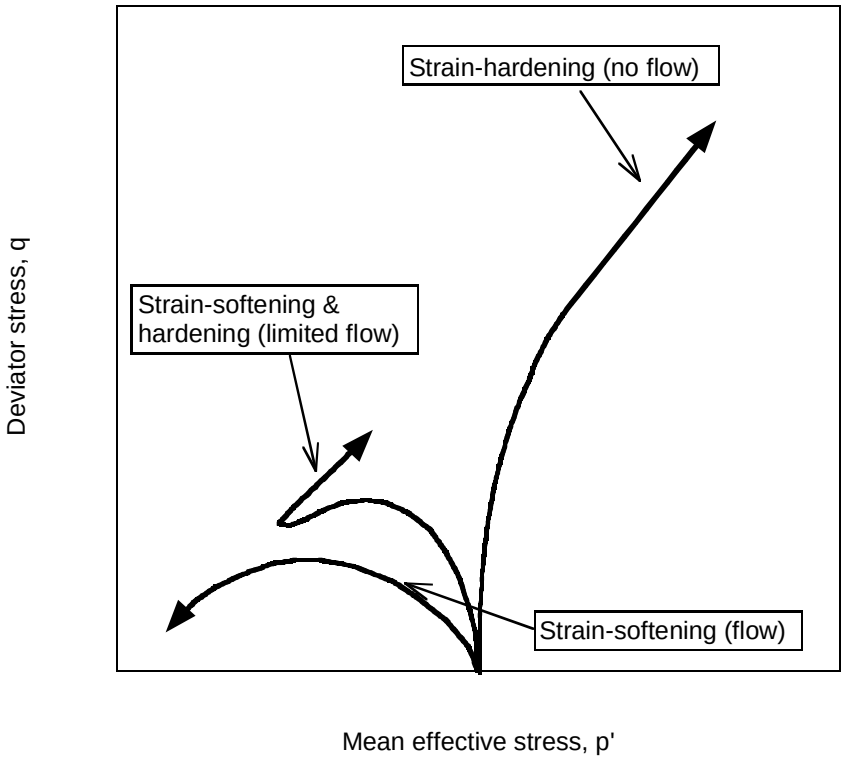

Figure 4-1 Schematic illustration of three types of undrained monotonic response of sand.

The steady state of deformation is considered to be the state at which a specimen will deform under constant shear stress, constant mean effective stress and constant volume (Castro and Poulos, 1977). The steady states for a given sand define a curve in $e - q - p'$

space (the steady state line), and the projection in the $e - p'$ plane is typically used for state characterization, as illustrated in Figure 4-2.

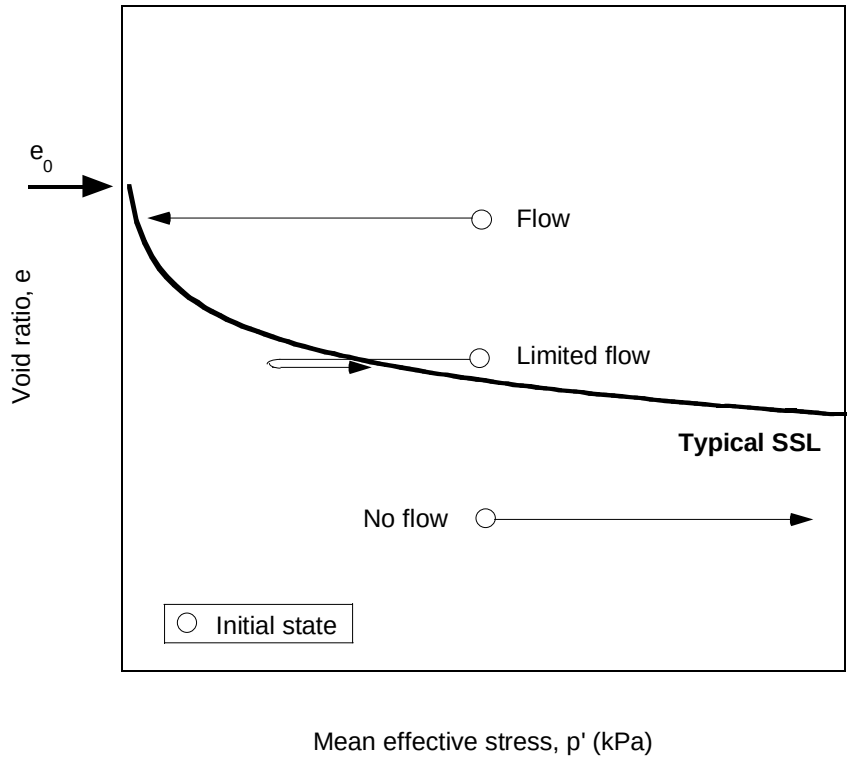

Figure 4-2 Schematic illustration of the state concept used to characterize undrained monotonic response.

Traditionally this line has been viewed as a division between initial states that will exhibit contractive (flow) or dilative (no flow) response (Casagrande, 1976). It has however been stated (Ishihara, 1993) that the true boundry between these states is the initial dividing line (ID-line). The steady state line does however approximate the ID-line reasonably well, and hence the steady state line has been used in the majority of state concept analyses in the literature.

The steady state line is the reference used to characterize the expected soil response during undrained monotonic loading. Specimens with initial states above the steady state line exhibit flow (fully contractive and strain-softening response), whilst specimens with initial states well below the steady state line show dilative and strain-hardening response. Note e_0 is the void ratio of the steady state line at $p' = 0$kPa.

Also note that the steady state is generally assumed to be unique for a given void ratio, regardless of the initial soil fabric (Zlatovic and Ishihara, 1997; Lee et al., 1999; Cubrinovski

and Ishihara, 2000). The experimental data typically shows some scatter but generally it can be reasonably approximated by a line (the steady state line).

4.1.2. Concept for Evaluation of Cyclic Resistance

The state concept as described for the undrained monotonic response in Section 4.1.1 does not apply to the undrained cyclic response. However a similar concept, in terms of an initial state reference being employed to characterize the expected response, can be used to interpret the undrained cyclic test data.

During this study the liquefaction resistance curves (LRC) of the sandy soils have been defined. These liquefaction resistance curves can be compared across different densities by selecting a constant value for the number of load cycles required to reach liquefaction, N_C, and comparing the cyclic stress ratios corresponding to that N_C value, as illustrated schematically in Figure 4-3.

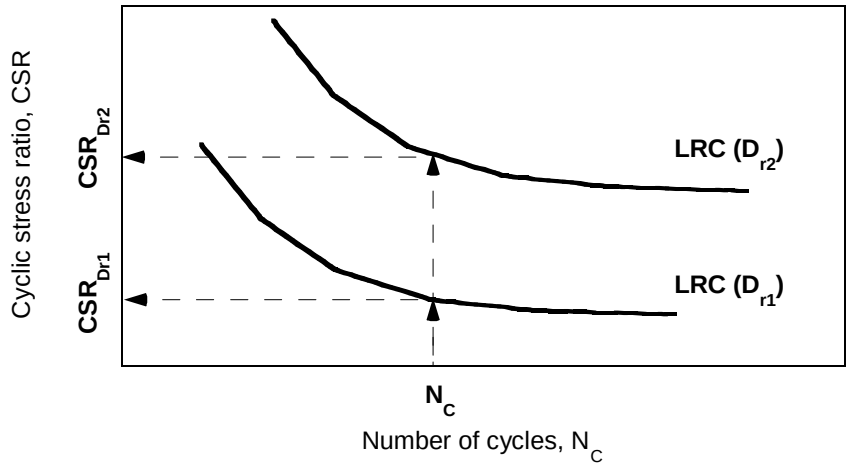

Figure 4-3 Schematic illustration showing typical sand liquefaction resistance curves (LRC) at two different densities (D_{r1} and D_{r2}) for a given sandy soil.

By comparing liquefaction resistance at a constant N_C value, a curve can be defined showing how the cyclic stress ratios corresponding to N_C vary with the density measure for a given soil. This curve is herein termed the cyclic resistance curve (CRC), and is used as the reference to characterize the required number of cycles for causing liquefaction.

Specimens with a density and cyclic stress ratio condition above the cyclic resistance curve will reach liquefaction in fewer cycles than the reference N_C value, corresponding to lower cyclic strength. Specimens with a combination of density and cyclic stress ratio below

the cyclic resistance curve will reach liquefaction after more cycles than the reference N_C value, corresponding to higher cyclic strength. This concept is schematically illustrated in Figure 4-4. Note that both the soil density (state) and cyclic stress ratio (load) are required to apply this concept.

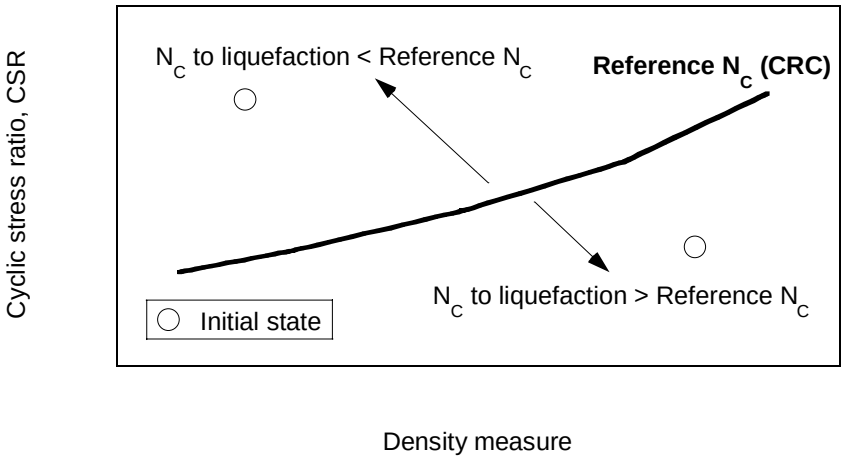

Figure 4-4 Schematic illustration of the cyclic resistance curve (CRC) of a sandy soil.

4.2. Undrained Monotonic Response of the FBM Soils

A series of 32 conventional triaxial compression tests were conducted on the FBM sandy soils to investigate the effects of fines on the undrained monotonic response of sand. The test specimens were prepared using the procedures discussed in Chapter 3, and were compressed during testing at a rate of 0.3mm / min under strain-controlled conditions. All specimens were tested from an initial mean effective stress p'_i = 100kPa, except for one FBM-10 specimen with e = 0.829 that was tested from p'_i = 200kPa. The visually observed deformations of the soils, the effects of density, and the effects of fines content on the monotonic response are discussed in the following sections.

4.2.1. Visually Observed Deformations of the FBM Soils

The response of the FBM soils during monotonic loading was initially observed through the test specimen deformations whilst in the triaxial cell. These deformations gave an indication of (a) the general stress-strain and stress-path soil response, and (b) the performance of the lubricated end membranes attempting to promote uniform radial deformations. There were typically three types of deformations observed during loading: (1)

softening, (2) barreling, and (3) caving. These deformations are presented and discussed in the following:

(1) Specimen softening was visually detected during loading by observing the change in the surface irregularities of the specimen membrane, and the change in specimen shape. The membrane tended to display small, noticeable inconsistencies following the consolidation of a specimen, which tended to reduce if strain-softening took place. This difference in surface irregularity is illustrated by the FBM-1 specimen with e = 0.907 at axial strains of ε_a = 0% and at ε_a = 20% in Figure 4-5 (a) and (b) respectively.

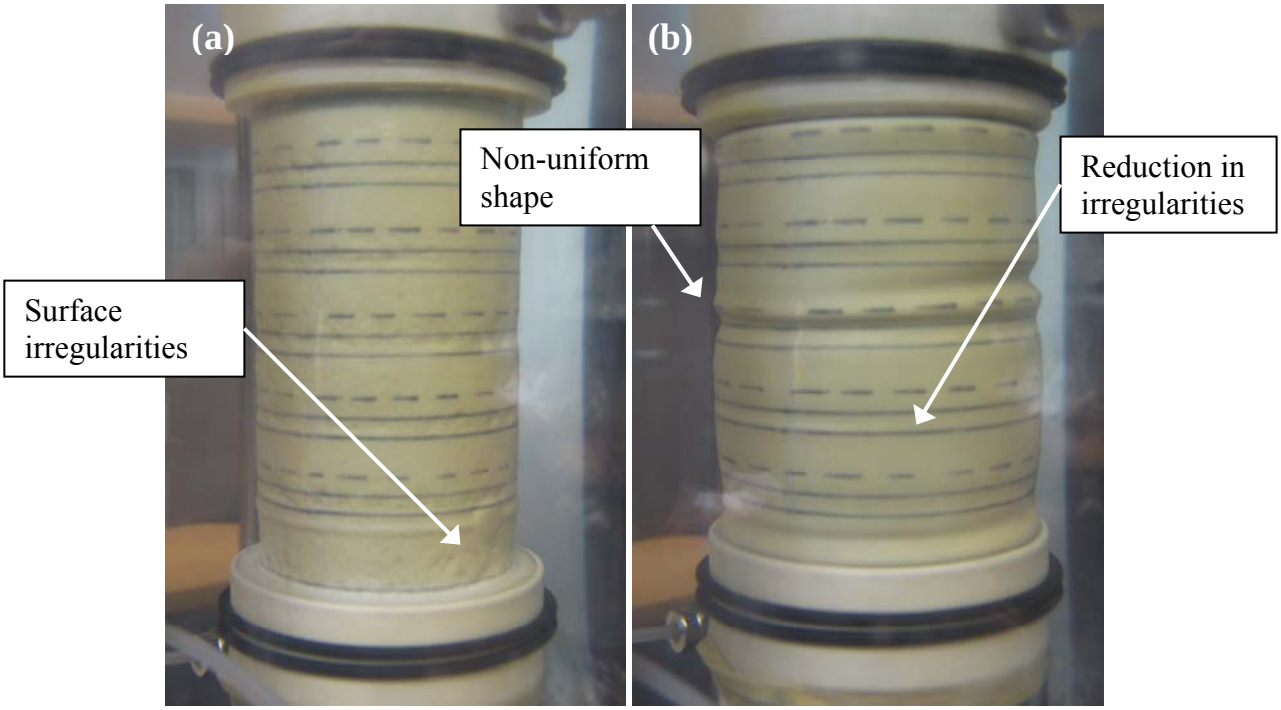

Figure 4-5 FBM-1 test specimen with e = 0.907 at (a) ε_a = 0%, and (b) ε_a = 20%. Note the inconsistencies in membrane texture at ε_a = 0%, and the texture uniformity when ε_a = 20%.

The change in specimen shape also signified if softening had occurred during loading. The shape tended to become very non-uniform, as shown in Figure 4-5 (b), suggesting the soil had become highly deformable.

Softening occurred during specimen compression as the mean effective stress p' of the soil approached p' = 0kPa. This signified strain-softening soil behaviour or undrained instability, coinciding with a reduction in deviator stress q as the axial strain was increased. In terms of stress-path, it represented highly contractive behaviour with the path heading to the

origin, where $q \approx 0$kPa and $p' \approx 0$kPa. The specimen could also be described as having zero residual strength.

(2) Specimen barreling was visually detected by observing the change in specimen shape throughout loading. Barreling corresponds to non-uniform radial deformations, with the mid-height specimen soil deforming more than the soil near the base pedestal and top-cap. This is shown in Figure 4-6 (b) for the FBM-10 specimen with $e = 0.829$ at $\varepsilon_a = 20\%$.

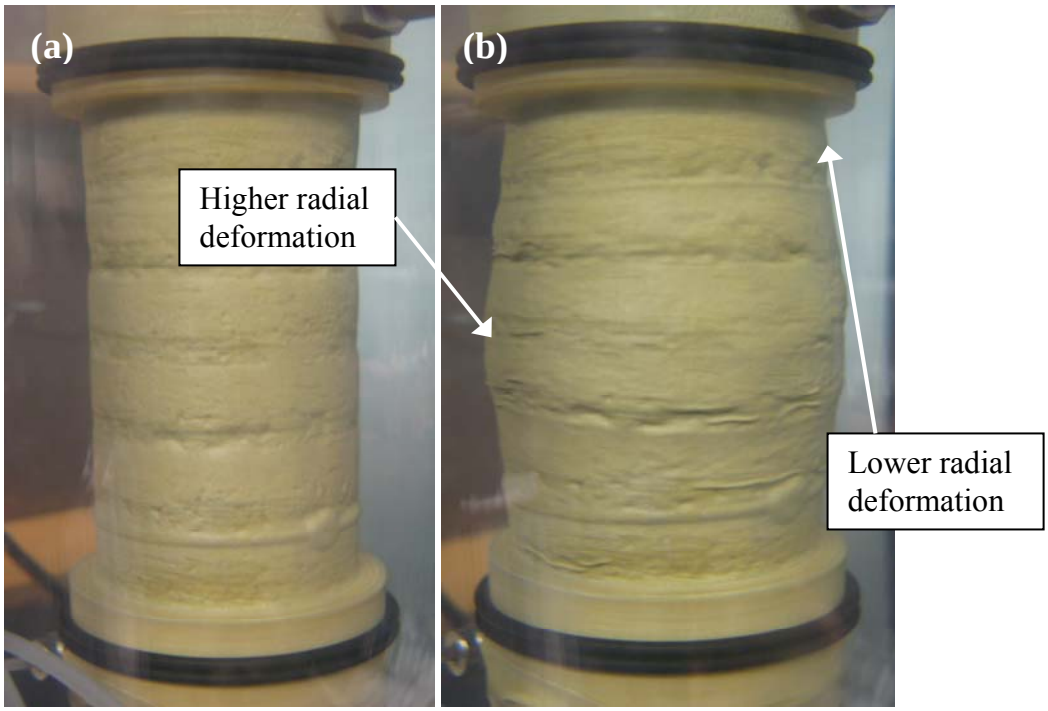

Figure 4-6 FBM-10 test specimen with $e = 0.829$ at (a) $\varepsilon_a = 0\%$, and (b) $\varepsilon_a = 20\%$. Note the increased radial deformation at the specimen mid-height when $\varepsilon_a = 20\%$.

An attempt was made to eliminate, or at least reduce, the non-uniform radial deformations associated with barreling by placing lubricated end membrane segments on the end platens (Tatsuoka and Haibara, 1985), as described in Chapter 3. The lubricated membranes were unsuccessful in completely preventing such deformations, but were observed to help reduce the non-uniformity in radial deformations.

Barreling deformations tended to become noticeable following the peak deviator stress q_{peak} being reached. It was often associated with some strain-softening behaviour of the soil, although it did also present during strain-hardening. Interestingly the barreling-shaped deformations reduced as the specimen densities were increased, giving way to caving-type deformation.

(3) Specimen caving was visually represented by a concave specimen shape occurring as axial compression was applied. Much like barreling it corresponds to non-uniform radial deformations, with the difference being that the mid-height specimen soil deforms less than the soil at the extremities. Figure 4-7 (b) illustrates the caving-type deformation for the FBM-30 specimen with e = 0.643 at ε_a = 10%.

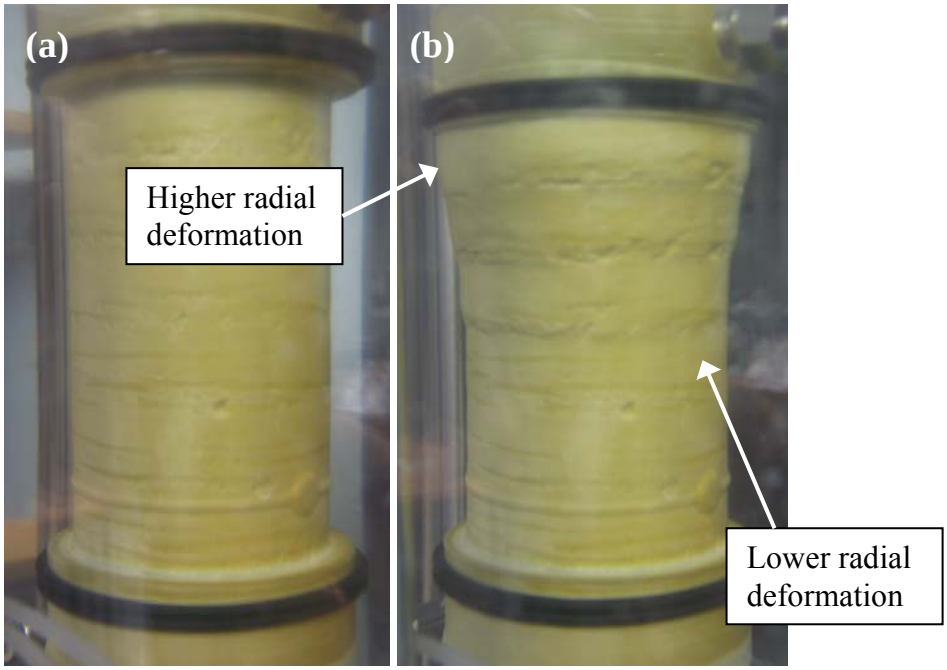

Figure 4-7 FBM-30 test specimen with e = 0.643 at (a) ε_a = 0%, and (b) ε_a = 10%. Note the reduced radial deformation at the specimen mid-height when ε_a = 10%.

Caving appeared to be due to the lubricated end membrane segments allowing more movement at the end platens than was occurring at the specimen mid-height. Typically one end platen (either the pedestal or top-cap) would show more movement of their lubricated membranes than the other. It is unknown why this type of deformation occurred, but it may have been due to subtle variations in the lubricated membrane arrangements created during mould preparation.

Caving deformations were typically associated with higher specimen densities than were seen for softening or barreling. Strain-hardening behaviour was the most common soil response when caving was observed, and the steady state of deformation was not reached if the soil specimen moved beyond the edge of the end platens during compression. If such

excessive movement occurred, the test was stopped due to the unreliability of any data recorded beyond that point. Such cases are noted in the list of test data in Chapter 3.

4.2.2. Effects of Density on the Stress-Strain Behaviour of FBM Soils

It is well documented that changes in density affect the undrained response of a sand. Density effects were therefore investigated for the FBM sandy soils by examining the respective stress-strain, stress path, and excess pore water pressure responses. Table 4-1 presents the density ranges achieved for the FBM test specimens. The minimum and maximum achieved densities, along with an in-between density, are used to discuss the effects of density on the undrained response of the four FBM soils with different fines contents.

Table 4-1 Density ranges of the monotonically-tested FBM soil specimens.

Soil	Void ratio range	Relative density range
FBM-1	$e = 0.907 – 0.821$	$D_r = 0 – 31\%$
FBM-10	$e = 0.863 – 0.691$	$D_r = 24 – 73\%$
FBM-20	$e = 0.722 – 0.652$	$D_r = 45 – 63\%$
FBM-30	$e = 0.693 – 0.626$	$D_r = 50 – 70\%$

Stress-strain responses of the four FBM sandy soils are presented in Figure 4-8 to Figure 4-11. The observed responses show typical undrained behaviour in which the peak and steady state strengths increase with the initial density of the soil. For example, Test M12 of the FBM-10 specimen with $e = 0.863$ ($D_r = 24\%$) reaches a $q_{peak} \approx 50$kPa in Figure 4-9, whilst test M15 of the FBM-10 specimen with $e = 0.806$ ($D_r = 40\%$) has a $q_{peak} \approx 190$kPa. Test M9 of the FBM-1 specimen with $e = 0.907$ ($D_r = 0\%$) experiences strain-softening and reaches a $q_{ss} \approx 5$kPa in Figure 4-8, however Test M8 of the FBM-1 specimen with $e = 0.873$ ($D_r = 12\%$) only responds with strain-hardening behaviour, and subsequently has a $q_{ss} \approx 260$kPa. Also note that very few FBM soil specimens exhibited quasi-steady state deformation (Ishihara, 1993) in these tests. The majority of specimens tended to shown either a reduction or increase in strength beyond $\varepsilon_a > 5\%$, rather than the reduction, steadying, and increase of strength observed for quasi-steady state deformation. This was due to very few initial states of the soils being in the region near the steady state line which produces quasi-steady state behaviour during compressive loading.

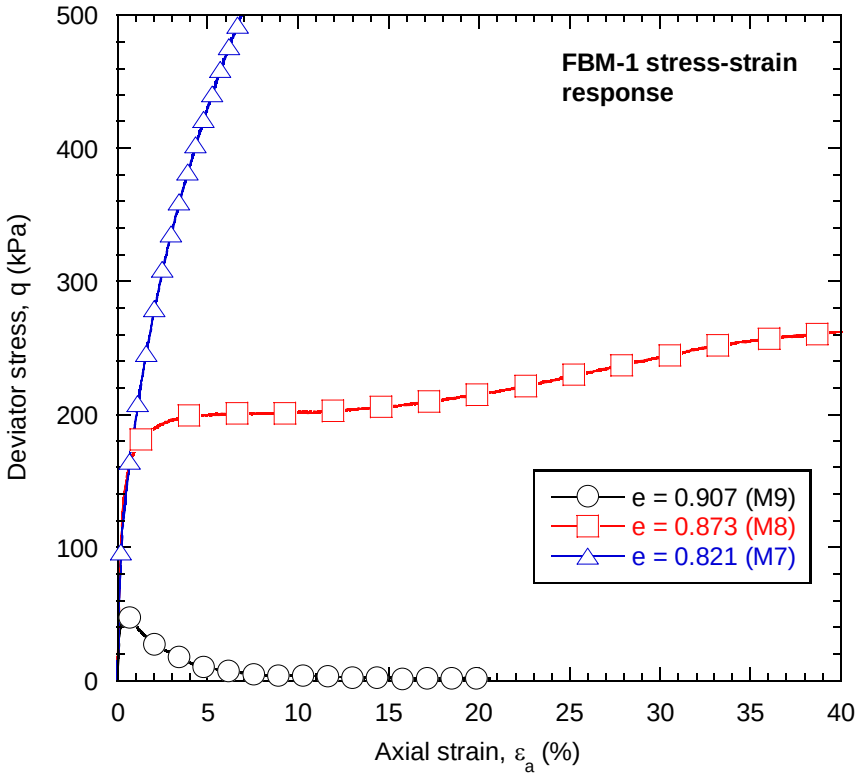

Figure 4-8 Stress-strain curves of three FBM-1 specimens tested using monotonic loading.

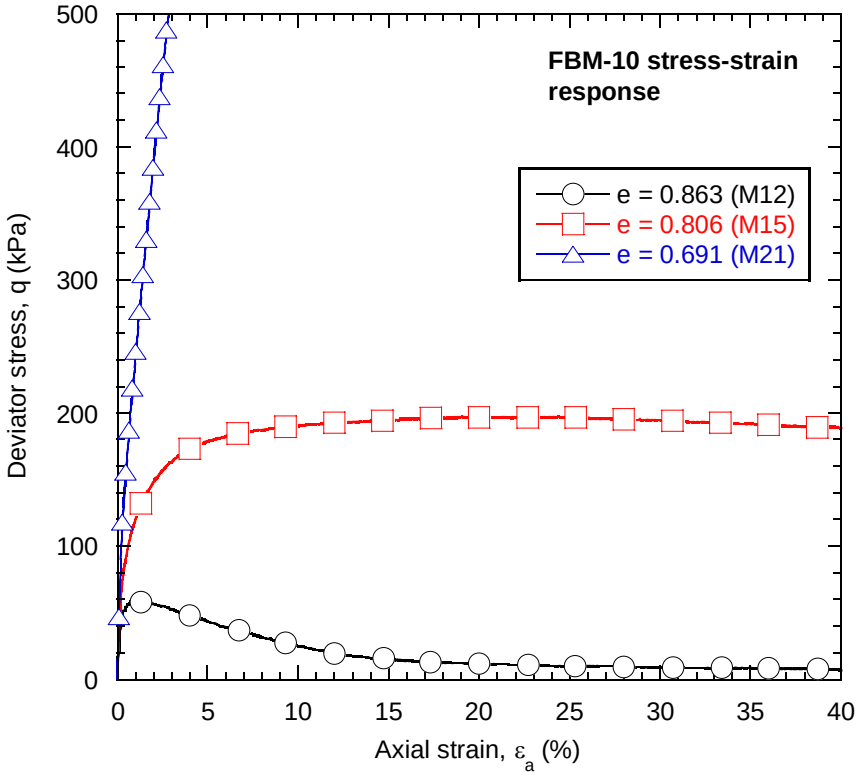

Figure 4-9 Stress-strain curves of three FBM-10 specimens tested using monotonic loading.

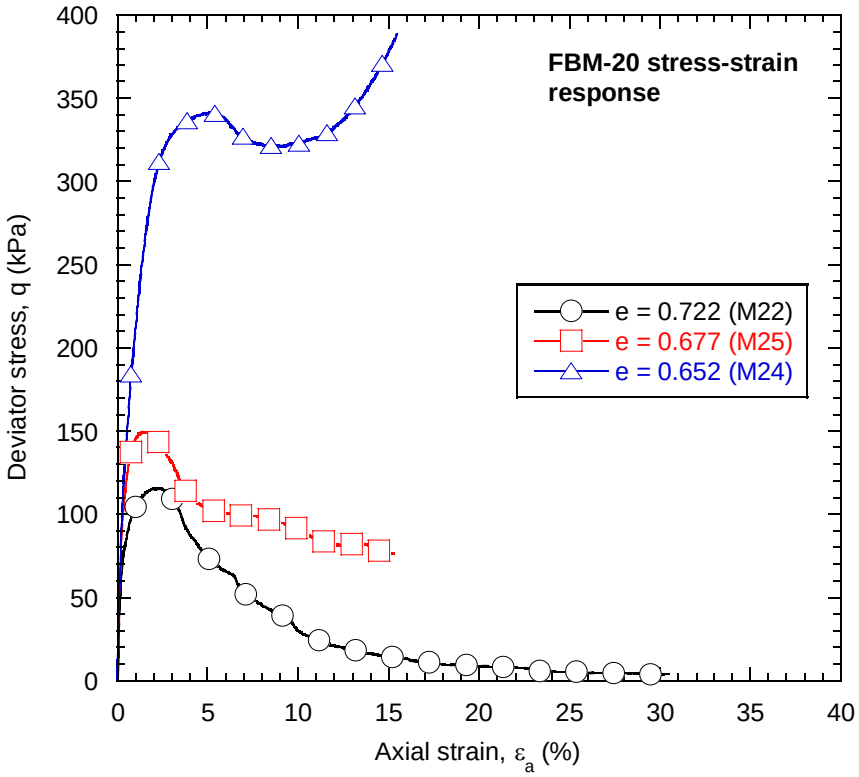

Figure 4-10 Stress-strain curves of three FBM-20 specimens tested using monotonic loading.

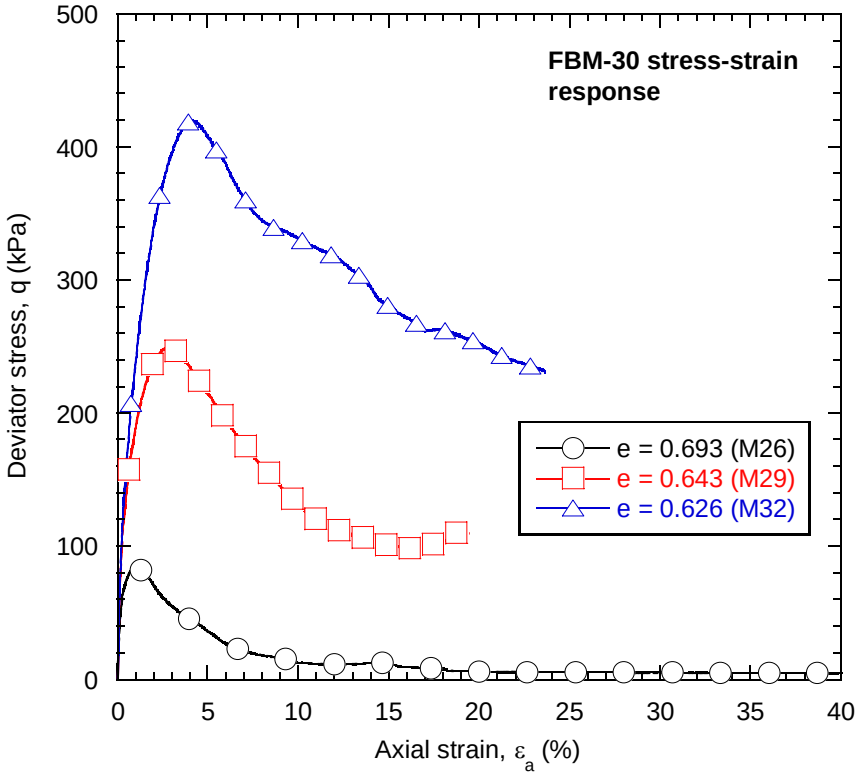

Figure 4-11 Stress-strain curves of three FBM-30 specimens tested using monotonic loading.

Effective stress-paths observed in the tests of the four FBM soils are presented in Figure 4-12 to Figure 4-15. These plots clearly show that increased soil density results in more dilative specimen response. For example test M22 of the FBM-20 specimen with e = 0.722 (D_r = 45%) in Figure 4-14 displays initially contractive behaviour, before a slight amount of dilative response occurs as the peak strength is reached. Following this the response is fully contractive, leading to a mean effective stress $p'_{ss} \approx$ 0kPa at the steady state of deformation. Test M24 with e = 0.652 (D_r = 63%) instead shows mainly dilative response to the axial compression, although there is a small drop in mean effective stress between $p' \approx$ 225 – 250kPa.

Also note that as the fines content of the FBM sand was increased, denser specimens tended to show contraction in their effective stress-paths after dilation had taken place. This is most evident for the FBM-20 specimen with e = 0.677 (M25) in Figure 4-14 and the FBM-30 specimens with e = 0.643 and 0.626 (M29 and M32) in Figure 4-15, which suddenly exhibit contractive response following dilation. This is not typical behaviour for sandy soils, and may be due to the additional fines creating a meta-stable soil structure which could collapse as the deviator stress increases. This behaviour has however been observed during other undrained compression tests on moist-tamped Masado soil specimens (Tsukamoto et al., 1998), which also contained a portion of fines (f_C = 8%) as well as a portion of gravel (55%).

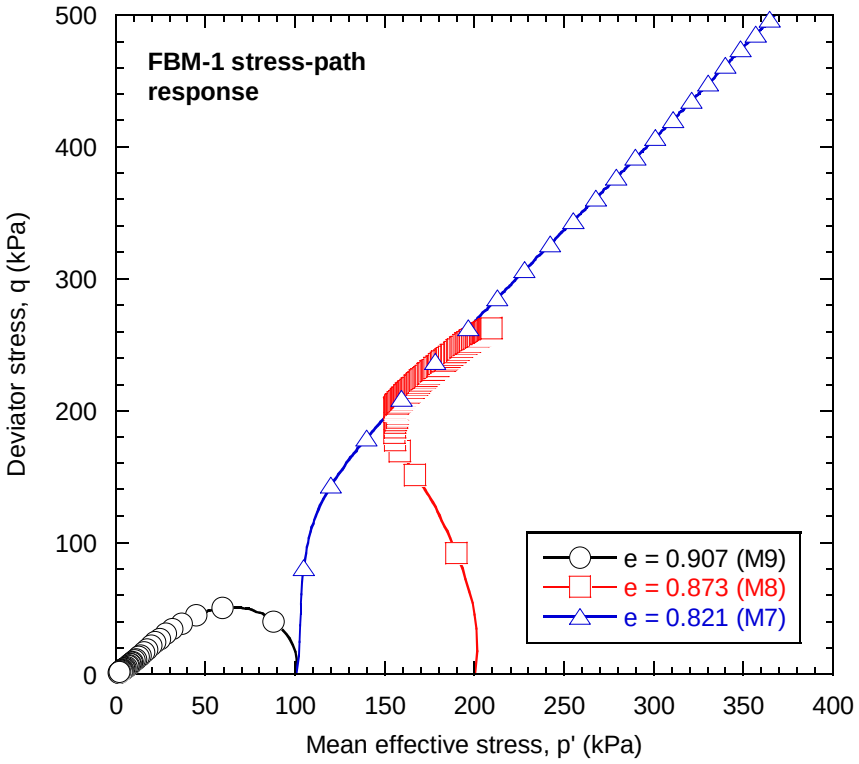

Figure 4-12 Effective stress-paths of three FBM-1 specimens tested using monotonic loading.

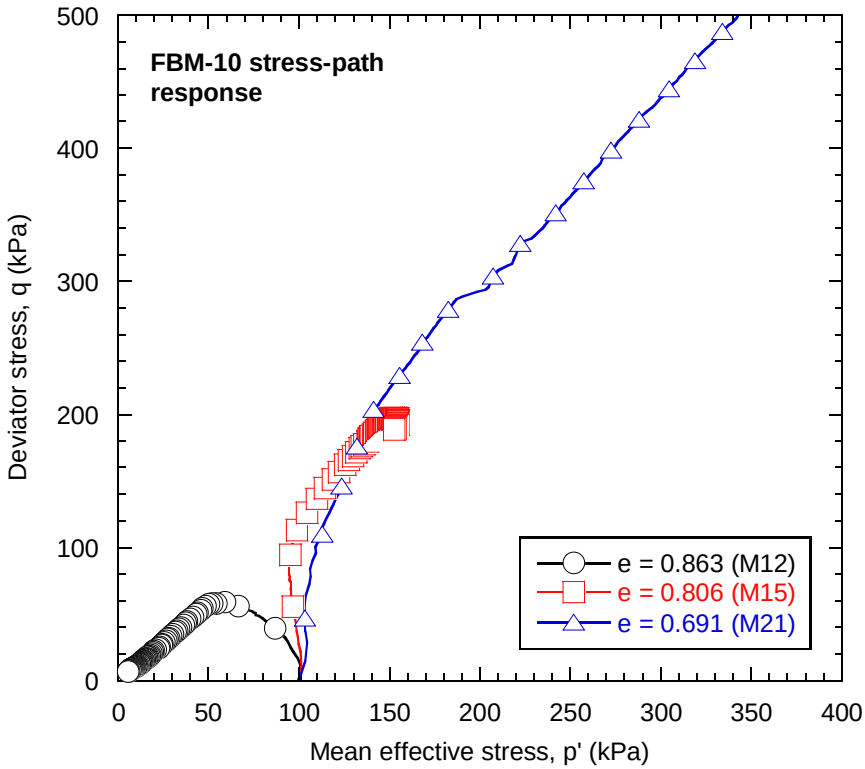

Figure 4-13 Effective stress-paths of three FBM-10 specimens tested using monotonic loading.

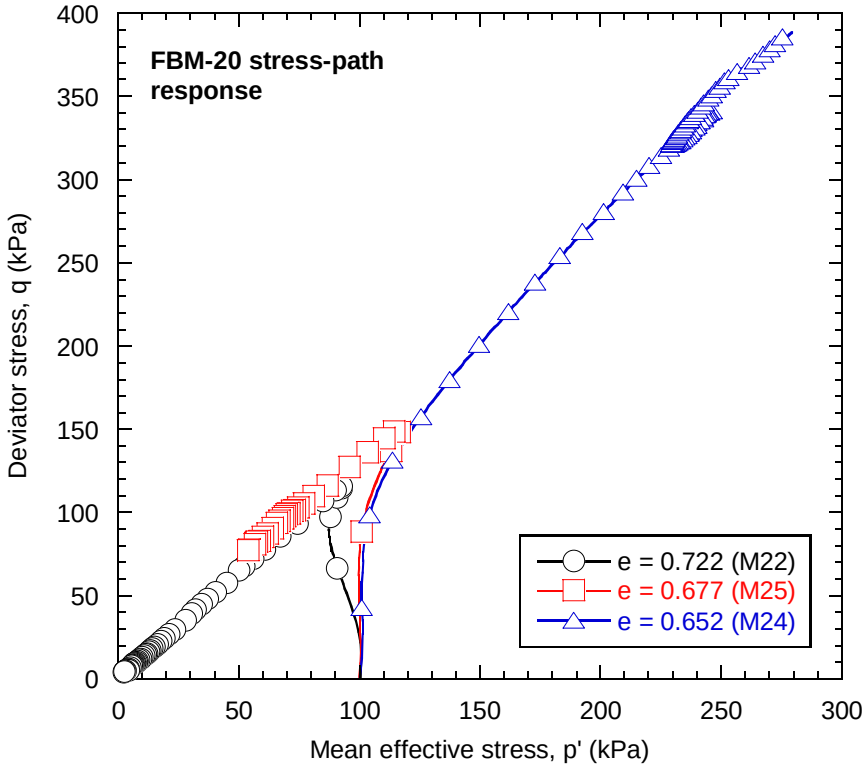

Figure 4-14 Effective stress-paths of three FBM-20 specimens tested using monotonic loading.

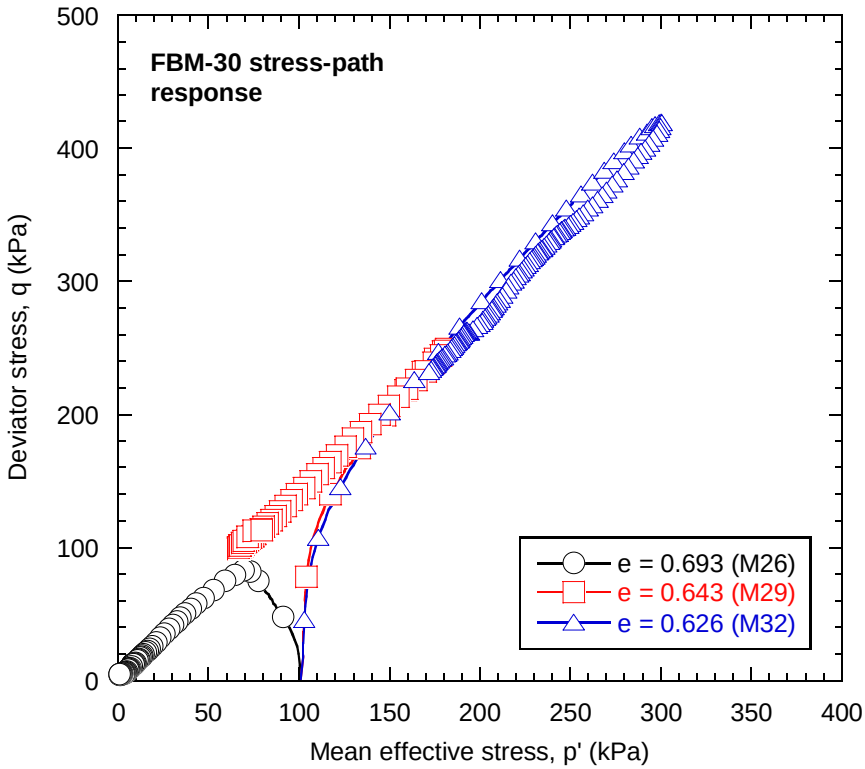

Figure 4-15 Effective stress-paths of three FBM-30 specimens tested using monotonic loading.

To further illustrate the effects of density on the contractive and dilative tendencies of the FBM soils, the excess pore water pressure responses are displayed in Figure 4-16 to Figure 4-19. The excess pore water pressure is normalized by the initial mean effective stress p'_i at the start of axial compression. This means that $\Delta u \,/\, p'_i = 1.0$ corresponds to 100% excess pore water pressure or a mean effective stress of $p' = 0$kPa. Note that the contractive behaviour that followed dilation in the FBM-20 and FBM-30 specimen stress-paths can be explicitly seen in Figure 4-18 and Figure 4-19. The excess pore pressure responses are otherwise typical of sandy soils.

The effects of an increased density on the undrained monotonic response of FBM soils were as expected and could be summarized as:

- Peak and steady state strength increase
- Less strain-softening behaviour
- Mean effective stress at the steady state of deformation increases
- More dilative response is observed
- Higher fines content soils exhibited some contraction after dilation.

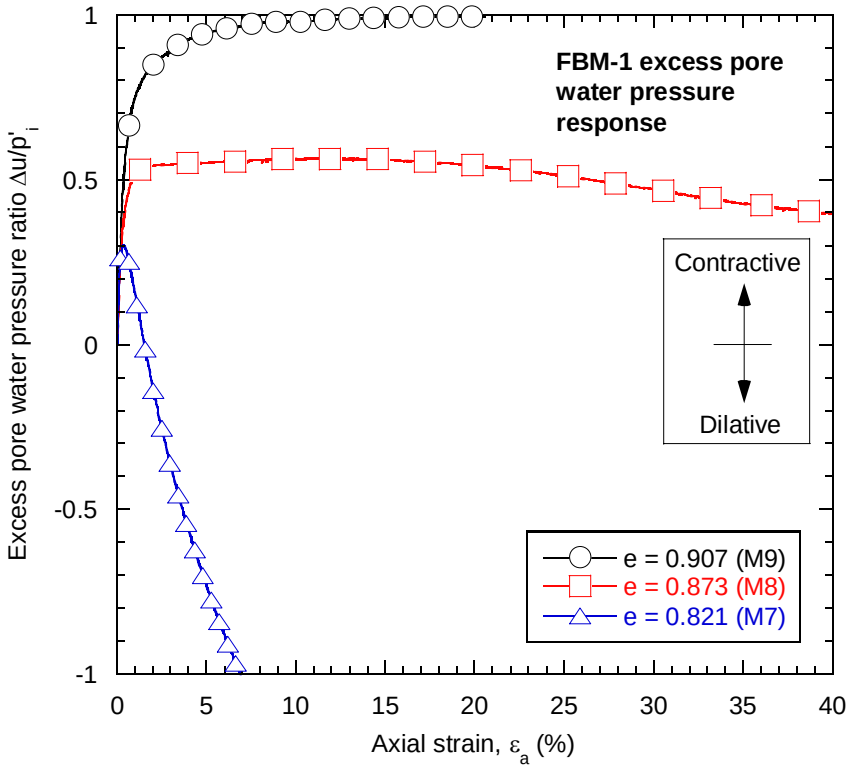

Figure 4-16 Excess pore water pressure curves of three FBM-1 specimens tested using monotonic loading.

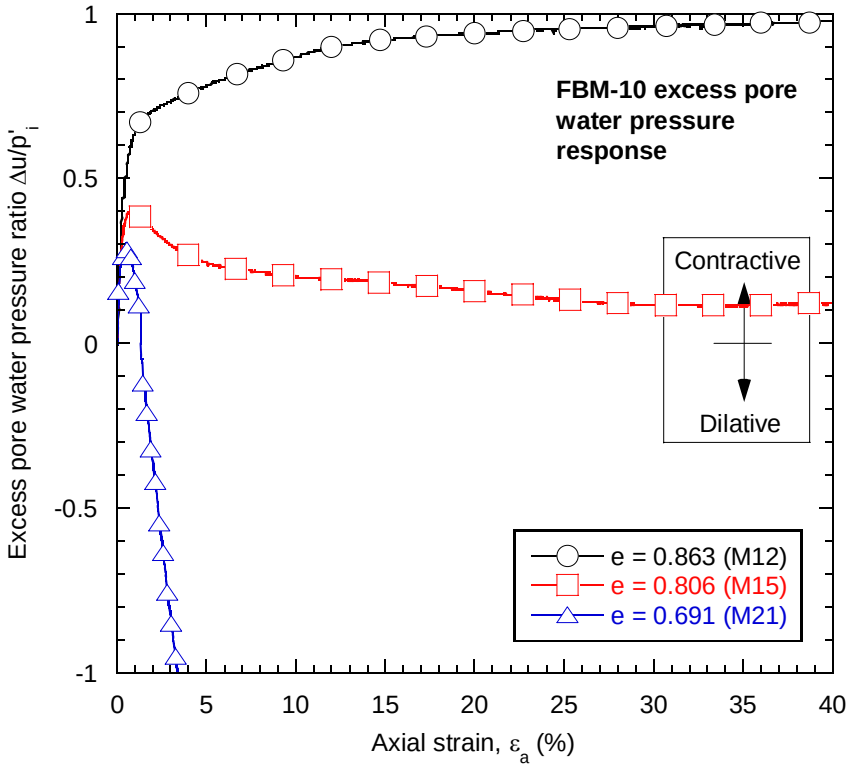

Figure 4-17 Excess pore water pressure curves of three FBM-10 specimens tested using monotonic loading.

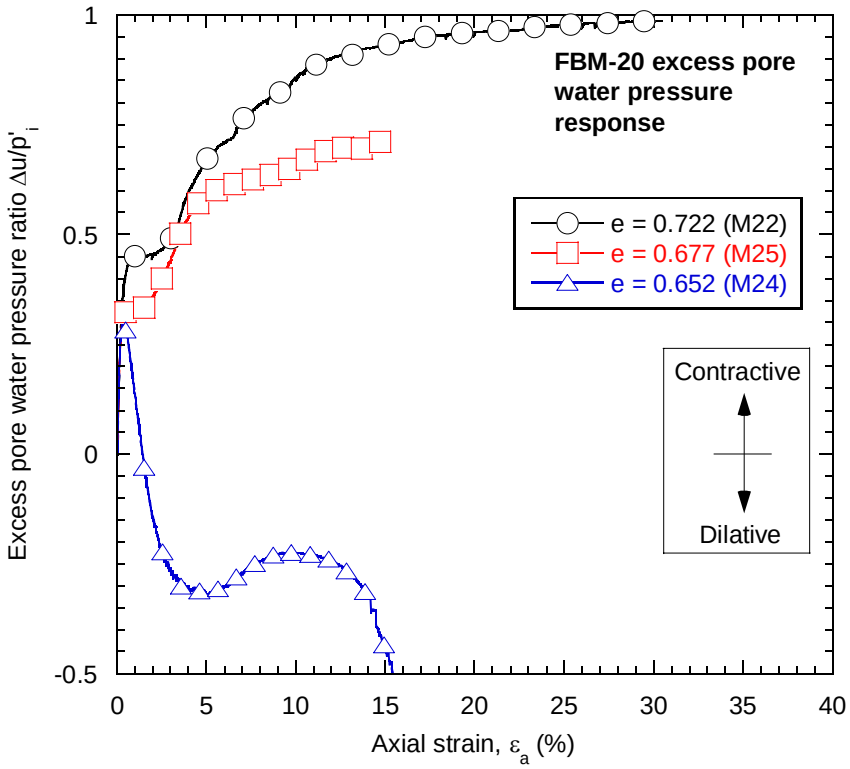

Figure 4-18 Excess pore water pressure curves of three FBM-20 specimens tested using monotonic loading.

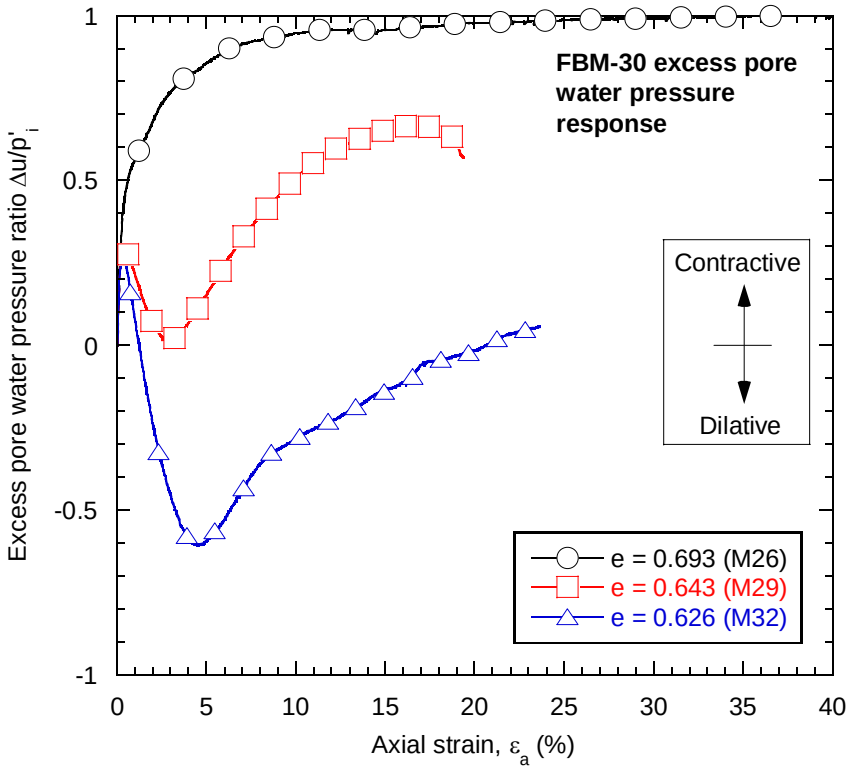

Figure 4-19 Excess pore water pressure curves of three FBM-30 specimens tested using monotonic loading.

4.2.3. Effects of Fines Content on the Stress-Strain Behaviour of FBM Soils

The effects of changes in the fines content of a sand are less understood than the effects of changing density, as discussed in Section 4.2.2. To investigate such effects of fines content, a representative undrained monotonic test from each of the four FBM soils was compared using their respective stress-strain, stress-path, and excess pore water pressure responses. The representative tests were chosen in such a way that the FBM-1 test specimen had the lowest density (e = 0.821, D_r = 31%) and the FBM-30 test specimen had the highest density (e = 0.659, D_r = 60%), since no undrained monotonic data was available for specimens across the four soils with similar void ratio or relative density values.

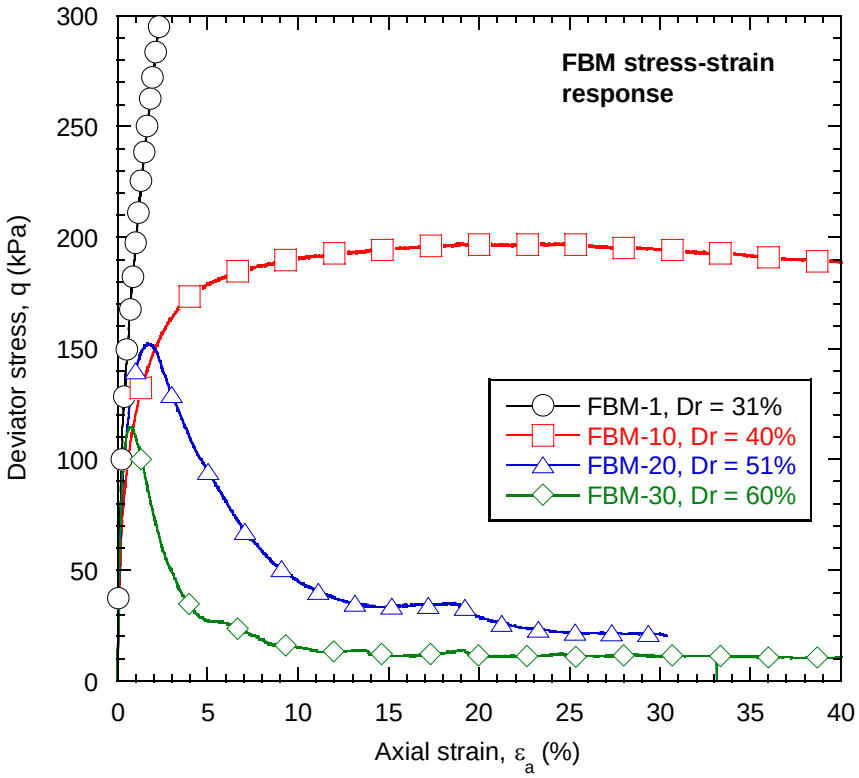

Figure 4-20 Stress-strain curves of four FBM specimens tested using monotonic loading.

Figure 4-20 compares the stress-strain curves of the four FBM soils. The peak strength q_{peak} and steady state strength q_{ss} both decrease as the fines content of the sands are increased. This occurs even though the soil density increases with the fines content, which otherwise should result in higher peak and steady state strengths, as discussed in Section 4.2.2.

These results suggest that an increase in fines content reduces the strength of the sand, and causes more strain-softening response under undrained axial compression. Similar effects of additional fines on the stress-strain response of sand has also been observed when Nevada sand with non-plastic fines was tested (Lade and Yamamuro, 1997). Chapter 2 discusses other studies that also stated this effect of fines.

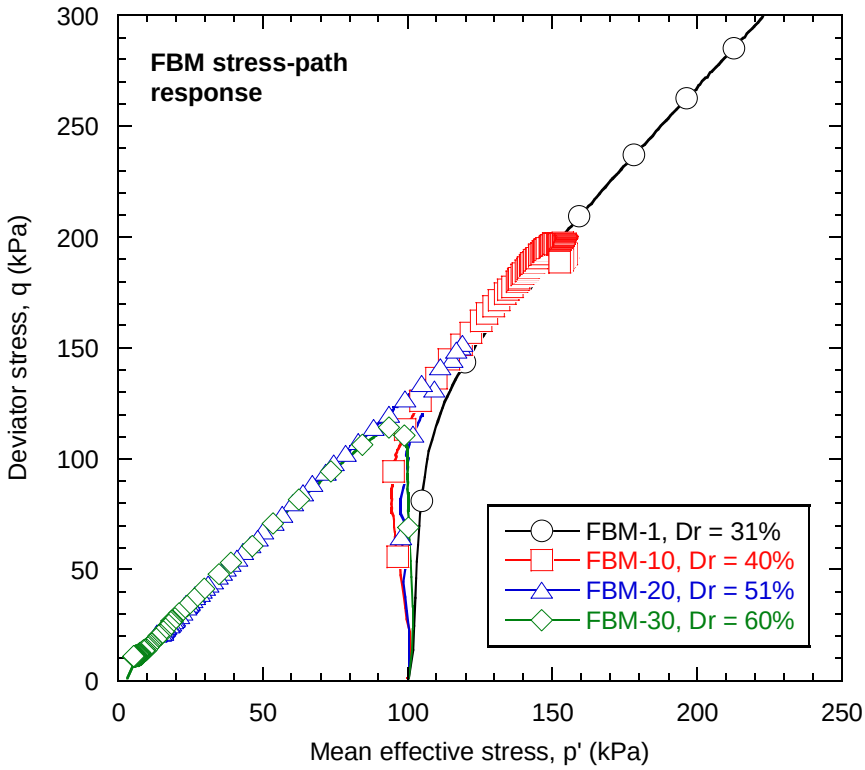

Figure 4-21 Effective stress-paths of four FBM specimens tested using monotonic loading.

Figure 4-21 compares the stress-paths of the four FBM soils, whilst Figure 4-22 compares the excess pore water pressure curves. The specimens initially show similar amounts of contraction, but the stress-paths begin to diverge as phase transformation occurs for the FBM-30 soil specimen. Once this specimen reaches a peak strength $q_{peak} \approx 115$kPa, the mean effective stress p' drops and eventually reaches $p'_{ss} \approx 5$ kPa. Note this is the densest specimen with the highest fines content. Conversely the FBM-1 soil specimen with the lowest density does not show any drop in p', and primarily displays dilative response to the axial compression.

The trend suggests that increased fines contents result in lower mean effective stresses at the steady state of deformation, and tend to cause increased specimen contraction when

comparing at similar densities. This trend was also observed by Lade and Yamamuro (1997) during tests performed on Nevada sand with fines.

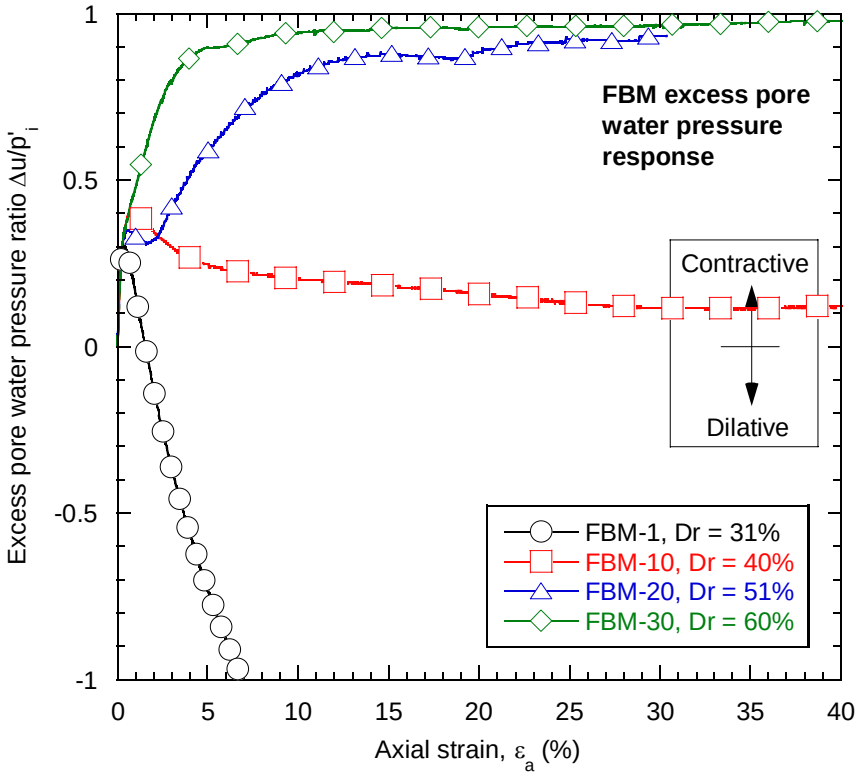

Figure 4-22 Excess pore water pressure curves of four FBM specimens tested using monotonic loading.

In summary, the effects of increasing fines content on the undrained monotonic response of the FBM sandy soils when using void ratio or relative density are are:

- Peak and steady state strengths reduce
- The behaviour is more contractive and strain-softening is more common.

4.2.4. Evaluation of the Steady State Line

The steady state of deformation for the undrained monotonic FBM soil tests was ideally defined at an axial strain ε_a = 40%. For clean sands, it is typically defined at axial strains ε_a > 20%. This strain level was chosen as it allowed the steady state of deformation to clearly develop, reducing the uncertainty as to whether or not steady state had actually been reached.

Figure 4-23 (a) provides a good example of why ε_a = 40% was used: the FBM-1 specimen with e = 0.873 appears to be deforming at a constant strength near $\varepsilon_a \approx$ 10%, but subsequently undergoes further strain-hardening until the steady state of deformation is reached.

Figure 4-23 (b) explains the process of determining the mean effective stress at steady state p'_{ss}: the steady state deviator stress is defined from the stress-strain response, and the stress-path response is then used to determine the steady state mean effective stress.

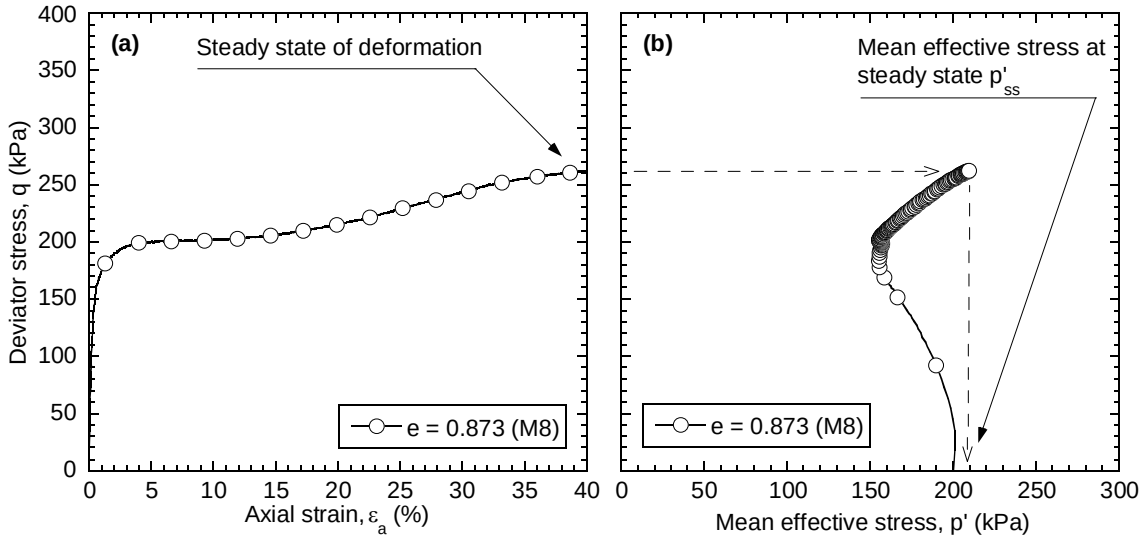

Figure 4-23 Derivation of the mean effective stress at the steady state of deformation p'_{ss}.

In the event that a specimen did not reach ε_a = 40%, p' at a lower strain value was used for p'_{ss}. This was selected on a test-by-test basis, and only employed for specimens that showed contractive response during loading. Specimens that had a dilative response without reaching the steady state of deformation were disregarded from the analysis and are not included in the evaluation of the steady state lines. This was due to the uncertainties associated with the steady states of a dilating specimen.

The steady state lines were determined by plotting the mean effective stress at steady state p'_{ss} against the void ratio. They were also plotted using relative density as the density measure. In all steady state line plots individual test data is shown as discreet points, with a logarithmic curve fit to the data in the stress range up to p' = 250kPa , which corresponds to a straight line in the e – log p' plot. Section 4.2.5 presents and discusses the steady state lines for the four FBM sandy soils.

4.2.5. Steady State Lines of the FBM Soils

As discussed in Section 4.1.1, the state concept is a useful framework for interpreting and comparing the undrained monotonic response of sands. Sand specimens with densities greater than those at the steady state line show dilative response under monotonic loading while specimens with lower densities show contractive response. This means that the steady state line provides a reference that can be used to determine the expected soil response based on the initial soil state (in terms of initial density and stress).

Hence, for the state concept interpretation it is necessary to compare how the location of the steady state line in the $e - p'$ plane changes as the fines content changes. For this purpose, the steady state lines of the four FBM sandy soils are presented in Figure 4-24 to Figure 4-27. The maximum and minimum void ratios, e_{max} and e_{min}, are also included in the figures to show the potential range of soil densities and the proximity of the respective steady state lines to these density limits.

Note that filled data points have been used when the steady state of deformation was defined at an axial strain ε_a = 40%. Open data points have been used when steady state was defined at lower strain values, such as for the FBM-20 and FBM-30 soils. In these latter cases the steady state points may in fact be showing the mean effective stresses at quasi-steady state, as the tests were stopped before ε_a = 40% could be reached. The presented open data points are however considered to reasonably represent the actual steady state line location.

The slope of the steady state lines of the four FBM soils is similar, with all lines being relatively flat in the $e - p'$ plane. This is typical for the steady state lines of sandy soils at low confining pressures, and has been observed in many other studies on sands (Verdugo, 1992). The flat nature of the steady state line means that small increases in soil density, when initial soil states are near the steady state line, can result in soil response changing from being mainly contractive to mainly dilative. The low mean effective stress range of p' = 0 – 300kPa for the FBM steady state lines was purposely chosen as it reflects the range of confining pressures for which soils are generally most susceptible to liquefaction in the field. This range was based on field case histories of observed level-ground liquefaction and the depths at which the liquefaction occurred (Stark and Olson, 1995), which tended to be less than 20m below the ground surface with effective vertical stresses less than 300kPa.

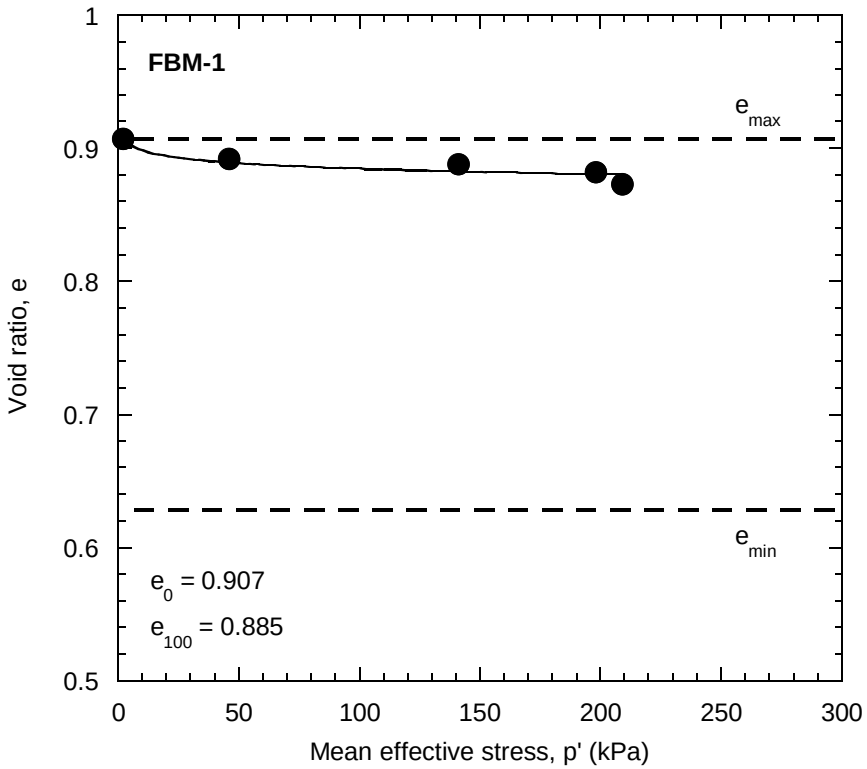

Figure 4-24 Steady state line of the FBM-1 soil.

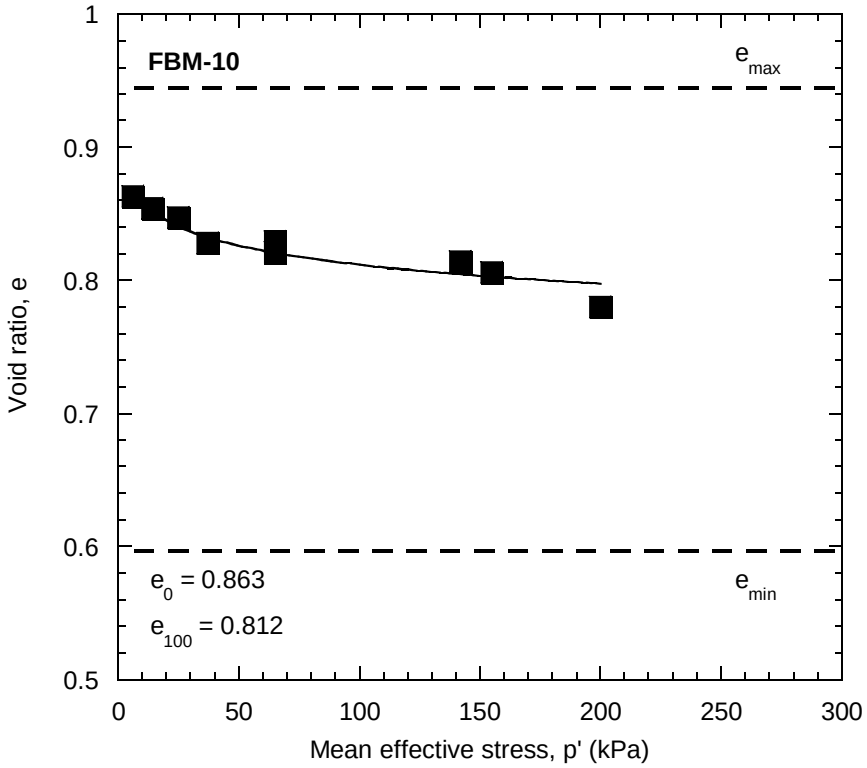

Figure 4-25 Steady state line of the FBM-10 soil.

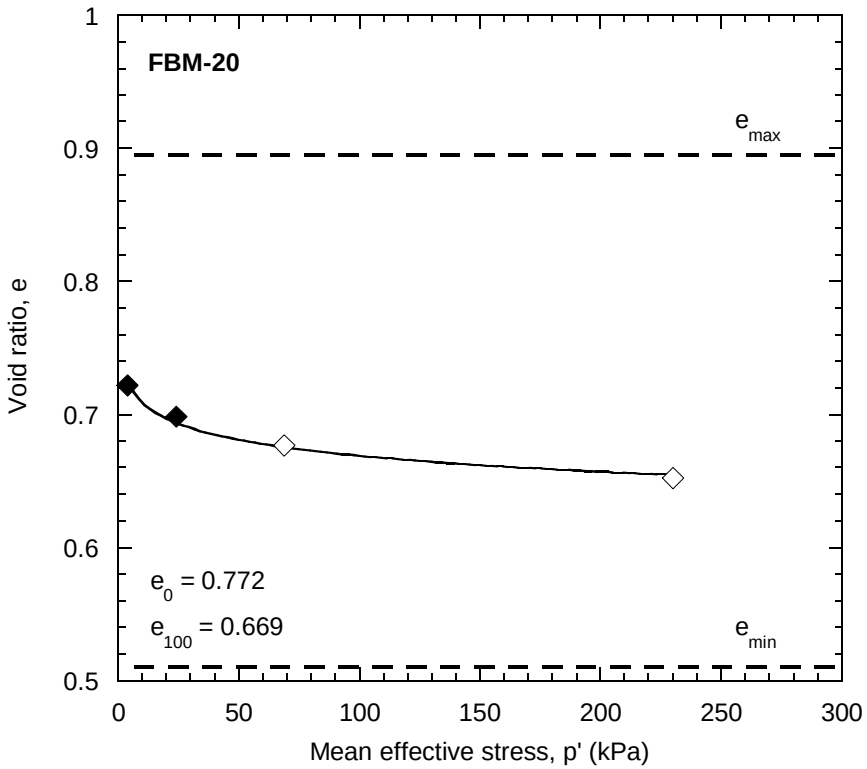

Figure 4-26 Steady state line of the FBM-20 soil.

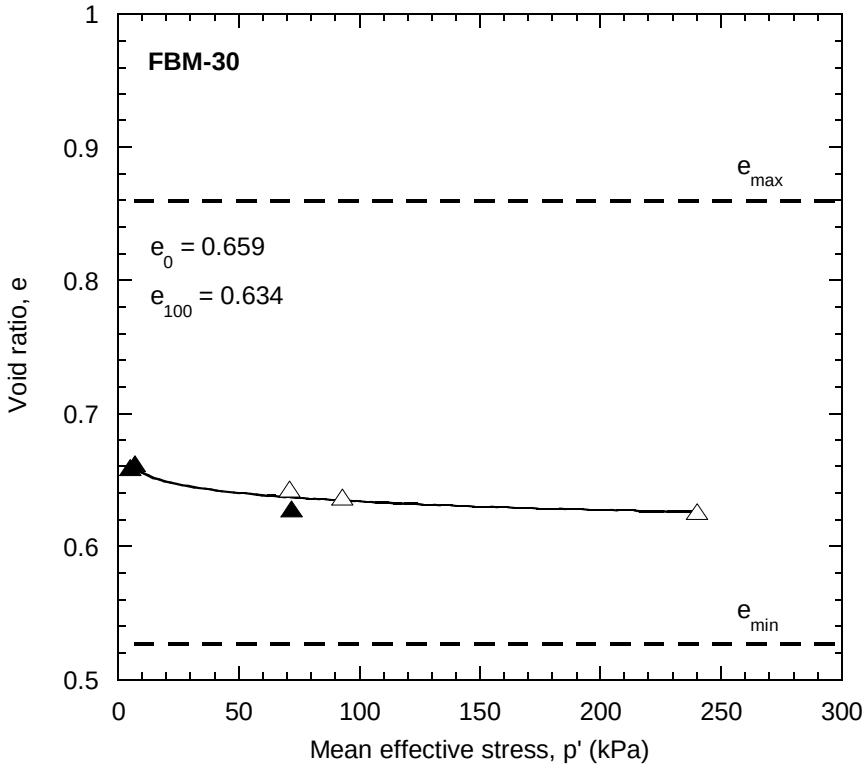

Figure 4-27 Steady state line of the FBM-30 soil.

The proximity of the FBM steady state lines to their respective void ratio limits, e_{max} and e_{min}, illustrates the potential range of soil response with respect to the initial states. The FBM-1 steady state line in Figure 4-24 is located very near to the e_{max} value – this means that when the sand is close to its loosest state (e_{max}), fully contractive behaviour will occur under axial compression. Contrary to this, the FBM-30 steady state line in Figure 4-27 is located nearer to the FBM-30 e_{min}. This means that many potential initial states could result in contractive soil behaviour during loading, as there are many possible densities less than those at the steady state line. This difference between the FBM-1 and FBM-30 steady state lines clearly suggests that the changing fines content affects the location of the steady state line of the FBM sand, and is discussed further in Section 4.2.6.

For reasons mentioned previously, it became more difficult to reach the steady state of deformation for the FBM sandy soils as the fines content was increased from $f_C = 1 \rightarrow 30\%$. Note that Figure 4-24 and Figure 4-25 for the FBM-1 and FBM-10 steady state lines respectively have only bold symbols, meaning that the steady state of deformation was able to be defined at approximately $\varepsilon_a = 40\%$. Figure 4-26 and Figure 4-27 however for the FBM-20 and FBM-30 steady state lines respectively have at least half open symbols, where the steady state of deformation was defined at $\varepsilon_a < 40\%$. It is thought that the increased densities of the FBM soils with higher fines contents caused the test specimens to behave in a manner that lead to increased movement of the end lubricated membrane segments and hence non-uniformity in the specimen response. It is also generally understood that higher strains are required to reach the steady state of deformation for fines-containing soils (Zlatovic, 1994).

4.2.6. Effects of Fines Content on the FBM Steady State Lines

It has been discussed and shown in Sections 4.2.3 and 4.2.5 that changing the fines content of a sand affects the undrained monotonic response of the sand. In general, when comparing soil response at a similar initial state, the FBM soils with higher fines contents displayed lower peak and steady state strengths, more contractive behaviour, and greater development of excess pore water pressures. To further investigate why these trends were observed, the steady state lines of the FBM soils were plotted together using two different measures of density as comparison.

- Void ratio, e, and
- Relative density, D_r

Note that the location of the steady state line is considered in the definitions of the state parameter ψ and state index I_s, as presented in Equations (4-3) and (4-4), and therefore using these produce no insightful information as to the difference in the steady state line locations as the fines content of the FBM sand is changed.

Figure 4-28 and Figure 4-29 respectively present the steady state lines of the FBM soils using void ratio and relative density as the measures of state.

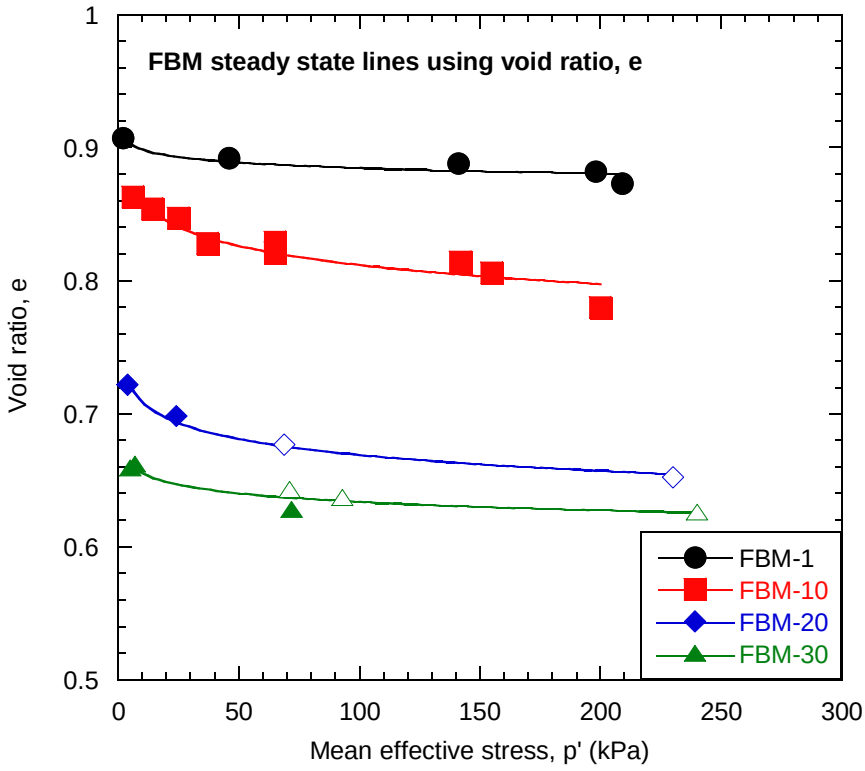

Figure 4-28 Steady state lines of the FBM soils using void ratio as the state measure.

Figure 4-28 and Figure 4-29 indicate that the primary effect of fines content on the steady state lines of the FBM soils is to move the steady state lines to higher densities as the fines content is increased. For example, the FBM-1 steady state line has densities at p' = 0kPa of approximately $e_0 \approx 0.91$ when using void ratio and $D_{r0} \approx 0\%$ when using relative density, whilst the FBM-30 steady state line has an $e_0 \approx 0.66$ and a $D_{r0} \approx 60\%$. This change in the steady state line location with increasing fines content is summarized in Figure 4-30, for both (a) void ratio, and (b) relative density. Note that the FBM-10 and FBM-20 steady state line locations fit within the observed trend.

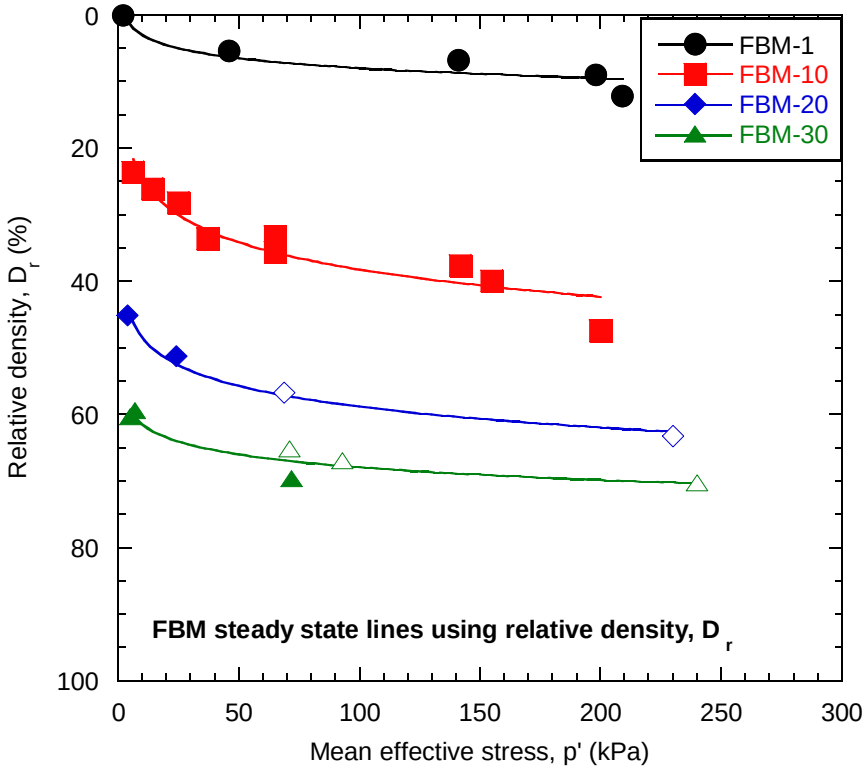

Figure 4-29 Steady state lines of the FBM soils using relative density as the state measure.

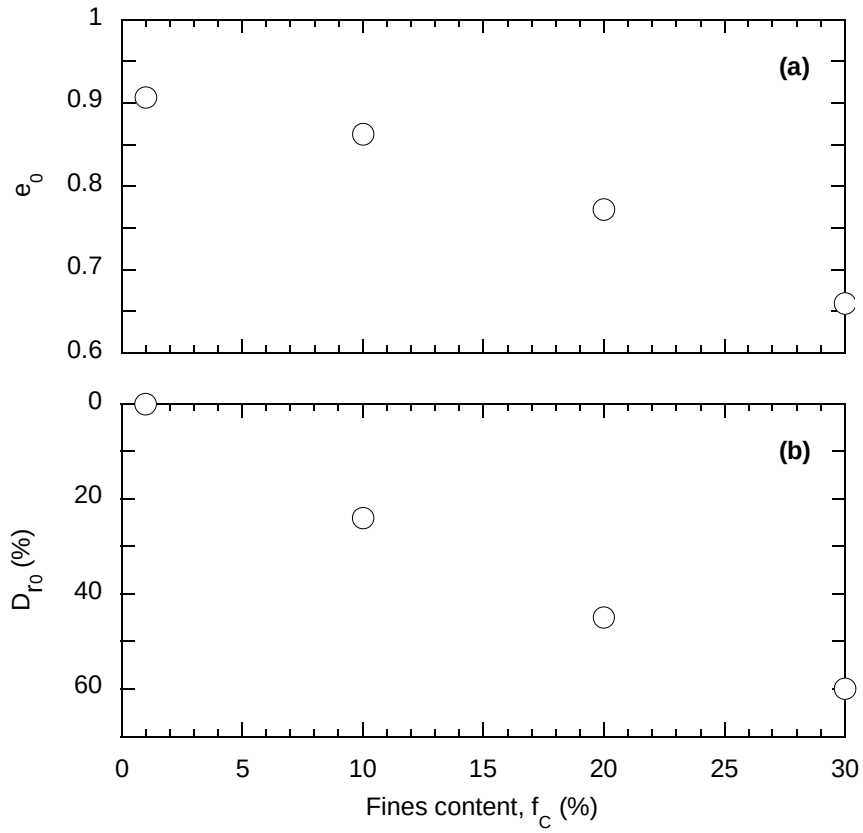

Figure 4-30 Change in steady state line location at p' = 0kPa for the FBM soils.

The FBM soils are not the only sandy soils for which this change in steady state line location with changing fines content has been noticed. Studies on other mixtures of sands and fines (Cubrinovski and Ishihara, 2000) have also presented data indicating that the addition of non-plastic fines to a sand causes the steady state line to move to higher-density locations.

The implication of this change in location is that sands with higher fines contents have more potential initial states that result in contractive soil behaviour during undrained axial compression. This is due to more potential soil densities existing that are lower than the steady state line densities. The trends observed and discussed in Section 4.2.3 can therefore be explained by the movement of the steady state lines – the soils with higher fines contents tend to be more contractive at densities where soils with lower fines contents tend to show dilative response. The contractive behaviour at higher fines contents leads to increased excess pore water pressure generation, which decreases the mean effective stresses and results in decreased soil strength.

The results shown in Figure 4-28, Figure 4-29 and Figure 4-30 can be summarized as follows:

- The FBM steady state lines are located at lower void ratios and higher relative densities as the fines content is increased
- There are more potential initial states that result in contractive soil behaviour for FBM soils with higher fines contents
- These steady state line trends have been observed in other mixtures of sands and fines
- The above observations explain why the FBM soils with higher fines contents displayed lower strengths and more excess pore water pressure generation when comparing the undrained monotonic response at similar void ratio and relative density.

4.2.7. Critical Assessment of Void Ratio and Relative Density

Section 4.2.6 presented the steady state lines for the four FBM soils, and showed that their location moves towards higher densities as the fines content of the soil is changed. This helped to explain why the FBM soils with higher fines contents and higher densities responded to axial compression with more contraction and lower strengths.

Ideally the response of the FBM soils would be similar, regardless of fines content, at similar void ratios or relative densities, if these density measures were valid for different fines contents. In such a case the steady state lines would be located at approximately the same densities in either the $e - p'$ plane or $D_r - p'$ plane. As displayed in Figure 4-30 however, showing e_0 and D_{r0} values with varying fines content, the FBM steady state lines are not located at similar densities. The difference in soil response due to the different steady state line location is illustrated in Figure 4-31, showing an initial soil state of D_r = 20% and p'_i = 150kPa. The soil response to axial compression will be contractive if the FBM-10 soil is compressed, and dilative if the FBM-1 soil is compressed.

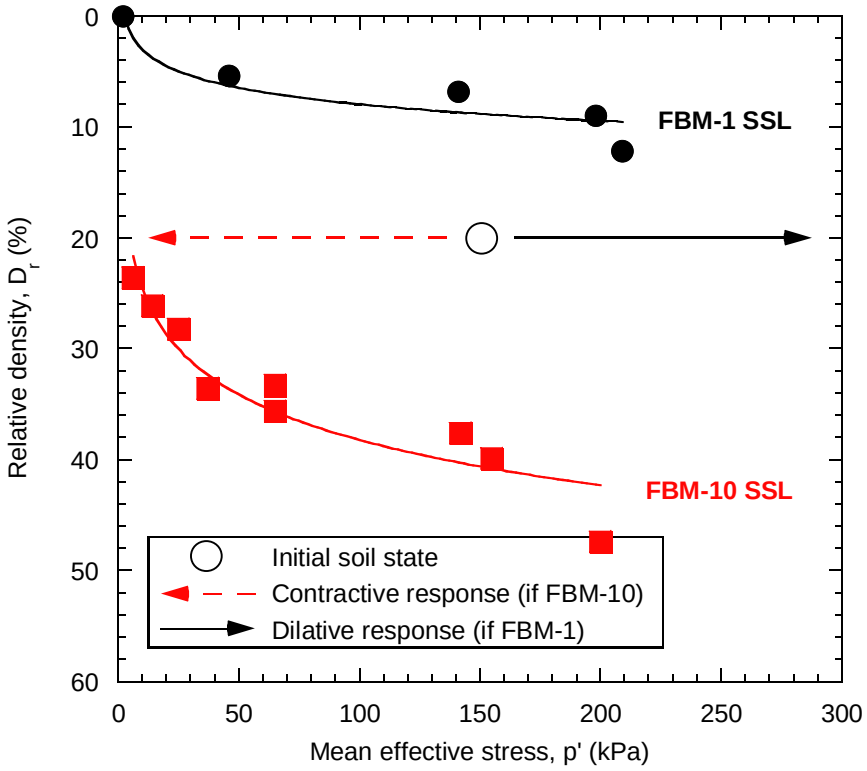

Figure 4-31 Potential soil responses from an initial state of D_r = 20%, p'_i = 150kPa for FBM-1 and FBM-10 soils.

The void ratio and relative density definitions are therefore critically assessed in the following to explain why similar values of these density measures do not correspond to similar undrained monotonic responses of the FBM sandy soils, using the state concept as a reference.

Void ratio (*e*) is defined in Equation (4-1) in Section 4.1, using the volume of voids (V_v) and volume of solid particles (V_s) within a soil specimen. This defines an index of soil particle contacts using only space filled by the soil particles, and space filled by pore water assuming full soil saturation. It is a calculation based on global soil properties, and does not account for micro-structural properties. As such, the void ratio has two important drawbacks when defining the density of a mixture of sand and fines:

(1) Void ratio provides no information on the potential soil density range
(2) Void ratio provides no information on the soil particle size composition

(1) The potential soil density range is typically described by the maximum and minimum void ratios, e_{max} and e_{min}. These are presented for the FBM soils in Figure 4-32. The void ratio limits help to locate the steady state line relative to reference densities that exist for a soil. This in turn provides insight into the soil densities that may exhibit contractive or dilative response during axial compression.

Figure 4-32 shows that the maximum and minimum void ratio limits change as the fines content of the FBM soils is increased, meaning that the range of potential soil densities also changes with fines content. If changes in these potential densities are not taken into account, it becomes difficult to assess how the changing steady state line position with increasing fines content, presented in Figure 4-28, really affects the number of possible contractive and dilative soil states. The actual density limits of each of the soils needs to be known, and this is one advantage of using the relative density as a density measure.

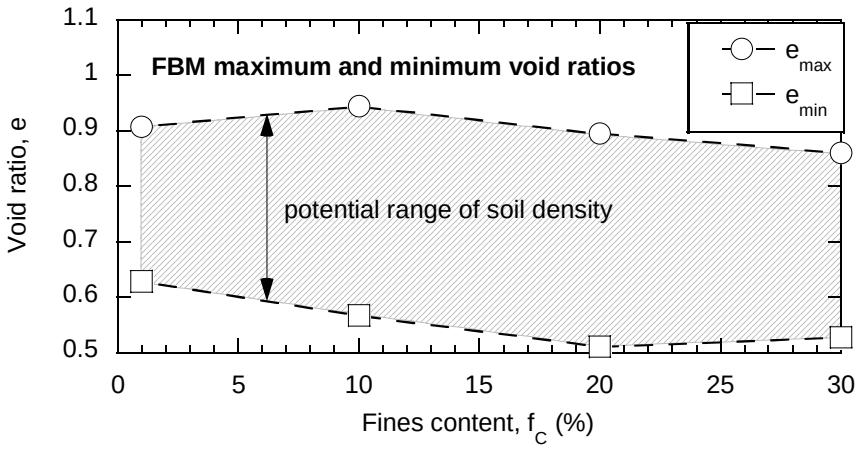

Figure 4-32 Maximum and minimum void ratios for the FBM sandy soils.

(2) The comment about the soil particle size composition refers to the volume of solid particles, V_s, and the lack of division between sand and fines particles in this parameter. V_s does not specify the relative amounts of sand and fines-sized particles within a soil, which clearly change as the FBM soil fines content is changed. This lack of division means that replacing sand particles with fines particles results in different numbers of soil particle contacts within the soil force-chain. Figure 4-33 provides a schematic illustration of the phase diagrams of clean sand, and sand with 25% fines.

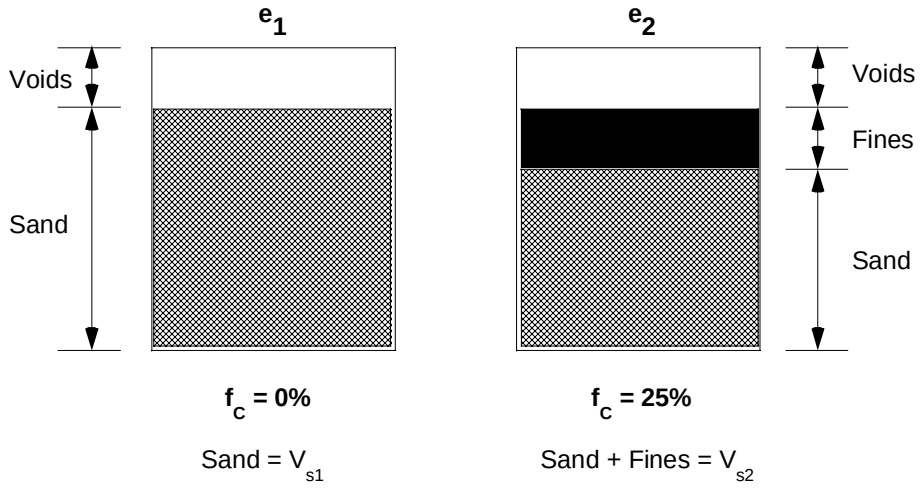

Figure 4-33 Phase diagrams of clean (f_C = 0%) and silty sand (f_C = 25%). Note that $e_1 = e_2$ because $V_{s1} = V_{s2}$.

The issue Figure 4-33 presents is that e_1 and e_2 are equal, even though the range of particle sizes are very different, as the silty sand would contain much smaller particles than the clean sand. Given that void ratio is an approximate index of particle contacts, this difference in particle size should physically result in a different arrangement of particle contacts in the internal force-chain as the sand and fines particles are mixed together. Thus by not differentiating between sand and fines particle sizes, similar void ratio values can potentially have very different particle contact arrangements in reality. Such differences can lead to the variation in the undrained monotonic response seen for the FBM soils at similar void ratio values. This issue is discussed further in Chapter 5, which discusses changes to the void ratio definition that includes parameters accounting for the different amounts of sand and fines-sized particles.

Relative density (D_r) is defined in Equation (4-2) in Section 4.1, using void ratio (e), maximum void ratio (e_{max}) and minimum void ratio (e_{min}). This defines the index of soil particle contacts in the same manner as void ratio, but includes the upper and lower limits for the void ratio as well (e_{max} and e_{min}). It avoids the complete lack of potential soil density range as discussed for the void ratio, but a number of extra issues arise when including the void ratio limits to help define the density of a mixture of sand and fines:

(1) e_{max} and e_{min} are not recommended for $f_C > 15\%$
(2) The procedures used to define e_{max} and e_{min} produce non-unique values
(3) e_{max} and e_{min} only truly apply to soil densities when normal stresses are nearly 0kPa

(1) Standards used throughout the world (American, British, Japanese, New Zealand) are all designed to determine e_{max} and e_{min} for clean sands, and sands with low fines content. These standards do not suggest using their procedures for fines contents above 15%. This makes e_{max} and e_{min} derived for soils with $f_C > 15\%$ potentially unreliable, such as those for FBM-20 and FBM-30. Some studies (Cubrinovski and Ishihara, 2002) have however shown that the use of the determination procedures for $f_C > 15\%$ soils do produce results consistent with the void ratio limits for soils with $f_C < 15\%$, making this an unresolved issue.

(2) The determination procedures used to define e_{max} and e_{min} vary across testing standards. Some standards, such as the American standard, provide multiple methods for determining e_{max} and e_{min} respectively. This means that the void ratio limits for a particular soil tend to vary when being determined using different procedures. It has also been shown (Cubrinovski and Ishihara, 2002) that different personnel using the same test procedure can produce reasonably different void ratio limit values for the same soil. This is illustrated in Figure 4-34 by the difference in e_{max} and e_{min} values for Toyoura Sand using JGS procedures.

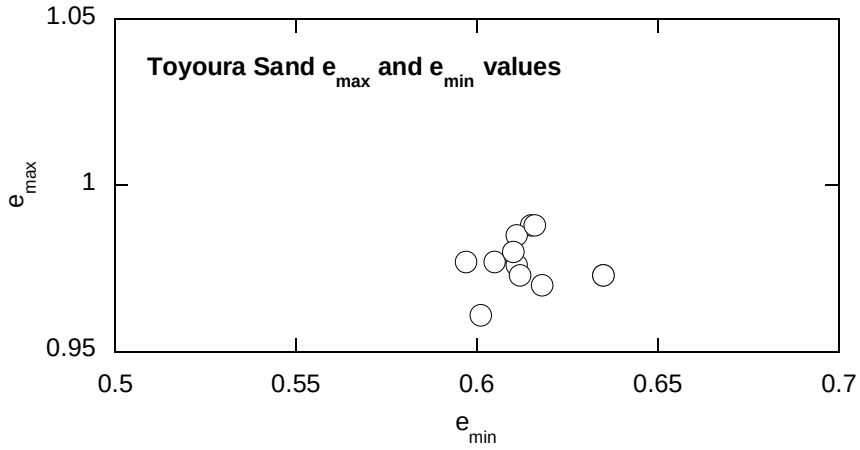

Figure 4-34 Variation in Toyoura Sand e_{max} and e_{min} values when performed by different personal (Cubrinovski and Ishihara, 2002).

(3) The void ratio limits are only accurate in describing the possible soil density range of a particular soil at a mean effective stress near to $p' \approx 0$kPa. The e_{max} and e_{min} limits should actually vary with mean effective stress, following the isotropic consolidation lines of the soil at the lowest and highest possible densities respectively. This difference is schematically illustrated in Figure 4-35.

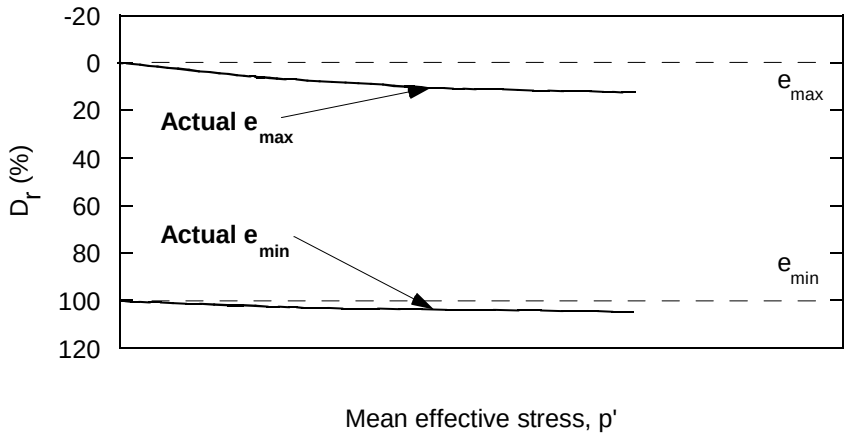

Figure 4-35 Schematic illustration of actual e_{max} and e_{min} values following the isotropic consolidation lines of the loosest and densest soil densities.

These three issues with the maximum and minimum void ratios are all relevant and must be considered when comparing the steady state lines of sand with changing fines content. They are not however, in the opinion of the author, more important than the lack of division between sand and fines-sized particles in the void ratio definition. This is clearly

supported by the consistent differences in the FBM steady state lines discussed in Section 4.2.6 when using both void ratio and relative density as the soil density measures. As such, two variations to the void ratio definition are discussed in Chapter 5 that treat the respective quantities of sand and fines particles separately.

4.3. Undrained Cyclic Response of the FBM Soils

A series of 57 cyclic triaxial tests were conducted on the FBM sandy soils to investigate the effects of fines on the undrained cyclic response of sand-fines mixtures. The test specimens were prepared using the procedures outlined in Chapter 3, and were loaded in a stress-controlled manner at a frequency of 0.0083Hz, or 2 min / load cycle. The targeted cyclic stress ratio (*CSR*) was fully-reversed, applying the same amplitude deviator stress (q) in both compression and extension, centering the symmetric loading around q = 0kPa. Cyclic liquefaction was defined as the number of load cycles required for specimens to reach 5% double amplitude axial strain during loading, which generally coincided with the initial liquefaction condition ($p' \approx$ 0kPa). The visually observed deformations of the soils, density effects, and the effects of fines content on the cyclic response are discussed in the following sections.

4.3.1. Visually Observed Deformations of the FBM Soils

The FBM specimens tended to respond to the load cycles by deforming in a similar manner, showing specimen softening. The similarity was due to the low levels of double amplitude axial strain being reached, which were $\varepsilon_a < 5\%$, as compared to the monotonic tests described in Section 4.2.1 which reached $\varepsilon_a = 40\%$.

Visual changes in the specimens were difficult to detect by eye at the beginning of loading, but became more apparent as the mean effective stress approached zero. This involved the inconsistencies visible on the specimen surface at the start of loading, as illustrated in Figure 4-36 (a), becoming less distinguishable. Once initial liquefaction had been reached the specimen surface had much fewer irregularities, as is displayed for the FBM-20 specimen with e = 0.606 in Figure 4-36 (b).

In some cyclic tests the loading was continued for a few cycles after cyclic liquefaction had been reached just to observe the post-liquefaction specimen response. This generally resulted in more deformation to the overall specimen shape than is shown in Figure 4-36 (b) when initial liquefaction was first reached. The post-liquefaction cycles caused slight necking

of the specimen near the base pedestal and top-cap respectively, along with increased non-uniformity in the shape of the specimen.

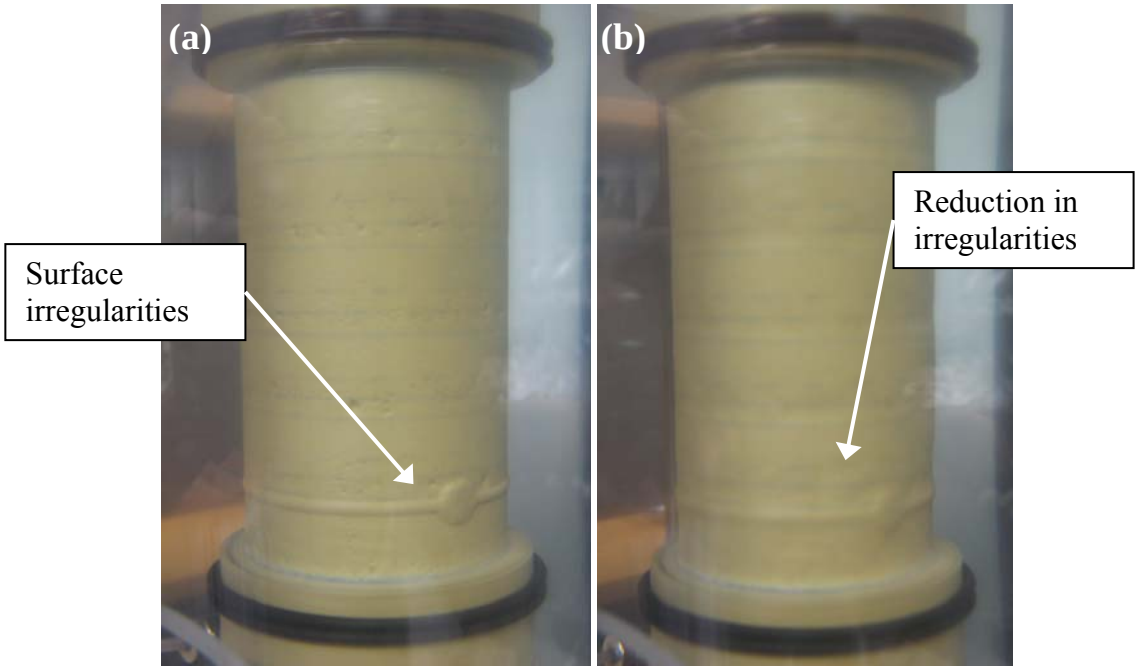

Figure 4-36 FBM-20 test specimen with e = 0.606 at (a) p'_i = 100kPa, and (b) p' = 0kPa. Note the inconsistencies in membrane texture at p'_i = 100kPa and the increased texture uniformity when p' = 0kPa.

4.3.2. Extrapolation of the Stress-strain Response Curves

The cyclic stress ratio applied to the FBM soils during cyclic loading degraded as the mean effective stress approached zero. This was an issue related to the triaxial apparatus limitations, as similar degradation occurred during the cyclic testing of clean Albany Sand (Roper, 2006) on the same apparatus. It appeared that as each specimen approached initial liquefaction, the motorised triaxial cell could not apply enough axial strain in the required load cycle time to reach the target deviator stress.

Some interpretation of the stress-strain curves was therefore required, due to the stress degradation, to enable the number of cycles to reach 5% double amplitude axial strain N_C to be identified. The interpretation is illustrated in Figure 4-37 for the FBM-20 specimen with e = 0.606.

The error between reaching N_C based on the extrapolated curves and based on the actual measured 5% double amplitude axial strain was estimated to be very small, generally less than one load cycle for N_C of about 20 cycles. This error corresponds to a relatively small change

in the position of the liquefaction resistance curve, which does not affect the overall trends observed for the FBM cyclic responses. Also note that initial liquefaction occurred within 1 – 2 cycles of cyclic liquefaction being reached (see Chapter 3).

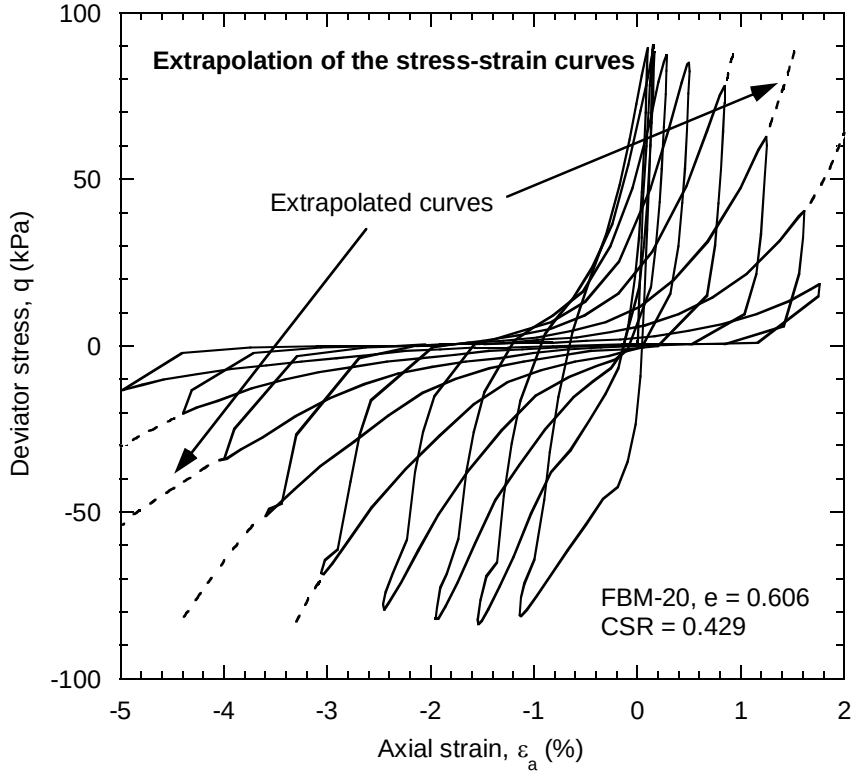

Figure 4-37 Interpretation of the stress-strain curves for the FBM-20 specimen with e = 0.606. The extrapolated sections of the curves are dashed. N_C = 6 based on the extrapolated curves, and N_C = 7 based on the actual measured curves.

4.3.3. Derivation of the Liquefaction Resistance Curve

The liquefaction resistance curves were derived by plotting the test cyclic stress ratio *CSR* against the number of cycles required to reach 5% double amplitude axial strain. The curves themselves were approximated by passing solid lines through test data with similar soil densities. The densities used in these tests are summarized in Table 4-2, in Section 4.3.4.

As discussed in Section 4.3.2, extrapolation of the stress-strain curves was required to identify the number of cycles to liquefaction N_C. Once this extrapolation had been performed, the stress-strain response was used to obtained (a) N_C, and (b) *CSR*. These are illustrated in the stress-strain response in Figure 4-38 of the FBM-30 specimen with e = 0.693 (D_r = 50%).

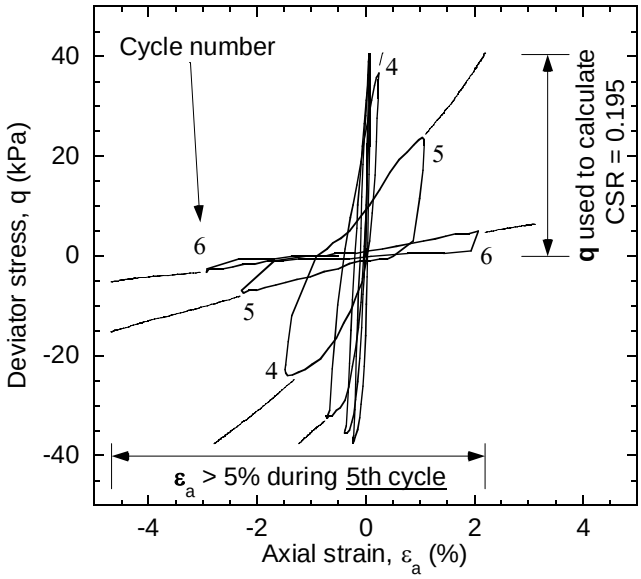

Figure 4-38 Derivation of N_C and *CSR* from the stress-strain response. In this example the double amplitude axial strain of 5% was reached in the 5th loading cycle.

4.3.4. Effects of Density on the Cyclic Response of FBM Soils

As discussed in Section 4.2.2 for the monotonic tests, an increase in soil density results in an increase in soil strength and a tendency for more dilative or less contractive response. Comparable trends were also observed during the cyclic tests of the FBM soils. To illustrate these, the stress-strain, stress-path, and excess pore water pressure responses of the FBM soils with different fines contents are compared across varying specimen densities. The cyclic stress ratio is kept constant at approximately *CSR* = 0.2, which allows response comparison at similar loading conditions for all tests. The liquefaction resistance curves of the FBM soils are also presented, and are used to summarize the increase in soil liquefaction resistance with increased soil density.

Note that 3 – 4 cyclic tests were performed at a given specimen density, with the cyclic stress ratio being varied for each test. Table 4-2 presents the tested specimen densities of the FBM sandy soils used in the cyclic tests.

Table 4-2 Representative specimen test densities of the FBM soils used for cyclic testing.

Soil	Test void ratios	Test relative densities
FBM-1	$e \approx 0.888, 0.823, 0.738$	$D_r \approx 7, 30, 60\%$
FBM-10	$e \approx 0.815, 0.789, 0.742, 0.711$	$D_r \approx 37, 45, 58, 67\%$
FBM-20	$e \approx 0.668, 0.604$	$D_r \approx 59, 76\%$
FBM-30	$e \approx 0.708, 0.693, 0.630, 0.592$	$D_r \approx 46, 50, 69, 80\%$

Figure 4-39 to Figure 4-42 present the stress-strain, stress-path, and excess pore water pressure responses during cyclic loading of the four FBM soils. The response of two tested specimens of each soil is shown, with the density and applied cyclic stress ratio being reported. Note there are no apparent differences in the general response as f_C is increased.

The stress-strain responses of the FBM soils indicate the number of cycles N_C required to reach cyclic liquefaction and also show the stiffness degradation of the soil specimens. The number of cycles to liquefaction clearly increases as the soil density increases. The FBM-1 test specimen with e = 0.890 (D_r = 6%) only requires two load cycles at a CSR = 0.209 to reach cyclic liquefaction. When the density is increased to e = 0.820 (D_r = 31%), cyclic liquefaction occurs after 14 load cycles at a CSR = 0.194. This expected trend of increasing liquefaction resistance is observed for all the FBM sandy soils, and is comparable to the increase in strength with increase in soil density seen for the FBM monotonic tests, discussed in Section 4.2.2. The liquefaction resistance of the soils, with particular attention as to the effects of fines, is discussed in more detail in Section 4.3.5 using cyclic resistance curves.

Note that the stiffness degradation of the cyclic test specimens is directly related to the liquefaction resistance. The majority of degradation occurs during approximately the final five cycles before cyclic liquefaction is reached, meaning that higher soil densities retain the bulk of their initial stiffness for a larger amount of load cycles than for the lower soil densities. Thus significant soil deformations are limited for longer when the soil density is higher. Also, the development of progressive deformation following liquefaction is slower for denser soils.

The rate at which the mean effective stress decreases in the FBM test specimens is best illustrated by the stress-path responses. Higher soil densities display smaller drops in mean effective stress during each load cycle, resulting in more cycles required to reach a mean effective stress of zero, or initial liquefaction. For example, the FBM-30 test specimen with e = 0.693 (D_r = 50%) reaches $p' \approx$ 0kPa after five load cycles – an average decrease of 20kPa / load cycle. The test specimen with e = 0.631 (D_r = 69%) however reaches $p' \approx$ 0kPa after 25 load cycles – an average decrease of 4kPa / load cycle. This shows that the denser specimens exhibit less contractive behaviour throughout the course of cyclic loading. Interestingly, the FBM-1 specimen with e = 0.890 (D_r = 6%) displays flow-type response when loaded in extension during the first load cycle, as shown in Figure 4-39 (c). This leads to cyclic liquefaction being reached in the subsequent load cycle.

Note that the mean effective stress does not remain constant once $p' \approx$ 0kPa is reached, unlike the response observed for the monotonic tests. Instead, the mean effective stress follows a ‘butterfly loop’ typical for cyclic mobility.

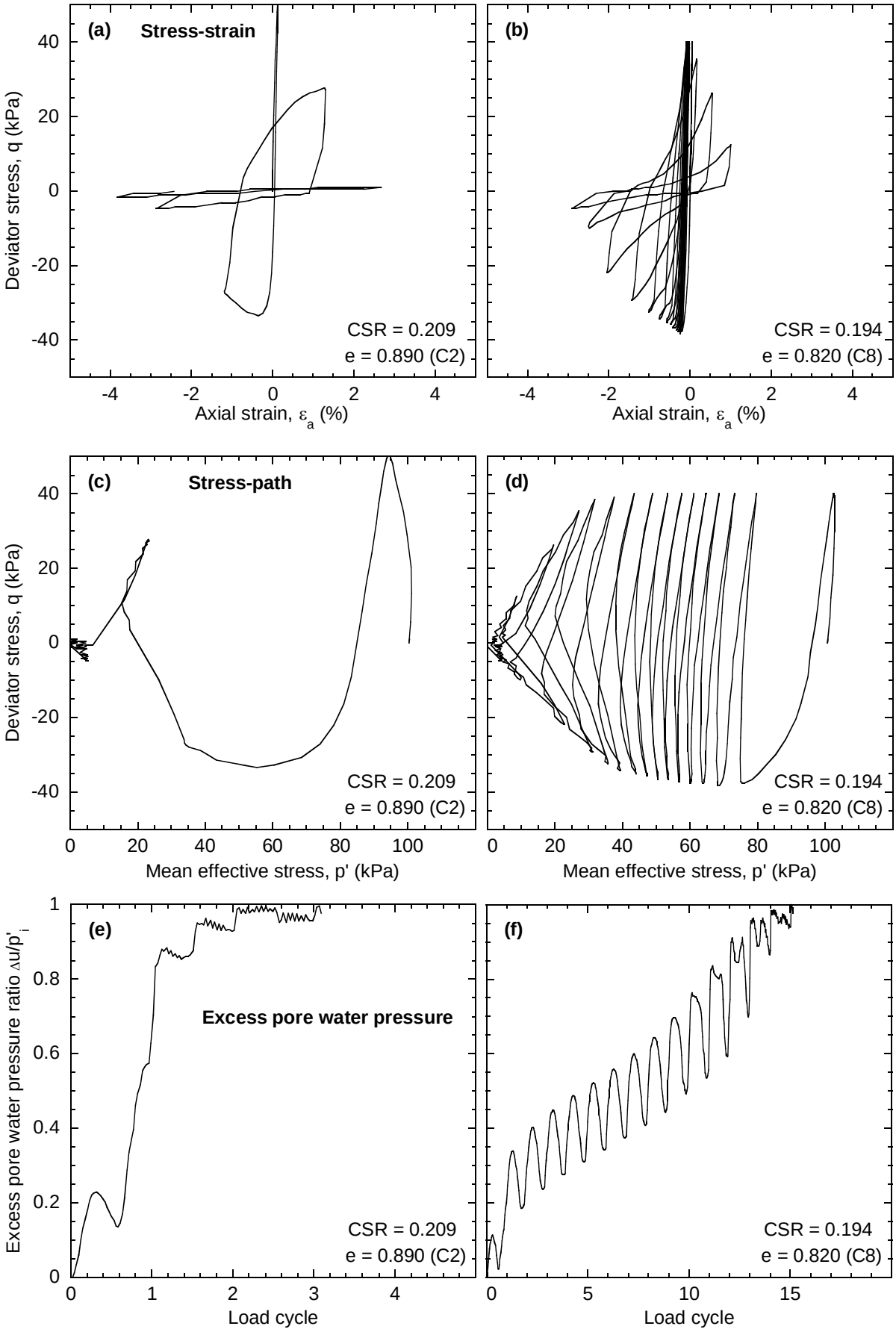

Figure 4-39 Cyclic response of two FBM-1 test specimens with $CSR \approx 0.2$, $D_r \approx 7$ and 30%.

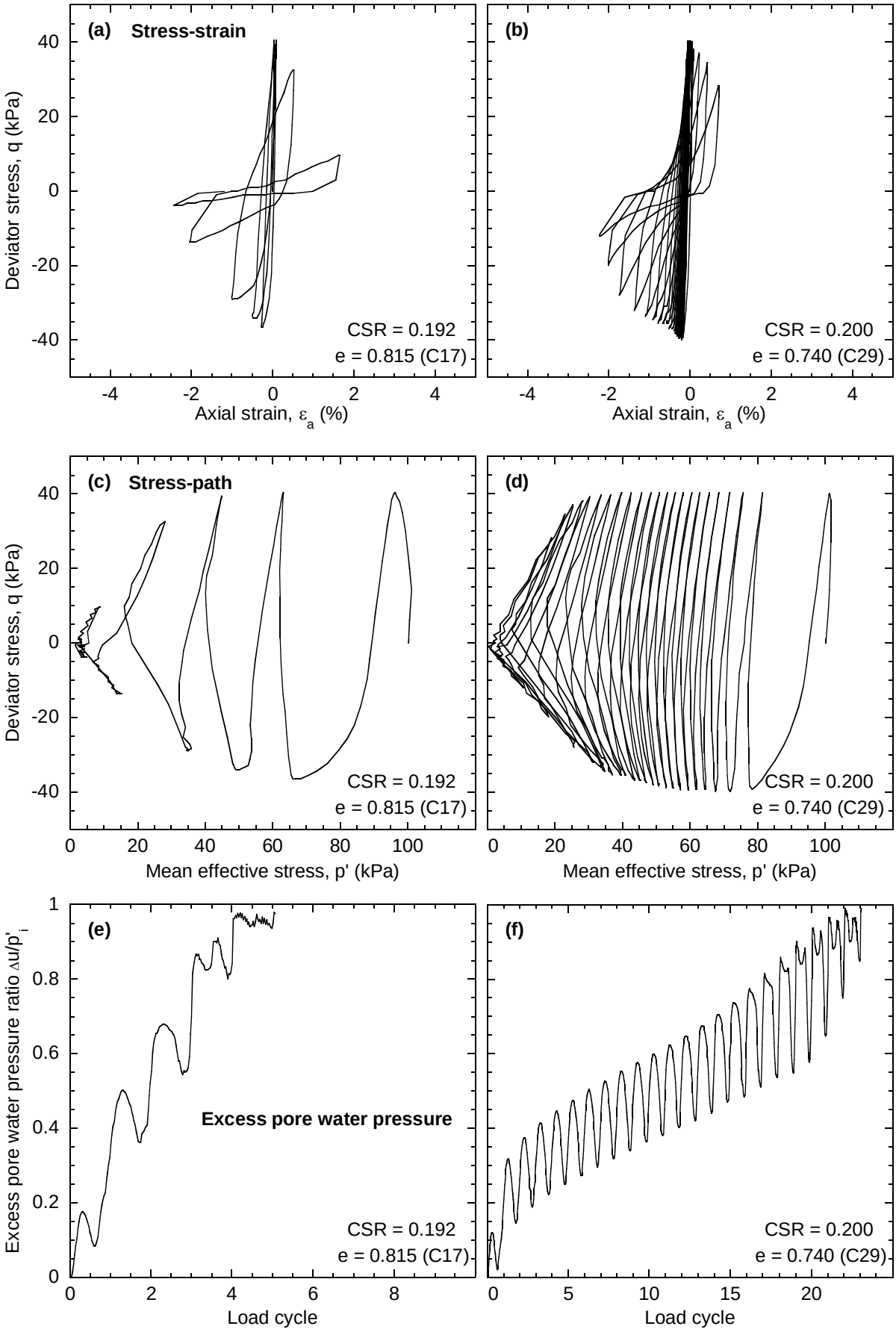

Figure 4-40 Cyclic response of two FBM-10 test specimens with $CSR \approx 0.2$, $D_r \approx 37$ and 58%.

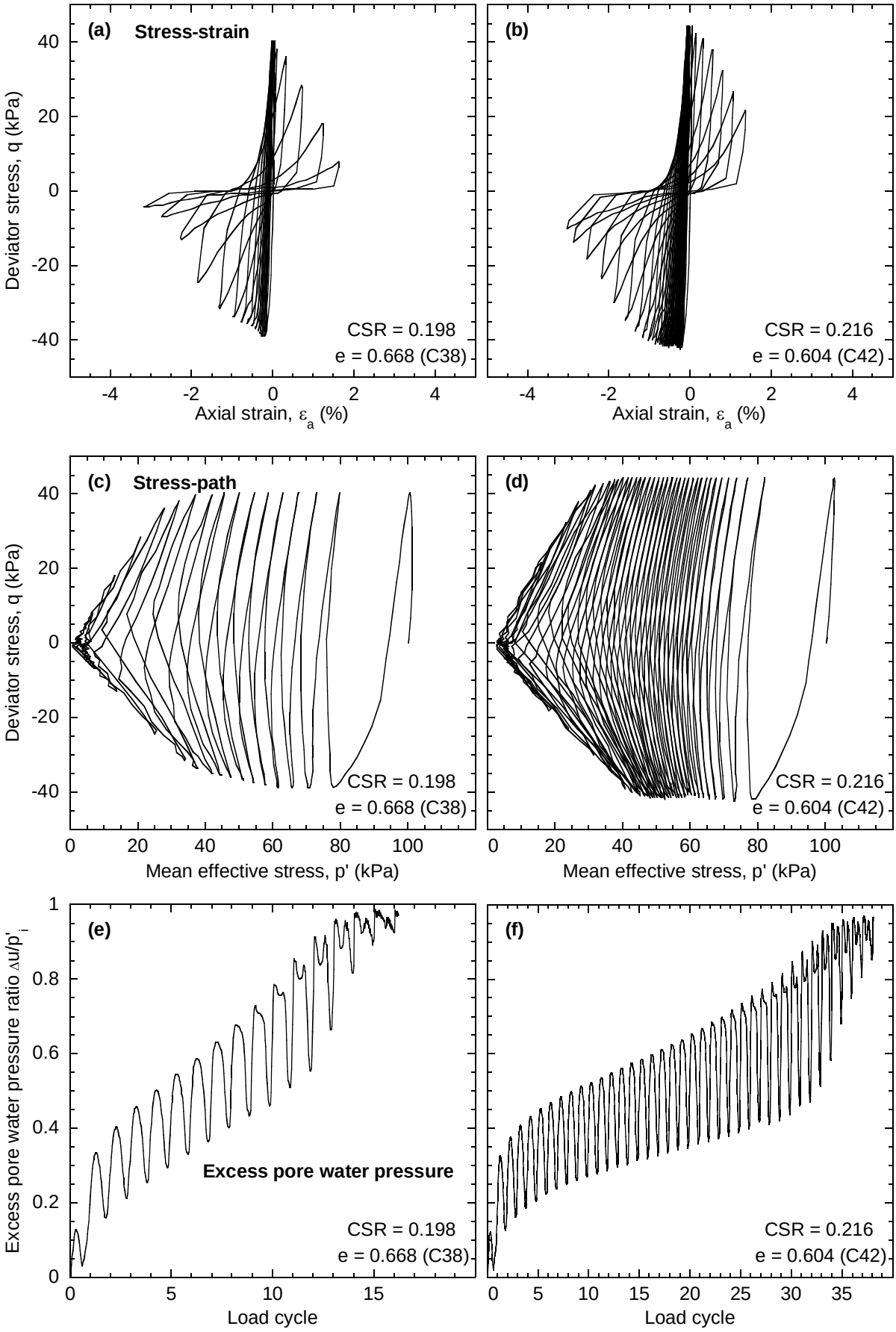

Figure 4-41 Cyclic response of two FBM-20 test specimens with $CSR \approx 0.2$, $D_r \approx 59$ and 76%.

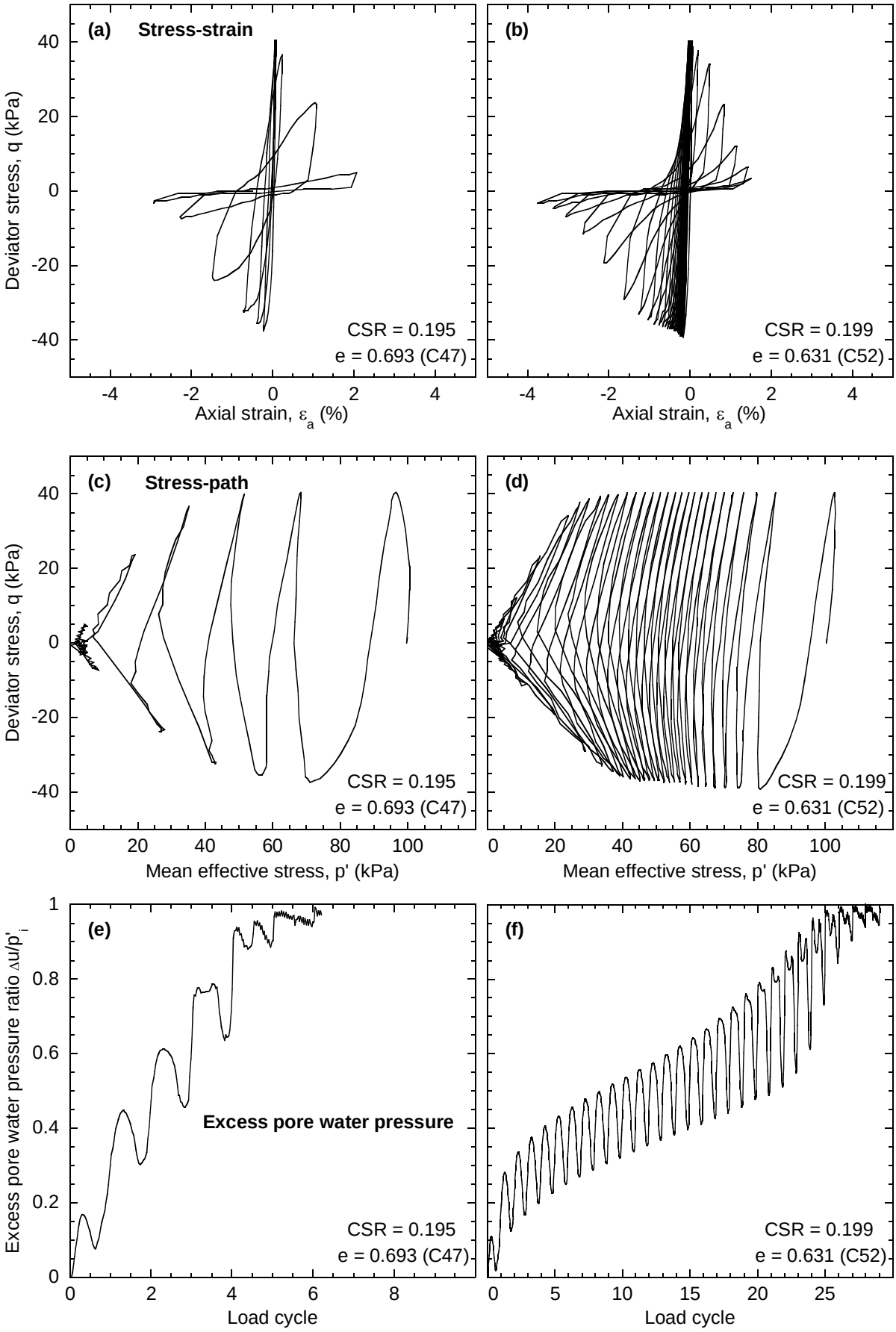

Figure 4-42 Cyclic response of two FBM-30 test specimens with $CSR \approx 0.2$, $D_r \approx 50$ and 69%.

Figure 4-43 to Figure 4-46 present the liquefaction resistance curves for different relative densities of the four FBM soils. These curves best summarize the increase in soil liquefaction resistance with increasing soil density, as previously discussed using the stress-strain responses.

The liquefaction resistance curves of the FBM soils also demonstrate how a change in density affects the number of load cycles required to reach liquefaction as the cyclic stress ratio is varied. This is essentially described by the shape of the liquefaction resistance curves – as the density of the soils increase, so do the slopes of the curves. This means that for a low specimen density, a small increase in the cyclic stress ratio may significantly reduce the number of cycles to liquefaction, N_C. However, as density increases, the same variation in the cyclic stress ratio will result in a smaller reduction in the number of cycles required to reach liquefaction. This makes the resistance to liquefaction of the FBM soils less sensitive to the cyclic stress ratio when the soil density is higher.

Note that this effect is most significant when cyclic liquefaction is reached in 10 load cycles or less. An interpretation of the liquefaction resistance curves of the FBM soils normalized by the cyclic stress ratio of each curve when N_C = 15 (Cubrinovski and Rees, 2008) showed that the normalized slopes of the curves were very similar when N_C > 10. However, the normalized liquefaction resistance curves showed significant differences in normalized slope in the region where N_C < 10, with the higher specimen density curves displaying greater slopes.

In summary, increased soil densities had the following effects on the undrained cyclic response of the FBM soils:

- Liquefaction resistance of the FBM soils increased
- More load cycles were needed for stiffness degradation to occur
- Mean effective stress decreased at a lower rate
- Greater slope of the liquefaction resistance curves. This corresponded to a reduction in sensitivity to variation in the cyclic stress ratio for the liquefaction resistance.

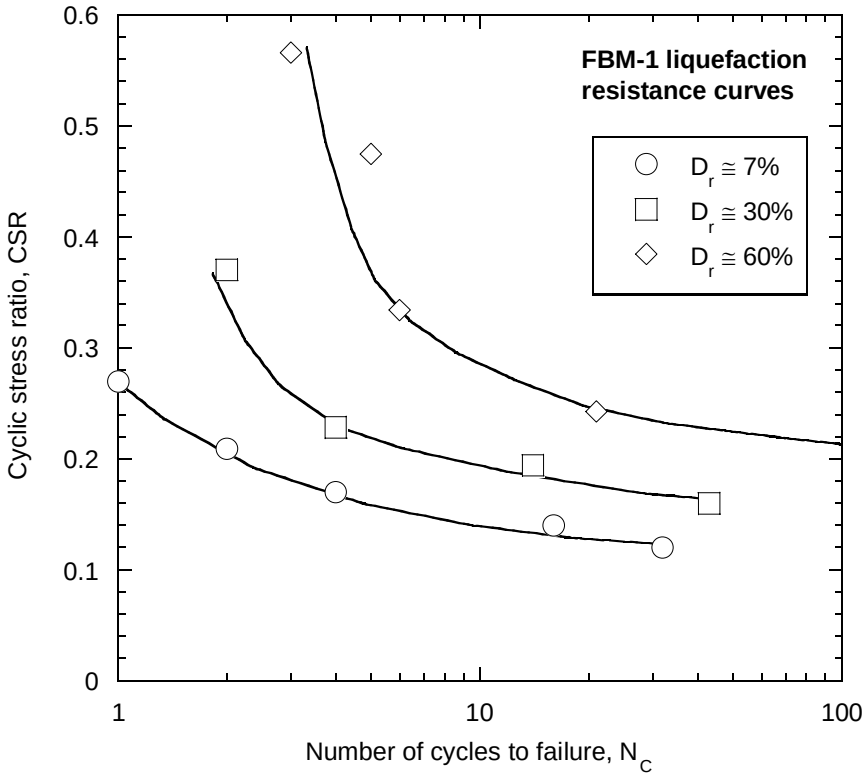

Figure 4-43 Liquefaction resistance curves of the FBM-1 soil.

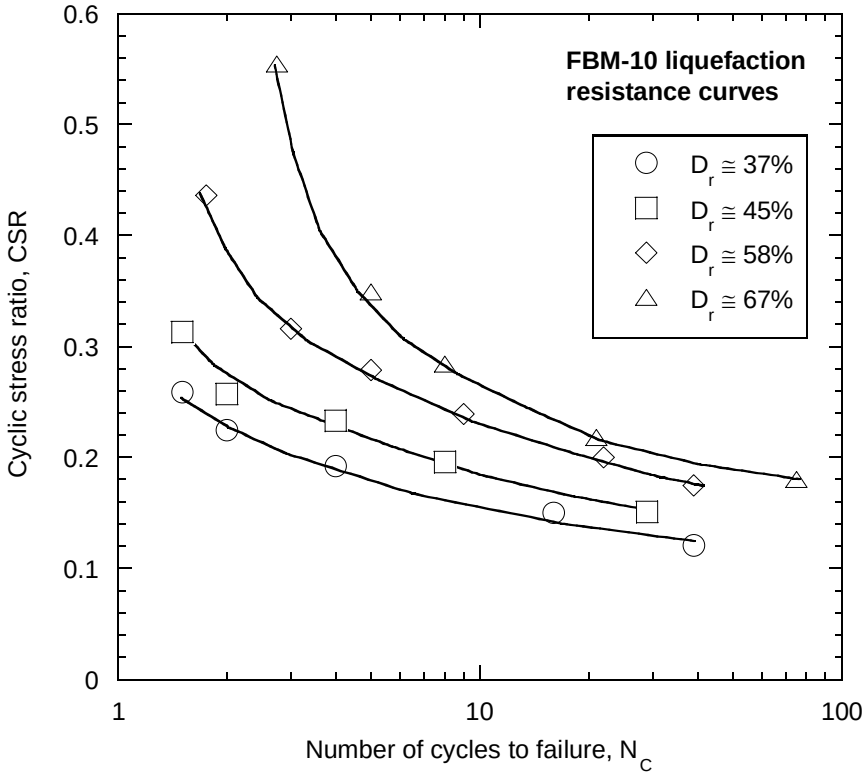

Figure 4-44 Liquefaction resistance curves of the FBM-10 soil.

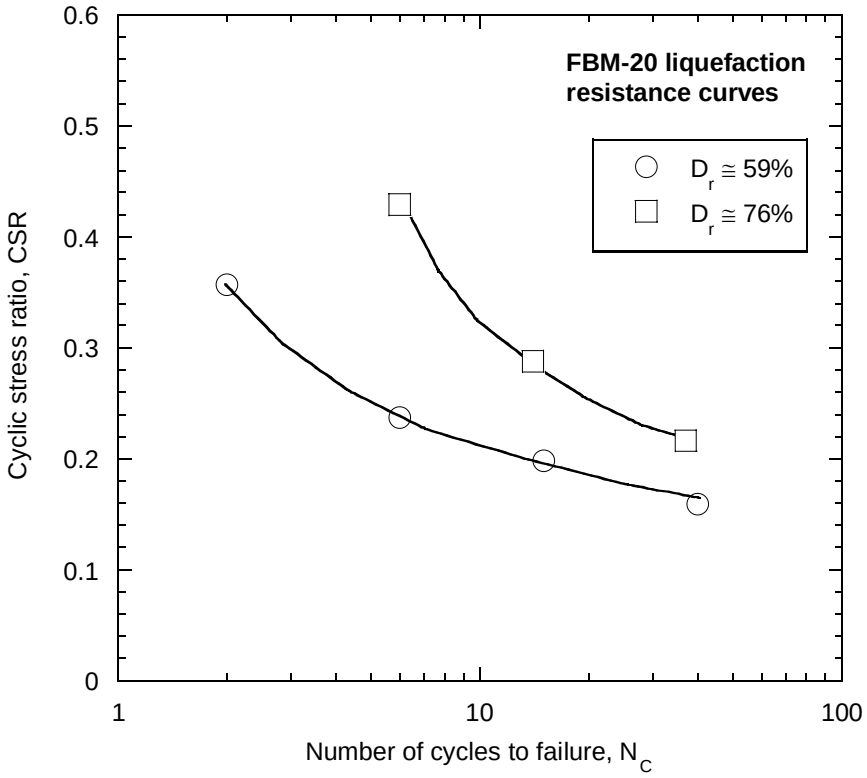

Figure 4-45 Liquefaction resistance curves of the FBM-20 soil.

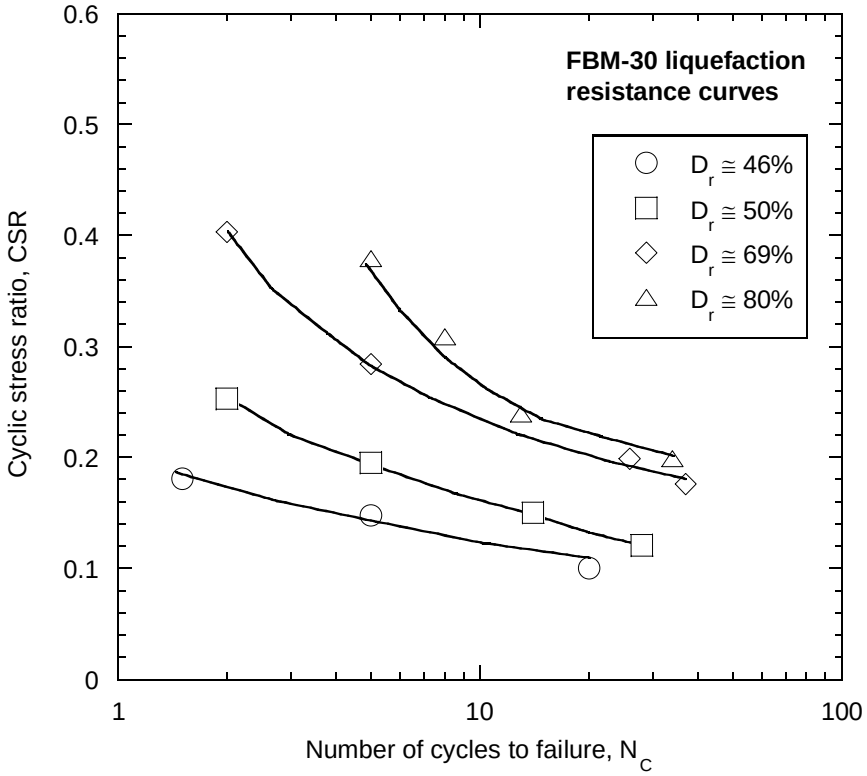

Figure 4-46 Liquefaction resistance curves of the FBM-30 soil.

4.3.5. Effects of Fines on the Cyclic Resistance of FBM Soils

Variation in the fines content of the FBM sands was shown in Section 4.2.3 to affect the undrained monotonic response through a change in the location of the steady state line in the e – p' plane. The fines content also has an effect on the undrained cyclic response of the FBM sands, and is investigated using the cyclic resistance curves as a reference for soil response. The definition and derivation procedure of the cyclic resistance curves are discussed in Section 4.1.2. The four state measures presented in Section 4.1 are used to compare the cyclic resistance curves of the FBM soils. Two of these parameters are purely density measures:

- Void ratio, e
- Relative density, D_r

The other two parameters are more robust state measures, and were first presented in Section 4.1:

- State parameter, ψ
- State index, I_s

Two different N_C values have been used to compare the liquefaction resistances of the FBM soils – the CSR at N_C = 5 and N_C = 15. Note that at N_C = 5 the liquefaction resistance curves in Section 4.3.4 have higher curvature than at N_C = 15. As discussed in Section 4.1.2, soils with density and applied cyclic stress ratio conditions well above the cyclic resistance curve will reach liquefaction in fewer cycles than N_C.

Figure 4-47 to Figure 4-50 display the cyclic resistance curves using void ratio and relative density for N_C = 5 and N_C = 15. In each of the plots the cyclic resistance curves of the FBM soils with higher fines contents are located at higher densities. This is summarized in Figure 4-51 using CSR = 0.2 and N_C = 15.

The observed trend means that, for a given density and cyclic stress ratio, the FBM soils with lower fines contents will reach cyclic liquefaction after more load cycles than the soils with higher fines contents. The liquefaction resistance of the FBM soils therefore appears to decrease as the fines content is increased. This trend has also been observed during other studies investigating the undrained cyclic response of sandy soils (Vaid, 1994; Carraro et al., 2003).

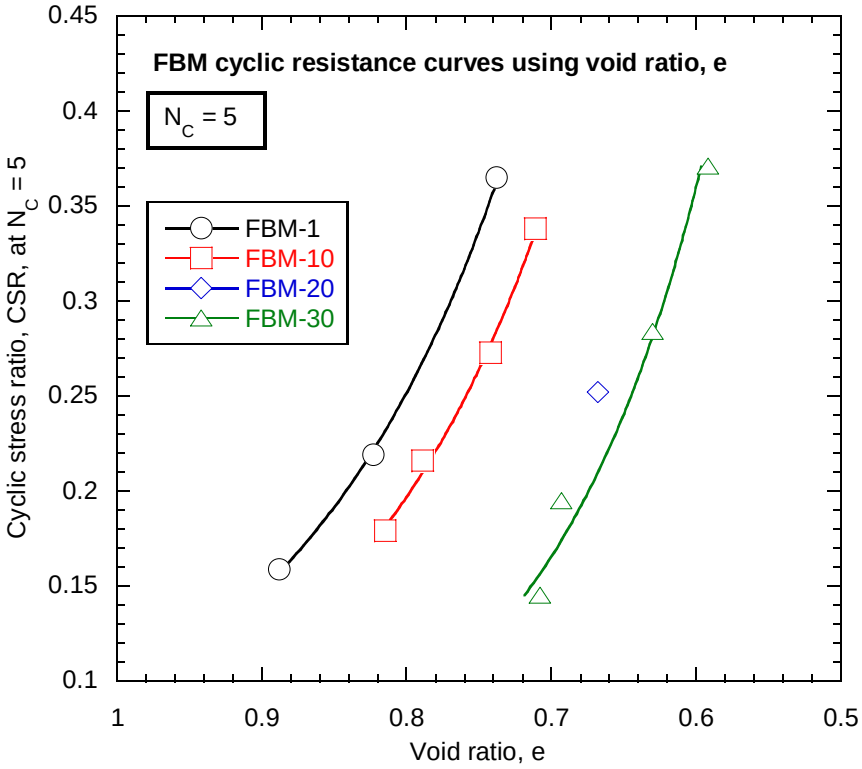

Figure 4-47 Cyclic resistance curves at $N_C = 5$ using void ratio, e.

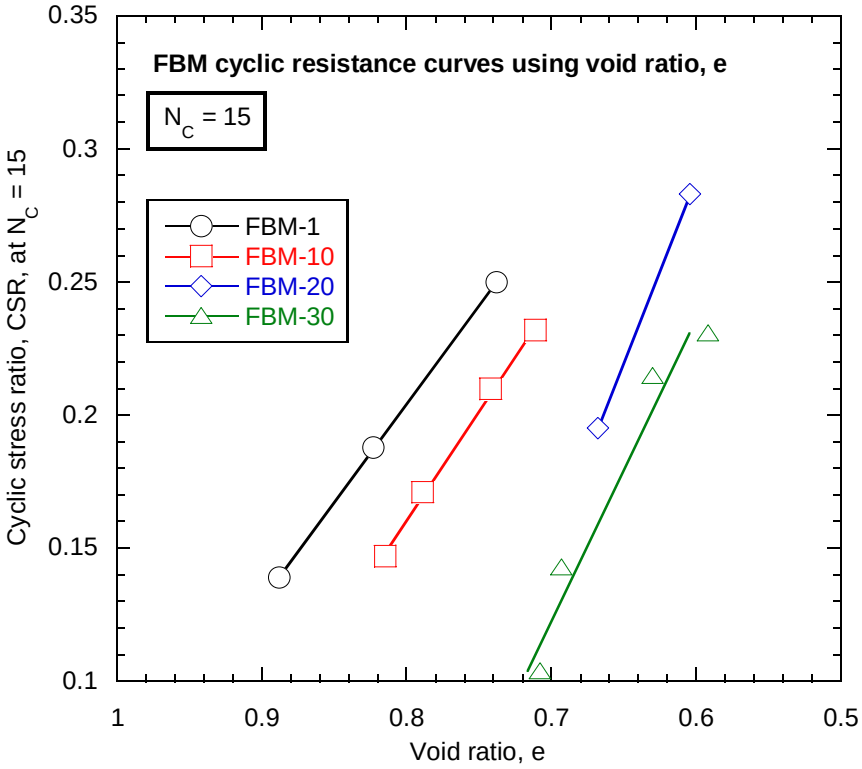

Figure 4-48 Cyclic resistance curves at $N_C = 15$ using void ratio, e.

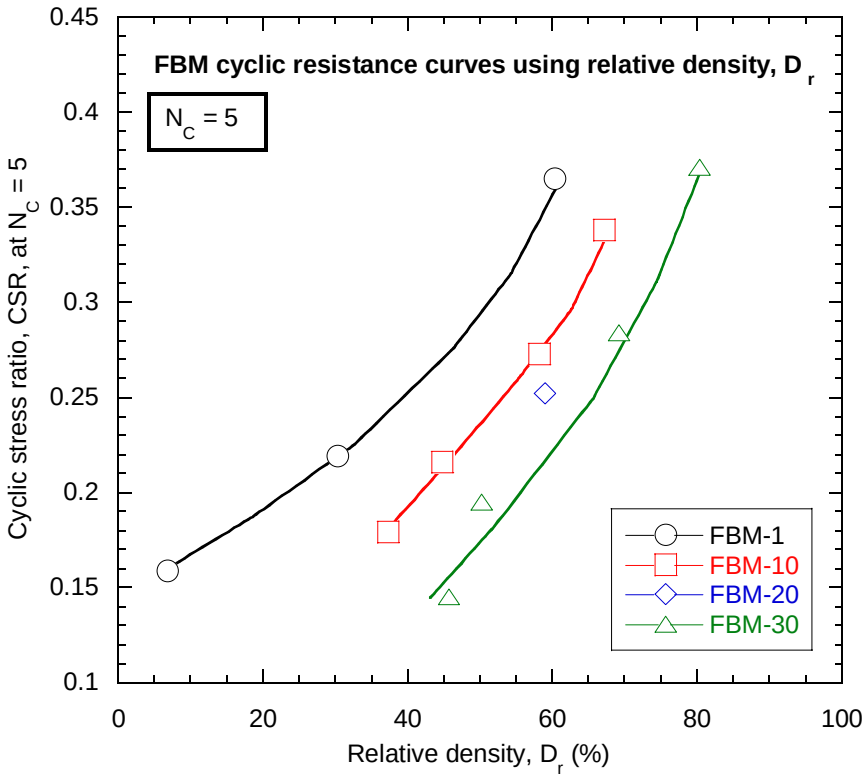

Figure 4-49 Cyclic resistance curves at $N_C = 5$ using relative density, D_r.

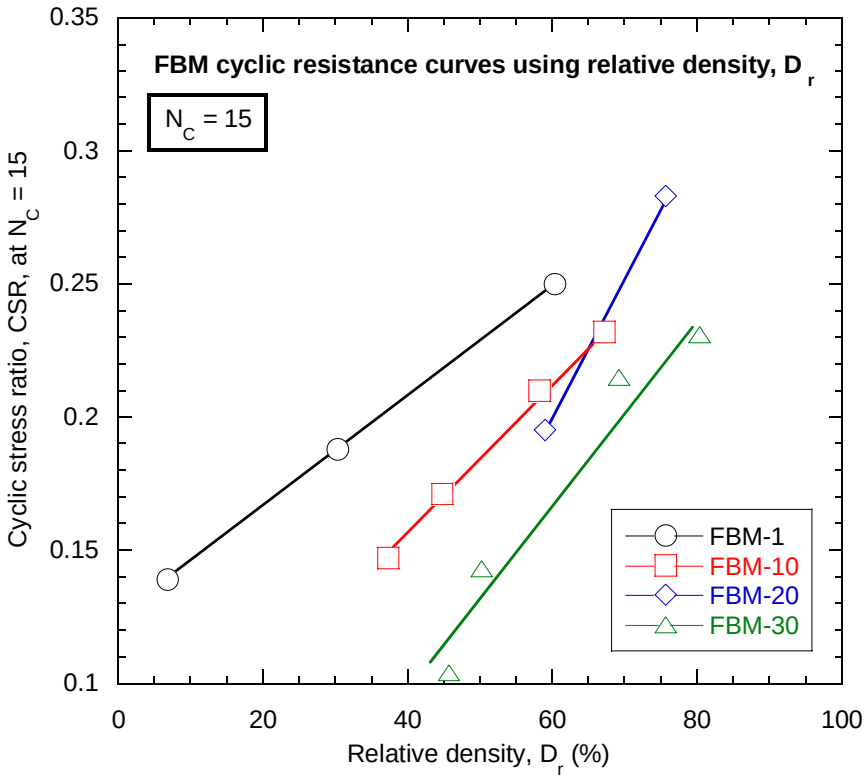

Figure 4-50 Cyclic resistance curves at $N_C = 15$ using relative density, D_r.

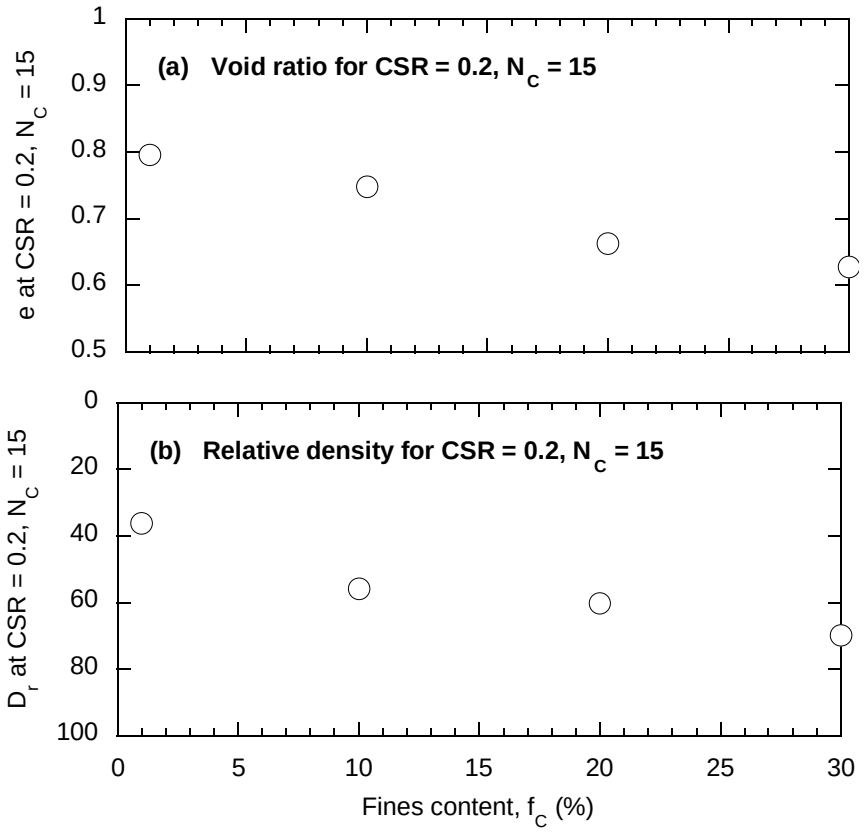

Figure 4-51 Change in cyclic resistance curve location when $CSR = 0.2$, $N_C = 15$ for the FBM soils using void ratio and relative density.

Physically these results suggest that the higher fines content soils are more contractive, causing a faster rate of excess pore water pressure generation and faster rate of decrease in mean effective stress when e or D_r is used as a basis for comparison. Note that these were the same effects discussed in Section 4.2.3 when comparing the effects of fines on the undrained monotonic response of the FBM soils. This means that when using void ratio or relative density to characterize the state of the FBM soils, the effects of fines on the undrained monotonic and cyclic responses are similar – higher fines contents correspond to more contractive soil behaviour.

The effects of increased fines content on the cyclic response of the FBM soils when using void ratio or relative density are summarized in the following:

- The response was more contractive
- Liquefaction resistances of the FBM soils decreased

Figure 4-52 to Figure 4-55 present the cyclic resistance curves using the state parameter and state index for N_C = 5 and N_C = 15. Negative values of the state parameter well below zero correspond to initial states well below the steady state line. Such states also correspond to higher soil densities, which result in more dilative soil response during undrained monotonic loading. It is interesting that the cyclic resistance curves of the FBM soils with higher fines contents are located at state parameter values closer to zero than the soils with lower fines contents, which are located at more negative state parameter values. This trend is summarized in Figure 4-56 using the curve locations at CSR = 0.2 and N_C = 15. It suggests that, when the state parameter is used as the state measure, the lower fines content soils are more contractive and have less resistance to cyclic liquefaction. This is opposite to the trend observed when using void ratio or relative density as the state measure.

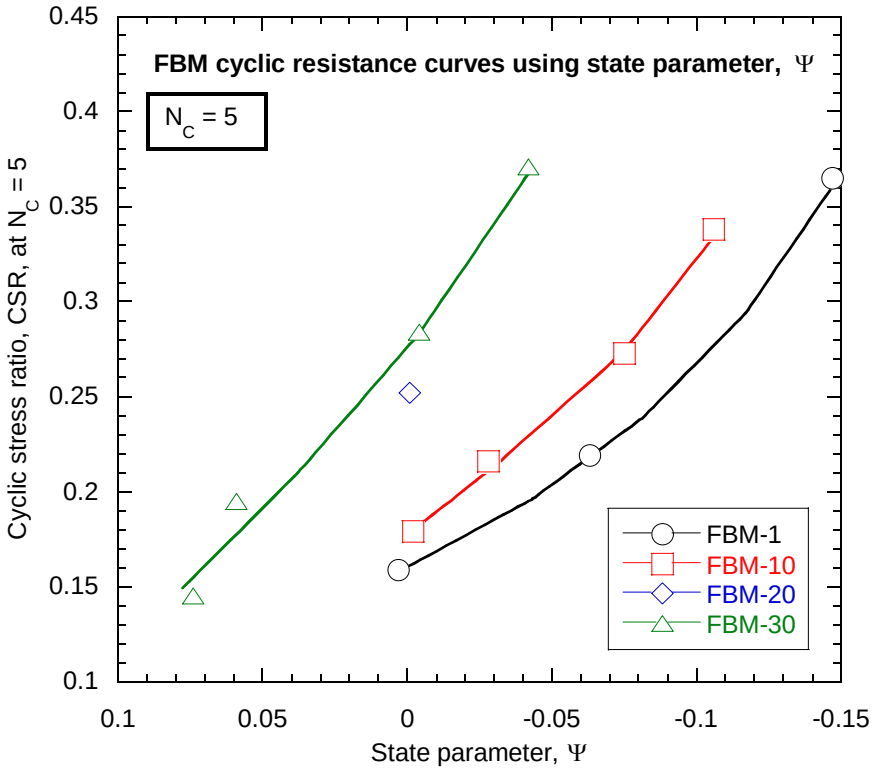

Figure 4-52 Cyclic resistance curves at N_C = 5 using state parameter, ψ.

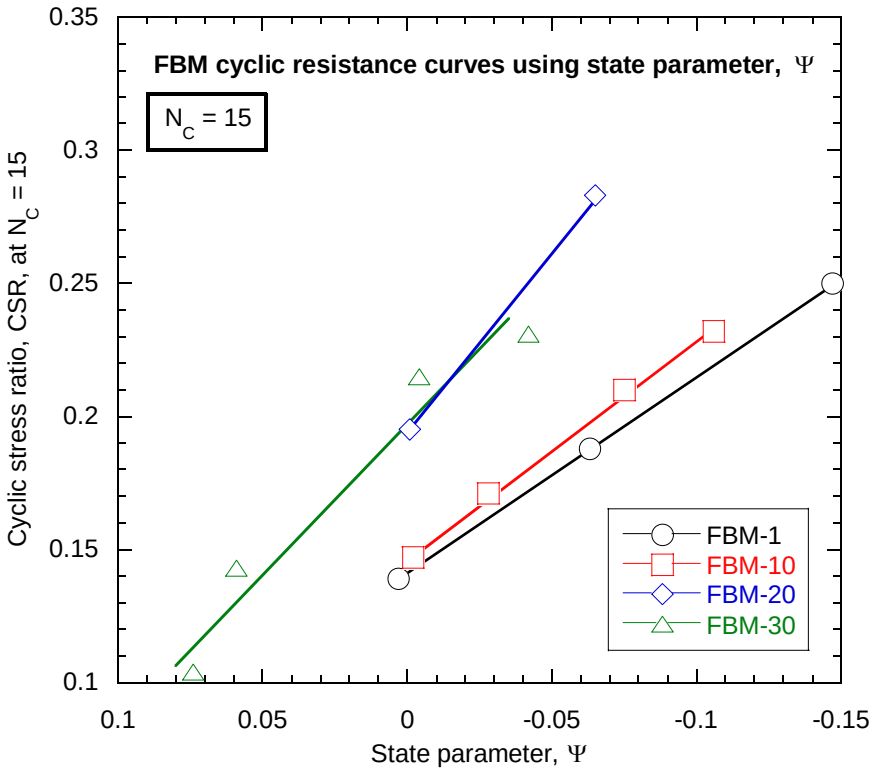

Figure 4-53 Cyclic resistance curves at $N_C = 15$ using state parameter, ψ.

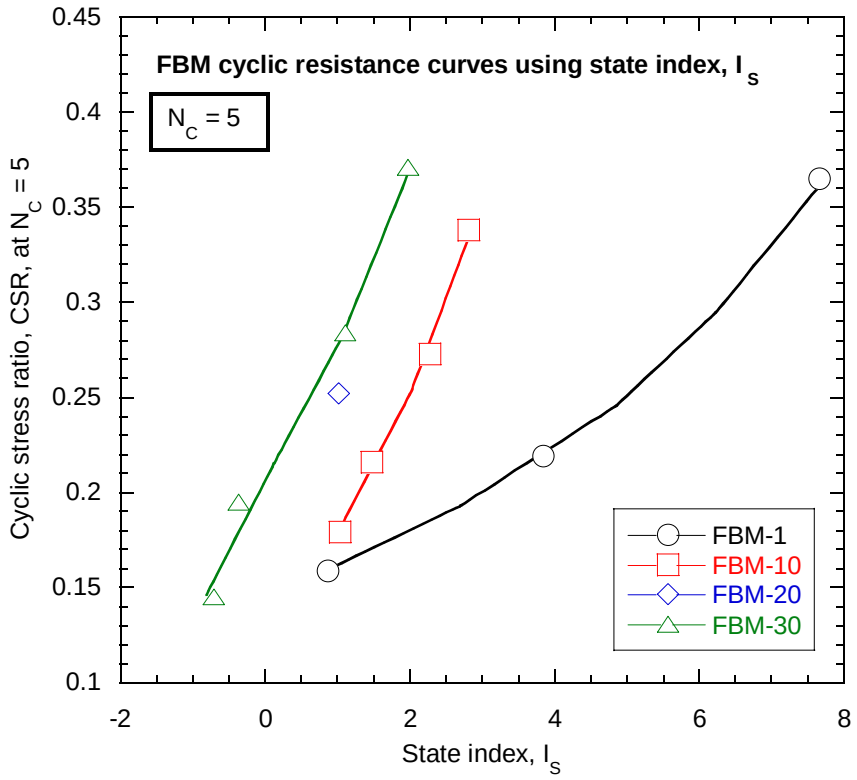

Figure 4-54 Cyclic resistance curves at $N_C = 5$ using state index, I_s.

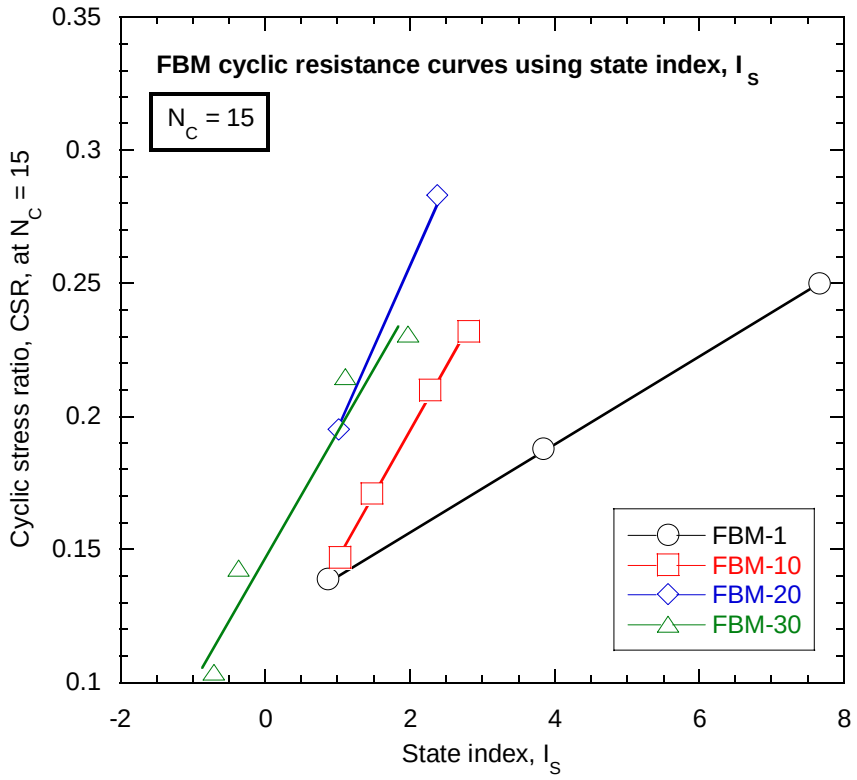

Figure 4-55 Cyclic resistance curves at N_C = 15 using state index, I_s.

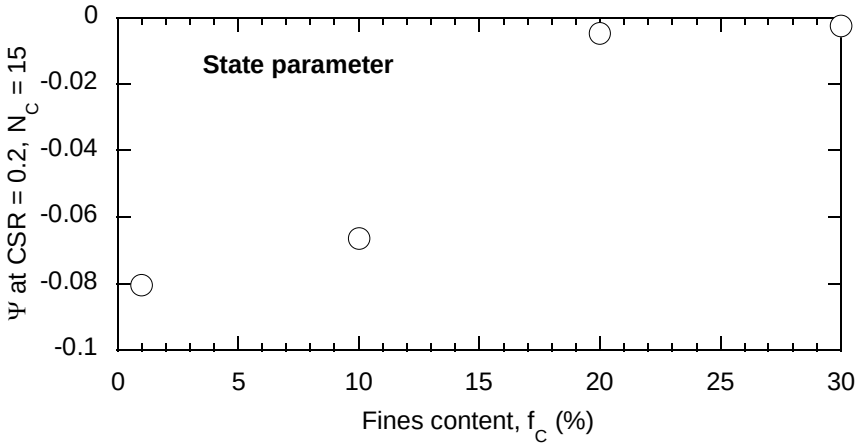

Figure 4-56 Change in cyclic resistance curve location when CSR = 0.2, N_C = 15 for the FBM soils using the state parameter.

As presented in Section 4.3.4 with the stress-strain responses, the majority of load cycles observed during a cyclic test on the FBM soils occurred at very low axial strains, ε_a < 1%. This means that the majority of excess pore water pressure generation also occurred at very low levels of axial strain. The state parameter however relates the soil void ratio (e) to the void ratio at the steady state of deformation (e_{ss}), which occurs at $\varepsilon_a \approx$ 40%. This means

that the monotonic strain levels used to define state do not relate to the relevant levels of strain associated with pore water pressure generation in the cyclic tests.

Figure 4-57 presents the excess pore water pressure development up to ε_a = 1% during the monotonic tests for FBM soil specimens with similar state parameter values. This plot clearly shows that up to 1% axial strain the soils with lower fines contents actually show a more contractive response, even though at the steady state of deformation the respective amounts of contraction for each soil are approximately similar. As such, Figure 4-57 explains why the FBM soils with lower fines contents display lower resistance to cyclic liquefaction when using the state parameter as a state measure – these soils are actually more contractive at the very low levels of axial strain which are relevant to the development of excess pore water pressures. This increased tendency for contraction results in fewer load cycles being required to reach cyclic liquefaction.

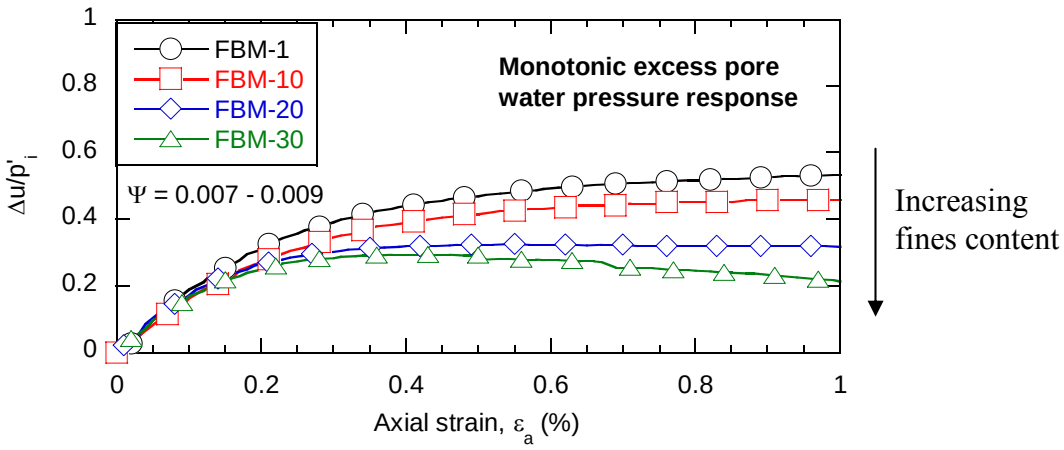

Figure 4-57 Monotonic excess pore water pressure response for the FBM soils with similar state parameter values.

The cyclic resistance curves in Figure 4-54 and Figure 4-55 using the state index also suggest that the lower fines content FBM soils have lower resistance to liquefaction, and the locations of these curves at CSR = 0.2 and N_C = 15 are summarized in Figure 4-58. The reasons for this apparent conclusion are the same as those for the state parameter, as discussed above. The state index relates initial state to the void ratio at the steady state of deformation for a given initial confining stress, and the void ratio of the steady state line at p' = 0kPa. As shown in Figure 4-57, similar amounts of contraction at the steady state of deformation do not correspond to similar amounts at very low levels of axial strain, causing the lower fines content soils to appear less resistant to cyclic liquefaction.

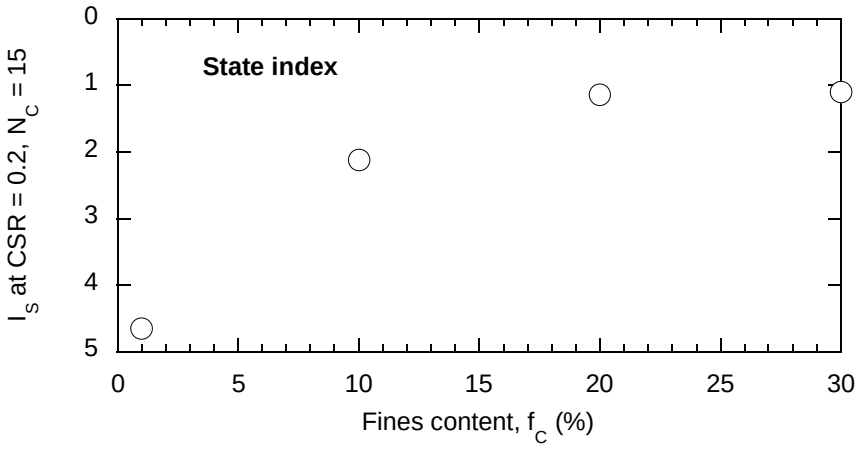

Figure 4-58 Change in cyclic resistance curve location when $CSR = 0.2$, $N_C = 15$ for the FBM soils using the state index.

Note that the FBM-30 cyclic resistance curve has two initial states with $I_s < 0$, or initial states at $e > e_0$. Previous studies using the state index to assess the undrained monotonic behaviour of sand (Cubrinovski and Ishihara, 1998) have indicated that parameters such as the peak stress ratio and steady state strength remain constant once $I_s < 0$ for a sandy soil. The FBM-30 cyclic resistance curve however shows that the liquefaction resistance continues to reduce as the state index value decreases.

The following summarizes the effect of increasing fines content of the FBM soils on the undrained cyclic behaviour when measuring initial state using the state parameter or state index:

- The response was less contractive
- Liquefaction resistance of the FBM soils increased

4.4. Summary

This chapter presented the results of undrained monotonic and cyclic triaxial tests on the four FBM sand-fines mixtures – FBM-1, FBM-10, FBM-20, and FBM-30. The monotonic test data was firstly discussed in terms of stress-strain, stress-path, and excess pore water pressure generation response. It was concluded that at similar void ratios or relative densities, FBM sandy specimens with higher fines contents exhibited more contractive behaviour than those with lower fines contents. This meant lower steady state strengths, lower effective stresses, and higher excess pore water pressures were observed during monotonic compression as $f_C =$

1% → 30%. Other studies (Lade and Yamamuro, 1997) have also noted such trends in the undrained monotonic response of sand as the fines content has been increased.

The steady state lines of the FBM sandy soils were secondly assessed, using void ratio, e, and relative density, D_r, as the measures of soil state. It was shown that when using either of these measures, the steady state lines of the FBM soils located at higher densities as the fines content was raised. This suggested that the potential for the FBM sand to experience flow liquefaction during monotonic compression also increased with increasing fines content. Each of the state measures were then discussed, critically assessing how the void ratio and relative density deal with measuring soil state when the respective amounts of sand and fines particles are changing. This led to a conclusion that a lack of differentiation within these parameters between the two different particle sizes (sand and fines) was the primary cause of variation in the steady state lines of the FBM soils as the fines content increased.

The cyclic test data was also presented using stress-strain, stress-path, and excess pore water generation response to firstly show the expected outcome that denser FBM specimens reach cyclic liquefaction after more load cycles than looser FBM specimens, for a given cyclic stress ratio. This data was then displayed in terms of the liquefaction resistance curves, which compiled all the test results to show the relationship between CSR and N_C for various specimen densities. These curves were used to define the cyclic resistances curves, which compared a range of state measures with the cyclic stress ratios of the FBM soils at $N_C = 5$ and $N_C = 15$. These measures included void ratio, e, relative density, D_r, state parameter, ψ, and state index, I_s. The comparisons showed that when the test specimens had similar void ratio or relative density values, the cyclic resistances of the FBM soils with higher fines contents were lower than those with lower fines contents. This suggested that the higher fines content FBM soils were more contractive, as was the case for the monotonically-loaded specimens when e and D_r were used to measure state.

When using the state parameter and state index however as the measure of soil state, it was the lower fines content FBM soils that displayed lower cyclic resistances. This reversal in trend was explained by comparing the excess pore water pressure generation of the FBM soils at the strain levels ($\varepsilon_a < 1\%$) that corresponded to the majority of load cycles observed during the cyclic tests. This concluded that, when using the steady state of deformation as a reference for soil state, the lower fines content FBM soils were more contractive than the higher fines content soils over this low range of strain. Overall it was suggested that using the steady state of deformation to help describe initial soil state, as ψ and I_s do, was not appropriate when

assessing cyclic liquefaction. This also highlighted how the choice of state measure can change the apparent effect of fines on the undrained response of sand. As such, Chapter 5 investigates two parameters that account for fines content in their definitions, in an attempt to better measure the state of sandy soils and quantify the effects of fines.

5. Intergranular and Equivalent Granular Void Ratios

5.1. Introduction

In Chapter 4, the parameters void ratio (e) and relative density (D_r) were used to interpret the undrained monotonic response of the FBM sand-fines mixtures. The state parameter (ψ) and state index (I_s) were also used to interpret the undrained cyclic response of these soils. The interpretation of the test data showed that as the fines content of the FBM soils increased, similar values of these state measures did not correspond to similar soil response. Soil strength at the steady state of deformation appeared to decrease at higher soil fines contents when using void ratio or relative density, whilst the liquefaction resistance increased with increasing fines content if the state parameter or state index were used.

The discussion in Chapter 4 suggested that the difference in soil response at similar values of the state measures may be due to these measures providing no differentiation between the sand and fines-sized particles within the soils. All particle sizes are assumed to contribute to the overall force-chain of the soil when using these measures (Thevanayagam and Mohan, 2000), but this assumption may not be physically true, especially when fines are mixed with sand. It therefore may be possible to account for the soil fines content with a new state measure – one that differentiates between sand and fines-sized particles, and produces similar soil response at similar values of the measure. Also note that from this chapter onwards in this thesis the conventional void ratio, e, will be referred to as the 'global void ratio' to avoid confusion between this and the modified void ratios – the intergranular and equivalent granular void ratios.

One proposed approach to account for the difference in sand and fines-sized soil particles was to consider the sand structure independently from the fines (Shen et al., 1977). This idea suggested that the undrained response of a sandy soil was controlled only by the sand particles within a soil – the fines were thought to play no role in the soil force-chain during loading. This parameter is often defined as the intergranular void ratio (Mitchell, 1993), e_g, which neglects the fines-sized particles in the global void ratio calculation. The concept of this parameter is further discussed in Section 5.2.1.

Following on from this idea, the intergranular void ratio was modified to allow some of the fines-sized particles to participate in the soil force-chain, rather than simply neglecting their effect. This resulted in the definition of the equivalent granular void ratio (Thevanayagam et al., 2000), e^*. The equivalent granular void ratio includes a term, b, which can be thought of as an influence factor that quantifies what fraction of the fines-sized particles participate in the soil force-chain during undrained loading. Because of this influence factor, the equivalent granular void ratio can be equal to either the global void ratio (e) or the intergranular void ratio (e_g). The concept of the equivalent granular void ratio is further discussed in Section 5.3.1.

These two density state measures – the intergranular (e_g) and equivalent granular (e^*) void ratios – are used in this chapter to interpret the monotonic and cyclic responses of the FBM soils presented in Chapter 4. Test data from the literature is also interpreted using these state measures to ensure the observed trends do not only correspond to the FBM soils, but to a range of sandy soils. A procedure to back-calculate the fines influence factor, b, is also discussed, as well as the effect of fines on the undrained monotonic and cyclic responses of sandy soils when using e_g and e^* as the measures of soil state.

5.1.1. Selection of Sandy Soil Test Data from the Literature

As discussed in Section 5.1, monotonic and cyclic test data from the literature is interpreted in this chapter using the intergranular and equivalent granular void ratios. The following summarizes the requirements used to select this data:

(1) The fines content of the sand must have been systematically varied – there could be no physical difference in the sand and fines respectively between each sand-fines mixture, only the relative amounts of each particle type.

(2) Only non-plastic or low plasticity fines were considered to keep the soil data within the scope of this study.

(3) Test data must have been available for the clean sand fraction ($f_C \approx 0\%$) – this data was used as a reference when back-calculating the influence factor, b.

(4) For each mixture of sand and fines, at least two soils with fines contents between $f_C = 5 – 30\%$ must have been tested. This was to allow the effect of fines on the undrained response to be properly discussed, and the fines influence factors to be accurately derived.

5.2. Interpretation using Intergranular Void Ratio

The intergranular void ratio, e_g, is used to interpret the monotonic and cyclic responses of a number of sandy soils from the literature, as well as the FBM soils which were discussed in Chapter 4. The concept and definition of this parameter are presented in Section 5.2.1. To compare responses of different soils, the steady state line is used as a reference for the monotonic data, and the cyclic resistance curves as a soil response reference for the cyclic data. The differences in the soil response at similar intergranular void ratio values are examined and this parameter is then critically assessed.

5.2.1. The Intergranular Void Ratio Concept

The concept of the intergranular void ratio, e_g, is based on a mixture of sand and fines being thought of as a binary material – only two particle sizes within the mixture (Mitchell, 1976). The sand is considered to be the dominate particle size, with the fines sitting in void space between the sand particles. A highly idealized schematic illustration of this concept is shown in Figure 5-1.

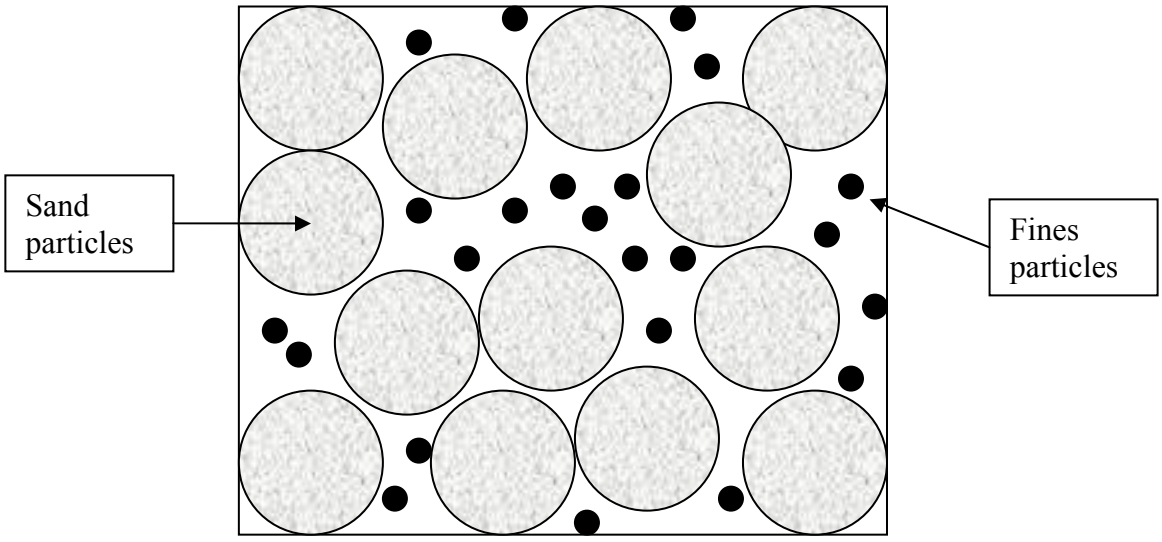

Figure 5-1 Highly idealized schematic illustration showing the intergranular void ratio concept. Sand particles are represented by open circles, and fines by the smaller solid circles.

As the fines particles are assumed to sit within the void space created by the sand, they are also assumed to have no involvement in the soil force-chain during loading (Thevanayagam, 1998). Hence the global void ratio, e, is essentially redefined so that only the

sand particles are considered to contribute to the volume of solids, as these provide the only active particle contacts in the soil. In making this assumption, a term indicating the fines content of the soil must be included in the intergranular void ratio definition.

Intergranular void ratio, e_g – where e = global void ratio, f_C = soil fines content in decimal form:

$$e_g = \frac{e + f_C}{1 - f_C} \tag{5-1}$$

Equation (5-1) defines the intergranular void ratio. When it is used as a state measure for clean sand with no fines, $f_C = 0$ and the intergranular void ratio value is equal to the global void ratio value. That is, $e_g = e$ for $f_C = 0$ in Equation (5-1).

If the soil fines content is increased, the numerator value in Equation (5-1) increases and the denominator value decreases. This leads to an overall increase in the intergranular void ratio value for any increase in fines content at a constant void ratio value. As such:

- If $f_C > 0$, then $e_g > e$

Physically an increase in the intergranular void ratio value corresponds to a looser soil state as compared to the global void ratio. This increase may occur even if the global void ratio value is decreasing due to the addition of fines. Based on the intergranular void ratio concept however, a looser packing or higher void ratio should correspond to more contractive soil behaviour.

It should be noted that the use of the intergranular void ratio is only considered relevant for fines contents below the threshold fines content, f_{Cth} (Thevanayagam et al., 2003). This is the point at which the soil structure fundamentally changes from being sand-dominated, or fines within the sand voids, to fines-dominated, or sand particles being separated by a 'sea of fines'. Schematics of these soil structures are illustrated in Figure 5-2. The threshold value is approximately located between f_C = 20 – 30% (Pitman et al., 1994; Thevanayagam and Mohan, 2000), with f_{Cth} = 30% being used in this study as a general approximation for f_{Cth}. It

should be noted that there are methods available to estimate the f_{Cth} value for a given mixture of sand and fines (Yang et al., 2006a).

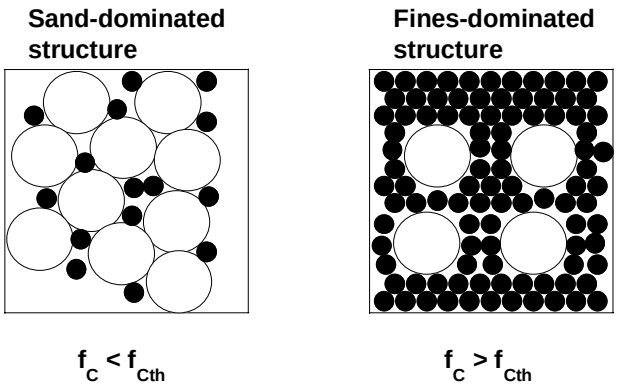

Figure 5-2 Schematic illustration showing the sand-dominated and fines-dominated soil structures respectively when the soil fines content is below and above the threshold fines content.

5.2.2. Interpretation of the Effects of Fines Content on the Steady State Line using the Intergranular Void Ratio

As discussed in Chapter 4, the state concept (Castro and Poulos, 1977) is a useful framework for comparing the undrained monotonic response of sandy soils. It gives insight into the volume change tendencies of a soil by comparing the initial soil state with the location of the steady state line. As such, the effects of fines content on the undrained monotonic response of sand are investigated using the intergranular void ratio as a measure of initial state and the steady state lines as a measure of soil response.

The steady state lines of the FBM soils are firstly presented in Figure 5-3. Intergranular void ratio values were calculated using Equation (5-1). Figure 5-3 shows that as the fines content of the FBM sand is raised, the steady state lines locate at higher intergranular void ratios, which corresponds to a looser packing of the sand particles. This trend is summarized in Figure 5-4, which plots the intergranular void ratio values, e_{g0}, when the mean effective stress at the steady state of deformation is equal to zero.

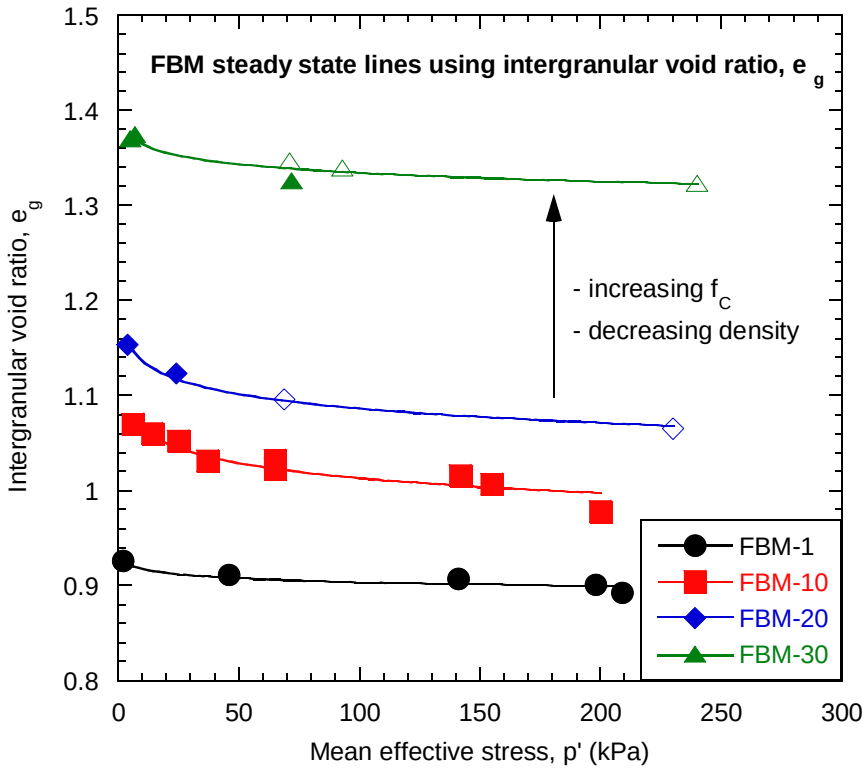

Figure 5-3 Steady state lines of the FBM soils using the intergranular void ratio as the state measure.

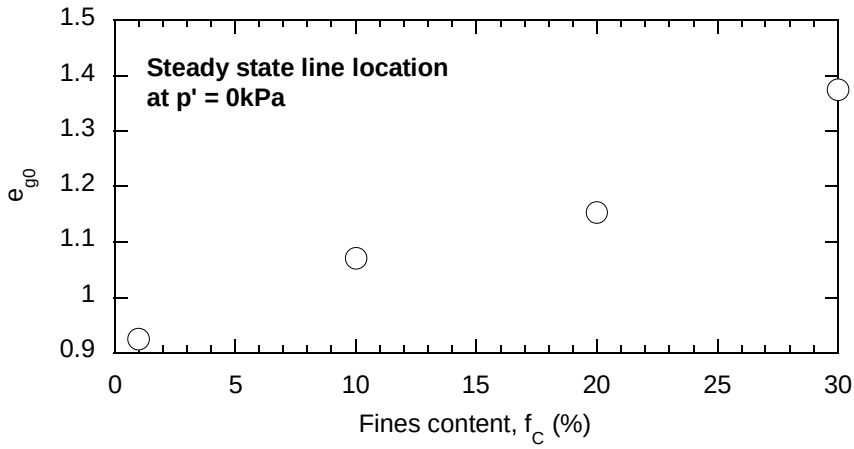

Figure 5-4 Change in steady state line location at p' = 0kPa for the FBM soils using the intergranular void ratio as the state measure.

The trend presented in Figure 5-4 suggests that, at a given intergranular void ratio, the FBM soils become more dilative as the fines content is increased. This has also been observed in other studies (Pitman et al., 1994; Thevanayagam, 1999) for silty sands tested at low confining stresses. The trend does however directly contrast to that observed in Chapter 4

using the global void ratio and relative density, where the soils appeared to become more contractive as the fines content was increased. Obviously there has been no change in the actual response of the soils, and this contrast is purely associated with the choice of the state measure. Most importantly however, similar intergranular void ratio values clearly do not correspond to similar monotonic response for the FBM soils.

Note that a significant change in the steady state line location when p' = 0kPa can be observed in Figure 5-4 from f_C = 20 – 30%, with e_{g0} increasing from e_{g0} = 1.153 → 1.375. This is maybe due to the soil fines content approaching the threshold fines content, f_{Cth}, as f_C = 30% is approached. In such a case the soil structure changes from being sand-dominated to fines-dominated, as discussed in Section 5.2.1. It therefore becomes unsuitable to try and report soil state for the FBM-30 soil using the intergranular void ratio, due to the inconsistency between the assumed lack of participation of the fines in the soil force-chain using this state measure, and the actual behaviour of the soil.

The steady state line data of eight mixtures of sand and fines were sourced from the literature, using the criteria listed in Section 5.1.1. These are interpreted to show that the general effects of fines on the observed undrained monotonic response of sand when using the intergranular void ratio as the state measure are the same as those observed for the FBM soils. The eight sandy soils are presented in Table 5-1 with their respective references and the plasticity of their fines.

Table 5-1 Sandy soils with monotonic steady state line data sourced from the literature.

Soil	**Plasticity of fines**	**Reference**
F55 Foundry Sand	NP	(Thevanayagam et al., 2002)
Ottawa Sand	NP	(Murthy et al., 2007)
M31 Artificial Sand	NP	(Papadopoulou and Tika, 2008)
Ardebil Sand	NP	(Naeini and Baziar, 2004)
Toyoura Sand	NP	(Zlatovic, 1994; Verdugo and Ishihara, 1996)
Hokksund Sand	NP	(Yang et al., 2006c)
Mai Liao Sand	PI < 8	(Huang et al., 2004; Chen and Liao, 1999)
Sydney Sand	PI = 11	(Rahman and Lo, 2007)

Note that the majority of the fines mixed with the sands in Table 5-1 are non-plastic (NP). The information that the Ardebil fines are non-plastic was obtained from a personal communication (Baziar, 2009). The two sandy soils with slightly higher fines plasticity indices, Sydney Sand and Mai Liao Sand, were considered in order to enlarge the database, though these soils should be treated with caution. This is because the stress-strain behaviour of fine-grained soils can change from being sand-like to clay-like if they have a $PI \geq 7$ (Boulanger and Idriss, 2006).

The primary method for obtaining the steady state of deformation data from the sources in Table 5-1 was to digitize the steady state line plots and extract the data into a spreadsheet format. Because of this digitization, there may be some discrepancy between the data presented herein and the actual obtained results from the respective tests. This discrepancy is considered to be minimal as care was taken to ensure the digitization was completed as accurately as possible, and in no way it affects the observed trends in soil response.

Only test data with mean effective stresses below 500kPa at the steady state of deformation were included in the following interpretation – any other data points were discarded. The reason for focusing on this range of mean effective stress values is that it reflects the range of confining pressures for which soils are generally most susceptible to liquefaction in the field, whilst still including enough data points to accurately define the steady state line. Case histories of observed level-ground liquefaction (Stark and Olson, 1995) have shown that liquefaction tends to occur less than 20m below the ground surface with effective vertical stresses less than 300kPa.

Also note that the soils are denoted in the same way as for the FBM soils – the name of the sand is listed first, followed by the fines content. For example, Toyoura-10 corresponds to Toyoura Sand with 10% fines content.

Figure 5-5 to Figure 5-12 present the steady state lines of the sand with fines mixtures listed in Table 5-1 using the intergranular void ratio as the state measure. There is a clear overall trend for the steady state lines of these soils to locate at higher intergranular void ratios as the fines content of the sands is increased. This was also observed for the FBM soils in Figure 5-3, and generally indicates more dilatant soil response with increasing fines content if the intergranular void ratio is used as a basis for comparison.

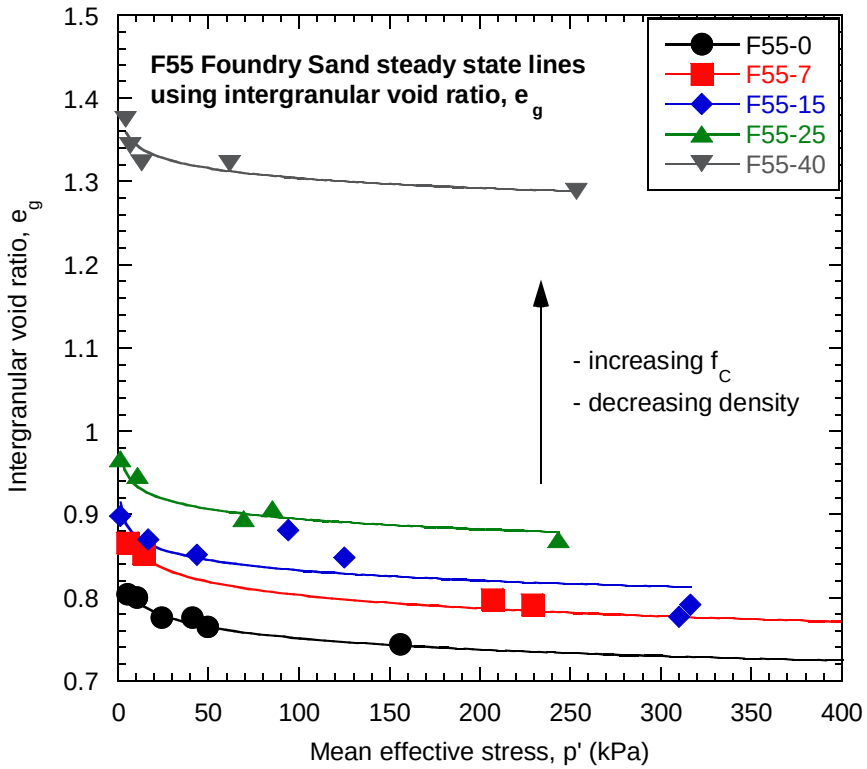

Figure 5-5 Steady state lines of the F55 Foundry Sand using the intergranular void ratio as the state measure.

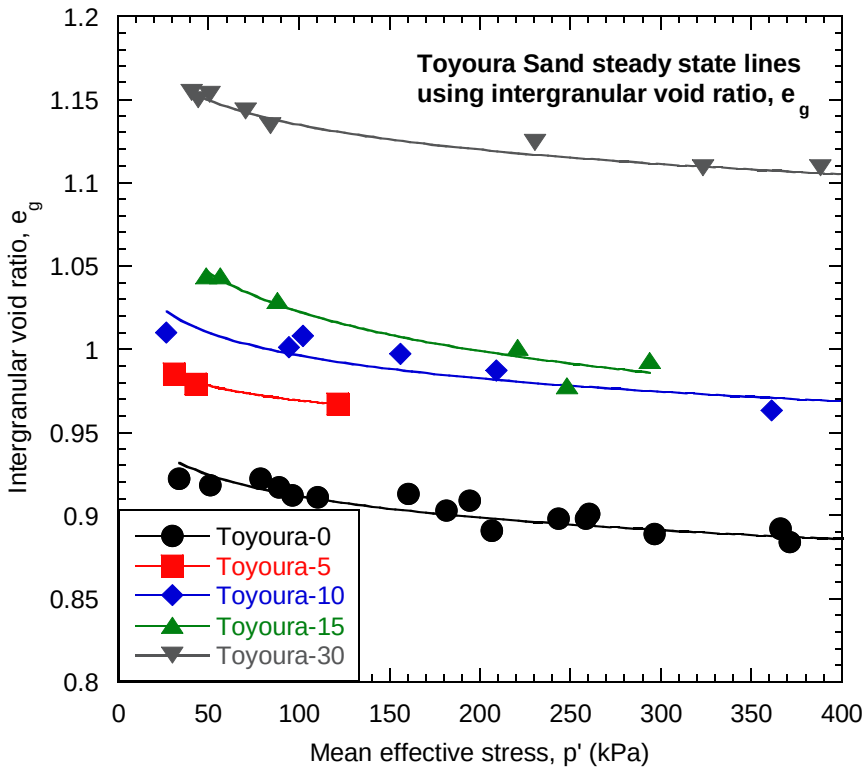

Figure 5-6 Steady state lines of the Toyoura Sand using the intergranular void ratio as the state measure.

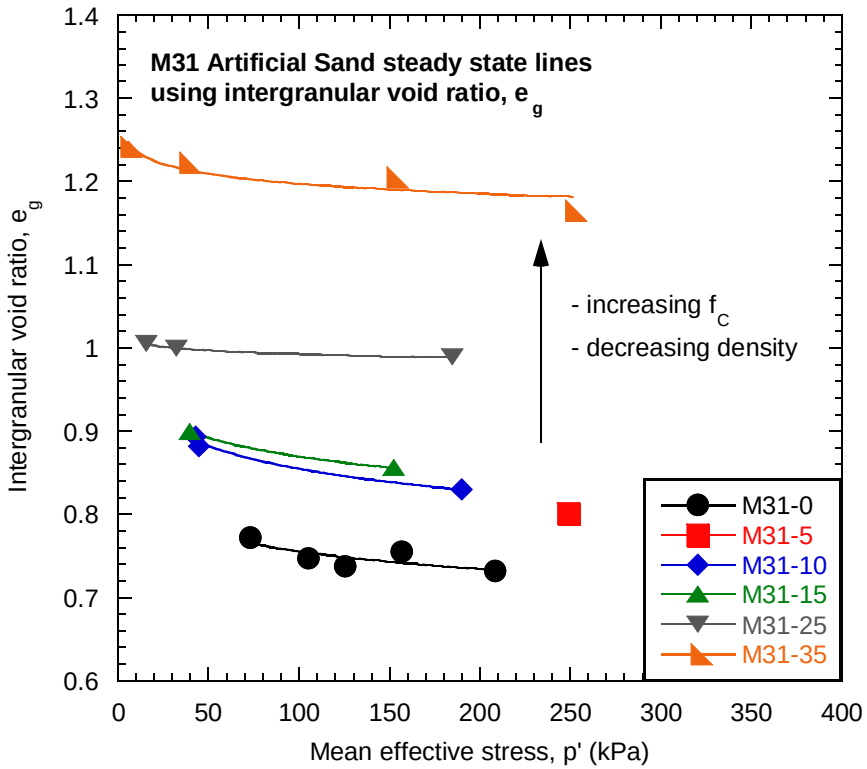

Figure 5-7 Steady state lines of the M31 Artificial Sand using the intergranular void ratio as the state measure.

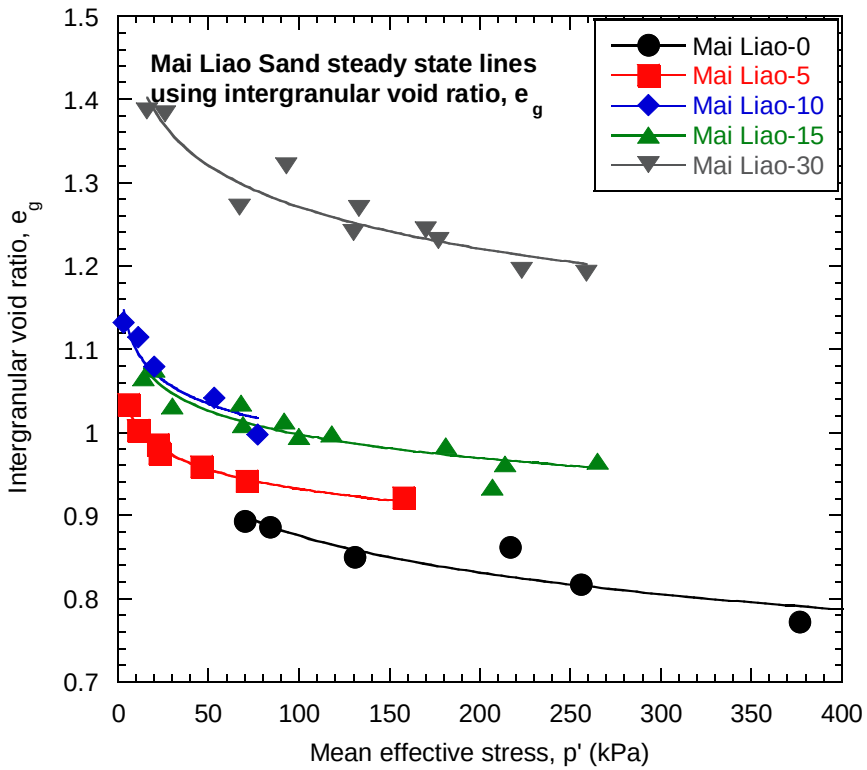

Figure 5-8 Steady state lines of the Mai Liao Sand using the intergranular void ratio as the state measure.

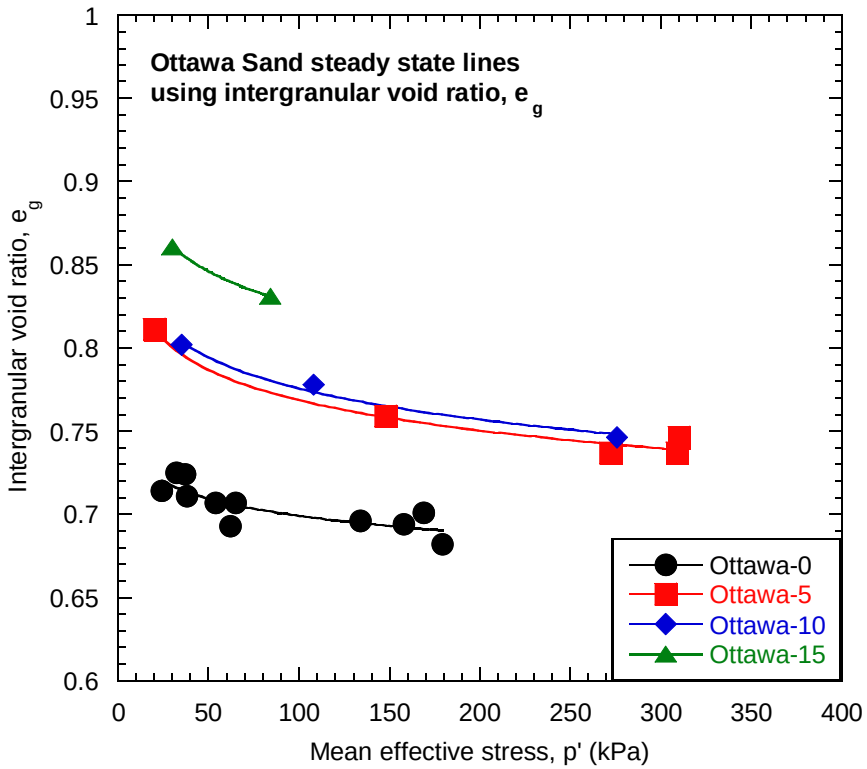

Figure 5-9 Steady state lines of the Ottawa Sand using the intergranular void ratio as the state measure.

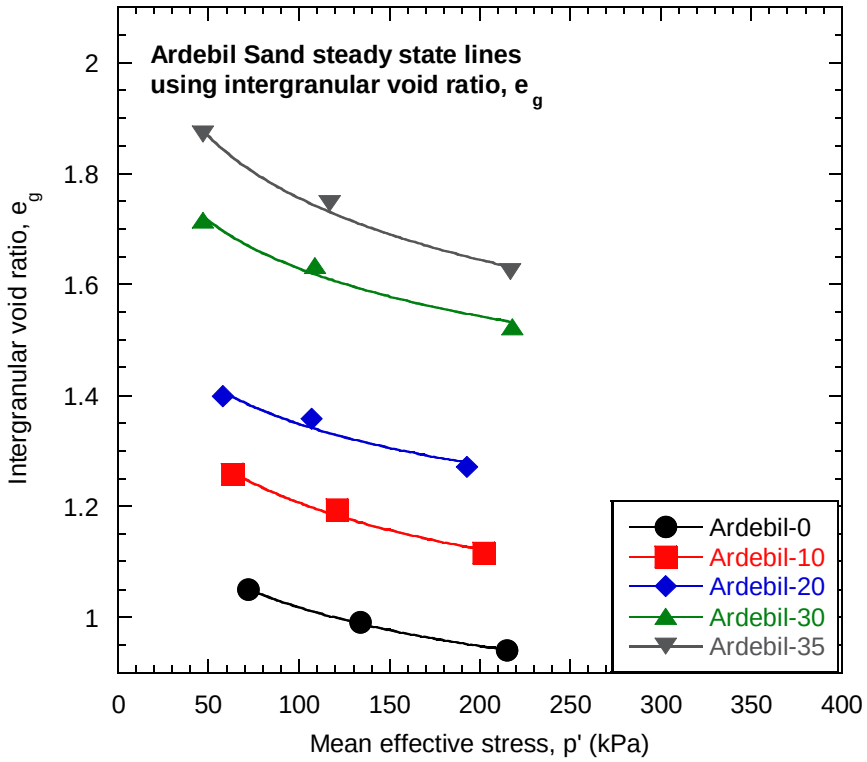

Figure 5-10 Steady state lines of the Ardebil Sand using the intergranular void ratio as the state measure.

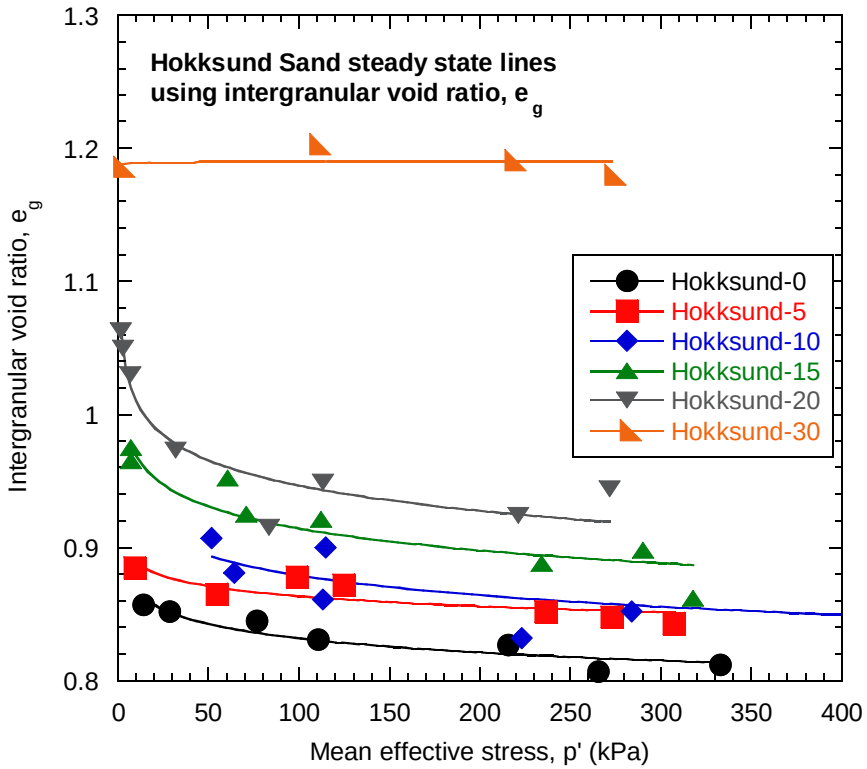

Figure 5-11 Steady state lines of the Hokksund Sand using the intergranular void ratio as the state measure.

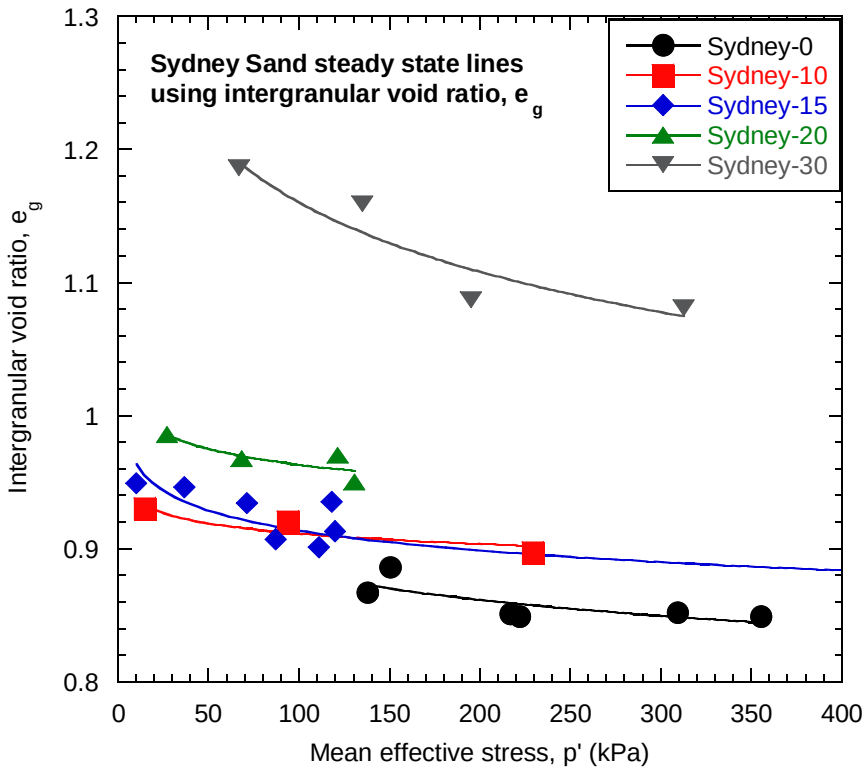

Figure 5-12 Steady state lines of the Sydney Sand using the intergranular void ratio as the state measure.

Interestingly for some of the soils, small increases in fines content do not cause a significant change in the location of the steady state line. For example, in Figure 5-7 the steady state lines of the M31 Artificial soils with f_C = 5%, 10% and 15% are located at similar positions in the e_g – p' plane. This means that similar e_g values correspond to similar monotonic response, instead of an increased dilatancy with increasing fines content. They do however show a significant difference in response from that of the M31 Artificial clean sand.

The steady state line locations for the FBM soils and each of the eight sandy soils listed in Table 5-1 are summarized in Figure 5-13, using e_g at p' = 100kPa, or e_{g100}. The intergranular void ratio at 100kPa was chosen as some steady state lines from the literature did not extend to p' = 0kPa, as shown by the Mai Liao-0 steady state line in Figure 5-8.

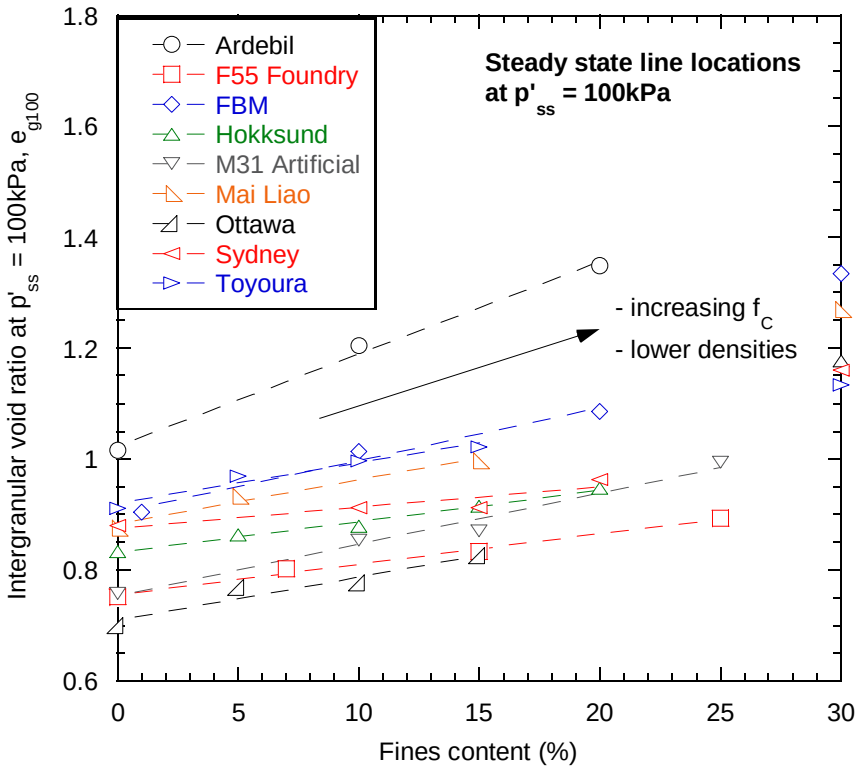

Figure 5-13 Change in steady state line location at p' = 100kPa for all sandy soils using the intergranular void ratio.

Figure 5-13 shows that the steady state lines for all nine reported sandy soils move to higher intergranular void ratios as the fines content is increased. This trend confirms that the addition of fines to a sand causes more dilative soil response during undrained monotonic loading, which is the opposite trend to that observed when the global void ratio was used as the state measure – increased fines content tended to cause more contractive response in that

case. Other studies (Pitman et al., 1994; Ni et al., 2004) have also noted this trend when the intergranular void ratio is used as the soil state measure.

Another interesting point observed in Figure 5-13 is the rate at which the steady state lines appear to move to lower densities with increasing fines content. There appears to be a roughly linear correlation between fines content and steady state line location up until f_C = 25 – 30%, with a significant jump in intergranular void ratio values e_{g100} between these fines contents. This jump is most likely due to the soil structure changing from sand-dominated to fines dominated (Thevanayagam, 1999), as discussed in Section 5.2.1.

5.2.3. Interpretation of the Effects of Fines Content on the Cyclic Resistance Curve using the Intergranular Void Ratio

In Chapter 4, the liquefaction resistance curves of the FBM soils were summarized by comparing the soil state with the cyclic stress ratio required to reach cyclic liquefaction (5% double amplitude axial strain) after a given number of load cycles (N_C = 5 and N_C = 15). The curves these comparisons produced were termed cyclic resistance curves, and are used here to compare the effects of fines on the undrained cyclic response of a number of sandy soils, using the intergranular void ratio as the state measure. Note that these curves have also been used in other studies to compare the undrained cyclic response of soils (Erten and Maher, 1995), (Polito and Martin II, 2003).

The cyclic resistance curves of the FBM soils are presented in Figure 5-14. This is followed by a summary of the sandy soils with cyclic data sourced from the literature, and some of their respective cyclic resistance curve plots. Also note that only the cyclic resistance curves for N_C = 15 have been used – as shown in Chapter 4, similar effects of fines on the cyclic response are observed when either N_C = 5 or N_C = 15 is used.

Figure 5-14 shows that the cyclic resistance curves of the FBM soils locate at lower densities as the fines content is increased. This corresponds to more dilative soil response at higher fines contents, which results in slower generation of excess pore water pressures and more load cycles being required to reach liquefaction. It also means that the liquefaction resistance of the soil is increasing with the addition of fines. Note that this tendency for increased soil dilation at higher fines contents is the same as the trend observed for the undrained monotonic response, as discussed in Section 5.2.2 using the FBM steady state lines. As such, the effects of increased fines content on the FBM soil response when using the intergranular void ratio are consistent across both monotonic and cyclic loadings.

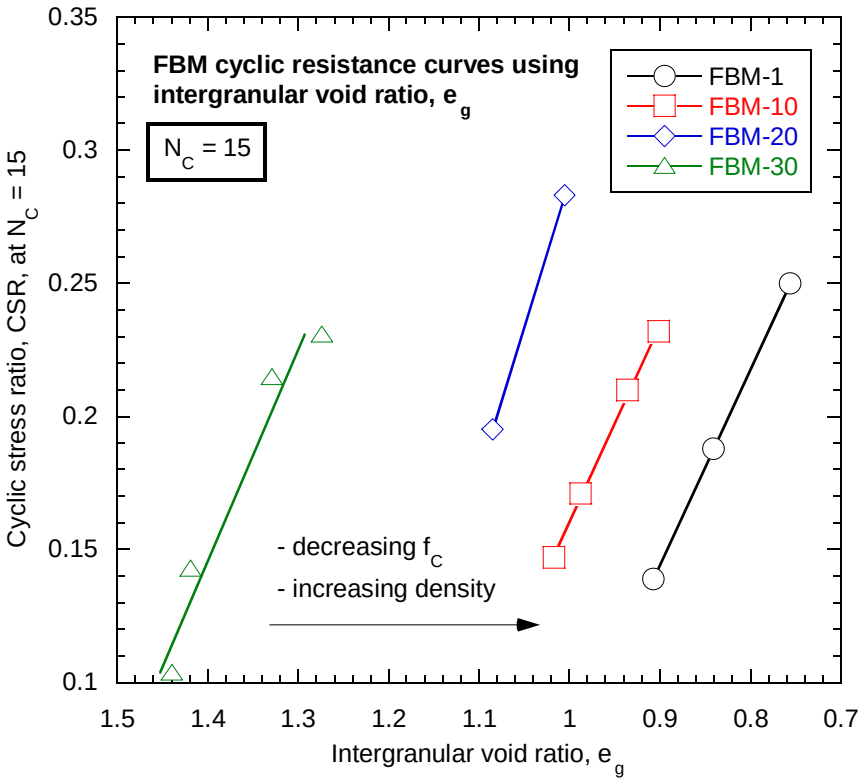

Figure 5-14 Cyclic resistance curves of the FBM soils at N_C = 15 using the intergranular void ratio as the state measure.

Another similarity observed in Figure 5-14 to the monotonic response in Figure 5-3 is the significant difference in location of the FBM-30 cyclic resistance curve relative to the curves with lower fines contents. It is located at e_g values between 1.3 – 1.5, which corresponds to very loose packing of the sand particles. The difference between this curve and the FBM-20 curve may again be due to the soil fines content approaching the threshold fines content.

In summary, when using the intergranular void ratio as state measure, the liquefaction resistance of the FBM soil increases with the fines content.

Table 5-2 presents eight mixtures of sand and fines with available liquefaction resistance data sourced from the literature. Note that not all of these soils are the same as those presented in Table 5-1 that were used to interpret the monotonic response. The method of deposition used to create the soil test specimens has been included in Table 5-2, as this affects the initial soil fabric and cyclic response (Vaid and Sivathayalan, 2000). The plasticity of the fines and the respective references are also included.

Table 5-2 Sandy soils with cyclic liquefaction resistance data sourced from the literature.

Soil	Plasticity of fines	Deposition	Reference
Monterey 0/30 Sand	NP	Moist tamping	(Polito and Martin II, 2001)
Yatesville Sand	NP	Moist tamping	(Polito, 1999)
Ottawa Sand	NP	Slurry	(Carraro et al., 2003)
F55 Foundry Sand	NP	Moist tamping and dry deposition	(Thevanayagam et al., 2000)
Brenda 20/200 Sand	NP	Slurry	(Vaid, 1994)
M31 Artificial Sand	NP	Moist tamping	(Papadopoulou and Tika, 2008)
Mai Liao Sand	$PI < 8$	Moist tamping	(Huang et al., 2004)
Yunlin Sand	NP	Moist tamping	(Chien et al., 2002)

The undrained cyclic resistance data was obtained from the literature through digitization. The liquefaction resistance curve plots from the various texts were generally used as the data source, and the cyclic stress ratio at N_C = 15 was digitized directly from these curves. As with the monotonic data, there may be some discrepancy between the cyclic data presented herein and the actual test results. However care was taken to ensure the digitization was as accurate as possible.

Note there were two exceptions to the cyclic stress ratio at N_C = 15 being used: the F55 Foundry Sand was tested at a constant CSR = 0.2, and hence the intergranular void ratio is plotted against the number of cycles required to reach liquefaction, N_C. The Brenda 20/200 Sand test only contained data for the cyclic stress ratio at N_C = 10, and therefore this number of load cycles has been used instead of the liquefaction resistance at N_C = 15.

Figure 5-15 to Figure 5-21 respectively present the cyclic resistance curves of all sand-fines mixtures listed in Table 5-2 (except F55 Foundry Sand) using the intergranular void ratio as the state measure. The curves tend to locate at higher intergranular void ratios as the fines content is increased, which corresponds to an increase in soil liquefaction resistance with increasing fines content. Note this also corresponds to a more dilative soil response as the fines content is increased, as discussed for the FBM soils.

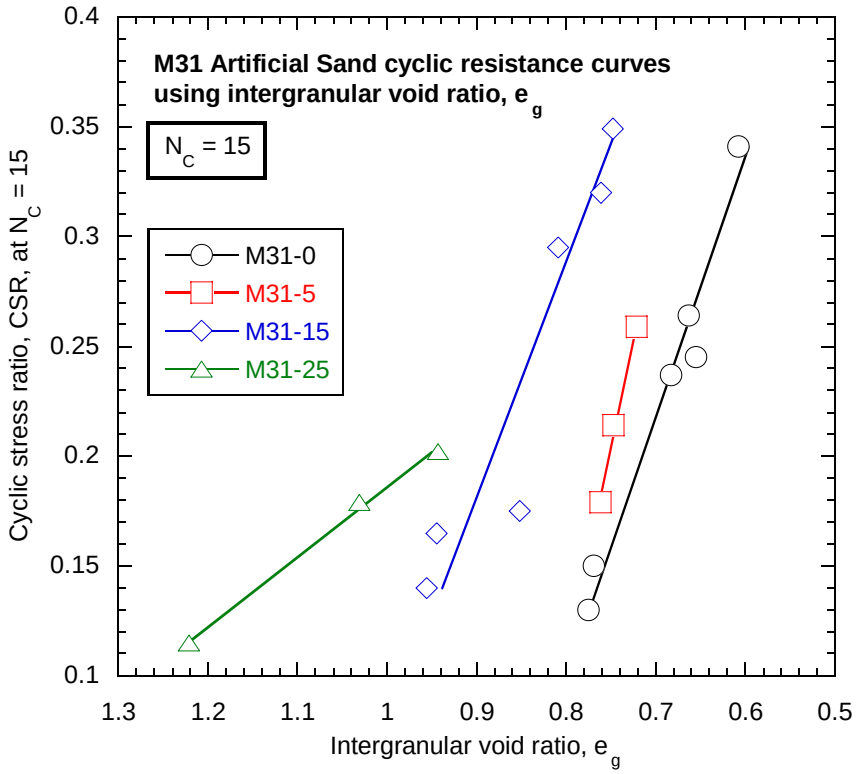

Figure 5-15 Cyclic resistance curves of the M31 Artificial Sand at N_C = 15 using the intergranular void ratio as the state measure.

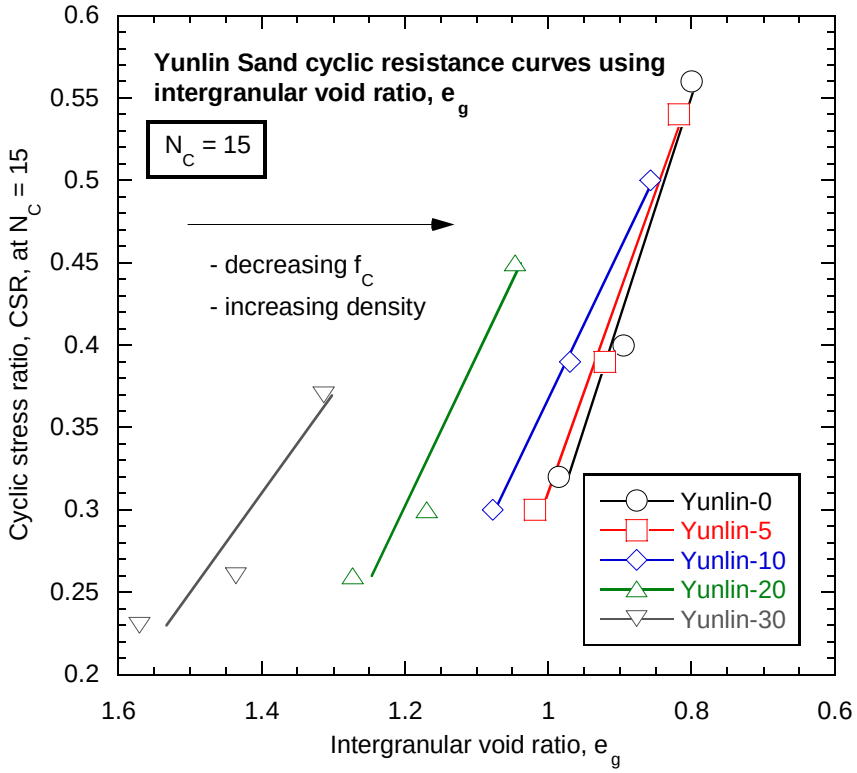

Figure 5-16 Cyclic resistance curves of the Yunlin Sand at N_C = 15 using the intergranular void ratio as the state measure.

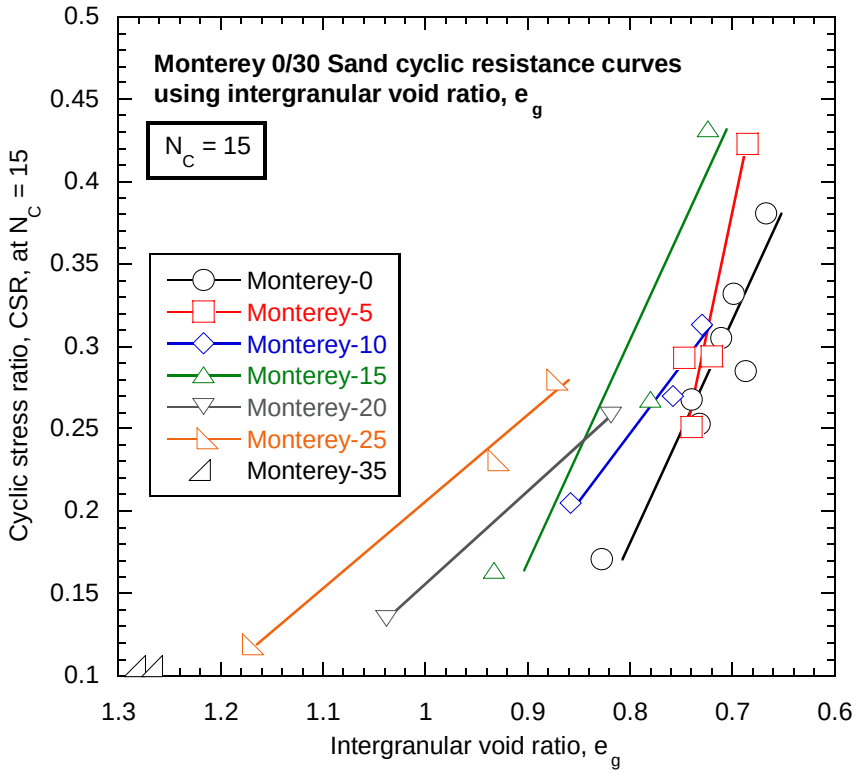

Figure 5-17 Cyclic resistance curves of the Monterey 0/30 Sand at N_C = 15 using the intergranular void ratio as the state measure.

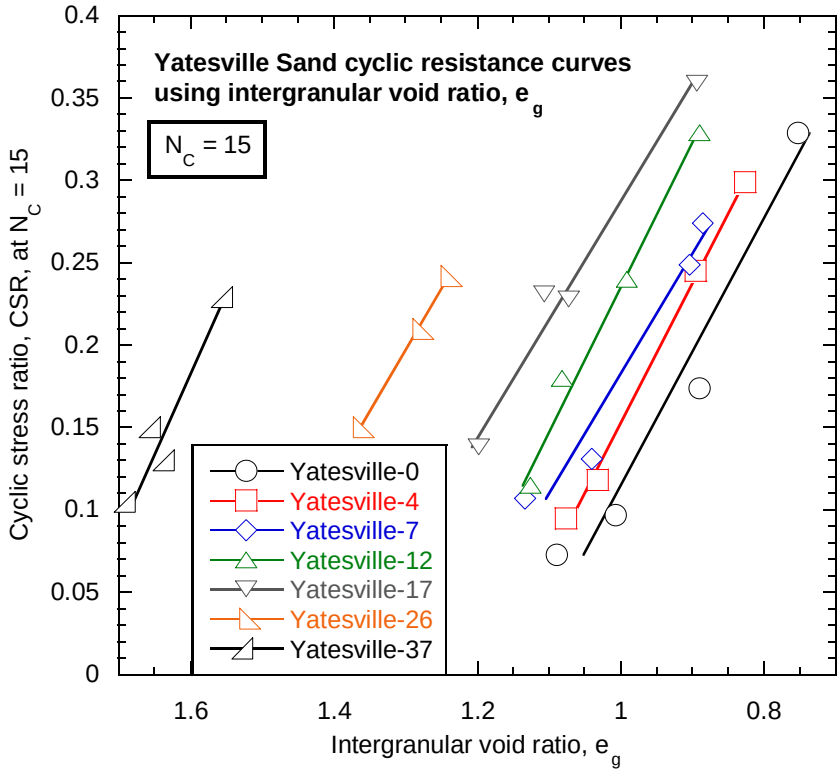

Figure 5-18 Cyclic resistance curves of the Yatesville Sand at N_C = 15 using the intergranular void ratio as the state measure.

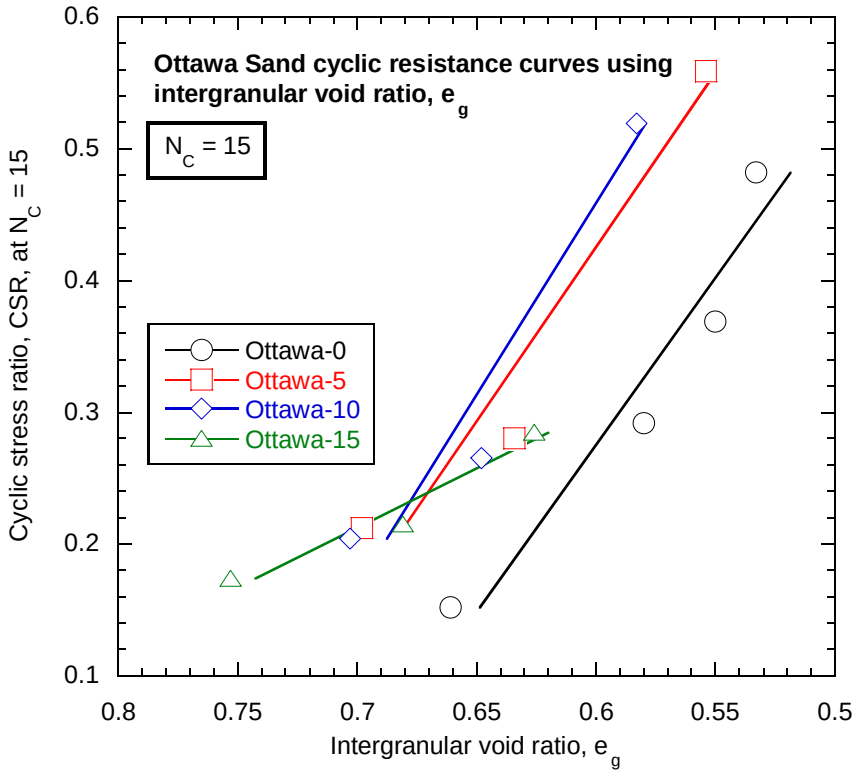

Figure 5-19 Cyclic resistance curves of the Ottawa Sand at N_C = 15 using the intergranular void ratio as the state measure.

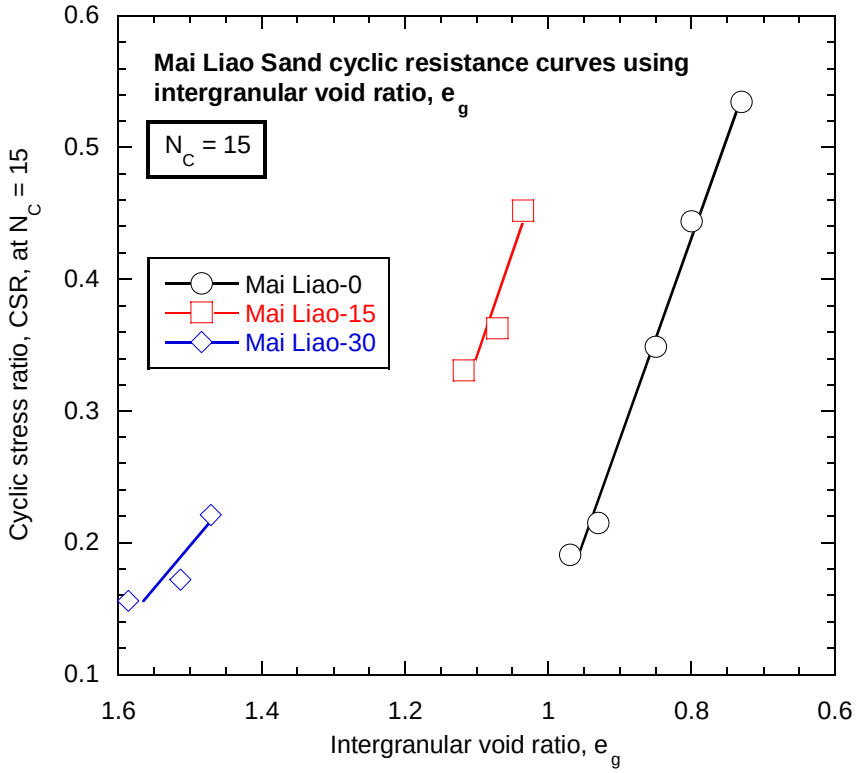

Figure 5-20 Cyclic resistance curves of the Mai Liao Sand at N_C = 15 using the intergranular void ratio as the state measure.

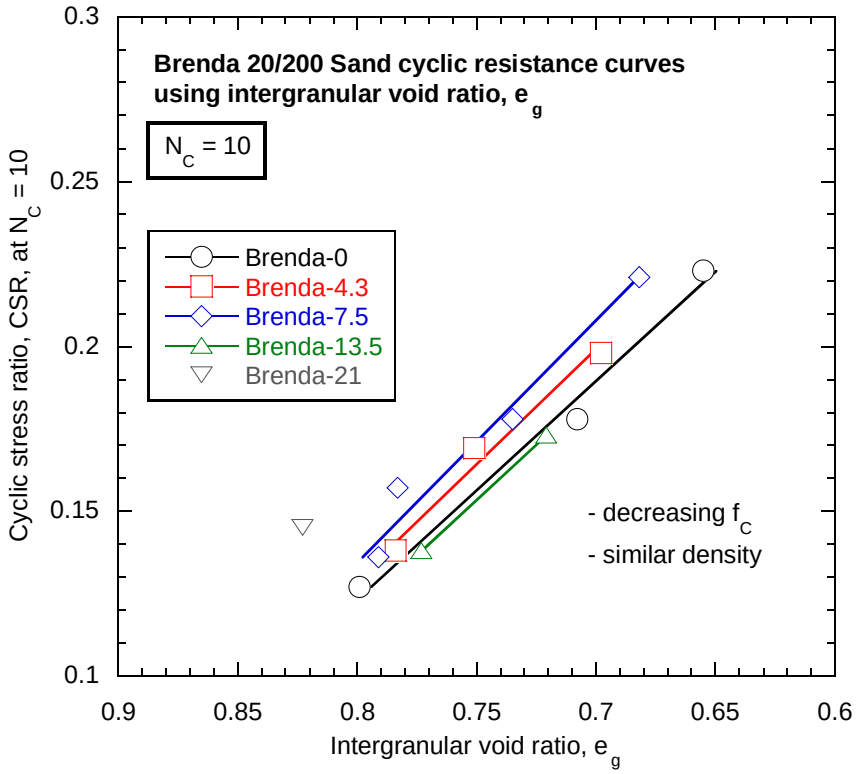

Figure 5-21 Cyclic resistance curves of the Brenda 20/200 Sand at N_C = 10 using the intergranular void ratio as the state measure.

The apparent increase in cyclic liquefaction resistance is most explicitly illustrated in Figure 5-22 for the F55 Foundry Sand, which displays the number of load cycles required to reach liquefaction when CSR = 0.2. It can be observed when considering a constant intergranular void ratio value of e_g = 0.780 that N_C = 1 for the F55 Foundry clean sand, whilst N_C = 10 for the F55-15 soil.

The Brenda 20/200 Sand cyclic resistance curves in Figure 5-21 are interesting as they are located in close proximity to one another – the Brenda-13.5 curve even sits at slightly higher densities than the Brenda-0 curve, contrasting with the general observed trend for the other sandy soils. For this sand, the intergranular void ratio concept provides a good approximation and 'unique' relationship with the cyclic soil response. Similar e_g values correspond to similar number of cycles being required to reach liquefaction for a given level of cyclic stress ratio.

Figure 5-23 displays the locations of the cyclic resistance curves at CSR = 0.2, $e_{gCSR=0.2}$, for all soils listed in Table 5-2 except Yunlin Sand. The data for this sand could not be included as none of the cyclic resistance curves pass through a CSR = 0.2. Also note that the Brenda 20/200 Sand and F55 Foundry Sand data points in Figure 5-23 correspond to N_C = 10.

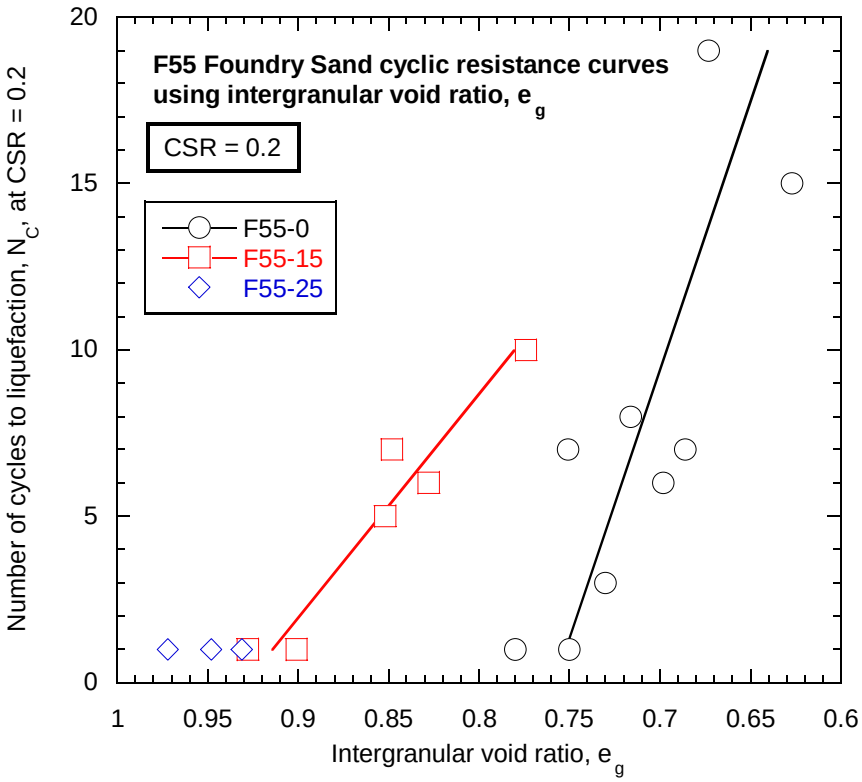

Figure 5-22 Cyclic resistance curves of the F55 Foundry Sand at *CSR* = 0.2 using the intergranular void ratio as the state measure.

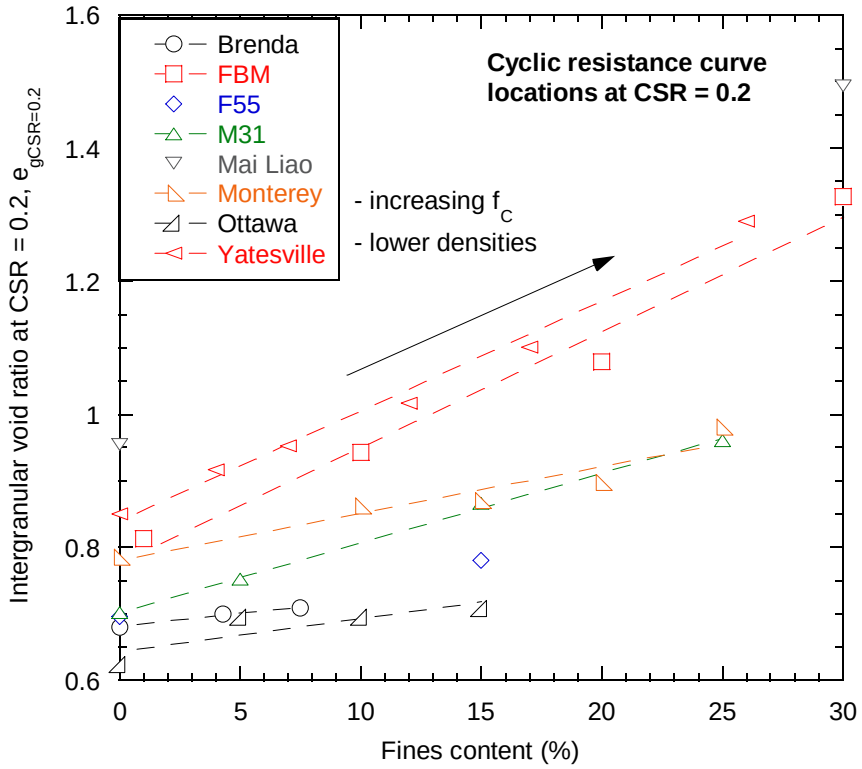

Figure 5-23 Change in cyclic resistance curve location at *CSR* = 0.2 for the sandy soils using the intergranular void ratio.

The general trend observed in Figure 5-23 shows the locations of the cyclic resistance curves for the sandy soils moving to lower densities (higher intergranular void ratio values) as the fines content is increased. As previously discussed, this suggests the liquefaction resistances of the sands are also increasing with the addition of fines. Note that there is also a roughly linear correlation between cyclic resistance curve location and fines content in Figure 5-23 – a similar trend was also observed in Figure 5-13 for the monotonic steady state line positions.

It is clear from the presented results that similar intergranular void ratio values for soils with different fines contents do not correspond to similar cyclic response. This was also the case when using the global void ratio as the state measure for the FBM soils, as shown in Chapter 4. Explanations for this outcome are discussed in the following section, which critically assesses the intergranular void ratio concept using the undrained monotonic and cyclic responses of the FBM soils.

5.2.4. Critical Assessment of the Intergranular Void Ratio

The effect of fines on the undrained response of mixtures of sand and fines using the intergranular void ratio as the state measure has shown to be consistent across both monotonic and cyclic loadings. Sections 5.2.2 and 5.2.3 presented the steady state lines and cyclic resistance curves of a range of sandy soils, and discussed the conclusion that the soil response becomes more dilative as the fines content is increased up to f_C = 30%. If the intergranular void ratio concept was accurate however, there should be no difference in the volume change tendencies of the soils as the fines content is altered. The reasons behind these inconsistencies between theory and observed soil response are firstly assessed by reviewing the assumptions made in defining the intergranular void ratio.

Intergranular void ratio (e_g) is defined by Equation (5-1) in Section 5.2.1. It includes the term f_C, which is used to neglect the fines particles from the soil density calculation. This is based on the idea that the fines play no part in transferring load in the soil force-chain, and instead sit in the void space created by the larger sand particles (Thevanayagam, 1998). Binary packing theory was used as the basis for this concept, considering the sand as uniform, spherical particles, and the fines as smaller uniform, spherical particles. In doing this, a ratio between the two different particle diameters can be defined. This ratio, herein termed the

particle diameter ratio R_d, is presented in Equation (5-2), where d_{large} = diameter of the sand particles, and d_{small} = diameter of the fines particles:

$$R_d = \frac{d_{large}}{d_{small}} \tag{5-2}$$

A minimum value of R_d exists such that, when the sand particles are arranged at their maximum density, the fines particles only just sit in the void space without pushing the sand particles apart (Lade et al., 1998). This is schematically illustrated in Figure 5-24, with the particle diameter ratio corresponding to this state being $R_d \approx 6.5$.

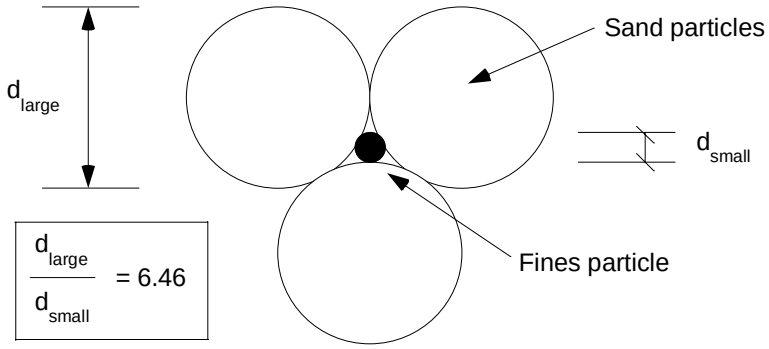

Figure 5-24 Minimum particle diameter ratio R_d at which the fines do not push apart the sand particles when the sand is at maximum density (Lade et al., 1998).

To simplistically assess the validity of the intergranular void ratio concept for real soils, representative particle sizes for both the sand (d_{large}) and fines (d_{small}) need to be defined. In this case d_{50} (the mean grain size) has been chosen as the representative particle size. Note that other studies examining R_d have also used d_{50} as a representative particle size (Thevanayagam et al., 2003). As such, the values of d_{large} and d_{small} are reported in Table 5-3 for the sandy soils, along with their R_d values.

Table 5-3 Particle diameter ratios of the sandy soils.

Soil	d_{large} (mm)	d_{small} (mm)	R_d
FBM Sand	0.168	0.015	11.2
F55 Foundry Sand	0.250	0.010	25.0
Ottawa Sand	0.390	0.023	16.7
M31 Artificial Sand	0.300	0.020	15.0
Ardebil Sand	0.150	0.025	6.0
Toyoura Sand	0.175	0.020	18.4
Hokksund Sand	0.440	0.032	13.8
Sydney Sand	0.274	0.027	10.1
Mai Liao Sand	0.127	0.044	2.9
Monterey 0/30 Sand	0.430	0.030	14.3
Yatesville Sand	0.180	0.030	6.0
Brenda 20/200 Sand	0.235	0.012	19.6
Yunlin Sand	0.292	0.060	4.9

Scanning through the R_d values listed in Table 5-3 shows that only four of the sandy soils out of 13 have $R_d < 6.5$ – Ardebil Sand, Mai Liao Sand, Yatesville Sand, and Yunlin Sand. This suggests that, using the representative values for d_{large} and d_{small}, the majority of the fines should be able to physically fit within the void space created by the sand particles. Of course a number of factors, such as particle shape, relative amounts of sand / fines, have not been considered in this assessment. Chapter 6 provides further discussion as to how fines may sit within a sand particle matrix and how this affects the fines influence factor, b.

If the fines did only sit within the void space created by the sand, then the maximum intergranular void ratio value would be equal to the maximum void ratio, e_{max}, as calculated for the clean sand. Any e_g value greater than e_{max} would correspond to an unstable and unobtainable sand particle structure. The results from the triaxial tests on the FBM soils, as well as the data from the literature, suggest that this does not occur in practice – many of the steady state lines for example are located at e_g values above e_{max} of the clean sand. This is explicitly illustrated in Figure 5-25 using the steady state lines of the FBM soils. The FBM-1 steady state line is located around e_{max}, but the FBM-10 and FBM-20 steady state lines are located well above e_{max}, at e_g values that correspond to very loose packing of the sand skeleton.

Actual soil response therefore demonstrates that the intergranular void ratio assumption of fines playing no part in the soil force-chain is incorrect, even though the relative particle sizes may suggest otherwise. Other studies also suggest this is the case (Lade and Yamamuro, 1997). The FBM-10 and FBM-20 soils were able to be deposited and tested at densities $e_g >>$

e_{max} of the clean sand, which should not be possible without the support of the fines particles in the soil structure. If these fines are supporting the sand particles, then they must also be participating in the soil force-chain to some degree during the loading of the soil.

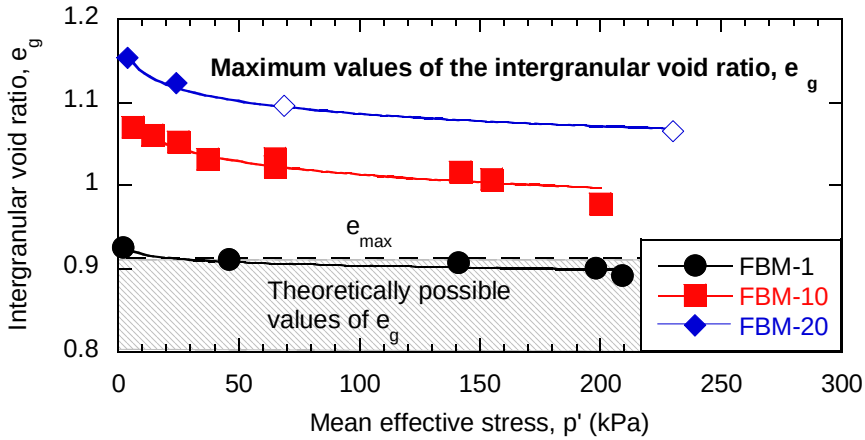

Figure 5-25 Steady state lines of the FBM soils relative to the theoretical maximum e_g value.

5.3. Interpretation using Equivalent Granular Void Ratio

The equivalent granular void ratio, e^*, is used to interpret the responses of the sandy soils presented in Section 5.2. The concept of the equivalent granular void ratio is presented in Section 5.3.1, along with its definition in Equation (5-3). The steady state lines and cyclic resistance curves of the sandy soils are again used as references for the soil response. A method is also presented in Section 5.3.2 for back-calculating the fines influence factor, b.

5.3.1. The Equivalent Granular Void Ratio Concept

The equivalent granular void ratio e^* was proposed (Thevanayagam et al., 2000) as an improvement to the intergranular void ratio, e_g, by allowing for some fines participation in the soil force-chain. This concept again bases around the idea of a binary mixture, with one set of sand-sized particles and another set of fines-sized particles interacting. The sand is still considered the dominant particle size, but the fines are considered to sit in between sand particles, as well as within the sand void space. This creates a soil structure whereby some fines participate in load transfer, and others do not, remaining inactive. Figure 5-26 illustrates this concept using a schematic of 13 sand particles and 23 fines particles. In this schematic, 11 fines particles actively participate in the soil force-chain, while 12 fines particles are shown as being inactive, or sitting in the sand void space.

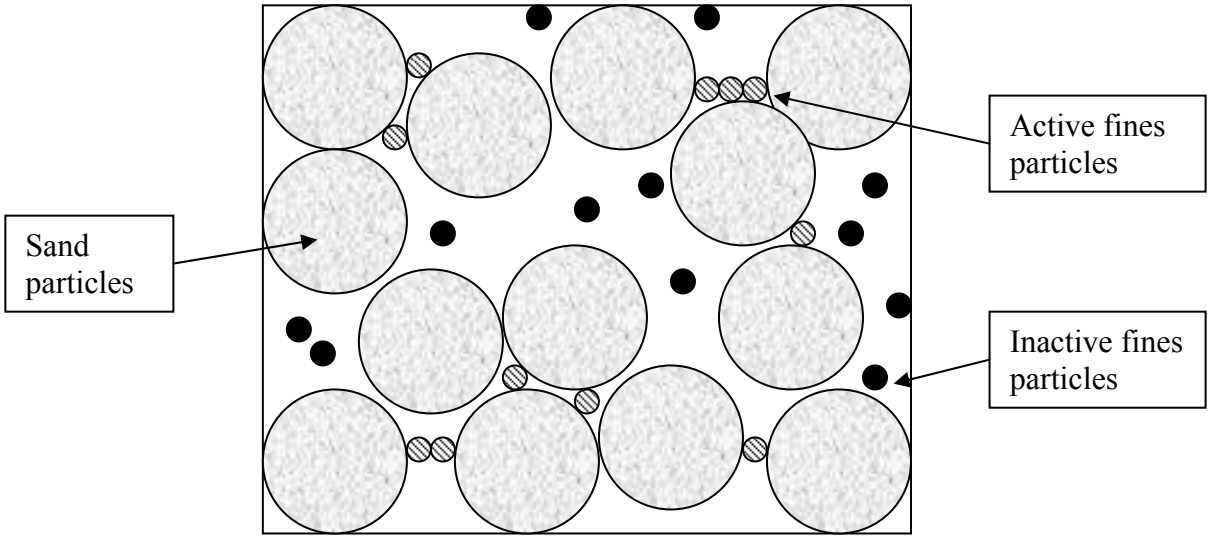

Figure 5-26 Schematic illustrating the equivalent granular void ratio concept. Sand particles are represented by open circles, inactive fines by smaller solid circles, and active fines by smaller hatched circles.

The equivalent granular void ratio, e^*, allows the active fines particles to be included in the state measure through the introduction of the fines influence factor, b. This factor adjusts the fines content of a soil so that a portion of the total fines are considered to be active in the soil force-chain. In the case of Figure 5-26, this portion would be b = 11 / 23 = 0.48 – the fraction of active fines. The equivalent granular void ratio is defined in Equation (5-3).

Equivalent Granular Void Ratio, e^* – where f_C = soil fines content in decimal form, and b = fines influence factor in decimal form:

$$e^* = \frac{e + (1-b) f_C}{1 - (1-b) f_C} \tag{5-3}$$

As displayed in Equation (5-3), the only difference from the intergranular void ratio definition is the addition of the *(1-b)* term multiplying the fines content, f_C. The fines influence factor represents the active portion of fines (Thevanayagam, 2007), and therefore *(1-b)* conversely represents the inactive portion of fines within a mixture of sand and fines.

The equivalent granular void ratio value is equal to the global void ratio value when a clean sand is being assessed ($f_C \approx 0\%$). It may also be equal to the global void ratio if the fines influence factor b = 1.0. In such a case all fines are considered to be participating in the soil force-chain, and there is no need to account for inactive fines, thus $(1-b)f_C = 0$.

The equivalent granular void ratio value can also be equal to the intergranular void ratio value. This occurs when all fines are inactive, or $b = 0$, and hence $(1-b)f_C = f_C$. These two extreme cases of $e^* = e$ and $e^* = e_g$ display the potential advantage of using the equivalent granular void ratio as a state measure – it incorporates full fines participation, no fines participation, and all states in between.

It should be noted that the equivalent granular void ratio concept is only relevant for mixtures of sand and fines below the threshold fines content, f_{Cth}. As discussed in Section 5.2.1, the soil structure fundamentally changes from being sand-dominated to fines-dominated as the threshold fines content is approached. There is however another parameter, the equivalent interfine void ratio (Thevanayagam et al., 2000), that can be used to describe the soil state when $f_C > f_{Cth}$, but as discussed earlier high fines content soils are outside the scope of this study.

Also note that all fines influence factor values are assumed to be constant for a given mixture of sand and fines in this chapter, regardless of individual soil fines content. A number of other studies, including the examination of the behaviour of F55 Foundry Sand (Thevanayagam et al., 2000), Toyoura Sand (Ni et al., 2004), Singapore Old Alluvium (Ni et al., 2006), Hokksund Sand (Yang et al., 2006b), and Silica Sand (Hyodo et al., 2008) have all used this assumption. The validity of this assumption is investigated further in Chapter 6. The notation b_{SSL} refers to the fines influence factor derived based on steady state lines, and b_{CR} derived based on cyclic resistance curves.

5.3.2. Determination of Fines Influence Factor, *b*

Section 5.3.1 presented the equivalent granular void ratio concept and discussed the meaning of the fines influence factor – it represents the portion of fines actively participating in the soil force-chain during loading. Some methods have been proposed to estimate the value of b for a soil based on material properties (Thevanayagam et al., 2003; Rahman et al., 2008), but the most accurate way to determine b is to back-calculate it based on observed soil response. As such, a back-calculation procedure for determining b is detailed below for a given mixture of sand and fines, using a sum of least squares approach. Note that the fines influence factor values b_{SSL} and b_{CR} are calculated separately – this is due to the apparent difference in fines activity between monotonic and cyclic soil response. These differences are discussed further in Chapter 6.

The objective of the back-calculation procedure is to determine a value of b that lets the soil response be similar at a constant value of e^*, independent of the soil fines content. This means that, for example, if $e^* = 0.8$ and $p'_{ss} = 100$kPa for clean sand, then $p'_{ss} \approx 100$kPa when $e^* = 0.8$ for the silty sands.

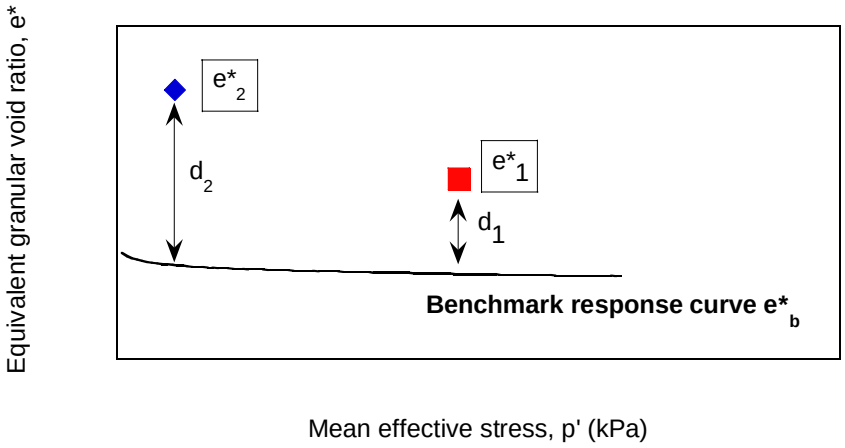

Figure 5-27 Definition of distance, d, from the clean sand benchmark response curve.

(1) The first step in the back-calculation procedure is to define the clean sand benchmark response curve. For monotonic tests, this is the clean sand steady state line. For cyclic tests, this is the clean sand cyclic resistance curve. Mathematical equations are fitted to test data points using a method of least squares to generate these response curves. A logarithmic function is used for the steady state line and a power function for the cyclic resistance curve. The power function was chosen based on observation of the cyclic resistance data presented in Section 5.2.

(2) The equivalent granular void ratio e^* is calculated for all test specimens using $b = 0.0$ - 1.0 in increments of 0.01 ($e^* = f(b)$ for each specimen, given that e and f_C are known). This covers the fines activity range from fully active to zero activity, meaning that all potential values of e^* for the soils are calculated.

(3) The distance d from the benchmark response curve, as illustrated in Figure 5-27, for each non-benchmark specimen e^* as calculated in Step 2, is measured. Note the equivalent granular void ratio values along the benchmark response curve are defined as e^*_b. Therefore to calculate d, e^* is subtracted from e^*_b, or $d = e^*_b - e^*$. The obtained values of d are then squared $\rightarrow d^2 = (e^*_b - e^*)^2$.

(4) The squared distances d^2 are summed up for all test specimens, and divided by the total number of test specimens, n. This summation gives the mean squared error value, *MSE*, for each specimen's e^* value calculated in Step 2. The lowest *MSE* is identified, and the corresponding b is chosen as the best fit for the fines influence factor. This final step is graphically shown for the FBM soil steady state line data in Figure 5-28.

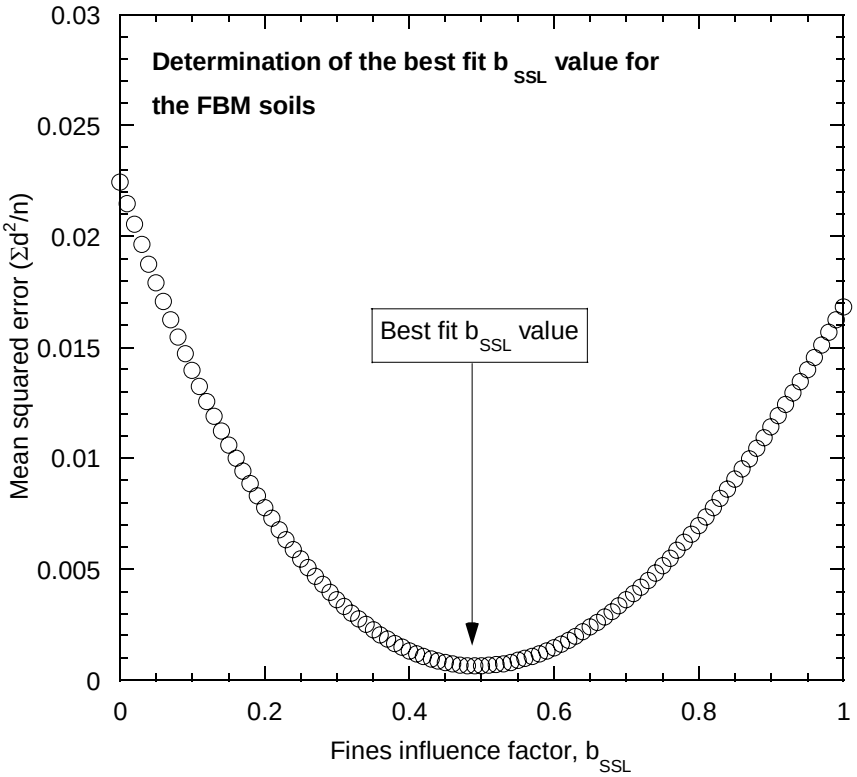

Figure 5-28 Determination of the best fit b_{SSL} value for the FBM soils.

Once the best fit b has been determined, the response curves of all the soils can be plotted together using the equivalent granular void ratio values that correspond to the best fit b as state measures. These response curves should be located in close proximity to one another, indicating that similar values of e^* give similar soil response, regardless of the fines content.

This back-calculation procedure was performed for all mixtures of sand and fines presented in this chapter. Note that when defining the benchmark response curves, any test specimens considered to be obvious outliers, identified through visual inspection of the data, were not included. Steady state lines were also only defined up to p'_{ss} = 500kPa. Specimens with fines contents equal to or above 30% were not included in the back-calculations, as f_C = 30% was used to approximate the threshold fines for all sandy soils.

5.3.3. Interpretation of the Effects of Fines Content on the Steady State Line using the Equivalent Granular Void Ratio

Section 5.2.2 presented and discussed the effects of fines on the steady state line using the intergranular void ratio as the state measure. In that case, the effect of increasing the fines content of sand appeared to make the soil response more dilative. This section instead uses the equivalent granular void ratio as the soil state measure, with the fines influence factor values, b_{SSL}, being derived using the procedure outlined in Section 5.3.2, and the equivalent granular void ratio values being calculated using Equation (5-3). The steady state lines of the FBM soils are presented in Figure 5-29, followed by the back-calculated values of the fines influences factors for the sandy soils sourced from the literature.

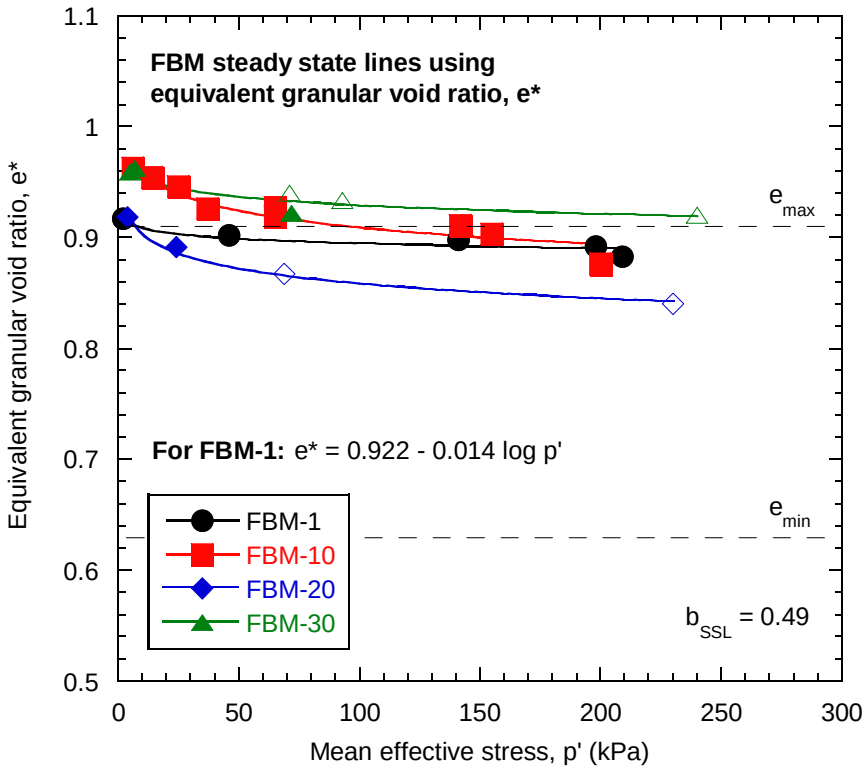

Figure 5-29 Steady state lines of the FBM soils using the equivalent granular void ratio as the state measure.

The steady state lines of the FBM soils in Figure 5-29 are displayed with the maximum and minimum void ratios of the clean sand. These void ratio limits are included to show the range of possible FBM clean sand soil densities, which help to show the relative proximity of all adjusted FBM steady state lines to the benchmark response curve.

Figure 5-29 firstly shows there is significantly less scatter in the steady state line locations when using the equivalent granular void ratio, as compared when using the global or intergranular void ratios as the state measure. This is not surprising given that the value of b_{SSL} = 0.49 was back-calculated to fit the observed test data, but does indicate that a constant b value produces similar undrained monotonic response in the FBM soils as the fines content is increased. Interestingly the FBM-30 soil fits within this conclusion, even though it was not used to calculate b_{SSL} and was shown in Section 5.2.2 to be near the threshold fines content.

Based on Figure 5-29, the steady state line of any FBM soil with $f_C < f_{Cth}$ could be estimated using the FBM-1 steady state line as a benchmark response curve. The state concept could then be used to estimate whether contractive of dilative soil response would occur for the soil at any given density. This is an improvement on using the global or intergranular void ratios as the state measure, where the FBM-1 steady state line could not generally be used as a benchmark for soil response.

Finally the back-calculated value of the fines influence factor, b_{SSL} = 0.49, also provides insight into the actual effect of increasing the soil fines content on the soil response. It suggests that approximately 50% of the fines added to the FBM sand actually participate in the soil force-chain, and 50% of the fines simply sit in the soil without contributing to load resistance. The inactive fines do however increase the overall soil density, which is why in Chapter 4 the steady state lines located at higher densities as the fines content was increased. The information that 50% of the fines are participating in the soil force-chain is important as it means the fines are having a significant effect on the overall soil response, and that the effect needs to be accounted for if the fines content of the soils are altered.

The sandy soils presented in Table 5-1 are restated in Table 5-4 with their respective b_{SSL} values derived using the back-calculation procedure from Section 5.3.2. Note the soils have a b_{SSL} range of 0.12 – 0.69, and that the FBM soil b_{SSL} = 0.49 sits within this range. The range illustrates how variable the participation of fines in the soil force-chain can be, depending on the properties of the respective sand and fines. Sydney Sand for example has approximately 12% of fines participating in the soil force-chain, whilst Ardebil Sand has around 69% participating. This also helps to explain why using the global or intergranular void ratio as the measure of soil state can often produce such differences in the soil response as the fines content is varied – the fines participation itself usually lies somewhere between the extremities assumed in the definitions of e and e_g.

Note that in the associated references, a b_{SSL} = 0.25 was used for both Hokksund Sand (Yang et al., 2006c) and F55 Foundry Sand (Thevanayagam et al., 2002). This value is very close to those calculated using the procedure in Section 5.3.2 (see Table 5-4). These sands, along with the Sydney Sand (Rahman and Lo, 2007), were also the only soil responses to be actually interpreted using the equivalent granular void ratio in the respective references.

Table 5-4 Sandy soils with monotonic steady state line data sourced from the literature, with their back-calculated fines influence factor values included.

Soil	Plasticity of fines	b_{SSL}	Reference
F55 Foundry Sand	NP	0.25	(Thevanayagam et al., 2002)
Ottawa Sand	NP	0.47	(Murthy et al., 2007)
M31 Artificial Sand	NP	0.39	(Papadopoulou and Tika, 2008)
Ardebil Sand	NP	0.69	(Naeini and Baziar, 2004)
Toyoura Sand	NP	0.35	(Zlatovic, 1994; Verdugo and Ishihara, 1996)
Hokksund Sand	NP	0.27	(Yang et al., 2006c)
Sydney Sand	PI = 11	0.12	(Rahman and Lo, 2007)
Mai Liao Sand	PI < 8	0.35	(Huang et al., 2004; Chen and Liao, 1999)

The steady state lines of the soils listed in Table 5-4 are presented in Figure 5-30 to Figure 5-37 using the equivalent granular void ratio as the state measure. The observed trend is similar to that seen for the FBM soils – the steady state lines tend to locate around the clean sand benchmark response curves for a constant value of b. Again this implies that similar e^* values correspond to similar monotonic soil response, for soils with f_C < 30%.

Figure 5-30 highlights the change in soil response as the threshold fines content is reached when using the equivalent granular void ratio concept. The F55 Foundry Sand steady state lines are located at densities between the minimum and maximum clean sand void ratios when f_C < 30%, but the F55-40 steady state line is located well above the e_{max} value. Clearly the equivalent granular void ratio concept, and the adopted constant value for b, are not applicable when f_C = 40%, as the fines are now the dominate particle size of the F55-40 soil.

This effect of changing soil structure on the monotonic response is also very evident for the Mai Liao-30 steady state line in Figure 5-33.

The steady state line locations for all soils, including the FBM soils, are presented in Figure 5-38. This is essentially Figure 5-13 re-plotted using the equivalent granular void ratio as the state measure, instead of the intergranular void ratio. Note that e^*_{100} corresponds to the equivalent granular void ratio e^* when the steady state of deformation is reached at a mean effective stress of 100kPa.

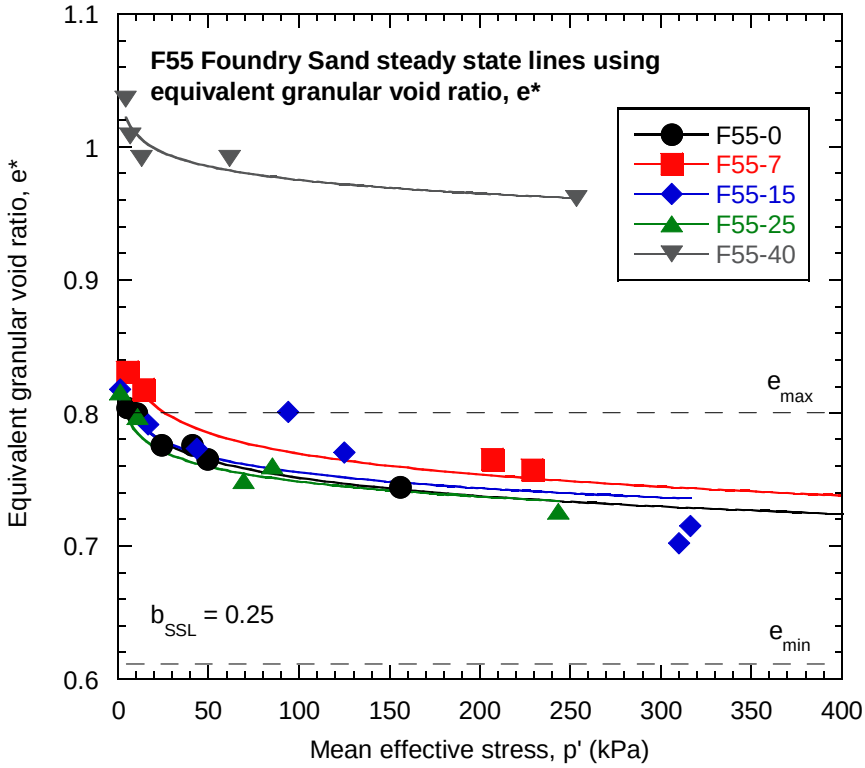

Figure 5-30 Steady state lines of the F55 Foundry Sand using the equivalent granular void ratio as the state measure.

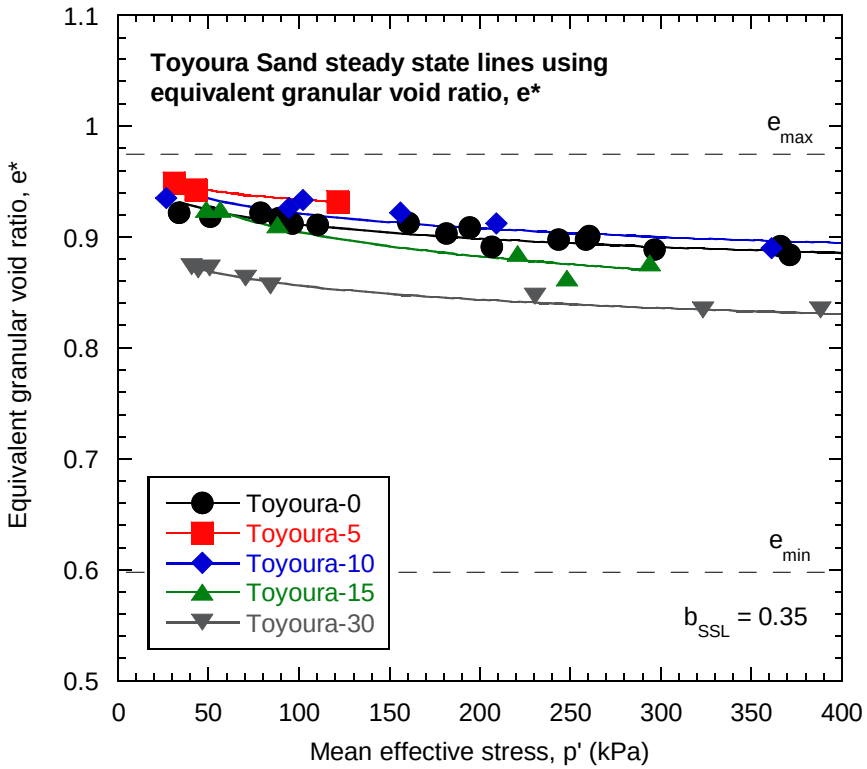

Figure 5-31 Steady state lines of the Toyoura Sand using the equivalent granular void ratio as the state measure.

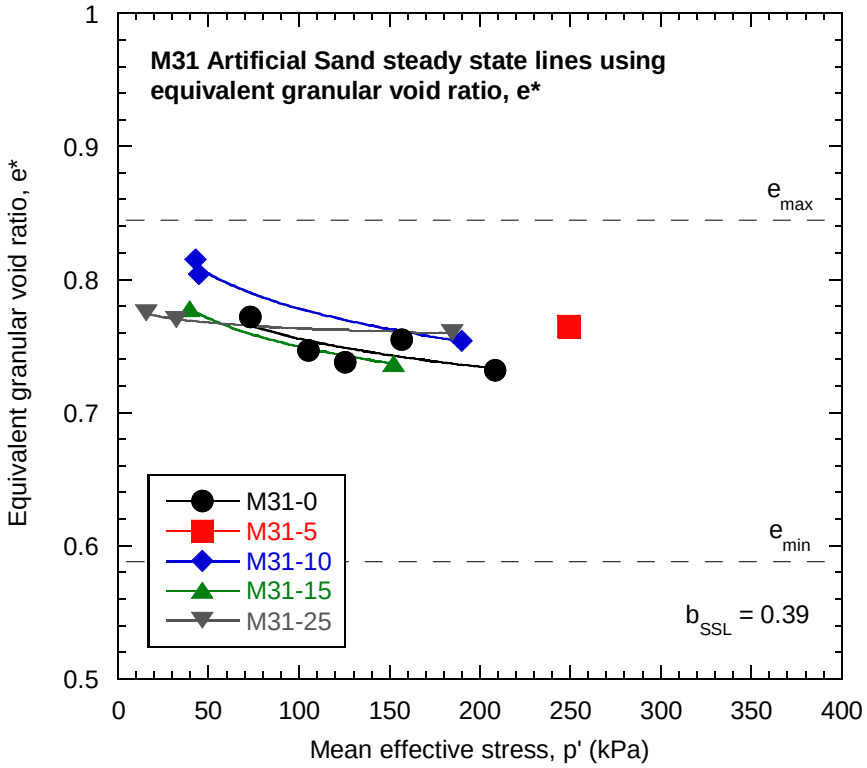

Figure 5-32 Steady state lines of the M31 Artificial Sand using the equivalent granular void ratio as the state measure.

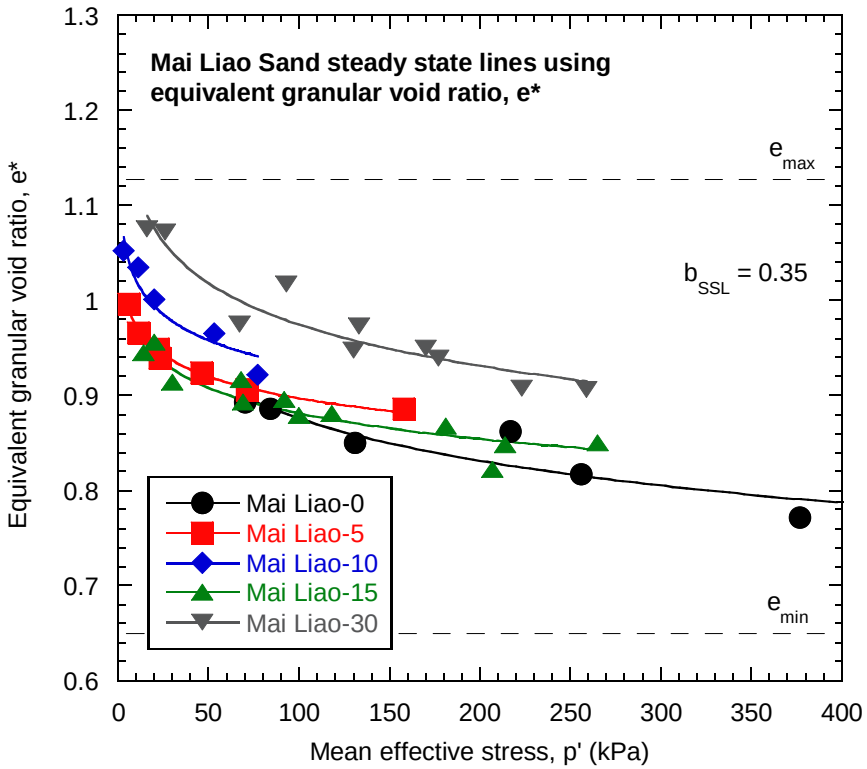

Figure 5-33 Steady state lines of the Mai Liao Sand using the equivalent granular void ratio as the state measure.

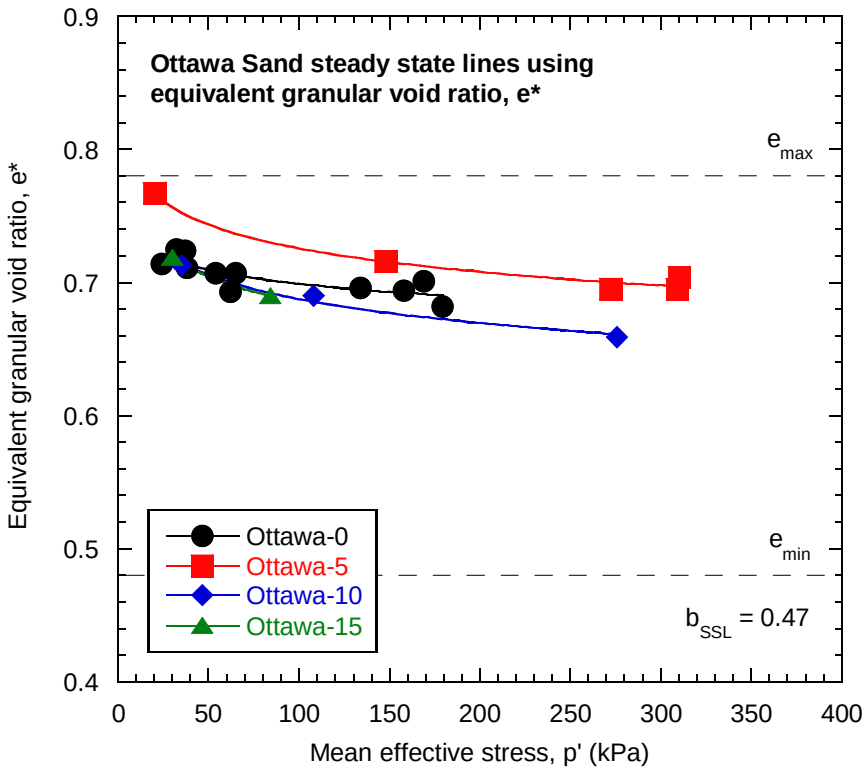

Figure 5-34 Steady state lines of the Ottawa Sand using the equivalent granular void ratio as the state measure.

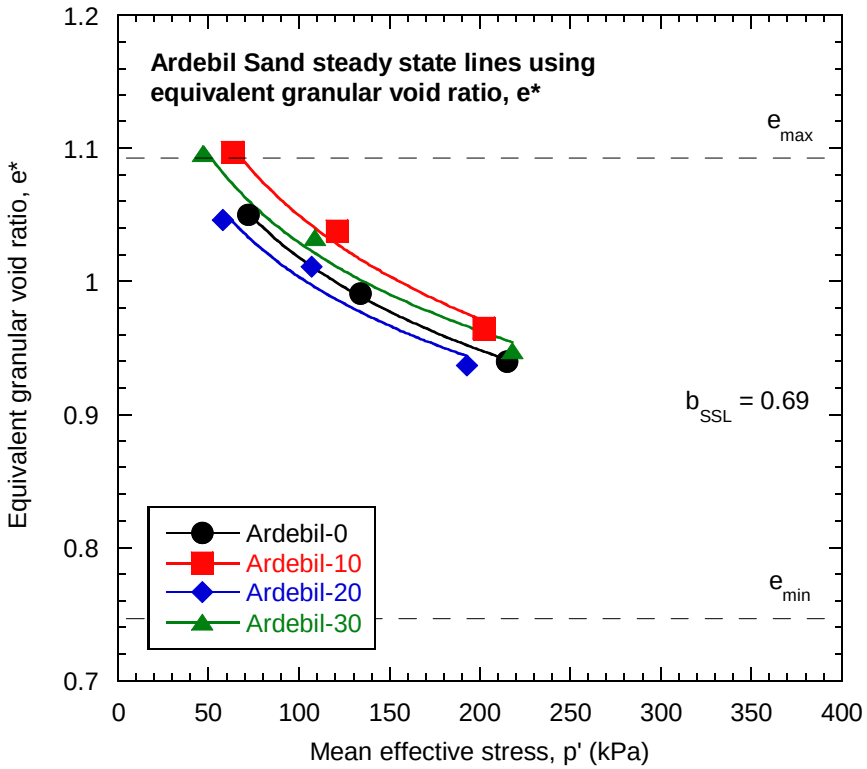

Figure 5-35 Steady state lines of the Ardebil Sand using the equivalent granular void ratio as the state measure.

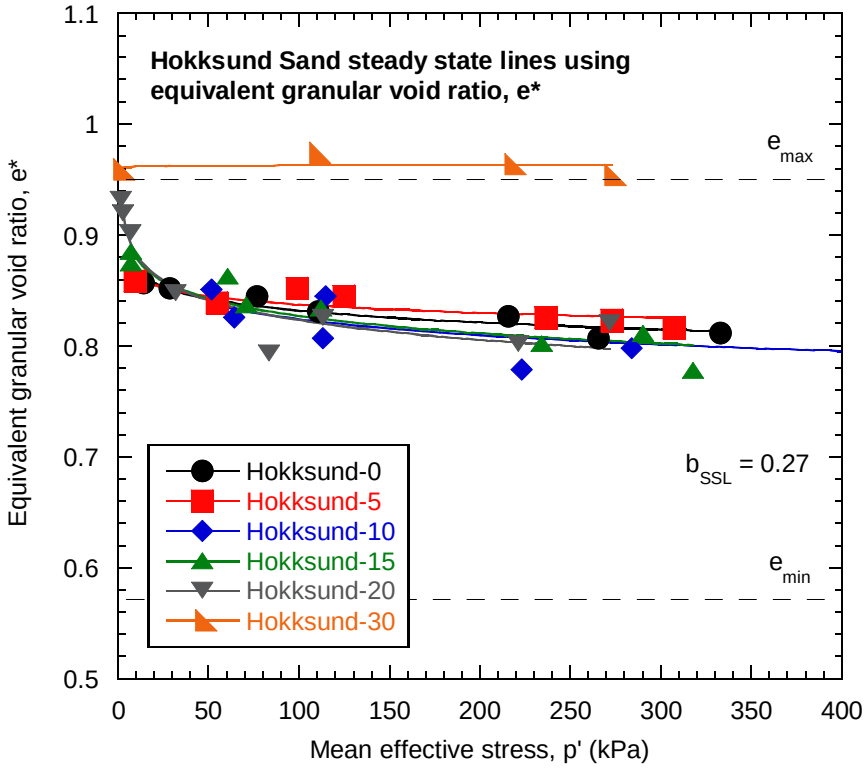

Figure 5-36 Steady state lines of the Hokksund Sand using the equivalent granular void ratio as the state measure.

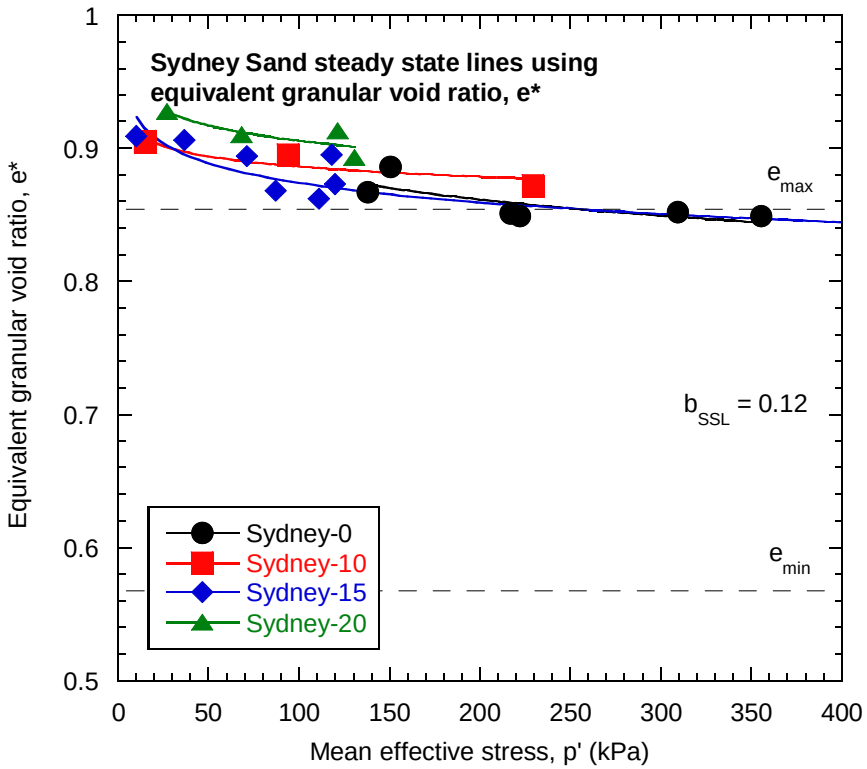

Figure 5-37 Steady state lines of the Sydney Sand using the equivalent granular void ratio as the state measure.

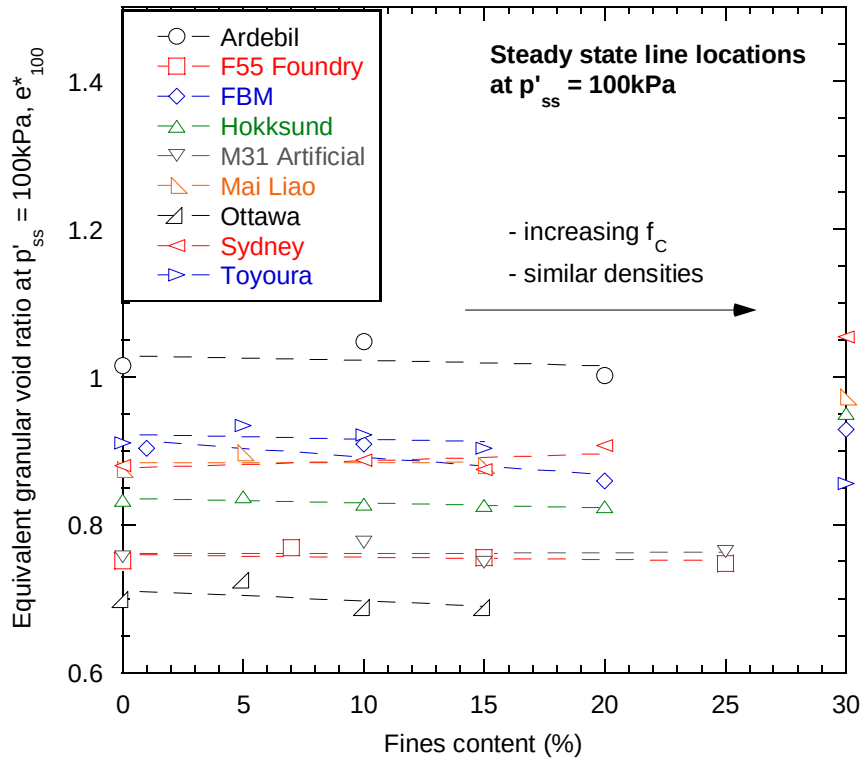

Figure 5-38 Change in steady state line location at *p'* = 100kPa for all sandy soils using the equivalent granular void ratio.

The data in Figure 5-38 confirms that the steady state lines of the sandy soils are located at roughly the same densities (in terms of equivalent granular void ratio values) as the fines content is increased from f_C = 0% to 25%. This makes the estimation of expected soil response at any fines content below 25% possible, as the response becomes largely independent of the fines content when using the equivalent granular void ratio to measure the soil state, assuming the best fit value for the fines influence factor b is used. It is however worth investigating the variability in the steady state line location as the fines content is increased, to quantify how independent the behaviour becomes from fines content. To do this, Figure 5-38 is re-plotted in Figure 5-39 displaying the difference between the steady state line location at a given fines content, and the steady state line location of the clean sand. As such, $e^*_{100\text{-}cs}$ corresponds to the value of e^*_{100} when f_C = 0%.

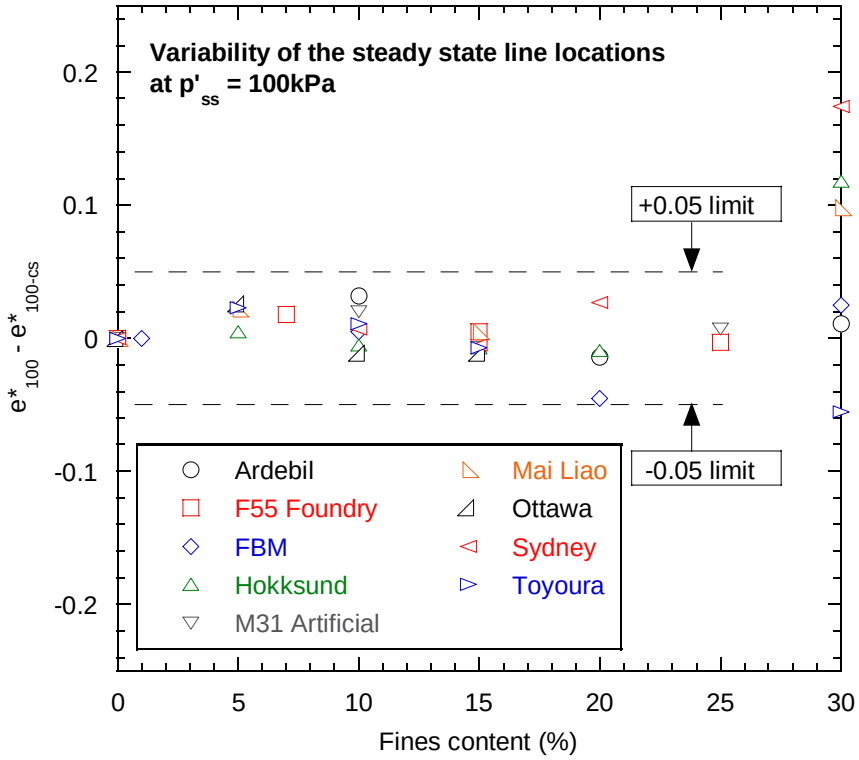

Figure 5-39 Steady state line location difference e^* - e^*_{cs} when p'_{ss} = 100kPa for all soils.

The dashed lines in Figure 5-39 display e^* ± 0.05 limits from the benchmark response curve, or the clean sand steady state line. As can be seen the steady state line locations when p'_{ss} = 100kPa for all the sandy soils sit within these limits when using the equivalent granular void ratio as the state measure. This quantifies the variability in the monotonic response as the fines content is increased – if the best fit fines influence factor value is used, the variation in

e^* at which the steady state of deformation occurs with p' = 100kPa will be within e^* ± 0.05. In terms of expected soil response when using the clean sand response as a reference:

(1) Initial states within e^* ± 0.05 of the clean sand steady state line may show either contraction or dilation;
(2) States e^* - 0.05 below the clean sand steady state line will show dilative soil response;
(3) States e^* + 0.05 above the clean sandy steady state line will show contractive soil response.

Note the scatter in Figure 5-39 is more pronounced once f_C = 30% is reached. As previously stated this fines content is the approximate threshold fines content for the sandy soils, and the equivalent granular void ratio concept is not expected to be applied at this fines content. Interestingly the f_C = 30% steady state lines of two soils sit within the ± 0.05 limit range (Ardebil, FBM) and three soils sit above the +0.05 limit (Hokksund, Mai Liao, Sydney), whilst the Toyoura-30 soil sits just on the edge of the -0.05 limit.

5.3.4. Interpretation of the Effects of Fines Content on the Cyclic Resistance Curve using the Equivalent Granular Void Ratio

The effects of fines on the liquefaction resistance of the sandy soils were also interpreted using the equivalent granular void ratio as the state measure. Figure 5-40 presents the cyclic resistance curves of the FBM soils, with a fines influence factor b_{CR} = 0.65 being back-calculated using the procedure described in Section 5.3.2.

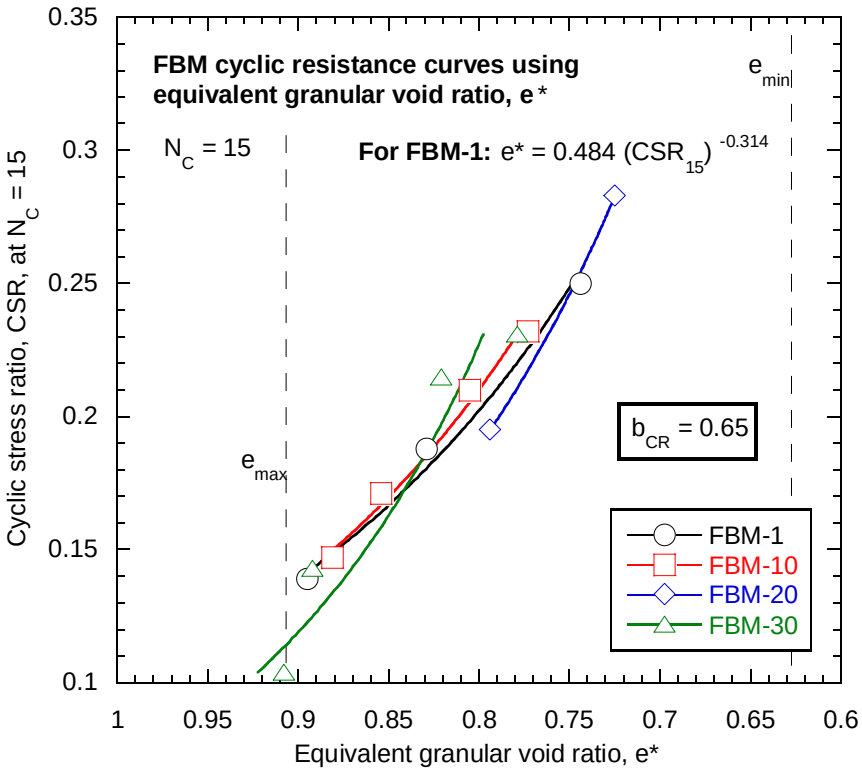

Figure 5-40 Cyclic resistance curves of the FBM soils at N_C = 15 using the equivalent granular void ratio as the state measure.

The cyclic resistance curves in Figure 5-40 are located in close proximity to one another, around the FBM clean sand curve. The maximum and minimum void ratios are also displayed to show the density range of the FBM clean sand. The data suggests that similar values of e^* correspond to similar cyclic resistance for the FBM soils, as was the case for the undrained monotonic response as discussed in Section 5.3.3. Using the clean sand cyclic resistance curve as a response reference, FBM soils with lower e^* values would show less contractive behaviour and reach liquefaction after more load cycles when comparing soil response at a constant level of cyclic stress ratio.

The difference between the two fines influence factors – b_{SSL} and b_{CR} – is also interesting to examine. Their values suggest that approximately 50% of the fines participate in the soil force-chain during monotonic loading, and 65% participate during cyclic loading. However the FBM test specimens were prepared using the same methods, discussed in Chapter 3, for both the monotonic and cyclic tests, meaning that the soil structures were similar before the actual loading of the specimens was begun. This suggests that the participation of fines in the soil force-chain is changing throughout loading, and is discussed in further detail in Chapter 6.

The sandy soils initially presented in Table 5-2 are restated in Table 5-5 including the back-calculated b_{CR} values for the soils. Note that a b_{CR} range of 0.11 – 0.81 is shown for these soils, with the FBM soil b_{CR} = 0.65 sitting within this range. Much like the fines influence factors for steady state lines, the range is wide and highlights how variable the participation of fines in the soil force-chain can be for different mixtures of sand and fines.

Table 5-5 Sandy soils with cyclic resistance curve data sourced from the literature, with their back-calculated fines influence factor values included.

Soil	Fines	b_{CR}	Deposition	Reference
Monterey 0/30 Sand	NP	0.29	Moist tamping	(Polito and Martin II, 2001)
Yatesville Sand	NP	0.67	Moist tamping	(Polito, 1999)
Ottawa Sand	NP	0.32	Slurry	(Carraro et al., 2003)
F55 Foundry Sand	NP	0.30	Moist tamping and dry deposition	(Thevanayagam et al., 2000)
Brenda 20/200 Sand	NP	0.11	Slurry	(Vaid, 1994)
M31 Artificial Sand	NP	0.55	Moist tamping	(Papadopoulou and Tika, 2008)
Mai Liao Sand	$PI < 8$	0.81	Moist tamping	(Huang et al., 2004)
Yunlin Sand	NP	0.35	Moist tamping	(Chien et al., 2002)

Figure 5-41 to Figure 5-48 display the cyclic resistance curves of the soils listed in Table 5-5 using the equivalent granular void ratio as the state measure. These plots show that the liquefaction resistances of the soils are similar for a given e^* value, largely independent from the fines content when $f_C < 30\%$.

Note that the Brenda 20/200 Sand curves in Figure 5-47 are located in closer proximity to the Brenda-0 curve than they were in Figure 5-21 when the intergranular void ratio was used as the state measure. This demonstrates the advantage of using the equivalent granular void ratio – a small amount of fines participation can be accounted for as in the Brenda 20/200 Sand case, or a large amount of participation can be accounted for, best illustrated by the b_{CR} = 0.81 for the Mai Liao Sand.

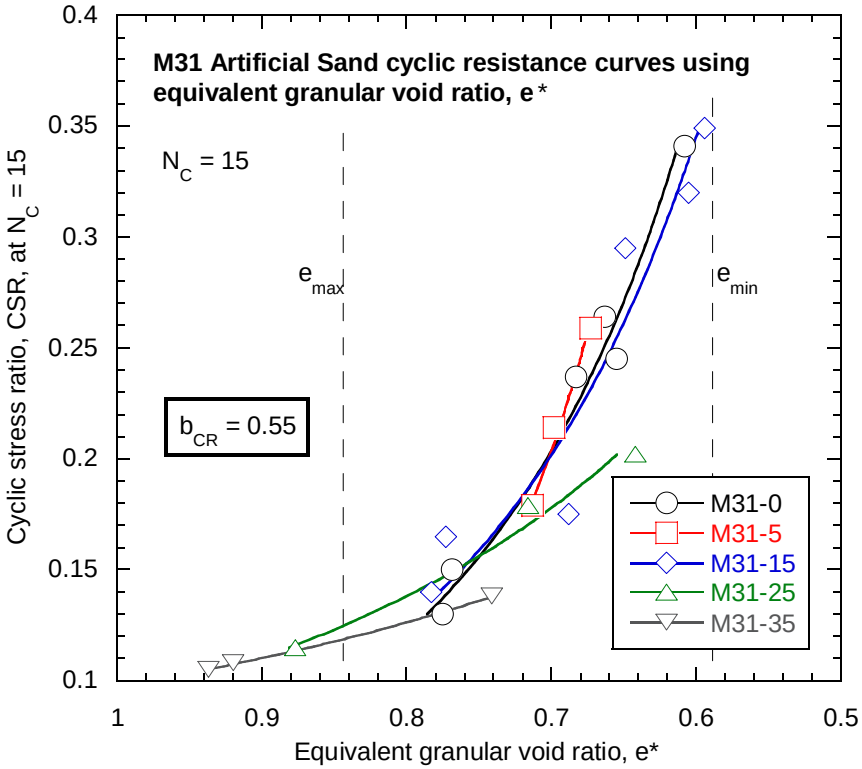

Figure 5-41 Cyclic resistance curves of the M31 Artificial Sand at N_C = 15 using the equivalent granular void ratio as the state measure.

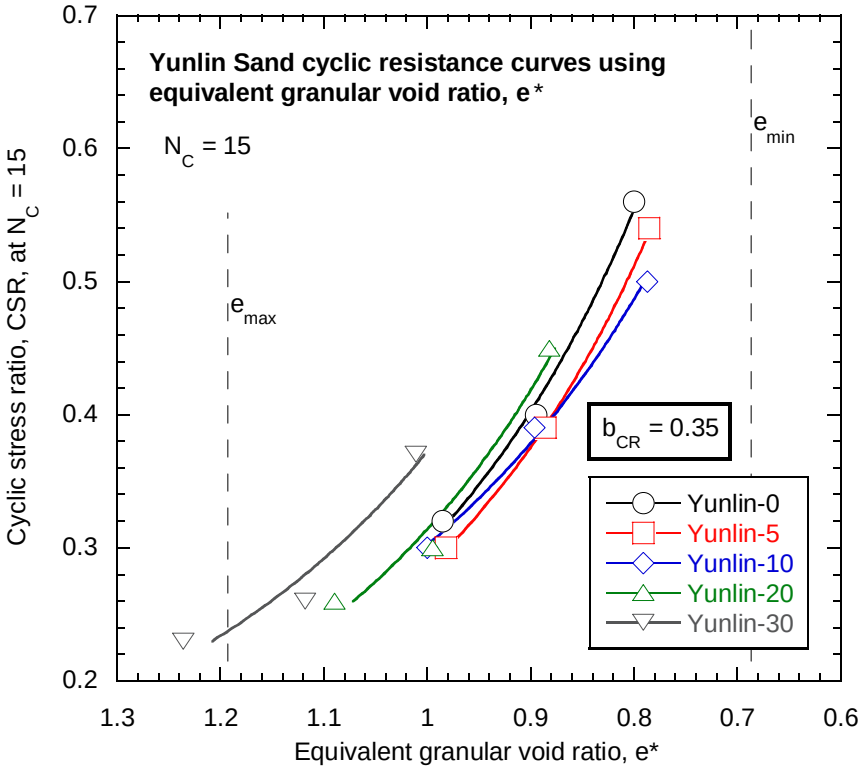

Figure 5-42 Cyclic resistance curves of the Yunlin Sand at N_C = 15 using the equivalent granular void ratio as the state measure.

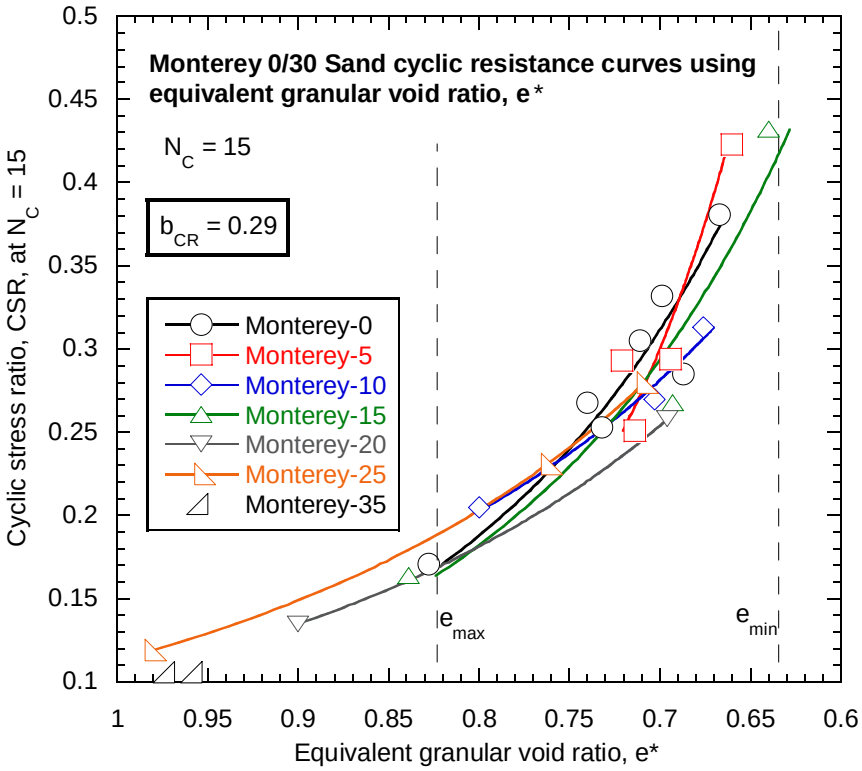

Figure 5-43 Cyclic resistance curves of the Monterey 0/30 Sand at N_C = 15 using the equivalent granular void ratio as the state measure.

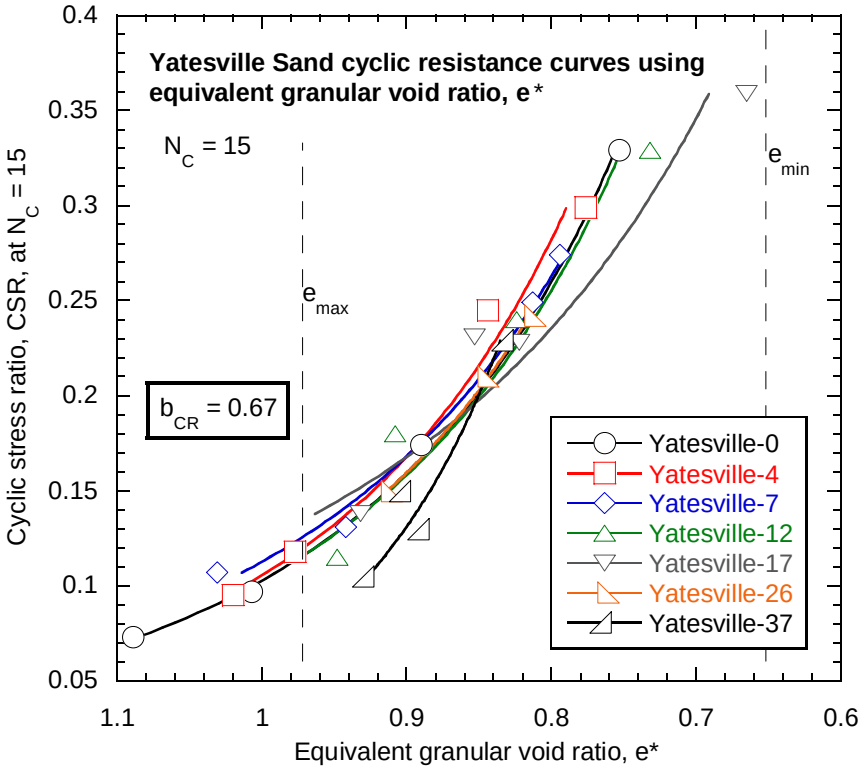

Figure 5-44 Cyclic resistance curves of the Yatesville Sand at N_C = 15 using the equivalent granular void ratio as the state measure.

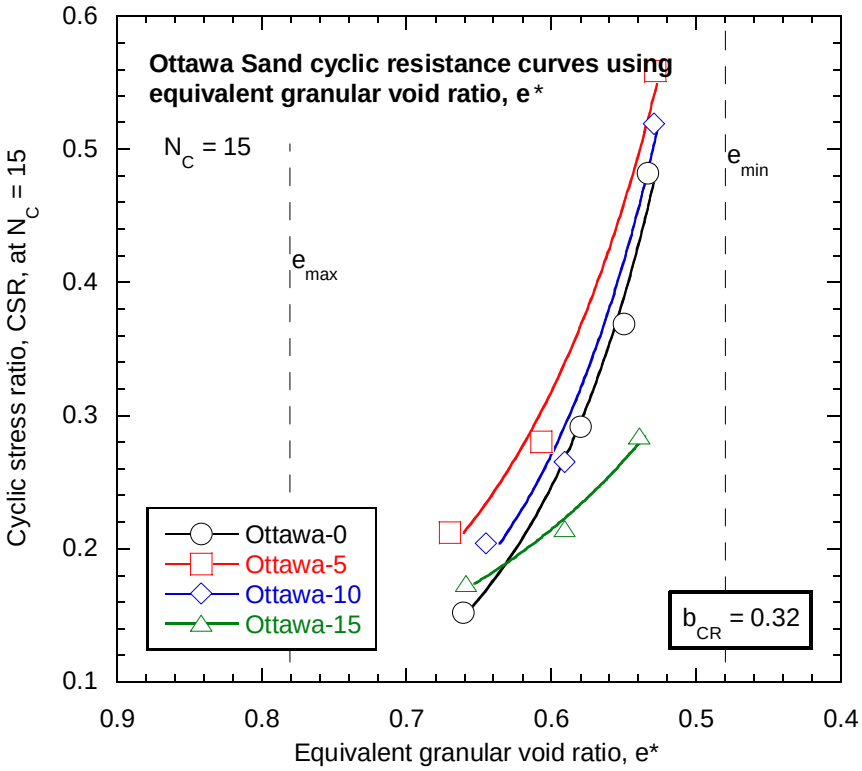

Figure 5-45 Cyclic resistance curves of the Ottawa Sand at N_C = 15 using the equivalent granular void ratio as the state measure.

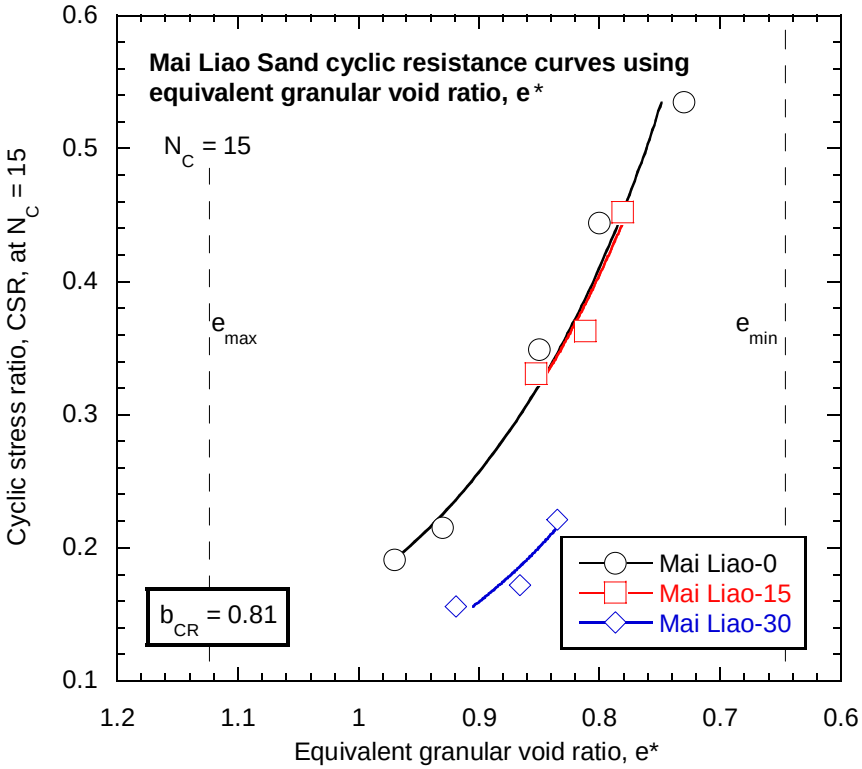

Figure 5-46 Cyclic resistance curves of the Mai Liao Sand at N_C = 15 using the equivalent granular void ratio as the state measure.

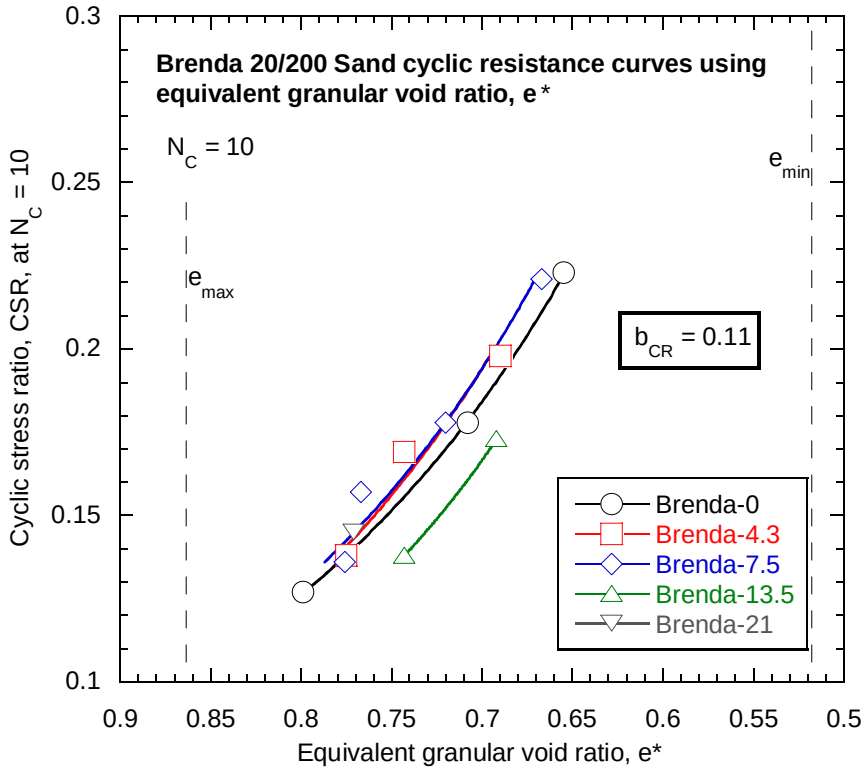

Figure 5-47 Cyclic resistance curves of the Brenda 20/200 Sand at N_C = 10 using the equivalent granular void ratio as the state measure.

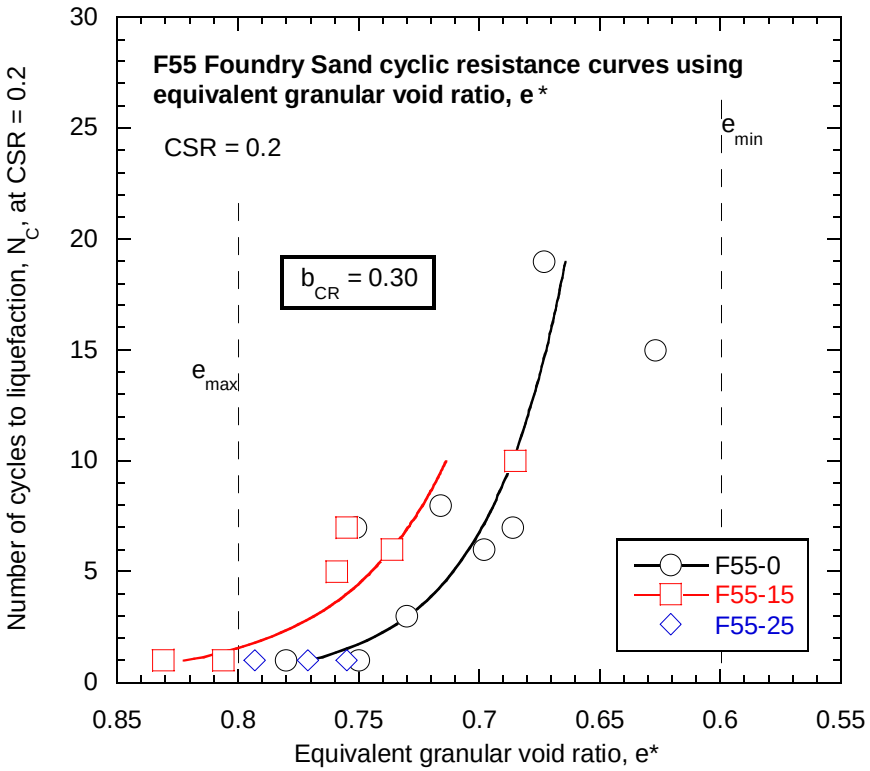

Figure 5-48 Cyclic resistance curves of the F55 Foundry Sand at N_C = 15 using the equivalent granular void ratio as the state measure.

The locations of the cyclic liquefaction curves at CSR = 0.2, $e^*_{CSR=0.2}$, for all soils presented in Table 5-5 except the Yunlin Sand, are shown in Figure 5-49. As can be seen, the curves are located at similar densities as the fines content is increased, unlike the trend observed in Figure 5-23 when the intergranular void ratio was used.

There is some scatter of the data points in Figure 5-49, indicating variability in the liquefaction resistances of the soils for a constant value of e^* as the fines content is increased. To quantify this variability, the difference in values between the equivalent granular void ratio of the clean sand, $e^*_{CSR=0.2\text{-}cs}$, and the other silty sands at CSR = 0.2 and N_C = 15 were calculated. This method was also used to quantify the variability of the steady state line locations in Section 5.3.3. It essentially compares the response of the silty sands, when using the equivalent granular void ratio, with the benchmark response. The calculated differences are plotted in Figure 5-50.

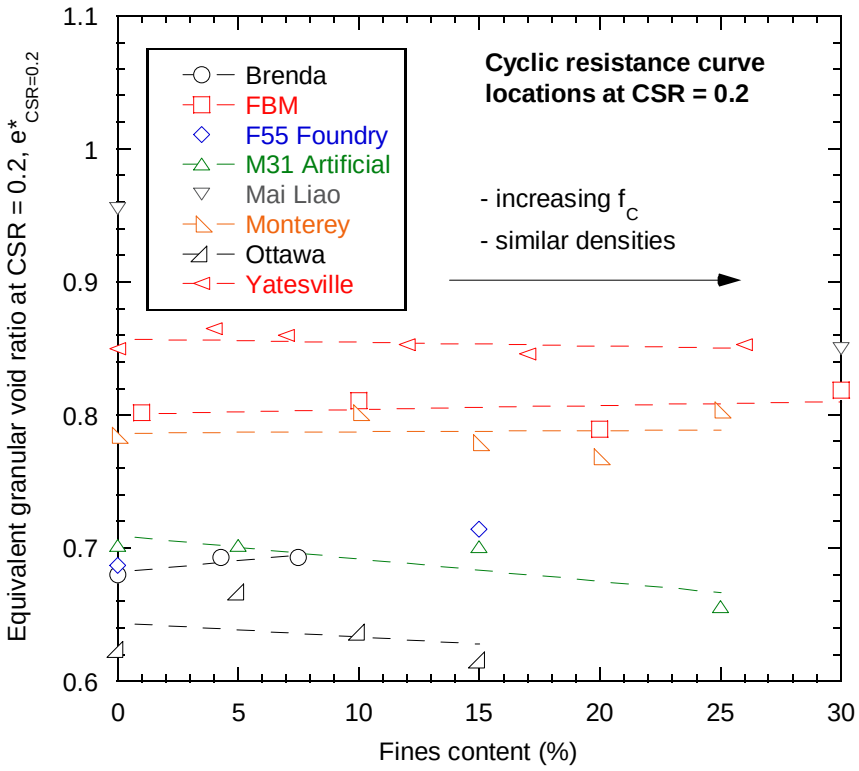

Figure 5-49 Change in cyclic resistance curve location at CSR = 0.2 for the sandy soils using the equivalent granular void ratio.

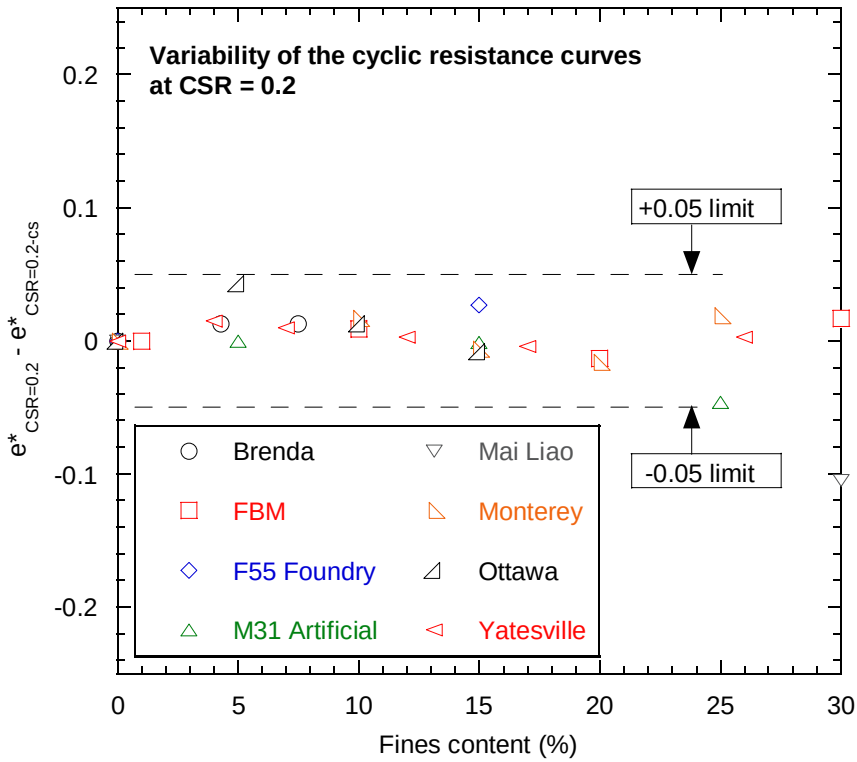

Figure 5-50 Cyclic resistance curve location difference e^* - e^*_{cs} at CSR = 0.2 for a selection of soils.

The dashed lines in Figure 5-50 are e^* ± 0.05 limits from the benchmark response curve. Note that the values of these limits are the same as those observed in Figure 5-39 for the monotonic steady state lines. All cyclic data points for the sandy soils, when f_C < 30%, sit between these limits. This suggests that when using the fines influence factors derived from the back-calculation procedure in Section 5.3.2, similar soil response occurs when the soil density is within e^* ± 0.05 of the clean sand soil density. Note that this has only been quantified at the steady state of deformation when p'_{ss} = 100kPa, and for cyclic liquefaction being reached after 15 cycles when the cyclic stress ratio is 0.2. Generally however, soils with e^* + 0.05 difference from the clean sandy density will exhibit more contractive response during undrained loading, and soils with e^* - 0.05 difference will show more dilative response during undrained loading.

5.4. Summary

This chapter interpreted the undrained monotonic and cyclic response of a number of sandy soils using two measures of soil state. These were the intergranular void ratio, e_g, and the equivalent granular void ratio, e^*. Both of these parameters differentiate between sand and

fines-sized particles in their respective definitions, and each accounts for different levels of fines participation in the soil force-chain during undrained loading.

The interpretation made using the intergranular void ratio, e_g, was discussed in Section 5.2. It showed that the undrained response of the investigated sandy soils became more dilative as the fines content increased, when comparing response at similar values of e_g. This meant that soil strengths at the steady state of deformation increased with the addition of fines, and that liquefaction resistances also increased as the fines content was raised. A critical assessment of the intergranular void ratio concept was also performed, which suggested that the relative sizes of the sand and fines particles within the sandy soils could potentially allow the fines to sit within the void space created by the sand without participating in the soil force-chain. The actual response of the soils however suggested that the fines do sit between the sand particles, and participate in the soil force-chain to some degree. This was due to soil densities, in e_g terms, well above the maximum void ratio of the clean sand being observed, which responded to load by exhibiting dilatant behaviour as the fines content was increased. From this it was concluded that the intergranular void ratio is not a consistenly useful parameter for measuring the soil state of sand and fines mixtures, as similar values of e_g do not generally correspond to similar soil response.

The interpretation made using the equivalent granular void ratio, e^*, was presented in Section 5.3. This firstly illustrated that the undrained response of the FBM soils, both monotonic and cyclic, was similar when the test specimens had similar values of e^*. It was therefore concluded that e^* could be used as a normalizing parameter for the effects of fines on the undrained behaviour if appropriate values of the fines influence factor, b, were used. Such values were back-calculated for the FBM soils, where $b_{SSL} = 0.49$ when interpreting the steady state lines, and $b_{CR} = 0.65$ when interpreting the cyclic resistance curves. The undrained responses of sandy soils presented in other studies were also interpreted using e^*, drawing the same conclusions as for the FBM soils. These interpretations highlighted the variability in the value of b, which ranged between $b_{CR} = 0.11$ for Brenda 20/200 Sand and $b_{CR} = 0.81$ for Mai Liao Sand. The steady state line fines influence factors ranged between $b_{SSL} = 0.12$ for Sydney Sand and $b_{SSL} = 0.69$ for Ardebil Sand. Finally, it was concluded that the undrained clean sand response of a particular sand-fines mixture can be used as a reference to estimate the soil response as the fines content of sand is increased, providing an appropriate value of the fines influence factor is known.

6. The Fines Influence Factor, *b*

6.1. Introduction

The equivalent granular void ratio e^* was introduced and defined in Chapter 5 based on previous research (Thevanayagam et al., 2000), and is reproduced again in Equation (6-1):

$$e^* = \frac{e + (1-b) f_C}{1 - (1-b) f_C} \tag{6-1}$$

This parameter was used as the state measure when interpreting the monotonic and cyclic responses of a number of sandy soils, and showed that at a given value of e^* the soil response is relatively similar, independent of the fines content.

The parameter b in Equation (6-1) is the fines influence factor, which in theory based on binary particle packing describes what portion of the fines participate in the soil force-chain during loading (Thevanayagam, 2007). As illustrated in Chapter 5, the fines influence factor can be back-calculated for a range of sandy soils for both undrained monotonic and cyclic test data. This allows such measures of soil response as the steady state line and cyclic resistance curve to be used as a reference to estimate the soil response of fines-containing sand. The equivalent granular void ratio has already been used in several studies (Thevanayagam et al., 2002; Ni et al., 2004; Rahman et al., 2008) to interpret such response.

There is however a current lack of knowledge available about the nature of the fines influence factor, b, and what it physically describes for natural soils. Considering the equivalent granular void ratio theory is based on binary packing, some differences must be present when such a concept is applied to real soil materials with continuous particle distributions. Other issues, such as how b varies with fines content, and why it has different values for monotonic and cyclic loadings respectively, have yet to be thoroughly investigated.

As such, this chapter firstly attempts to define the fines influence factor by considering physical soil properties and characteristic responses. It then moves on to show that b can be assumed to be constant for fines contents below the adopted threshold fines content of f_C = 30%. The difference between the fines influence factor values at the steady state of

deformation and cyclic liquefaction is discussed, and the back-calculated values of *b* for a range of sandy soils are correlated with material properties. Finally a simplified method for estimating values of *b* using material properties of the soil is presented.

6.2. Soil Properties and the Fines Influence Factor

The fines influence factor, *b*, was derived from binary packing theory (Thevanayagam et al., 2000), in which all particles are assumed to be spherical, and only two particle sizes are present – one unique size for sand particles and one unique size for fines particles. In reality however, mixtures of sand and fines have a continuous particle size distribution and variable particle shapes that can be relatively rounded to highly angular. This is illustrated in Figure 6-1 by Scanning Electron Microscope (SEM) images of the FBM sand and fines. As is shown, natural soils differ greatly from the binary assumption.

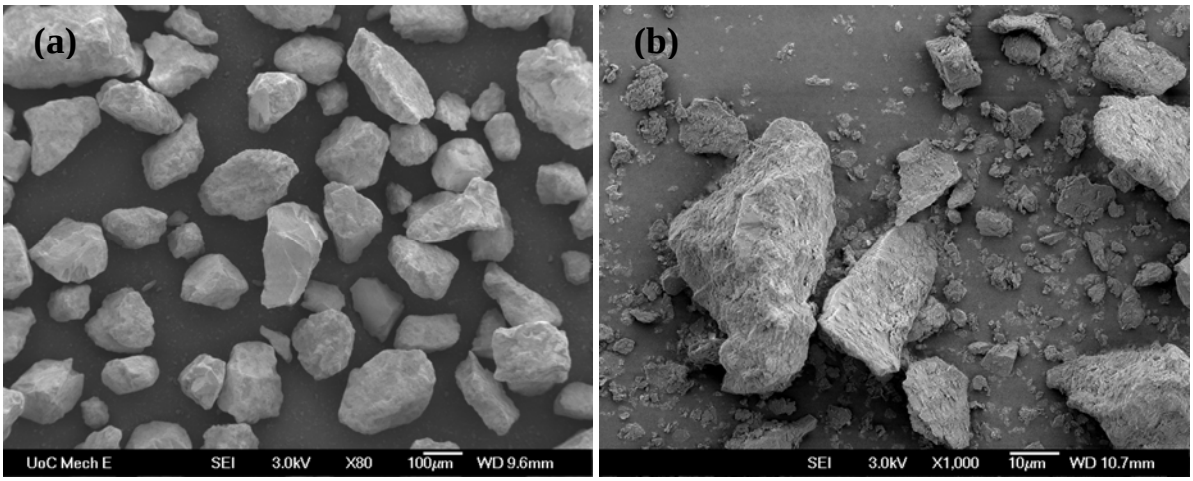

Figure 6-1 SEM images of the FBM (a) sand particles, and (b) fines particles.

It is therefore expected that the binary packing concept, and theoretical meaning of *b*, do not precisely describe the actual interactions between sand and fines particles of natural soils. The equivalent granular void ratio has however been shown to be very useful in measuring the states of these soils, and hence the fines influence factor in particular needs to be properly defined in light of such differences between the theoretical assumption and reality.

In shifting from the idealized binary packing concept to real soils, a number of additional factors relating to the soil particle properties must be accounted for. All of these factors are known to affect the undrained behaviour of soils, and it is therefore suggested that

they may also affect the participation of the fines in the soil force-chain. These factors include:

- Continuous particle size range
- Angularity of particles
- Plasticity of fines particles
- Mineralogy of particles

(1) Continuous particle size range – the shift from two particle sizes in the binary assumption to a continuous size distribution is a major issue. Instead of having two different particle sizes, there are two distinct and different particle size distributions: one for the sand (particles >75μm in diameter) and one for the fines (particles <75μm in diameter). This means there are most likely particles within each of these individual distributions not actively participating in the soil force-chain (Thevanayagam and Mohan, 2000), not just the fines. For example, sand particles close to 75 μm in size may sit in void spaces between other larger sand particles, even when the sand is clean. This would clearly not occur if all sand particles were of the same size, and is more likely to be an issue when the soil is looser (at a higher value of e). An inherent assumption when using any form of void ratio to measure state is that all sand particles are actively participating in the soil force-chain, which becomes inaccurate when real soils are considered.

(2) Fines participation – there is also the issue of how particle activity relates to number of active contacts when using the equivalent granular void ratio. The global void ratio definition is a global parameter, providing an approximation of the index of active particle contacts. The fines content parameter in the equivalent granular void ratio is also global, and quantifies the amount of fines within a soil by weight. The fines influence factor, b, acts on this term meaning that $(1-b)f_C$ theoretically gives the quantity of inactive fines particles within the whole specimen by weight also. Therefore for a constant b value, there could potentially be a small number of larger fines participating in the soil force-chain, or a large number of smaller fines being active, assuming the specific gravity of all fines is equal. These two cases are quite misleading in terms of the number of active contacts: the former case (larger fines) would result in fewer active contacts, and the latter case (smaller fines) would result in more active contacts. The main point is that the fines influence factor, even when considering fully active sand particles, does not give information on the number of active fines contacts. It only

considers the global effect of the fines, which may be due to a small number of larger particles. Hence a high fines influence factor value does not necessarily mean a high number of fines particles are participating in resisting load.

(3) Other factors – the three other particle factors – angularity, plasticity, mineralogy – also affect the undrained behaviour of sandy soils in complex ways. Angularity can change the void ratio (Miura et al., 1997) and the way particles move in relation to each other. Plastic fines can alter the frictional characteristics between the particles and potentially increase the liquefaction resistance of a soil (Polito, 1999). Given that all these factors must also be taken into account when considering how fines may affect the undrained behaviour of sand, it seems inappropriate to explicitly define the fines influence factor as the percentage of active fines (by weight) participating in the soil force-chain. Instead, the following definition has been used for the fines influence factor in this study:

Fines influence factor, b – "*a factor that accounts for all the combined effects of different parameters on the undrained response of sand due to the addition of fines below the threshold fines content*".

This definition clearly does not give a purely physical interpretation for the fines influence factor, as other studies have (Thevanayagam, 2007). Rather it assumes that the mechanisms in which fines interact with other particles are very complex, and depend on a whole range of soil particle factors. The fines influence factor is therefore currently viewed as a convenient parameter to combine all such effects coming from the physical changes in the sand response as fines are introduced, based on theoretical concepts that approximate the actual soil particle interactions. When correlating the values of b with the material properties of soil in Section 6.5 however, the theoretical concepts are still used to try and explain the observed trends.

6.3. The Constant Fines Influence Factor Assumption

The fines influence factor, b, has most commonly been used in the literature as a constant value for sands with fines contents below the threshold fines content (Thevanayagam and Martin, 2002; Ni et al., 2004). Some studies have modified the b value once the f_{Cth} is reached (Yang et al., 2006a), and some have varied the b value as the fines content is

increased (Rahman et al., 2008). However, there has yet to be a detailed assessment of how b may change as the fines content is varied, meaning the constant b value assumption has not been verified. To investigate this issue, the b values at varying fines contents were analyzed for a range of sands. These include the soils from the literature presented in Chapter 5 to assess the intergranular and equivalent granular void ratios, and the FBM soils tested in this study.

All b values were derived using the same method described in Chapter 5. The best fit for each individual soil (unique fines content) was found in relation to the clean sand benchmark response, with the factor $(1-b)f_C$ being plotted against the soil fines content. The comparison has been done in this way to clearly show how the global void ratio is altered by the additional parameters b and f_C contained within the equivalent granular void ratio definition in Equation (6-1).

6.3.1. Variation of $(1-b)f_C$ with Increasing Fines Content

Figure 6-2 illustrates how the fines influence factor varies with increasing fines content for the FBM soils, using both the b_{SSL} values obtained from the steady state lines, and b_{CR} values obtained from the cyclic resistance curves. The line $b = 0$ corresponding to zero fines influence is displayed for reference, and $b = 1.0$ corresponds to the horizontal x-axis. The lines indicating the constant b_{SSL} or b_{CR} values for the soils as derived in the Chapter 5 analysis are also displayed in Figure 6-2.

Figure 6-2 firstly shows that the constant fines influence factor value is higher for the cyclic test data ($b_{CR} = 0.65$) compared with the monotonic test data ($b_{SSL} = 0.49$). This is the case for all individual FBM soils at all tested fines contents, suggesting the fines have more effect, or more influence within the internal soil force-chain, during the undrained cyclic response than the monotonic response. The importance of this is that the fines influence factor values vary with loading type, which has only been considered in one other study using the equivalent granular void ratio to measure soil state (Thevanayagam et al., 2003). All other studies have assumed that the value of the fines influence factor for a given mixture of sand and fines is the same for both monotonic and cyclic loadings. An explanation for the difference between b_{SSL} and b_{CR} is given in Section 6.4.

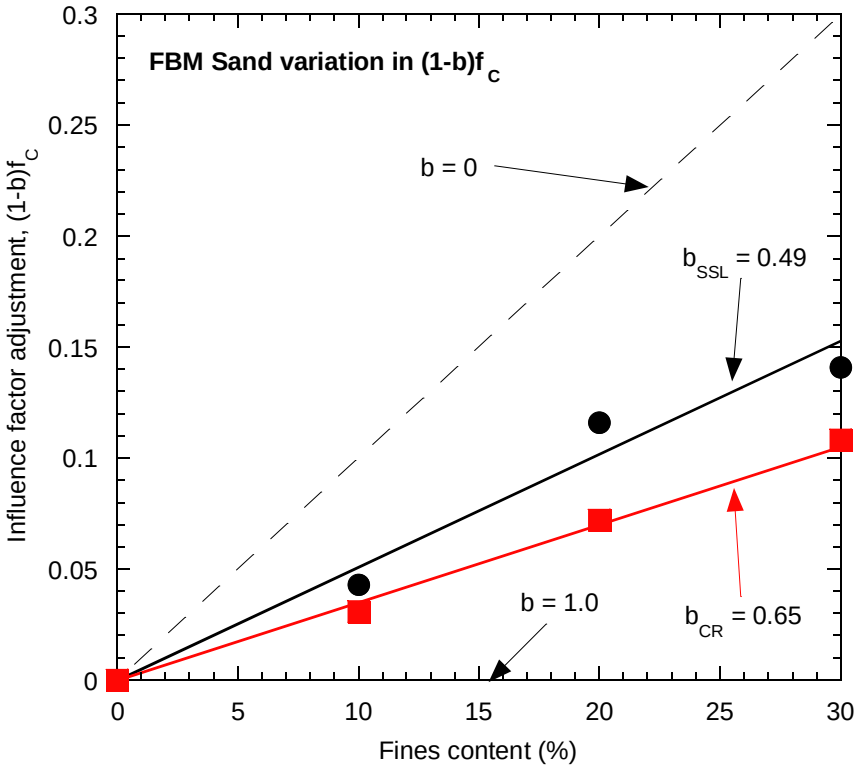

Figure 6-2 Variation in $(1-b)f_C$ as the fines content of the FBM soils is increased.

There also appears to be more variation in the individual b_{SSL} values from the constant b_{SSL} value than for the individual b_{CR} values from the constant b_{CR} value. This was visually noticed in Chapter 5, whereby the steady state lines tended to show more scatter about the clean sand benchmark response than the cyclic resistance curves did when the equivalent granular void ratio was used as the state measure. This may be due to the greater difficulty in accurately defining the steady state lines, as the mean effective stress reached at the steady state of deformation, p'_{ss}, is very sensitive to the soil density. The steady state line can therefore be thought more of as a band (Cubrinovski and Ishihara, 2000), rather than a distinct line. However the increased scatter may also be a physically occurring phenomenon, with the individual b_{SSL} naturally not fitting closely to the constant b_{SSL} value. This would imply that the effect of fines on the undrained monotonic response varies more significantly with changing soil fines content than for the cyclic response. Given that the cyclic liquefaction resistance is also very sensitive to differences in soil density and loading, it is difficult at this stage to truly determine if b_{SSL} is more naturally variable than b_{CR} for the FBM soils.

Another interesting observation that can be seen in Figure 6-2 concerns the relative locations of the individual fines influence factors. For f_C = 10%, both the indiviual $(1-b_{SSL})f_C$ and $(1-b_{CR})f_C$ points sit below the linear approximations. This means that the individual b

values are slightly higher than the constant values, or there is more fines influence at f_C = 10% than the average. This reverses at f_C = 20%, where the individual $(1-b_{SSL})f_C$ value clearly sits above the constant b value line, and the $(1-b_{CR})f_C$ point sits on the constant b_{CR} line. This is somewhat expected – only f_C = 10% and 20% were used for the FBM soils to define the constant b_{SSL} and b_{CR} values (f_C = 30% was omitted due to proximity to the threshold fines content). Thus if the individual b values were higher than average at 10%, they would be expected to be lower than average at 20%. The interesting point is that they are not constant, but are relatively higher at lower fines contents, f_C = 10%, and relatively lower at higher fines contents, f_C = 20%, for both monotonic and cyclic loadings. This trend implies that the fines actually influence the undrained soil response more at lower fines contents than they do at higher fines contents, relative to the fines content of the soil. Of course the absolute influence of the fines is greater at higher fines contents, as shown by the increasing influence factor adjustment values in Figure 6-2. Note that this trend should be treated with caution, as there is currently a very limited amount of data available about the value of the fines influence factor as the fines content is varied.

Thus the following conclusions can be taken from the individual fines influence factor assessment for the FBM soils:

- The required adjustment $(1-b)f_C$ to the global void ratio increases with increasing fines content, meaning the fines affect the undrained response of the FBM sand proportional to the fines content
- Fines influence factor b values are slightly higher at lower fines contents
- The b_{SSL} values (monotonic) for FBM soils show more variation than the b_{CR} values (cyclic)
- The b_{CR} values (cyclic) are higher than the b_{SSL} values (monotonic) for all fines contents, suggesting fines influence the cyclic response more than the monotonic response as represented by the steady state of deformation

Importantly, it does appear based on Figure 6-2 that using a constant value for the fines influence factor is a reasonable approximation for the FBM soils. However, a different value of b applies to the monotonic behaviour and cyclic resistance of the FBM soils.

The variation of $(1-b)f_C$ was also assessed for the other presented sandy soils to examine how b_{SSL} and b_{CR} vary with increasing fines content. Note however that only the soils that were tested using both monotonic and cyclic loadings are displayed in individual plots – these were the M31 Artificial Sand, Ottawa Sand, Mai Liao Sand, and F55 Foundry Sand. Their respective plots are shown in Figure 6-3 to Figure 6-6. It should also be kept in mind that the test data from soils with $f_C \geq 30\%$ was not used to calculate the constant values of b_{SSL} and b_{CR} in Chapter 5. This is why the lines indicating constant b_{SSL} and b_{CR} values in Figure 6-5 for the Mai Liao Sand vary significantly from the individually-calculated b_{SSL} and b_{CR} values when f_C = 30%.

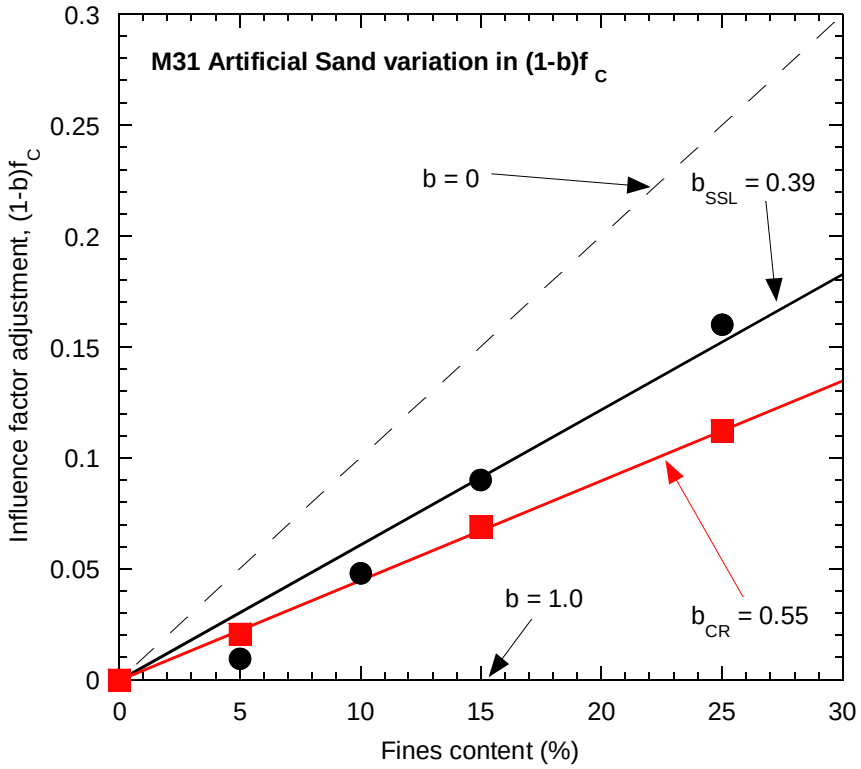

Figure 6-3 Variation in $(1-b)f_C$ as the fines content of the M31 Artificial Sand is increased.

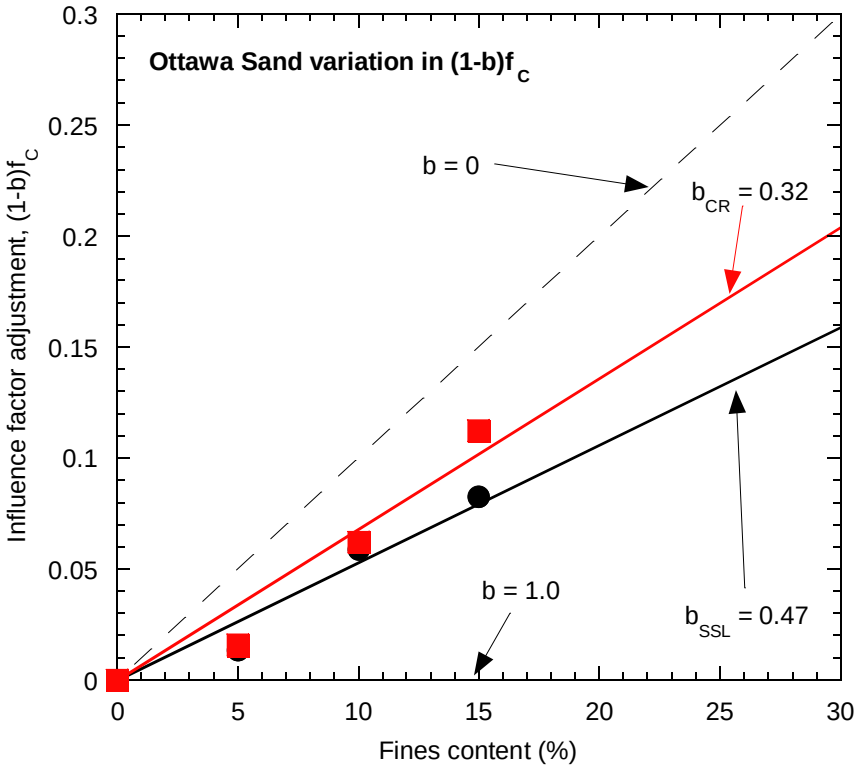

Figure 6-4 Variation in *(1-b)f_C* as the fines content of the Ottawa Sand is increased.

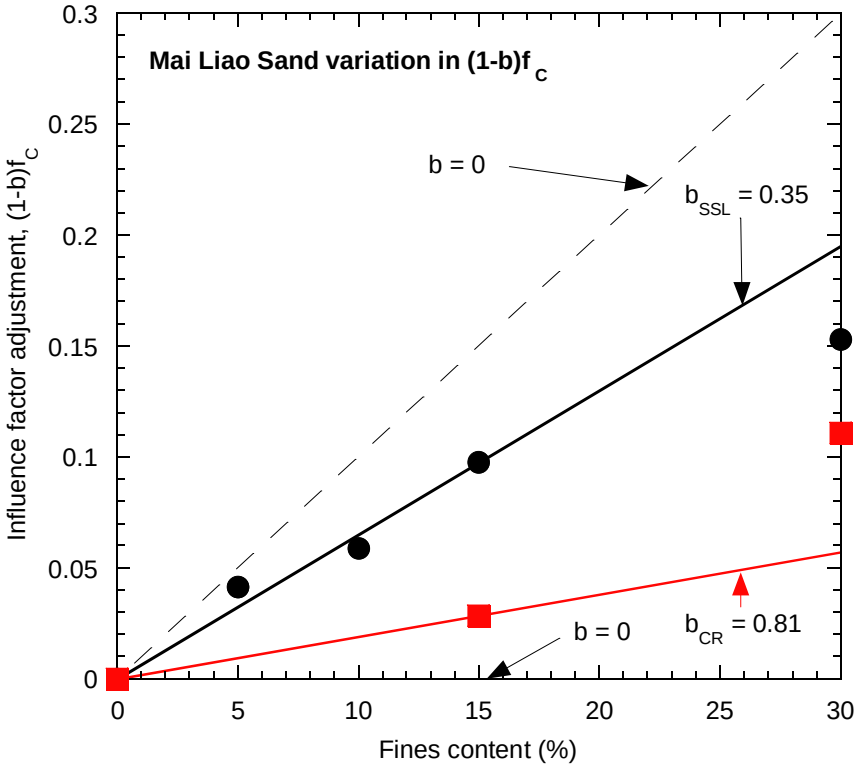

Figure 6-5 Variation in *(1-b)f_C* as the fines content of the Mai Liao Sand is increased.

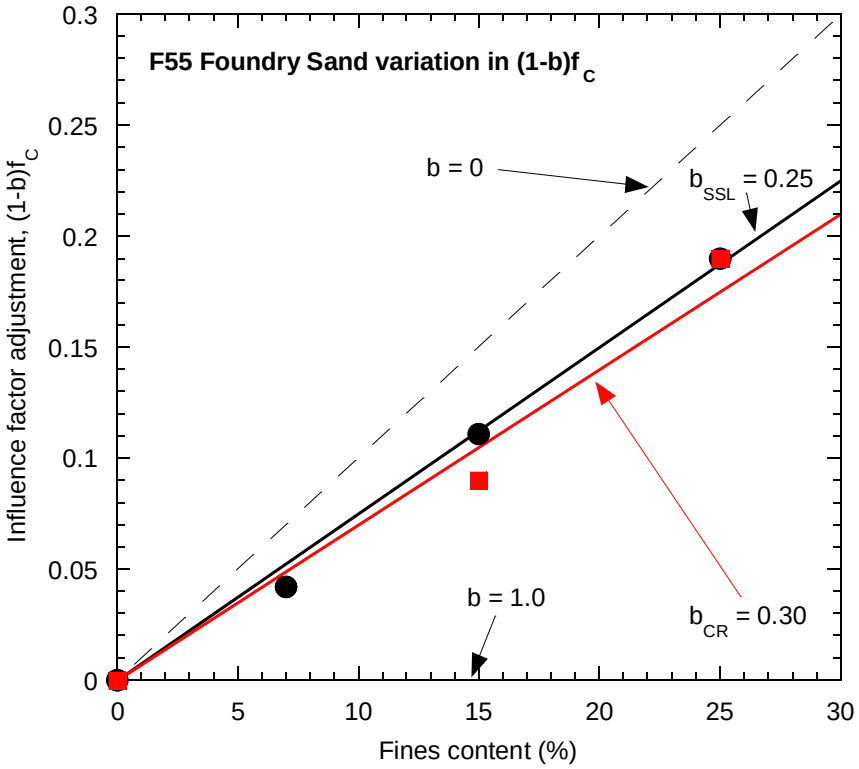

Figure 6-6 Variation in $(1\text{-}b)f_C$ as the fines content of the F55 Foundry Sand is increased.

1. ***(1-b)f_C* increases with increasing fines content** – this is also the case for the four sandy soils presented in Figure 6-3 to Figure 6-6. It is expected, as the effect of fines on the undrained response of sandy soils has shown to increase as the fines content increases during Chapter 4 and Chapter 5. An increased value of $(1\text{-}b)f_C$ simply signifies that the response curves, be them steady state lines or cyclic resistance curves, require a larger modification to the global void ratio to locate them closer to the clean sand benchmark response as the fines content is increased.

2. **Values of b_{SSL} vary more from the average than b_{CR} values do** – this appears not to be true for all sandy soils, which is further proven by the variation in $(1\text{-}b)f_C$ values for monotonic and cyclic loading in Figure 6-7 and Figure 6-8 respectively. It would appear that the fines influence factor can vary as much for cyclic loading as it can for monotonic response, which suggests some consistency in the effect of fines between the two methods of loading, as also discussed in Chapter 5.

3. **Values of b_{CR} are higher than those for b_{SSL}** – this is generally true for the sandy soils, except for the Ottawa Sand shown in Figure 6-4. In this case the fines appear to

have less effect on the undrained response during cyclic loading than they do during monotonic loading. The major difference in the preparation of the Ottawa Sand specimens is that slurry deposition was used. All other presented soils with both monotonic and cyclic data used moist tamping for deposition. The difference in depositional method most likely created a different soil fabric in the Ottawa Sand test specimens from those created using moist tamping. As noted in Chapter 4, the steady state line is considered to be independent of the soil fabric at the beginning of loading (Cubrinovski and Ishihara, 2000). Thus the fines influence factors derived for the steady state lines should also be independent of initial specimen fabric. However, Chapter 4 noted that the cyclic soil response is dependant on initial soil fabric (Mulilis et al., 1977), and as such the b_{CR} values should also depend on the initial fabric. Hence it is possible that the difference in soil depositional method led to the effect of fines being lower for cyclic loading than for monotonic loading in the Ottawa Sand. This effect of soil fabric on the value of b_{CR} is further discussed in Section 6.5, and is used as a method for determining b_{CR} based on material properties.

The variability of $(1-b_{SSL})f_C$ with increasing fines content for all sandy soils with steady state line information available is presented in Figure 6-7. It displays the difference in the value of $(1-b_{SSL})f_C$ from the constant b_{SSL} values derived in Chapter 5 when interpreting the steady state lines using the equivalent granular void ratio.

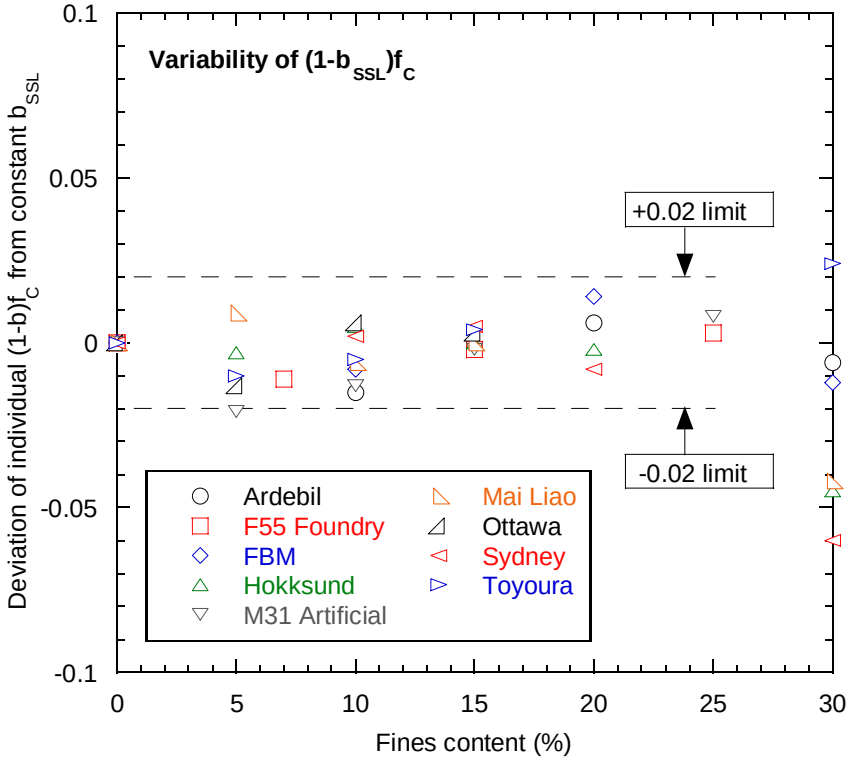

Figure 6-7 Variation in individual $(1-b_{SSL})f_C$ values from the constant value of b_{SSL}.

As is shown in Figure 6-7, all points plot either within, or very close to (M31 Artificial at f_C = 5%), the ± 0.02 limits for fines contents below the threshold fines content of f_{Cth} = 30%. This means that in using a constant value of b_{SSL} derived from the procedure in Chapter 5, the influence factor adjustment to the global void ratio for the presented sandy soils is only ever ± 0.02 in difference from the actual best fit value for each fines content across all soils.

This difference corresponds to differing inaccuracies when using the equivalent granular void ratio, as the adjustment operates on both the numerator and denominator of the e^* equation. High and low values of the void ratio can of course be considered to gain an understanding of the magnitudes of these errors. As such, a high global void ratio of e = 1.0 and a low global void ratio of e = 0.5 have been used in the following examples:

Example 1. If e = 1.0, and the actual value of $(1\text{-}b)f_C$ = 0.1:

- e^* = 1.222

Now, if the lower limit of $(1\text{-}b)f_C$ = 0.1 – 0.02 = 0.08 is used:

- e^* = 1.174

When an upper limit of $(1\text{-}b)f_C$ = 0.1 + 0.02 = 0.12 is used:

- e^* = 1.273

Thus the variation in e^* from the actual value is approximately ± 0.050.

Example 2. If e = 0.5, and the actual value of $(1\text{-}b)f_C$ = 0.1:

- e^* = 0.667

If a lower limit of $(1\text{-}b)f_C$ = 0.1 – 0.02 = 0.08 is used:

- e^* = 0.630

When an upper limit of $(1-b)f_C = 0.1 + 0.02 = 0.12$ is used:

- $e^* = 0.705$

Thus the variation in e^* from the actual value is approximately ± 0.038.

Figure 6-8 displays the same type of data as Figure 6-7, except using the b_{CR} values derived from the cyclic resistance curves. Again the maximum deviation from the constant b_{CR} value is ± 0.02 for all fines contents below f_C = 30%. The same errors in e^* as for the monotonic response therefore also apply to the cyclic response.

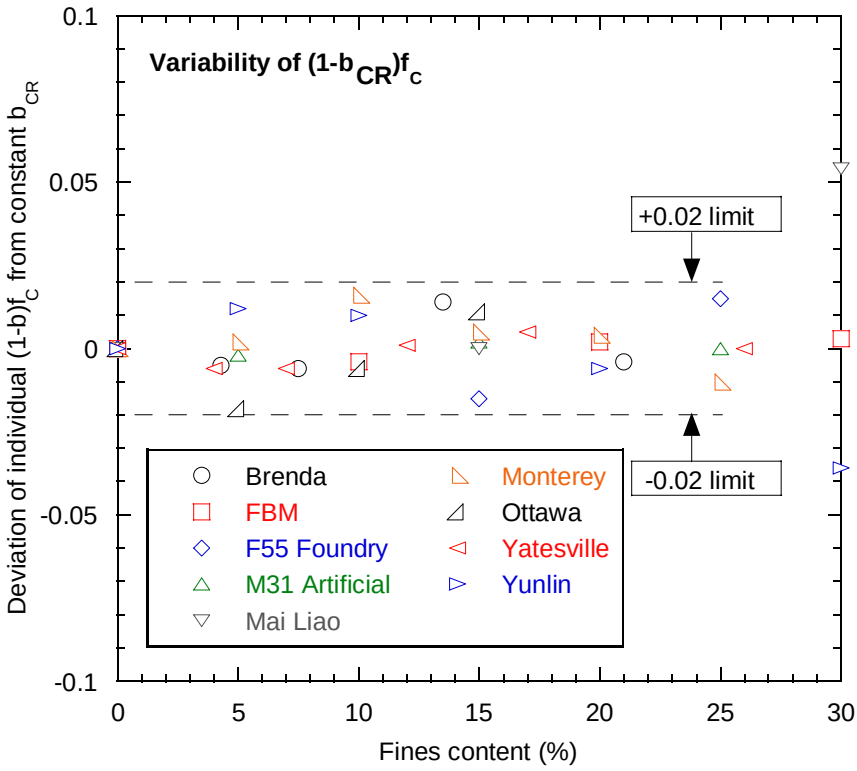

Figure 6-8 Variation in individual $(1-b_{CR})f_C$ values from the constant value of b_{CR}.

6.3.2. Using a Constant Value of Fines Influence Factor

The plots and discussion in Section 6.3.1 show that assuming a constant value of the fines influence factor is reasonable. Figure 6-7 and Figure 6-8 firstly suggest that the maximum deviation of the adjustment $(1-b)f_C$ to the global void ratio is no more than ± 0.02 from the best fit value when using a constant b. This corresponds to different inaccuracies when considering the actual value of e^*, due to the dependence of e^* on the value of the global

void ratio. It has however been shown, using typical e and $(1-b)f_C$ values, that the difference in e^* from the actual value is likely to be somewhere around ± 0.050 at most. This error is considered to be generally acceptable given the much larger differences other state measures create when interpreting the effect of fines on sand response, such as the global and intergranular void ratios, e and e_g.

Therefore, whilst it is understood that the fines influence factor may slightly vary across fines content for a given sandy soil, using a constant value of b below the threshold fines content is a reasonable and useful assumption to make. It also simplifies the parameter itself as well as the equivalent granular void ratio, as a single fines influence factor value can provide fast understanding of how additional fines affect the undrained response of a sand. Low b values suggest that fines have little influence on the undrained soil response, and are largely unimportant when quantifying the state of a soil. Conversely, high fines influence factor values suggest that additional fines have a significant influence on the undrained response, and must be considered when measuring the state of the sandy soil.

6.4. Difference in Fines Influence Factors b_{SSL} and b_{CR}

It was discussed in Chapter 5, and has been shown in Section 6.3, that the value of the fines influence factor differs when considering the steady state of deformation and cyclic liquefaction. In Section 6.3, the majority of sandy soils with both monotonic and cyclic response information showed $b_{CR} > b_{SSL}$, although this was reversed for the Ottawa Sand. The reasons for this difference are discussed below.

(1) Void ratio as an index of active particle contacts – Thevanayagam and Mohan (2000) discussed the global void ratio and how this parameter is an index for active particle contacts in uniform sand. When considering undrained triaxial compression, it was suggested that the active contacts within the soil could not remain the same throughout the entire deformational process. Based on this, the void ratio could not be considered as an index of active particle contacts at all points throughout deformation, but rather corresponded to an index of contacts at the steady state of deformation where the soil force-chain would not longer be altered. This led to the statement that "void ratio is an index of the microstructure of active particle at critical state."

Extending this idea to sandy soils with some amount of added fines, the equivalent granular void ratio should also only be viewed as an index of active particle contacts at the

steady state of deformation. This means that the fines influence factor b_{SSL} for the steady state lines fit within this definition of index for active particle contacts, but that b_{CR} for liquefaction resistance does not. This is because cyclic liquefaction is obtained at much lower levels of deformation than observed for the steady state of deformation, and hence the active particle contacts are most likely different at the onset of cyclic liquefaction compared with the steady state of deformation. As such, the equivalent granular void ratio at cyclic liquefaction could rather be viewed as an index of average active particle contact effects from the beginning of loading until liquefaction is reached, which includes the influence of initial soil fabric as well. This also would mean that the fines influence factor b_{CR} for the cyclic resistance curves describes a different effect of fines on the undrained soil response compared with b_{SSL}, as it corresponds to active particle contacts at much different levels of deformation to that of steady state, and is dependent on the soil fabric.

(2) Evidence that $b_{CR} > b_{SSL}$ for the FBM soils based on observed soil response – in Chapter 4 the cyclic response of the FBM soils was interpreted using the state parameter as the measure of soil state. It was shown that for similar values of state parameter, the liquefaction resistance of the FBM sand increased as more fines were added to the sand. This trend also corresponded to a less contractive soil response with increasing fines content. To explain why the FBM soil with higher fines content displayed more dilative response, even though the values of state parameter were similar, the monotonic excess pore water pressure generation was plotted in the range of axial strains corresponding to the development of cyclic liquefaction (ε_a = 0 – 1%). This is displayed again in Figure 6-9.

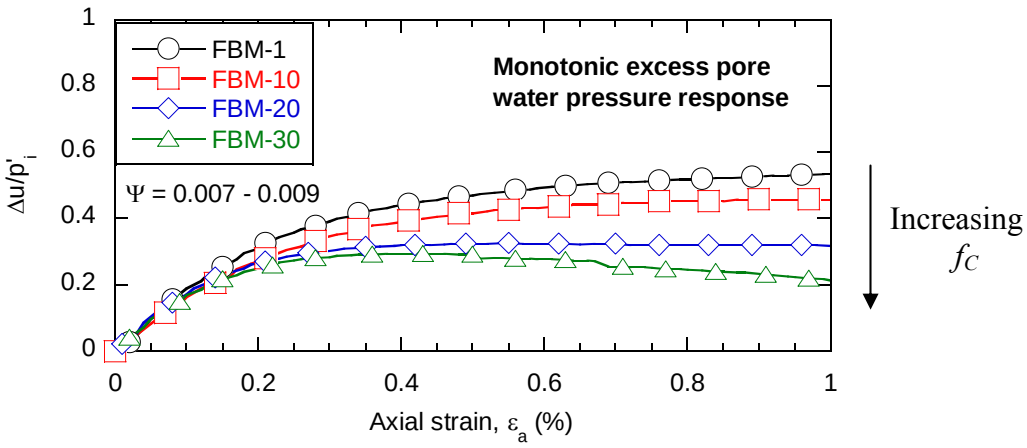

Figure 6-9 Monotonic excess pore water pressure generation of the FBM soils.

Figure 6-9 illustrates that the higher fines content FBM soils responded with less contractive behaviour from ε_a = 0 – 1% when undergoing triaxial compression, even though they reached very similar $e - p'$ states at the steady state of deformation. This implies that the higher fines content soils showed response corresponding to relatively denser soil when being compressed from ε_a = 0 – 1%, which directly led to the observed higher liquefaction resistances for increased fines contents when comparing at similar state parameter values. As such, the additional fines appear to have a higher cumulative effect on the undrained soil behaviour from ε_a = 0 – 1% than they do from ε_a = 0 – 40%. This in turn leads to a higher expected value of the fines influence factor being observed for cyclic liquefaction as opposed to the fines influence factor for the steady state of deformation, which was the case for the FBM soils as b_{CR} = 0.65 and b_{SSL} = 0.49.

In summary, the differences in the fines influence factor values for cyclic liquefaction and the steady state of deformation can be explained by the following:

- Active particle contacts in a sandy soil vary throughout the course of deformation
- When using the equivalent granular void ratio, the active contacts in a soil must be compared at similar levels of deformation
- This means the fines influence factors are also unique to their respective soil states: b_{CR} corresponds to low levels of axial strain under cyclic deformation; b_{SSL} corresponds to high levels of axial strain under monotonic loading
- b_{CR} is dependent on the initial fabric of the soil – this is not the case for b_{SSL}
- $b_{CR} > b_{SSL}$ for the FBM soils is consistent with the observed undrained behaviour in monotonic and cyclic tests

6.5. Correlation of b_{SSL} and b_{CR} with Material Properties

It was shown in Chapter 5 that the equivalent granular void ratio e^* is a useful parameter for measuring the soil state of sandy soils with varying fines contents. Using this parameter requires the fines influence factor, b, to be known for a given mixture of sand and fines. As shown in Section 6.3, b can be assumed to be constant up to the threshold fines content, and from Section 6.4 that it differs when considering the steady state of deformation or

liquefaction resistance respectively. Thus far, the fines influence factors presented in this study have been derived from the data of a number of triaxial tests on sandy soils with varying fines contents. For example, FBM soils were tested at f_C = 1, 10%, and 20% to define the FBM b_{SSL} and b_{CR} values. Practically, it is more useful to estimate the fines influence factors based on material properties of the sand and fines fractions of these soils. This would enable the undrained response of a sandy soil at any fines content below 30% to be estimated based purely on an estimated value of b, and the actual undrained response of the sand (preferably using the f_C = 0% clean sand response as a benchmark for e^*).

Three different methods for estimating the fines influence factors have already been suggested in the literature. These are summarized in the following:

(1) The first proposed method (Thevanayagam et al., 2003) correlated the fines influence factors b_{SSL} and b_{CR} with the particle size disparity ratio R_d ($d_{50,\ sand}$ / $d_{50,\ fines}$), sand uniformity coefficient C_{uc} ($d_{60,\ sand}$ / $d_{10,\ sand}$), and fines uniformity coefficient C_{uf} ($d_{60,\ fines}$ / $d_{10,\ fines}$). The form of these correlations are shown in Equation (6-2):

$$b = f\left(\frac{C_{uc}C_{uf}^{\ 2}}{R_d}\right) \tag{6-2}$$

(2) Following this, it was suggested (Ni et al., 2004) that the fines influence factor b_{SSL} be correlated with a revised particle size disparity ratio χ ($d_{10,\ sand}$ / $d_{50,\ fines}$). This was based on representative particle sizes being used to indicate the mean fines size ($d_{50,\ fines}$) and the mean void space ($d_{10,\ sand}$). The correlation form is displayed in Equation (6-3):

$$b = f(\chi) = f\left(\frac{d_{10,sand}}{d_{50,fines}}\right) \tag{6-3}$$

(3) The most recent method of estimating the fines influence factors b_{SSL} and b_{CR} (Rahman et al., 2008) uses a semi-empirical correlation primarily containing the disparity ratio χ, fines content f_C, threshold fines content f_{Cth}, and a fitting constant m = 2.5. Within Equation (6-4), $r = \chi^{-1}$ and $k = (1 - r^{0.25})$:

$$b = \{1 - \exp[-m(f_C)^2 / k]\}(rf_C / f_{thre})^r \quad (6\text{-}4)$$

Method (1) was initially derived with a limited amount of available data, namely from three different mixtures of sand and fines. When this method was assessed using the data set shown in this study (the sandy soils in Chapter 5), the correlation of R_d, C_{uc}, and C_{uf} with b was observed to be less reliable than initially proposed. The practicality of defining $d_{10,\,fines}$ is also questioned, due to the often near-horizontal slope of a particle size distribution curve around this particle size percentile for fines. As the C_{uf} term is squared in the correlation with b, there is also a high sensitivity to the value of $d_{10,\,fines}$. Interestingly this is the only method that estimates b_{SSL} and b_{CR} independently, recognizing a difference in fines influence factors values between monotonic and cyclic loading.

Method (2) is the simplest of the three methods, only using the disparity ratio $\chi = d_{10,\,sand} / d_{50,\,fines}$. It also intuitively makes physical sense, as it attempts to relate the effects of the fines to the size of the fines relative to the void space in which they can sit. This correlation does display a trend of increasing b values as the disparity ratio χ decreases. When correlating χ alone with the set of sandy soils used in this study however, there is a large amount of scatter in the points, as illustrated in Section 6.5.1.

Method (3) is the only method that estimates b based on the fines content of a given soil. This means that b is not constant for a particular mixture of sand and fines, but varies up to the threshold fines content. This has been shown to be useful over a range of sandy soils (Rahman et al., 2008), most of which are presented in this study, but not all soils. It is also considered to be a rather complex method for accounting for the effects of fines on undrained sandy soil response.

The aim in this study was to provide a simplified method for estimating the fines influence factors b_{SSL} and b_{CR} based on a number of physical considerations, using the largest available data set of sandy soils. In doing this, a number of concepts from the three methods already proposed were incorporated. The variables considered in this simplified method are:

- Relative size of fines compared with available void space
- Effect of sand particle angularity on void space
- Effect of initial soil fabric on b_{SSL} and b_{CR}

Each of these variables is correlated with the back-calculated b values presented in Chapter 5, and discussed to physically explain the observed trends. Note that the b_{SSL} values are investigated first as the soil response at the steady state of deformation is independent of the initial soil fabric. Following this, a final simplified method for estimating the fines influence factors b_{SSL} and b_{CR} is given in Section 6.6.

6.5.1. Available Void Space for Fines based on Relative Particle Size

The equivalent granular void ratio e^* concept is based on binary packing, and fines within sand voids are thought to be inactive in the soil force-chain. From this, it seems appropriate to try and relate the fines influence factor to the available void space in which the fines can sit. This was carried out in Method (2) and Method (3) using two variables: $d_{50,\ fines}$ representing the mean fines particle size, and $d_{10,\ sand}$ representing the mean void space, which was chosen based on earlier work (Aberg, 1992). The ratio of these gives a particle size disparity χ, as defined in Equation (6-3).

Particle size properties for sandy soils with monotonic steady state line data presented in this study are displayed in Table 6-1, with $d_{10,\ sand} = D_{10}$ and $d_{50,\ fines} = d_{50}$ used herein.

Table 6-1 Particle size properties of the sandy soils with steady state line data.

Soil	D_{10} (mm)	d_{50} (mm)	$\chi = (D_{10} / d_{50})$	b_{SSL}	Reference
FBM Sand	0.089	0.015	5.9	0.49	This study
F55 Foundry Sand	0.160	0.010	16.0	0.25	(Thevanayagam et al., 2002)
Ottawa Sand	0.227	0.023	9.7	0.47	(Murthy et al., 2007)
M31 Artificial Sand	0.228	0.020	11.4	0.39	(Papadopoulou and Tika, 2008)
Ardebil Sand	0.090	0.025	3.6	0.69	(Naeini and Baziar, 2004)
Toyoura Sand	0.120	0.010	12.6	0.35	(Zlatovic, 1994; Verdugo and Ishihara, 1996)
Hokksund Sand	0.220	0.032	6.9	0.27	(Yang et al., 2006b)
Sydney Sand	0.237	0.027	8.8	0.12	(Rahman and Lo, 2007)
Mai Liao Sand	0.083	0.044	1.9	0.35	(Huang et al., 2004)

As is shown in Table 6-1, the size disparity χ ranges from χ = 1.9 for Mai Liao Sand, to χ = 16.0 for F55 Foundry Sand. D_{10} ranges from 0.083mm for Mai Liao Sand to 0.237mm for Sydney Sand, and d_{50} ranges from 0.010mm for the fines used with F55 Foundry Sand and Toyoura Sand, to 0.044mm for Mai Liao Sand.

The fines influence factor b_{SSL} values are plotted against the disparity ratio χ in Figure 6-10. The included error bars correspond to b_{SSL} values that gave mean squared errors (*MSE*) ≤ 0.0009 during the back-calculation of b_{SSL}, as described in Chapter 5. *MSE* ≤ 0.0009 was chosen as it corresponds to a mean error of $e^* \leq 0.03$, which was considered to be a reasonable limit based on the example calculations in Section 6.3.1. Note that the Mai Liao Sand data point has no error bars as the minimum *MSE* = 0.0010 when calculating the b_{SSL} value.

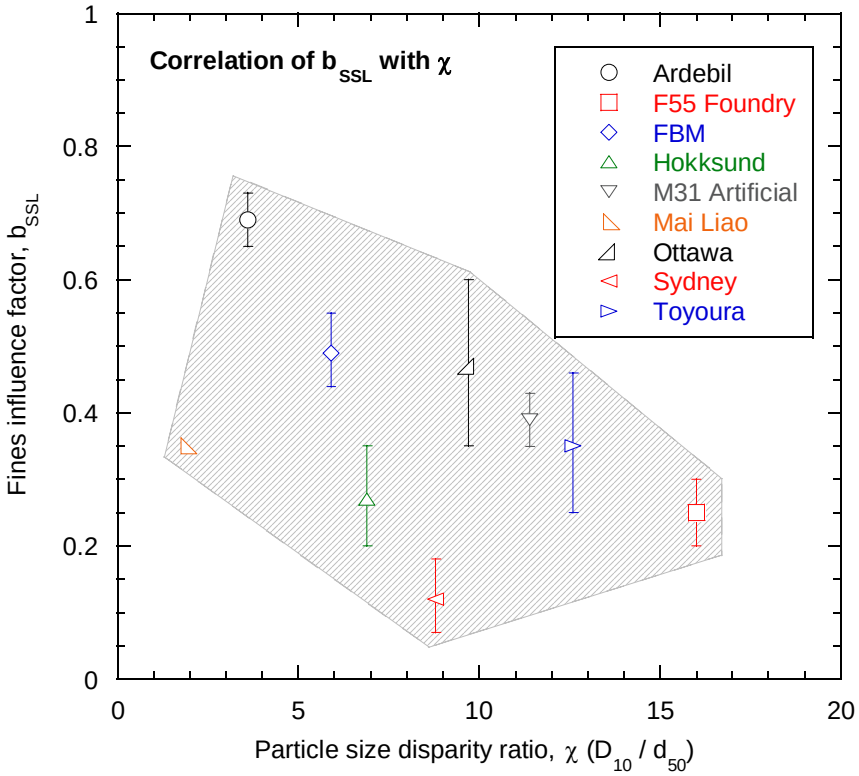

Figure 6-10 Correlation of the fines influence factor values b_{SSL} with the particle size disparity ratio χ.

There is clearly a large amount of scatter in the b_{SSL} values in Figure 6-10 when the particle size disparity ratio χ is solely used to describe the relative available void space. For example, Ottawa and Sydney Sands have similar disparity values (χ = 9.7 and 8.8 respectively), yet have very different fines influence factor values (b_{SSL} = 0.47 and 0.12 respectively) and no overlap of error bars. Figure 6-10 does however show a general trend of

increasing b_{SSL} values with decreasing χ values. This is the expected trend due to physical considerations, in that decreasing particle disparity results in less void space for the fines, which in turn leads to more force-chain participation from the fines, or higher b_{SSL} values. Despite this, it is clear that χ alone does not satisfactorily correlate with b_{SSL}.

6.5.2. Effects of Sand Particle Angularity

It has been previously discussed in other studies (Miura et al., 1997; Cubrinovski and Ishihara, 2002; Cho et al., 2006) that particle angularity affects material properties such as the maximum and minimum void ratio limits, e_{max} and e_{min}, of a sandy soil. These limits tend to shift apart as sand particle angularity increases. Thus, if $(e_{max} - e_{min})$ for a particular mixture of sand and fines is increasing with increasing particle angularity, the void space available for fines to sit within may also be increasing. In such a case the fines would potentially have less participation in the soil force-chain, leading to a lower fines influence factor value.

The angularity of the sand particles for the soils considered is summarized in Table 6-2. Angularity was defined using standard qualitative classification of round to angular particles reported in each of the source references, where R = round, SR = sub-round, SA = sub-angular, A = angular.

Table 6-2 Sand angularity properties of the presented sandy soils.

Soil	$\chi = (D_{10} / d_{50})$	**Sand Angularity**	b_{SSL}	A_f
FBM Sand	5.9	SA - SR	0.49	3.1
F55 Foundry Sand	16.0	R	0.25	0.0
Ottawa Sand	9.7	R	0.47	0.0
M31 Artificial Sand	11.4	R	0.39	0.0
Ardebil Sand	3.6	SR	0.69	0.0
Toyoura Sand	12.6	SR - SA	0.35	0.3
Hokksund Sand	6.9	SA	0.27	8.3
Sydney Sand	8.8	SA	0.12	10.5
Mai Liao Sand	1.9	A	0.35	11.0

Figure 6-10 is re-plotted in Figure 6-11 including the sand particle angularity as a parameter. Although this is based purely on qualitative angularity descriptions, a clear trend can be observed. Sandy soils with rounded sand particles tend to have higher b_{SSL} values, whilst soils with angular sand particles have lower b_{SSL} values. The sandy soils with

subangular to subrounded particles – Toyoura and FBM Sand – tend to sit within the rounded particle trend or slightly below. The idea that angular particles have lower b_{SSL} values follows the reasoning that angular particles create larger void spaces, which in turn produce less fines participation in the soil force-chain, hence the lower b_{SSL} values.

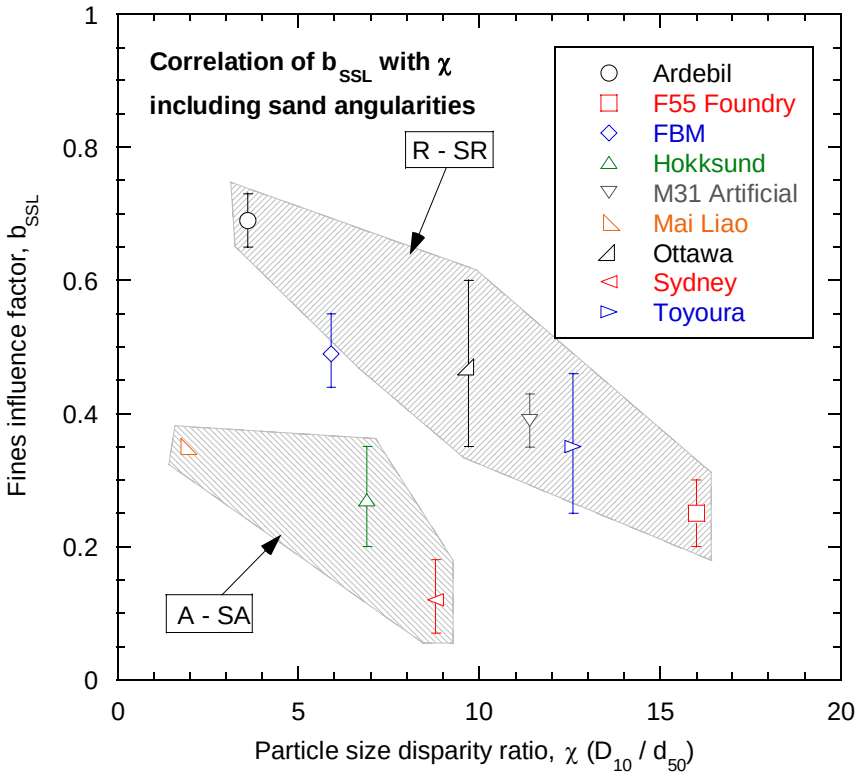

Figure 6-11 Correlation of the fines influence factor values b_{SSL} with the particle size disparity ratio χ, and the angularity of the sand particles.

A new parameter χ_e was defined to allow angular b_{SSL} points to horizontally shift in line with the R – SR points displayed in Figure 6-11. χ_e is termed the effective particle size disparity ratio, and accounts for particle angularity effects on the available void space for fines to sit within. It contains the parameter A_f, or angularity effect, which quantifies the horizontal shift required for the angular sand particles. χ_e is defined in Equation (6-5):

$$\chi_e = \chi + A_f \tag{6-5}$$

More angular particles are expected to have higher A_f values, whilst rounded particles are expected to have $A_f \approx 0$ values. To estimate A_f values for the sandy soils, a linear

relationship was fitted through the R – SR points in Figure 6-11, as defined in Equation (6-6). Note that the condition of $b_{SSL} = 0.815$ when $\chi_e = 0$ does not make physical sense, as the effect of fines should be the same as sand when the respective particles are of similar size ($b_{SSL} = 1.0$). There is however no available data for such mixtures of sand and fines, and as such it is suggested that the response of soils with $\chi_e < 3.0$ not be interpreted using the equivalent granular void ratio concept at this stage.

$$b_{SSL} = 0.815 - 0.036\chi_e \tag{6-6}$$

A_f values were then determined using Equation (6-6) for each of the sandy soils by using the back-calculated b_{SSL} values and particle size disparity ratios χ. These estimated A_f values provide the following ranges based on qualitative angularity. Note that these ranges are based purely on the sandy soils presented in this study, hence the gap in A_f values between SR – SA particles and A – SA particles.

- R – SR sand particles → $A_f \approx 0$
- SR – SA sand particles → $A_f \approx 1$ - 3
- SA – A sand particles → $A_f \approx 8$ - 11

Effective particle disparity ratios were calculated using the determined A_f values. For example, Mai Liao Sand has $\chi = 1.9$, and is qualitatively described as having angular (A) particle shape, which corresponded to $A_f = 11$. Therefore $\chi_e = (1.9 + 11) = 12.9$ for Mai Liao Sand. Figure 6-11 is re-plotted in Figure 6-12 using the effective particle disparity ratio χ_e, also showing the linear curve defined in Equation (6-6).

Figure 6-12 shows how the angularity effect A_f and effective particle size disparity ratio χ_e shift the b_{SSL} points for all sandy soils in line with the one defined for sand with R – SR particles.

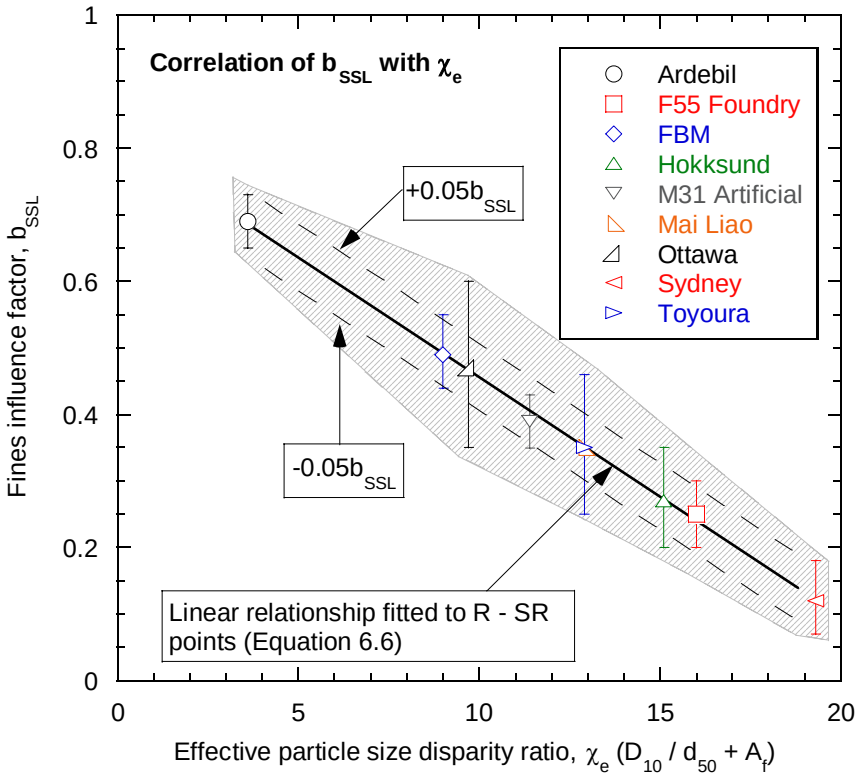

Figure 6-12 Correlation of the fines influence factor values b_{SSL} with the effective particle size disparity ratio χ_e.

It is recognized that particle angularity changes from round to angular not in a discrete manner and that qualitative descriptions only provide a rough guide for classification. Accounting for the angularity effect on χ can be improved if A_f is estimated based on quantitative angularity measures. As such, two methods to correlate the angularity effect with quantitative angularity measures were subsequently investigated to increase the influence factor estimation accuracy. These methods were:

- Angularity A_{2D} (Lees, 1964) using the parameter $(e_{max} - e_{min})$
- Roundness R, and sphericity S chart (Krumbein and Sloss, 1963) and regularity ρ (Cho et al., 2006) using the parameter e_{max}

Angularity A_{2D} determines the degree of angularity of a soil particle in two dimensions (Lees, 1964). A_{2D} values have been defined to range from A_{2D} = 0 – 1600, with A_{2D} = 0 corresponding to very rounded particles, and A_{2D} = 1600 corresponding to very angular particles. Note however that sand particles typically have values of A_{2D} < 1000, as evidenced in Figure 6-13. A_{2D} can be determined visually using a chart, but has also been correlated with

other material parameters such as $(e_{max} - e_{min})$. Using $(e_{max} - e_{min})$ to determine A_{2D} is considered to be more objective than determining A_{2D} visually from a chart, which is clearly user-subjective.

The fact that there are numerous ways of determining e_{max} and e_{min} from different standards must however be kept in mind when using these void ratio limits. The mixtures of sand and fines presented in this study use American, Japanese, British and New Zealand standards as guidelines for calculating e_{max} and e_{min}, with some literature not reporting the determination methods. These differences were difficult to account for in this assessment of particle angularity, and as such all $(e_{max} - e_{min})$ values have been used together without differentiating between the determination methods.

Figure 6-13 was employed to estimate the degree of angularity of sand particles based on the $(e_{max} - e_{min})$ and D_{50} values reported in Table 6-3. Note that all sand samples used to define the correlations in Figure 6-13 were clean sands, as any particles larger than 2.000mm or smaller than 0.075mm were removed from the natural sand samples for that particular study (Miura et al., 1997).

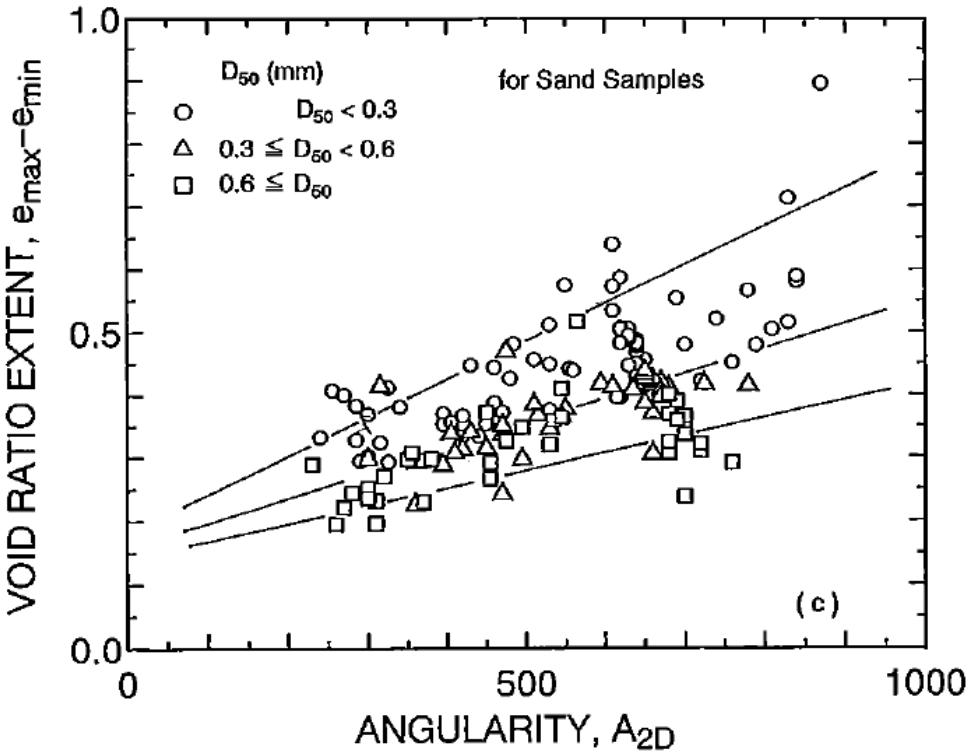

Figure 6-13 Degree of angularity A_{2D} correlated with $(e_{max} - e_{min})$ (Miura et al., 1997).

Table 6-3 Clean sand e_{max} and e_{min} values of the sandy soils.

Soil	D_{50} (mm)	e_{max}	e_{min}	$(e_{max} - e_{min})$	A_{2D}	Qualitative Angularity
F55 Foundry Sand	0.250	0.800	0.608	0.192	14	R
Ottawa Sand	0.390	0.780	0.480	0.300	360	R
M31 Artificial Sand	0.300	0.842	0.588	0.254	245	R
Ardebil Sand	0.150	1.090	0.746	0.344	264	SR
FBM Sand	0.168	0.907	0.628	0.278	157	SA - SR
Toyoura Sand	0.175	0.977	0.597	0.380	323	SR - SA
Hokksund Sand	0.440	0.949	0.572	0.377	552	SA
Sydney Sand	0.274	0.855	0.565	0.290	175	SA
Mai Liao Sand	0.127	1.125	0.646	0.479	486	A

The ranges of A_{2D} shown in Table 6-3 for the various particle shapes are listed in the following:

- For R – SR particles, A_{2D} = 14 – 360
- For SR – SA particles, A_{2D} = 157 – 323
- For A – SA particles, A_{2D} = 175 – 552

These ranges display a general trend of rounded particles having the lowest A_{2D} value, and angular particles having the highest A_{2D} value. There is however a larger amount of overlap, and interestingly the maximum A_{2D} = 552 is relatively low considering that A_{2D} values for sand can reach about 1000 (Miura et al., 1997). Note that Figure 6-13 contains a large amount of scatter in the data points used to define the $A_{2D} - (e_{max} - e_{min})$ correlations. Hence it is not unexpected to see wide and overlapping ranges of A_{2D} values. The estimated A_{2D} values are compared with the estimated A_f values for the sandy soils in Figure 6-14.

It is difficult, even with some data points neglected, to define a useful trend in Figure 6-14 for estimating A_f based on estimated A_{2D} values using $(e_{max} - e_{min})$. The range of A_{2D} values, particularly for the more rounded particles, is too large given the maximum estimated A_{2D} = 552. This means that A_{2D} values estimated using $(e_{max} - e_{min})$ are not considered to sufficiently describe the effect of particle angularity on the fines influence factor b_{SSL} for the presented range of sandy soils.

- A_{2D} values derived using $(e_{max} - e_{min})$ do not correlate well with the angularity effect A_f on b_{SSL}

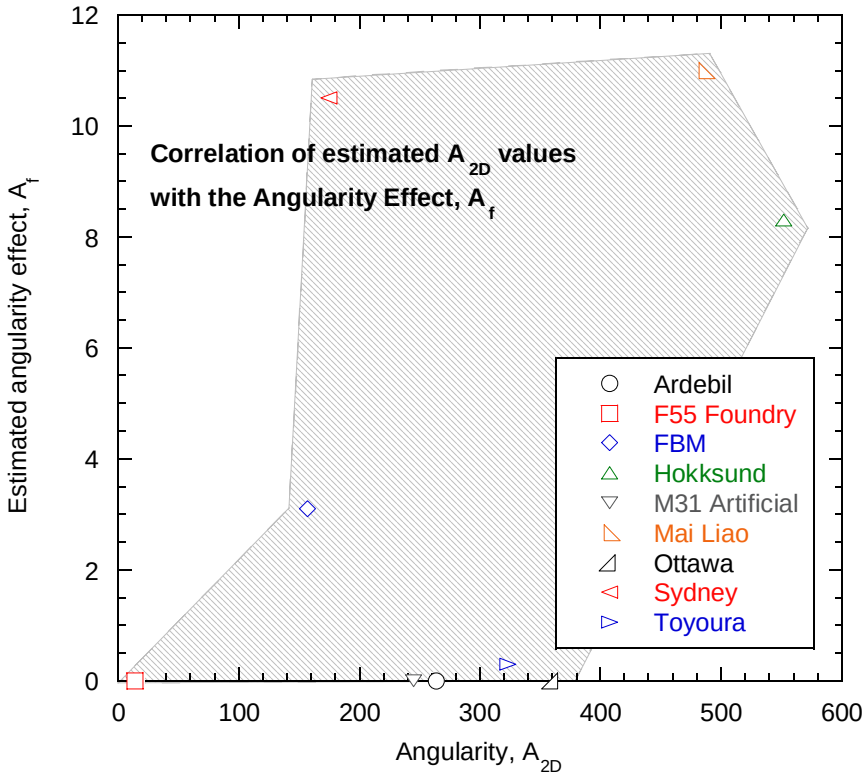

Figure 6-14 Estimated angularity effect A_f values correlated with estimated A_{2D} values.

Roundness *R* and sphericity *S* (Wadell, 1932) describe two different aspects of particle shape: sphericity refers to the global particle length, height and width; roundness refers to the smaller scale features, typically an order of magnitude below the particle size (Cho et al., 2006). These aspects of shape have also been combined to produce particle **regularity *ρ***, defined in Equation (6-7):

$$\rho = \frac{R + S}{2} \tag{6-7}$$

At a high degree of sand particle roundness, $R = 1.0$; at low sand particle roundness, $R = 0$. These same values also correspond with high and low degrees of sphericity respectively. As such, a highly regular particle has $\rho = 1.0$, whereas a highly irregular particle has $\rho = 0$. Charts such as that shown in Figure 6-17 to visually assess R and S for sand particles are available, as do correlations with other material parameters such as e_{max} and e_{min} (Cho et al., 2006).

In this study R, S and ρ were estimated using e_{max} values as opposed to visual assessment for the same reasons as discussed during the A_{2D} analysis. The parameter e_{max} was preferred over e_{min} as the r^2 correlation factors with R, S and ρ were greater by approximately

r^2 = 0.2. The *R*, *S*, and ρ correlations with e_{max} sourced from Cho et al. (2006) are reported in Equations (6-8), (6-9), and (6-10):

$$e_{\max} = 1.3 - 0.62R \tag{6-8}$$

$$e_{\max} = 1.6 - 0.86S \tag{6-9}$$

$$e_{\max} = 1.5 - 0.82\rho \tag{6-10}$$

Particle roundness, sphericity and regularity values estimated using Equations (6-8), (6-9), and (6-10) are reported in Table 6-4. Regularity ρ was considered the best particle shape parameter to correlate with angularity effects, as it combines both roundness and sphericity. Note that expected ρ values for natural sand range from ρ = 0.4 – 0.9 (Cho et al., 2006).

Table 6-4 Estimated values of sand particle roundness, sphericity, and regularity using e_{max}.

Soil	e_{max}	**Roundness** ***R***	**Sphericity** ***S***	**Regularity** ρ	**Qualitative Angularity**
F55 Foundry Sand	0.800	0.81	0.93	0.85	R
Ottawa Sand	0.780	0.84	0.95	0.88	R
M31 Artificial Sand	0.842	0.74	0.88	0.80	R
Ardebil Sand	1.090	0.34	0.59	0.50	SR
FBM Sand	0.907	0.63	0.81	0.72	SA - SR
Toyoura Sand	0.977	0.52	0.72	0.64	SR - SA
Hokksund Sand	0.949	0.57	0.76	0.67	SA
Sydney Sand	0.855	0.72	0.87	0.79	SA
Mai Liao Sand	1.125	0.28	0.55	0.46	A

Clearly e_{max} does not correlate perfectly with particle regularity, but it does show a general trend of higher ρ values for rounder particle shapes. For example, Ottawa Sand is qualitatively classified as being round (R), and has ρ = 0.88 (very regular). However Ardebil Sand is classified as being sub-round (SR), yet ρ = 0.50 (very irregular) using e_{max} as the estimation parameter. It is therefore proposed that e_{max} can be used to estimate particle regularity when assessing angularity effects on b_{SSL}, but that ρ should remain within limits based on qualitative particle shape classification. Based on the values and classifications in Table 6-4, the proposed limits are:

- Regularity ρ = 0.75 – 0.90 for R – SR particle shapes
- Regularity ρ = 0.65 – 0.75 for SR – SA particle shapes

- Regularity ρ = 0.40 – 0.65 for A – SA particle shapes

Using these limits means that some ρ values shift for the sandy soils listed in Table 6-4. For example, Ardebil Sand ρ shifts inside the R – SR limits from ρ = 0.50 → 0.75, and Sydney Sand shifts from ρ = 0.79 → 0.65. The adjusted regularity values are plotted against the estimated angularity effect A_f values in Figure 6-15.

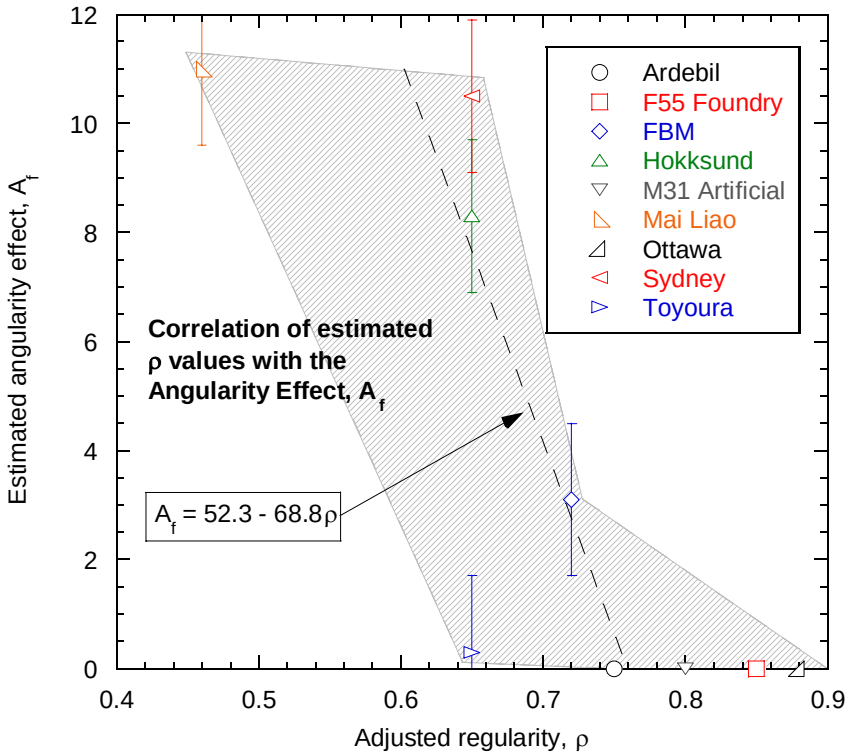

Figure 6-15 Estimated angularity effect A_f values correlated with estimated and adjusted ρ values.

Figure 6-15 illustrates that the adjusted regularity ρ estimated using e_{max} can be used to reasonably estimate the angularity effect A_f on the sandy soil b_{SSL} values. It is suggested that regularity ρ be determined using e_{max} and Equation (6-10), and the qualitative particle shape used to ensure ρ is within the proposed limits. The approximate value of A_f can then be found from Figure 6-15, using the fitted linear trend. This trend implies that rounded particles will have zero adjustment due to particle angularity, and that A – SA particles will have $A_f > 7$. Note that there is still an amount of subjectivity in the A_f estimation process, but also that angularity effects can be estimated in a straightforward manner.

In summary, the fines influence factor b_{SSL} has been correlated with three main material parameters:

- Particle size disparity ratio $\chi = D_{10} / d_{50}$
- Clean sand e_{max}
- Clean sand qualitative particle shape classification

The clean sand particle shape classification can be used in conjunction with clean sand e_{max}, Equation (6-10) and the criteria in Figure 6-15 to estimate sand particle regularity ρ and estimate the angularity effect A_f. A_f can then be used with the particle size disparity ratio χ and Equation (6-5) to estimate the effective particle size disparity ratio χ_e. Finally χ_e can be used as the input in Figure 6-12 to estimate the upper, lower and expected b_{SSL} values for a sand-fines mixture. This process is schematically illustrated in Figure 6-16.

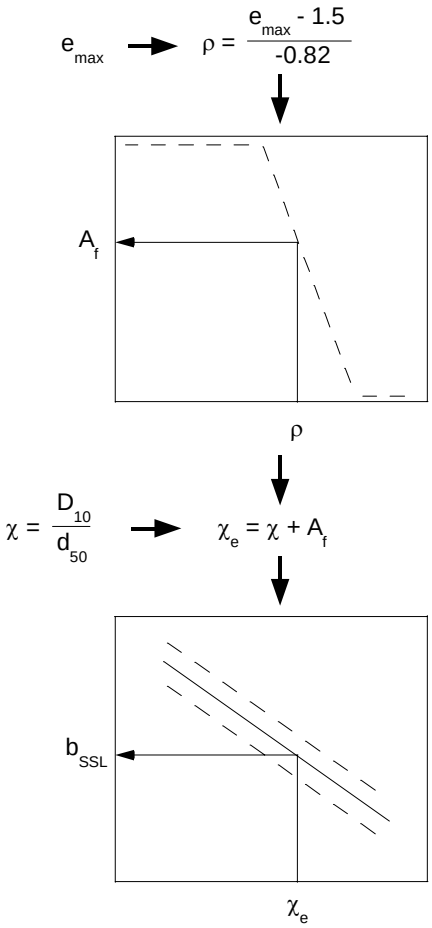

Figure 6-16 Schematic illustration of the process for estimating b_{SSL} based on the material properties of a soil.

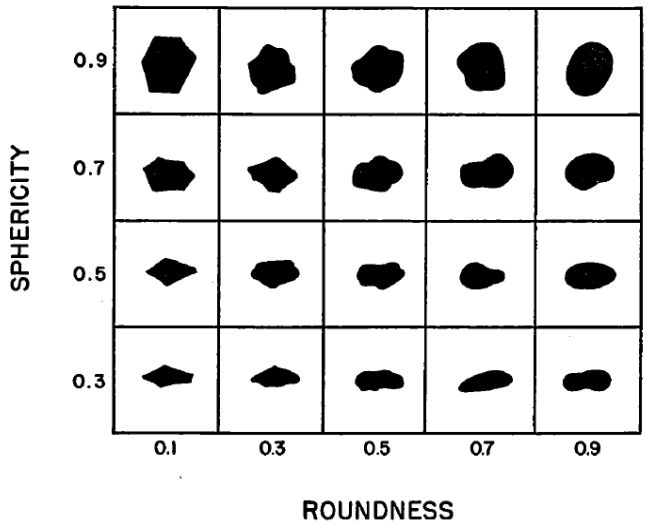

Figure 6-17 Particle sphericity and roundness chart (Krumbein and Sloss, 1963).

6.5.3. Effect of Initial Soil Fabric on b_{CR}

The plots in Figure 6-2 through Figure 6-6 clearly show significant differences in the back-calculated b_{SSL} and b_{CR} values for particular mixtures of sand and fines. These differences were discussed in Section 6.4, concluding that the cumulative dilatancy effects on the undrained behaviour leading up to large strains (those needed to define the steady state line) were different from those exhibited during the development of cyclic liquefaction, explaining why the values of b_{SSL} and b_{CR} were not equal. As such, the same material correlations with b_{SSL} values may not apply to b_{CR} values.

Chapter 4 discussed the state concept and the assumption that steady state deformation was independent from initial specimen fabric. This assumption means that the method of soil deposition does not need to be considered when estimating b_{SSL} values for a sandy soil. The cyclic response however of these soils is very dependant on initial specimen fabric, as well as other factors such as initial confining stress and stress-strain history (Mulilis et al., 1977; Castro and Poulos, 1977; Seed, 1979).

In this section the effect of soil deposition method, or initial soil fabric, on the value of b_{CR} is investigated by firstly correlating the fines influence factor with the particle size disparity ratio and sand particle angularity. Following this, the value of b_{SSL} is used as a reference to compare the effect of depositional method on the value of b_{CR}.

Particle size, depositional methods and angularity properties for sandy soils with cyclic response data presented in this study are displayed in Table 6-5. These are the same soils as presented in Chapter 5. Note that Yunlin Sand has been classified as angular (A) based on an e_{max} = 1.191, which corresponds to an estimate of ρ = 0.38 (very irregular particle shape).

Table 6-5 Particle size properties of the sandy soils with cyclic response data.

Soil	D_{10} (mm)	d_{50} (mm)	χ	b_{CR}	Deposition method	Sand Angularity	Reference
FBM Sand	0.089	0.015	5.9	0.65	Moist tamping	SA - SR	This study
F55 Foundry Sand	0.160	0.010	16.0	0.30	Moist tamping and dry deposition	R	(Thevanayagam et al., 2000)
Ottawa Sand	0.262	0.023	11.4	0.32	Slurry	R - SR	(Carraro et al., 2003)
M31 Artificial Sand	0.228	0.020	11.4	0.55	Moist tamping	R	(Papadopoulou and Tika, 2008)
Monterey 0/30 Sand	0.300	0.030	10.0	0.29	Moist tamping	SA - SR	(Polito and Martin II, 2001)
Yatesville Sand	0.089	0.030	3.0	0.67	Moist tamping	SA - SR	(Polito, 1999)
Mai Liao Sand	0.083	0.044	1.9	0.81	Moist tamping	A	(Huang et al., 2004)
Brenda 20/200 Sand	0.091	0.012	7.6	0.11	Slurry	A	(Vaid, 1994)
Yunlin Sand	0.150	0.060	2.5	0.35	Moist tamping	A	(Chien et al., 2002)

Figure 6-18 displays the b_{CR} values of the sandy soils correlated with the particle size disparity ratio, χ. The error bars again correspond to b_{CR} values that have a $MSE \leq 0.0009$, or an average e^* deviation from the benchmark response curve of ≤ 0.03. Note that M31 Artificial Sand has no error bars due to a minimum $MSE = 0.00095$, and F55 Foundry Sand due to a minimum $MSE = 0.00137$.

The general trend observed in Figure 6-18 of increasing b_{CR} values with decreasing particle size disparity ratio χ was also observed when correlating χ with the b_{SSL} values. Clearly χ does not properly correlate with the b_{CR} values alone, as there is a large amount of scatter in the b_{CR} data points. Sand particle angularity has been included in Figure 6-19 based on the qualitative descriptions listed in Table 6-5.

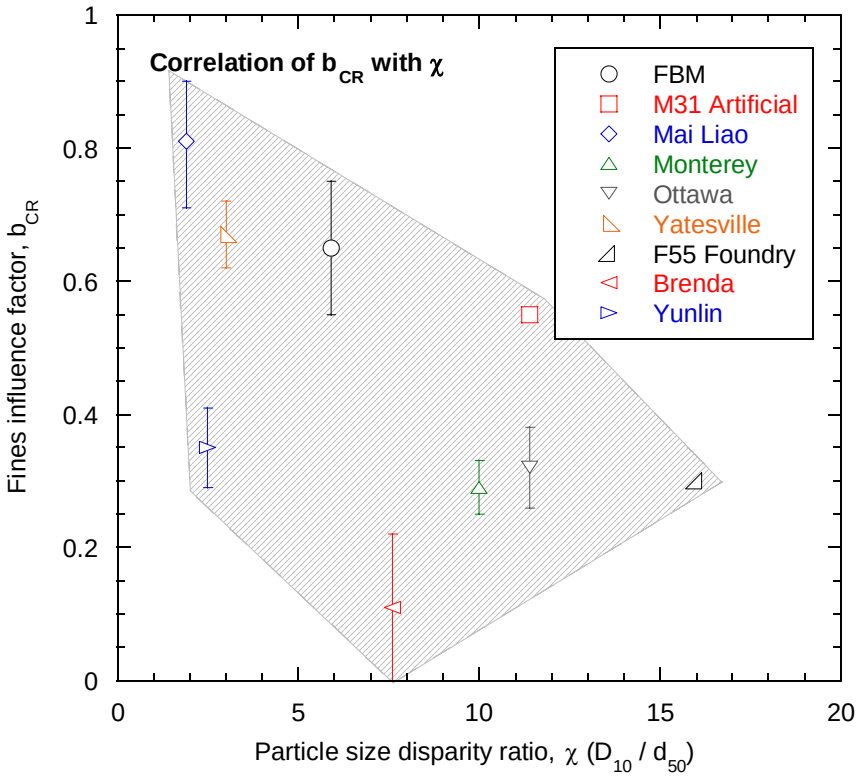

Figure 6-18 Correlation of fines influence factor b_{CR} with the particle size disparity ratio χ.

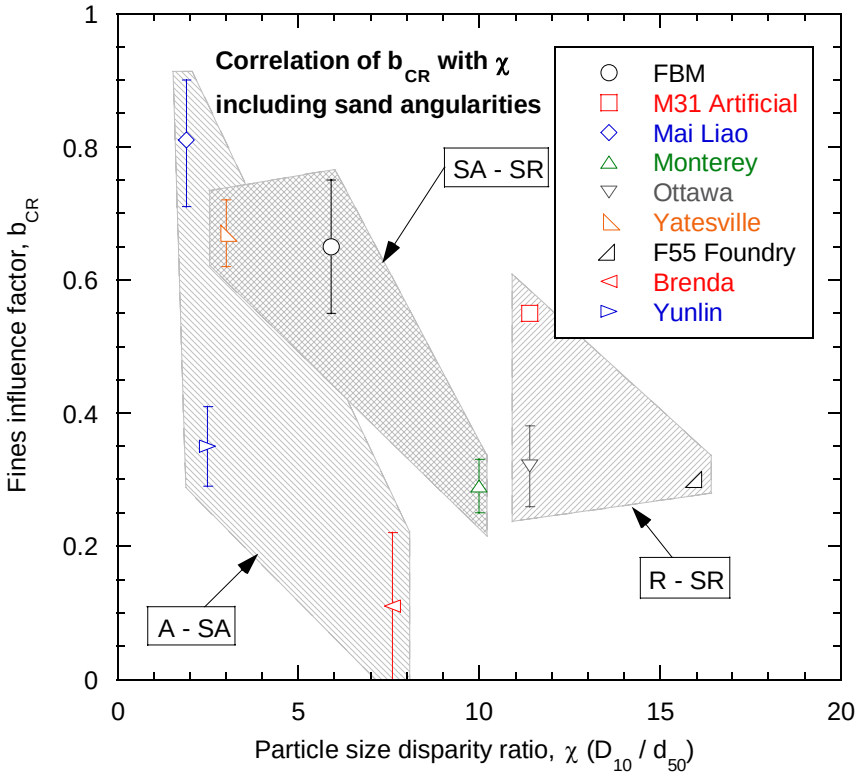

Figure 6-19 Correlation of fines influence factor b_{CR} with the particle size disparity ratio χ, and sand angularity.

Figure 6-19 illustrates that sand particle angularity has a similar effect on the b_{CR} values as it did for the b_{SSL} values. Sandy soils with more angular sand particles tend to have lower b_{CR} values for a similar particle size disparity ratio χ. This trend means that an effective disparity ratio, such as that defined in Equation (6-5), could also be used in adjusting the cyclic data to account for sand particle angularity effects.

It was discussed that initial soil fabric has a significant effect on the cyclic response of sandy soils, but not on the steady state response. The deposition method for the cyclic test specimens has therefore been included as another parameter that possibly affects the fines influence factor b_{CR}. As such, Figure 6-20 has been produced with only b_{CR} points for sandy soils that employed moist tamping as their depositional method, allowing comparison of fines influence factors derived from specimens with similar initial soil fabrics.

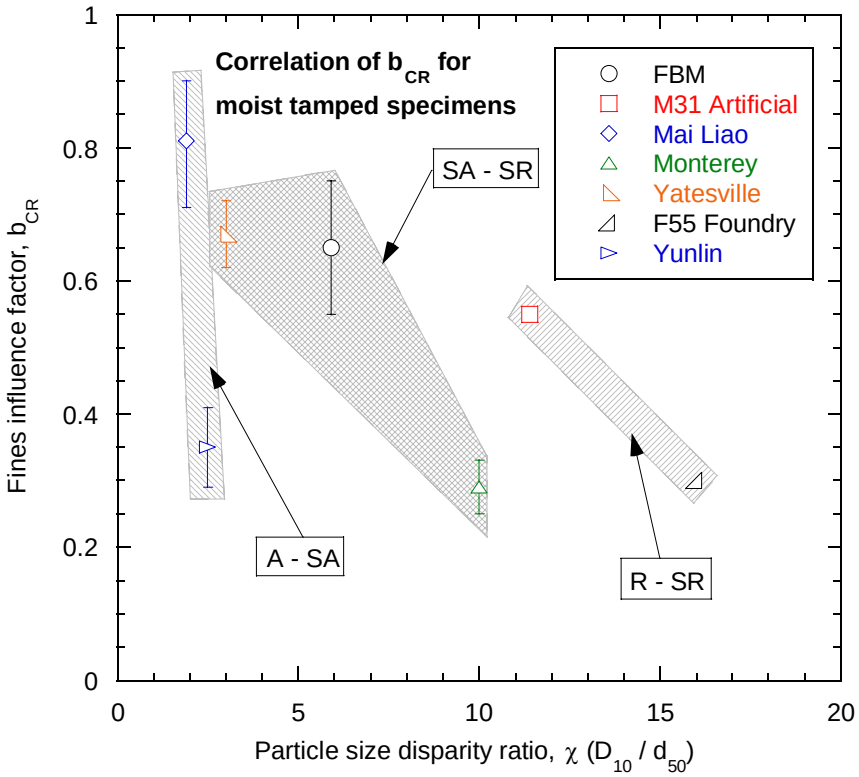

Figure 6-20 Correlation of fines influence factor b_{CR} with the particle size disparity ratio χ, and sand angularity for moist tamped specimens only.

The effect of sand angularity on b_{CR} becomes clearer in Figure 6-20 when only moist tamped specimen data is used. The two mixtures prepared by slurry – Ottawa Sand and Brenda 20/200 Sand – have lower b_{CR} values than their moist tamped counterparts. It also

appears that b_{CR} values are more sensitive to changes in particle size disparity than for the b_{SSL} values, based on the increased slopes qualitatively observed in Figure 6-20.

These points lead to the following conclusions based on the presented mixtures of sand and fines with available cyclic data:

- b_{CR} values tend to decrease with increasing particle size disparity ratio χ
- Increased sand particle angularity decreases b_{CR}
- Specimen depositional method appears to affect b_{CR} (only moist tamping and slurry methods were used in this data set)
- b_{CR} may be more sensitive to changes in χ than b_{SSL}

Given that the cyclic resistance curve fines influence factor b_{CR} shows the same trends as the steady state line influence factor b_{SSL}, it is potentially beneficial to relate the two factors and estimate b_{CR} based on b_{SSL} values. This means that b_{SSL} can be used as a reference for the effect of fines on undrained soil response, as it has no dependency on initial soil fabric as discussed earlier, and is unique for a given mixture of sand and fines.

Relating b_{CR} to b_{SSL} is carried out in this study by simply taking the difference between the two factors. The difference is defined in Equation (6-11) as the change in fines influence factor, Δb:

$$\Delta b = b_{CR} - b_{SSL} \tag{6-11}$$

Equation (6-11) implies that sandy soils with $b_{CR} > b_{SSL}$ have $\Delta b > 0$, and indicate greater influence of fines in cyclic loading relative to that in monotonic loading.

Five mixtures of sand and fines had both monotonic and cyclic data available, allowing Δb to be defined based on test data. These mixtures were: FBM Sand, F55 Foundry Sand, Ottawa Sand, M31 Artificial Sand and Mai Liao Sand. Note that all bar the cyclic Ottawa Sand test specimens were prepared using moist tamping. Δb for each of these mixtures is correlated with χ_e in Figure 6-21, using filled data points. Error bars correspond to the $MSE \leq 0.0009$ limits for the b_{CR} values.

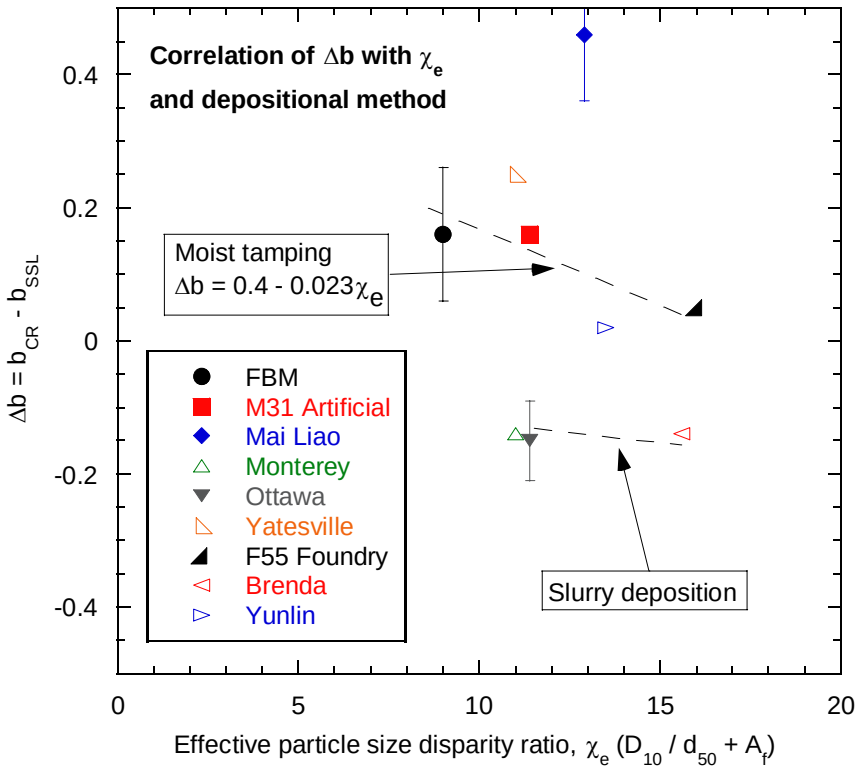

Figure 6-21 Difference in fines influence factors Δb using χ_e.

Figure 6-21 also displays Δb values for the four other sandy soils that had cyclic resistance data: Monterey 0/30 Sand, Brenda 20/200 Sand, Yatesville Sand and Yunlin Sand. The steady state line b_{SSL} values were estimated for these soils using the procedure discussed in Section 6.6. Note these sandy soils have open data points in Figure 6-21 to identify the fact that they are purely estimated Δb values.

The general trend in Figure 6-21 suggests the moist tamped specimens have positive Δb values, or $b_{CR} > b_{SSL}$. This is the case for all four moist tamped sandy soils with both back-calculated b_{SSL} and b_{CR} values (FBM Sand, F55 Foundry Sand, M31 Artificial Sand, and Mai Liao Sand). Estimated Δb values for Yatesville Sand and Yunlin Sand are also positive, with only the estimated Δb for Monterey 0/30 Sand being negative. Overall it would appear that b_{CR} values for moist tamped soil specimens can be estimated reasonably well by adding some value of Δb to the b_{SSL} fines influence factor. In total, six out of seven sandy soils prepared using moist tamping had $\Delta b > 0$.

The test specimens of two mixtures of sand and fines, Ottawa Sand and Brenda 20/200 Sand, were prepared using slurry deposition. $\Delta b < 0$ for each of these mixtures, but only Ottawa Sand Δb was back-calculated from both monotonic and cyclic test data. Based on these two mixtures, it appears that slurry deposited specimens have $b_{CR} < b_{SSL}$. This difference

is likely due to the difference in initial soil structure, and subsequent effect on cyclic response, created by slurry deposition compared with that created by moist tamping.

It is proposed based on Figure 6-21 that b_{CR} can be estimated by using Δb and the steady state line fines influence factor b_{SSL}. The data suggests that Δb depends on the soil depositional method, and that different correlations with χ_e exist, as illustrated in Figure 6-21 for moist tamping and slurry deposition. This idea essentially uses the steady state line fines influence factor as a base reference for a given sandy soil, and allows b_{CR} to be estimated for differing soil depositional methods.

It should also be noted that these conclusions are based on a small amount of data, particularly as only five sandy soils had both monotonic and cyclic data available. The apparent difference in b_{CR} values due to initial soil fabric needs further testing to confirm, and would benefit from an undrained cyclic testing regime on one mixture of sand and fines using varying depositional methods.

- b_{CR} can potentially be estimated using b_{SSL} and Δb
- Further study is required to confirm different depositional methods produce different b_{CR} values

6.6. Simplified Estimation Method for Steady State Lines and Cyclic Resistance Curves

The following details a simplified method to estimate the steady state line and cyclic resistance curve across varying fines contents, up to f_C = 30%, for a particular mixture of sand and fines. The method uses material properties of the sand and fines fractions to estimate fines influence factors b_{SSL} and b_{CR}, based on the correlations in Section 6.5. These factors are used in conjunction with the equivalent granular void ratio definition and clean sand data to estimate the undrained response as fines are added. A method overview is outlined below:

- Define the material properties of the sand and fines particles
- Estimate angularity effects on the particle size disparity ratio
- Estimate the steady state line fines influence factor, b_{SSL}
- Estimate the cyclic resistance curve fines influence factor, b_{CR}
- Define the benchmark response curves for the steady state of deformation and liquefaction resistance

- Generate the expected response curves for steady state and cyclic resistance using b_{SSL}, b_{CR} and benchmark response curves

6.6.1. Definition of Material Properties

The material properties of the sandy soils must firstly be defined. These can be separated into requirements for the sand fraction and fines fraction:

Sand properties:

- Particle size distribution to determine D_{10}
- Void ratio limits, e_{max} and e_{min}
- Qualitative particle angularity (R → A)

Fines properties:

- Particle size distribution to determine d_{50}
- Plastic and liquid limit tests to check fines are non-plastic (NP)

The particle sizes of the sand and fines fraction can be used to calculate the particle size disparity ratio χ. This ratio estimates the relative available void space for the fines to sit within without considering any angularity effects. The ratio χ is defined in Equation (6-12):

$$\chi = \frac{D_{10}}{d_{50}} \tag{6-12}$$

The calculated particle size disparity ratio is the first **combined material property**:

- Particle size disparity ratio χ

6.6.2. Estimation of Angularity Effects

Sand particle angularity has been shown in Section 6.5.2 to increase the effective available void space for the fines to sit within. To estimate the angularity effect A_f on the particle size disparity ratio χ, the sand particle regularity ρ is firstly estimated using Equation (6-13):

$$\rho = \frac{e_{max} - 1.5}{-0.82} \tag{6-13}$$

The sand particle regularity is then checked with the proposed regularity ranges based on the qualitative particle angularity description. The suggested ranges are:

- ρ = 0.75 – 0.90 for R – SR particle shapes
- ρ = 0.65 – 0.75 for SR – SA particle shapes
- ρ = 0.40 – 0.65 for A – SA particle shapes

If the estimated particle regularity ρ is outside of these limits, it should be adjusted to the closest ρ value based on the qualitative descriptions. For example, ρ = 0.72 for a R – SR sand particle → ρ = 0.75 – the lower limit for R – SR particles. Figure 6-22 can then be used to estimate the angularity effect A_f on the particle size disparity ratio χ.

Equation (6-14) can also be used to calculate the estimated A_f.

$$A_f = 52.3 - 68.8\rho \quad , \quad 0.60 \le \rho \le 0.76 \tag{6-14}$$

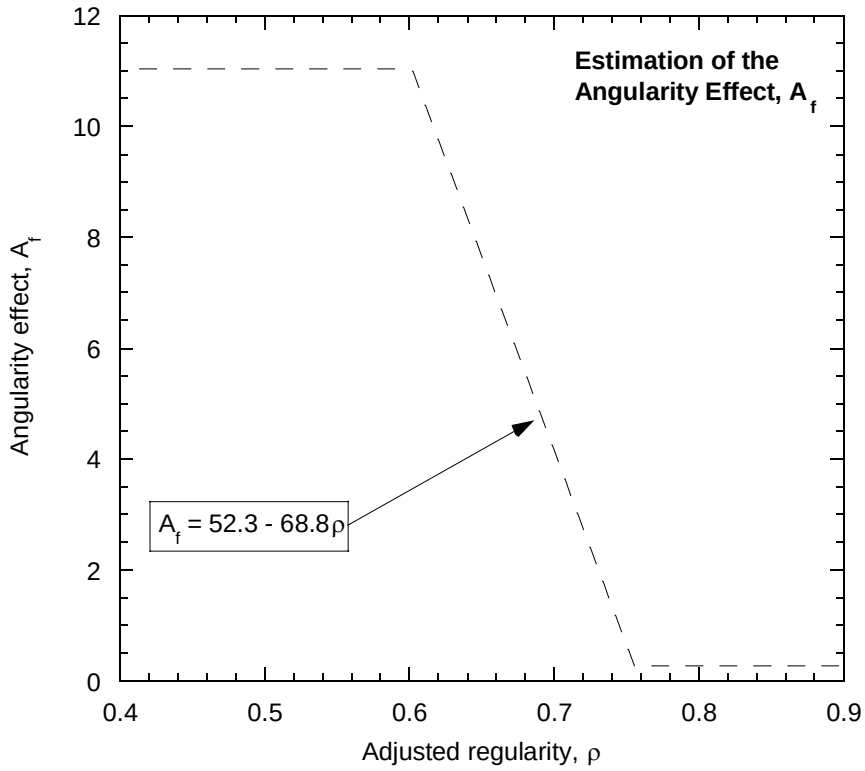

Figure 6-22 Estimation curve for angularity effect A_f using the adjusted particle regularity ρ.

Once the angularity effect A_f has been estimated, the effective particle size disparity ratio χ_e is calculated. The effective particle size disparity ratio accounts for increased available void space for the fines due to sand particle angularity, and is defined in Equation (6-15):

$$\chi_e = \chi + A_f \tag{6-15}$$

The **sand properties** estimated in this step are:

- Sand particle regularity ρ
- Angularity effect A_f

The **combined material property** is:

- Effective particle size disparity ratio χ_e

6.6.3. Estimation of Steady State Line Fines Influence Factor, b_{SSL}

The fines influence factor b_{SSL} for the steady state of deformation is estimated using the effective particle size disparity ratio χ_e. This ratio is used in conjunction with Figure 6-23, which also shows the b_{SSL} ± 0.05 limits. It is recommended that these limits are used to generate a range of potential steady state lines, rather than a single specific curve. Note that this range will increase in $e - p'$ space as the fines content is increased, due to the increasing variability in potential steady state line location with increasing fines content.

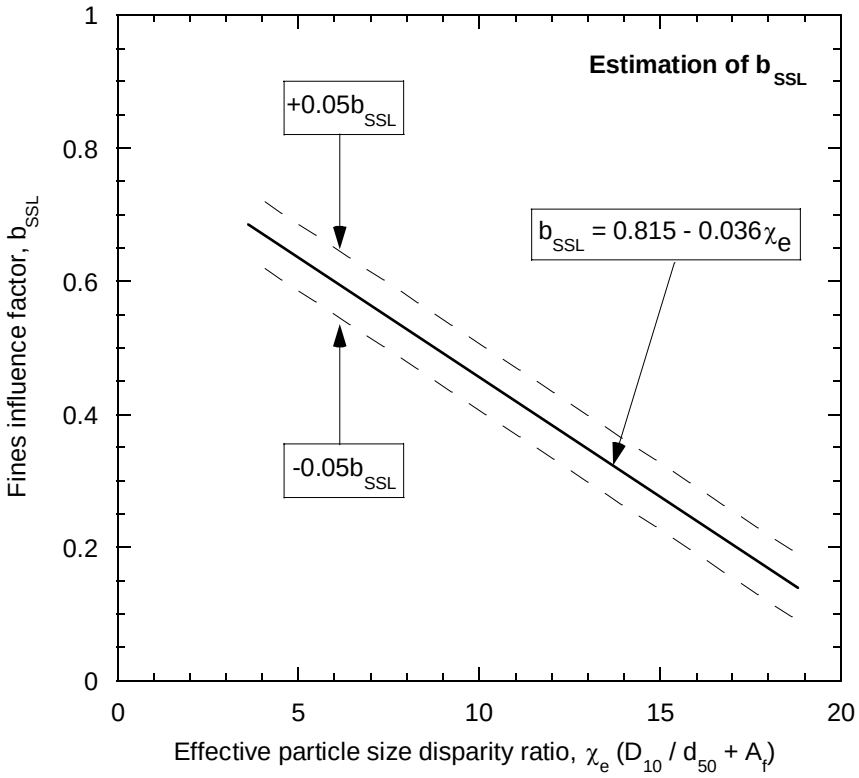

Figure 6-23 Estimation curve for b_{SSL} using the effective particle size disparity ratio χ_e.

Note that b_{SSL} can also be estimated using Equation (6-16):

$$b_{SSL} = 0.815 - 0.036\chi_e \tag{6-16}$$

The **fines influence factor** estimated in this step is:

- Monotonic steady state fines influence factor, b_{SSL}

It is recommended that this factor is only used for fines contents < 30%, or below a known value of the threshold fines content. Beyond this fines content, the internal soil structure is likely to change from sand-dominated to fines-dominated, moving out of the scope of the equivalent granular void ratio concept.

6.6.4. Estimation of Cyclic Resistance Curve Fines Influence Factor, b_{CR}

The fines influence factor b_{CR} for cyclic resistance is estimated using the effective particle size disparity ratio χ_e and the depositional method employed for creating the soil specimens. This estimation should currently only be made for moist tamped specimens, as there is a lack of data confirming the depositional method trends.

The first step is to use χ_e and Figure 6-24 to estimate Δb, which is the change in fines influence factor moving from steady state to cyclic resistance. Note that this takes account of sand particle angularity effects and specimen depositional method. The curves in Figure 6-24 have not been defined beyond the values of χ_e of the soils presented in this study, as it is unclear how the value of Δb may vary as $\chi_e = 0$ is approached.

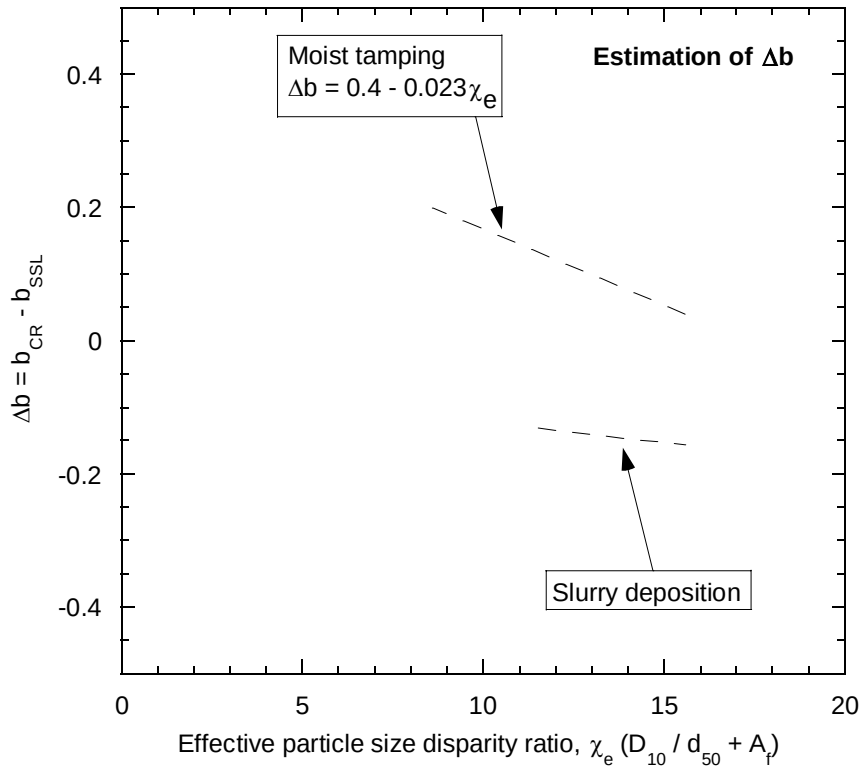

Figure 6-24 Estimation curves for Δb using the effective particle size disparity ratio χ_e and soil depositional method.

Once the change in influence factor is estimated, b_{CR} can be calculated using Equation (6-17). Note that the value of b_{SSL} has been estimated in Section 6.6.3.

$$b_{CR} = b_{SSL} + \Delta b \tag{6-17}$$

The same ± 0.05 limits as for b_{SSL} can also be applied to the b_{CR} values. This enables a range of cyclic resistance curves to be generated rather than a single specific curve. Again note that this range will increase as the fines content is increased, due to the increasing variability in potential cyclic resistance curve location with increasing fines content.

The **fines influence factors** estimated in this step are:

- Change in fines influence factor, Δb
- Cyclic resistance fines influence factor, b_{CR}

6.6.5. Definition of Benchmark Response Curves

The clean sand benchmark response curves are required to enable generation of response curves for additional fines contents. These benchmark curves are the steady state line derived from undrained monotonic loading, and the cyclic resistance curve derived from undrained cyclic loading. They define the expected undrained response of the sandy soils in $e^* - p'$ space and $e^* - CSR$ space.

The steady state line can be defined in terms of a logarithmic relationship between e^* and p', and the cyclic resistance curve by a power relationship between e^* and CSR. Such relationships are described in Equations (6-18) and (6-19) respectively, where K, M, A and D are all constants:

$$e^* = K - M \log p' \tag{6-18}$$

$$e^* = A(CSR)^D \tag{6-19}$$

Sand response references:

- Steady state line → requires 3 – 4 undrained monotonic tests
- Cyclic resistance curve → requires 2 – 3 cyclic resistance points. Each point is taken from the CSR at a given N_C on a single liquefaction

resistance curve, which requires 3 – 4 cyclic tests to define. Therefore 6 – 12 cyclic tests are required to define a cyclic resistance curve.

6.6.6. Generation of Response Curves for Varying Fines Contents

The expected response curves for any fines content below f_{Cth} are generated using the fines influence factor b_{SSL} range estimated in Section 6.6.3, the b_{CR} range estimated in Section 6.6.4, and the benchmark response curves defined in Section 6.6.5. Equation (6-20) shows a rearrangement of the equivalent granular void ratio definition, allowing the global void ratio e for a given fines content to be determined. Note that $b = b_{SSL}$ or b_{CR}:

$$e = e^{*}[1-(1-b)f_C]-(1-b)f_C \tag{6-20}$$

Equation (6-20) is used to move the benchmark response curves, as described in Equations (6-18) and (6-19), to generate the expected response curves. This process is qualitatively shown in Figure 6-25 using the steady state line as an example.

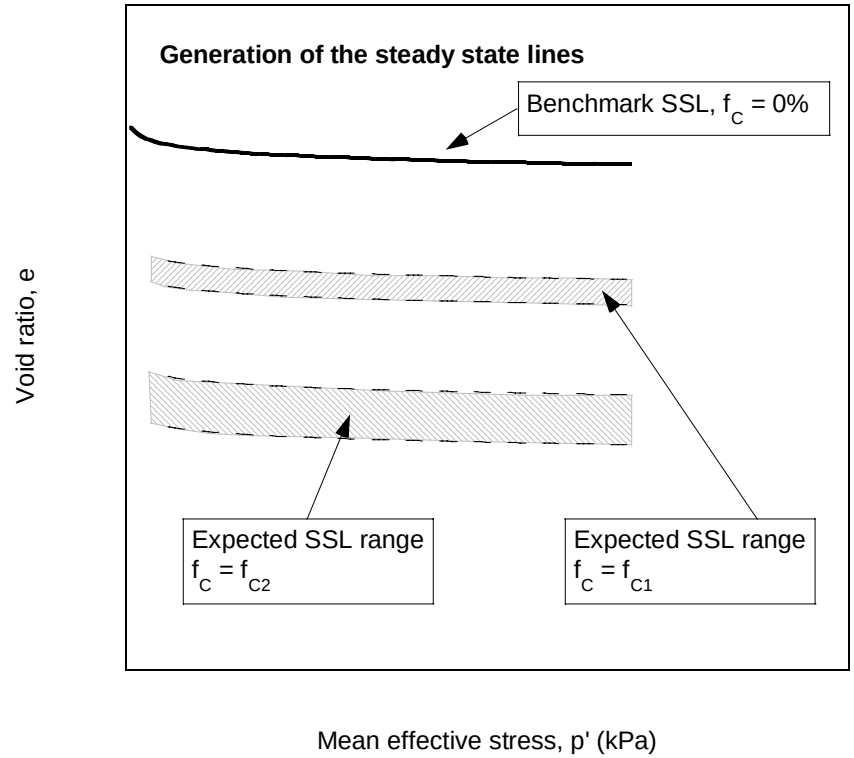

Figure 6-25 Benchmark steady state line used to generate expected steady state line ranges.

Note that $f_C = 0\% < f_{C1} < f_{C2}$ in Figure 6-25, meaning the steady state line ranges move to higher densities, in terms of the global void ratio, as fines content is increased. This was the typical trend observed in Chapter 4 when interpreting the FBM soil response using the global void ratio as the fines content was increased. The response generation process is comparable when generating the cyclic resistance curves.

6.6.7. Limitations of the Simplified Estimation Method

A number of known limitations exist when using the simplified estimation method. These are listed in the following:

Sand and Fines properties:

- The sand should be mixed with no more than 30% fines. The equivalent granular void ratio concept is not applicable beyond the threshold fines content, f_{Cth}.
- The method should not be used when $\chi_e < 3.0$ for a sand-fines mixture, and $b \geq 0$, as predicted by the equivalent granular void ratio concept.
- The fines should be non-plastic (NP). It is currently unclear how plasticity affects the fines influence factor, with some research (Ni et al., 2004) suggesting that plastic fines shift the influence factor values outside of the range $0 \leq b \leq 1.0$.

Expected response curves:

- Steady state lines should only be estimated using the procedure for mean effective stress $p' \leq 500$kPa. This limit is based on the p' values used to create the procedure.
- Cyclic resistance curves should only be estimated for moist tamped specimens, preferably with $\chi_e > 9$. It is currently unclear how other depositional methods affect Δb and b_{CR} values.

Finally it is important to note that this procedure has been created from the data of a limited number of sandy soils. As such, it should currently be treated with caution. The overall procedure can be improved in particular through the addition of extra back-calculated fines influence factor values derived from further test data to improve the correlations defined in Section 6.5.

6.7. Summary

This chapter investigated the fines influence factor, b, which was defined as "a parameter that accounts for the variation in the undrained response of sand due to the addition of fines below the threshold fines content." Note that separate values of b_{SSL} and b_{CR} were defined for monotonic and cyclic responses respectively.

The definition of the equivalent granular void ratio, e^*, was firstly given to demonstrate how the fines influence factor, b, and fines content, f_C, modify the global void ratio of a sandy soil. The physical properties of sandy soils were then discussed, suggesting that the fines influence factor cannot be explicitly defined as the percentage of fines participating in the soil force-chain during loading.

The use of a constant value of the fines influence factor in the equivalent granular void ratio, for soils below the threshold fines content, was then assessed using test data from the FBM soils presented in Chapter 4, and the sandy soils from the literature presented in Chapter 5. Ultimately it was concluded that using a constant b value was a reasonable assumption to make, as the variation in the individual influence factor adjustment, $(1-b)f_C$, varied at most ± 0.02 from the constant back-calculated b value.

The difference between the influence of the fines on the undrained monotonic response at the steady state of deformation, and cyclic response at liquefaction, was explained. It appears the cumulative dilatancy effects change throughout the course of soil deformation, and that the differences in levels of axial strain at the steady state of deformation and cyclic liquefaction reflect the differences in the values of the fines influence factors, b_{SSL} and b_{CR}.

Following this, the material properties of the sandy soils were correlated with the fines influence factors b_{SSL} and b_{CR}. It was found that the value of b_{SSL} increases as the particle size disparity ratio χ decreases, and that b_{SSL} is higher for soils with more rounded sand particles than for soils with more angular sand particles. The value of b_{SSL} was also used as a reference for comparing the effects of initial soil fabric, or depositional method, on the value of b_{CR}. It was found that typically $b_{CR} > b_{SSL}$ when moist-tamped specimens were being considered.

Lastly a simplified method was presented to estimate the locations of the steady state lines and cyclic resistance curves of sandy soils using the material properties of the soil, the depositional method, and the actual response of the clean sand. This method was based on the correlations presented in this chapter.

7. Critical Review of the Simplified Estimation Method

7.1. Introduction

In Chapter 6 a simplified method was proposed to estimate the effects of fines content on the steady state line and cyclic resistance of sandy soils using only: (1) the material properties of the soil, and (2) the undrained response of the clean sand. This method uses the equivalent granular void ratio concept (Thevanayagam et al., 2000) as a basis for estimating such soil response. To critically review this proposed method, two sandy soils sourced from Christchurch – PSM1 and PSM2 – were triaxially tested under monotonic and cyclic loading conditions, with the responses of the silty sands predicted using the simplified method before testing occurred. Detailed information on the two PSM sandy soils can be found in Chapter 3.

Material property tests, such as particle size distributions and void ratio limits, were firstly carried out on the two mixtures of sand and fines before any triaxial testing was begun. These allowed the fines influence factors, b_{SSL} and b_{CR}, to be estimated before testing using the process outlined in Figure 7-1. Initial triaxial tests were then performed on the clean sand fraction of the mixtures to define the benchmark response curves. These curves enabled the expected steady state lines and cyclic resistance curves to be estimated as fines were added to the PSM sands, using the estimated b_{SSL} and b_{CR} values.

This chapter firstly details the estimation of the fines influence factors for the PSM1 and PSM2 soils. Following this, the predicted and observed steady state lines and cyclic resistance curves of the two soils are compared. Finally the simplified estimation method is critically reviewed based on the results obtained from the PSM soil laboratory tests.

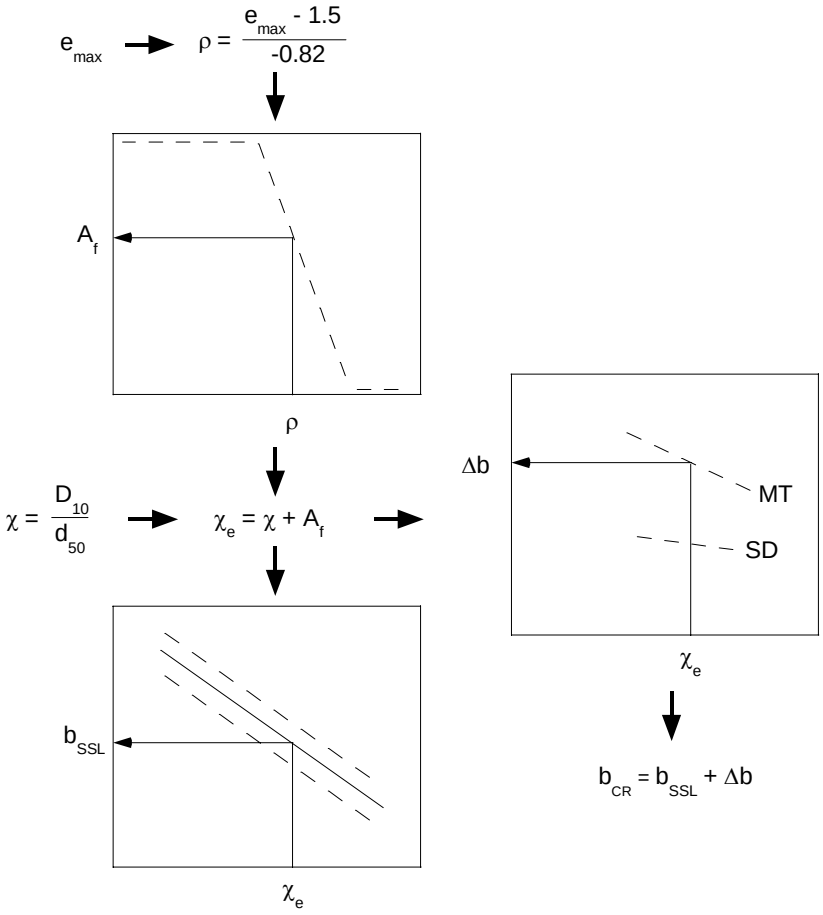

Figure 7-1 Schematic illustration of the process used to estimate b_{SSL} and b_{CR}.

7.2. Estimation of b_{SSL} and b_{CR} for PSM1 and PSM2 Soils

The simplified method for estimating the steady state lines and cyclic resistance curves of sandy soils, as outlined in Chapter 6, was firstly used to estimate the fines influence factors, b_{SSL} and b_{CR}, of the PSM1 and PSM2 soils. The material properties of the soils required to estimate the fines influence factors are presented in Table 7-1. The particle size distributions of the PSM1 and PSM2 soils are shown in Figure 7-2 and Figure 7-3 respectively. Figure 7-3 highlights the gap-graded nature of the PSM2 soils that include fines – this gap was due to the removal of particles sizes from 37 - 75μm, as discussed in Chapter 3.

Table 7-1 Material properties of the PSM1 and PSM2 soils required to estimate b_{SSL} and b_{CR} using the simplified estimation method.

Soil	Sand D_{10} (mm)	Fines d_{50} (mm)	Sand e_{max}	Qualitative sand angularity	Fines plasticity
PSM1	0.104	0.016	0.927	SR - SA	NP
PSM2	0.091	0.009	0.941	SR - SA	NP

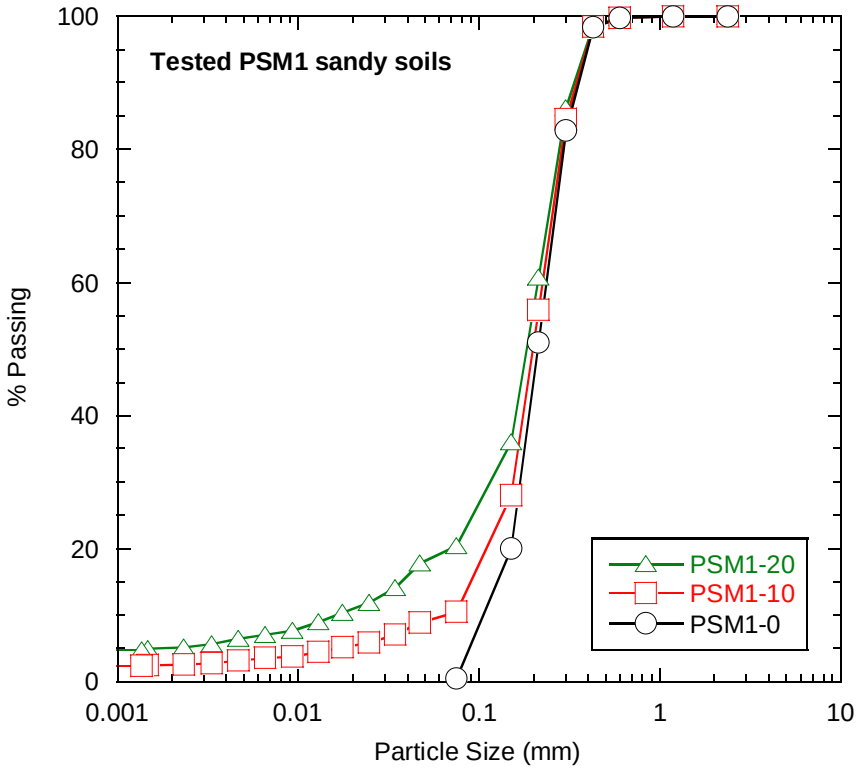

Figure 7-2 Particle size distributions of the tested PSM1 sandy soils.

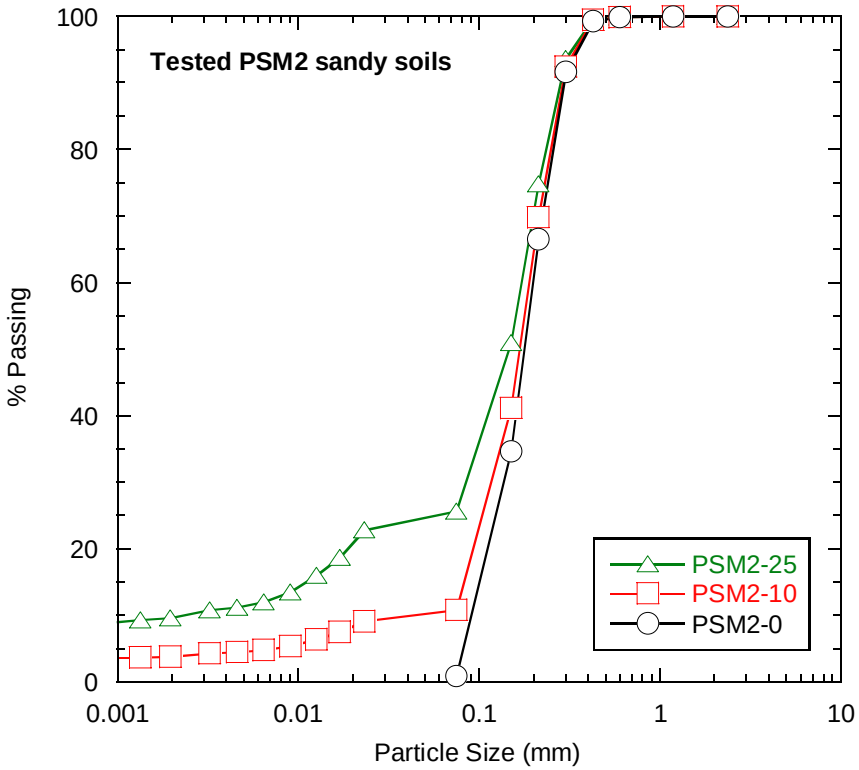

Figure 7-3 Particle size distributions of the tested PSM2 sandy soils.

Using the properties listed in Table 7-1, the fines influence factors b_{SSL} and b_{CR} were estimated for the PSM1 and PSM2 soils using the following steps:

(1) The particle size disparity ratios χ firstly were calculated using D_{10} and d_{50}. These were:

PSM1 χ = Eq. (6-12) = (0.104mm / 0.016mm) = 6.5

PSM2 χ = Eq. (6-12) = (0.091mm / 0.009mm) = 10.1

(2) The sand particle regularities ρ were then estimated using e_{max} of the sand fraction. These were:

PSM1 ρ = Eq. (6-13) = (0.927 – 1.5 / -0.82) = 0.70

PSM2 ρ = Eq. (6-13) = (0.941 – 1.5 / -0.82) = 0.68

As each of the ρ values were within the SR – SA range of ρ = 0.65 – 0.75, no adjustment to the estimated values of ρ was required. The angularity effect A_f was estimated using these ρ values:

PSM1 A_f = Eq. (6-14) = 52.3 – 68.8(0.70) = 4.1

PSM2 A_f = Eq. (6-14) = 52.3 – 68.8(0.68) = 5.5

The A_f values were then combined with the calculated χ values to give the effective particle size disparity ratios χ_e:

PSM1 χ_e = Eq. (6-15) = 6.5 + 4.1 = 10.6

PSM2 χ_e = Eq. (6-15) = 10.1 + 5.5 = 15.6

(3) The steady state line fines influence factors, b_{SSL}, were estimated using the χ_e values:

PSM1 b_{SSL} = Eq. (6-16) = 0.815 – 0.036(10.6) = 0.43

PSM2 b_{SSL} = Eq. (6-16) = 0.815 – 0.036(15.6) = 0.25

The b_{SSL} range was defined for each soil using ± 0.05 limits:

PSM1: $0.38 \leq b_{SSL} \leq 0.48$

PSM2: $0.20 \leq b_{SSL} \leq 0.30$

(4) The change in fines influence factors, Δb, from b_{SSL} to b_{CR} were estimated using the χ_e values, and the moist tamping depositional method curve:

PSM1 $\Delta b = 0.4 - 0.023(10.6) = 0.16$ from Fig. 6-23
PSM2 $\Delta b = 0.4 - 0.023(15.6) = 0.04$ from Fig. 6-23

The cyclic resistance curve fines influence factors, b_{CR}, were then estimated using the b_{SSL} and Δb values:

PSM1 b_{CR} = Eq. (6-17) = 0.43 + 0.16 = 0.59
PSM2 b_{CR} = Eq. (6-17) = 0.25 + 0.04 = 0.29

The b_{CR} range was defined for each soil using ± 0.05 limits:

PSM1: $0.54 \leq b_{CR} \leq 0.64$
PSM2: $0.24 \leq b_{CR} \leq 0.34$

The calculated parameters used to estimate the b_{SSL} and b_{CR} values are summarized in Table 7-2.

Table 7-2 PSM1 and PSM2 calculated parameters from the simplified estimation method.

Soil	χ	ρ	A_f	χ_e	b_{SSL}	Δb	b_{CR}
PSM1	6.5	0.70	4.1	10.6	0.43	0.16	0.59
PSM2	10.1	0.68	5.5	15.6	0.25	0.04	0.29

These first four steps were the only parts of the simplified estimation method that could be completed before any triaxial testing was carried out. The remaining steps of the procedure used to estimate the steady state line and cyclic resistance curve ranges require the clean sand benchmark response data, which was obtained from the initial undrained monotonic and cyclic tests on the PSM1 and PSM2 soils.

7.3. Predicted and Observed Steady State Lines

To test the validity of the simplified estimation method outlined in Chapter 6, the steady state lines of the PSM soils obtained from the triaxial tests were compared with those estimated using the simplified method. The steady state lines of the PSM clean sands were firstly obtained to define the benchmark response curves. Following this the expected locations of the steady state line for different fines contents were predicted using the clean sand benchmark response and the fines influence factors, b_{SSL}, calculated in Section 7.2. Monotonic compression tests on the PSM sandy soils were then performed to define the actual steady state lines at f_C = 10% and f_C = 20% for the PSM1 sand, and f_C = 10% and f_C = 25% for the PSM2 sand.

The PSM1 steady state lines are presented first, with the PSM2 steady state lines following. Note that the general undrained monotonic response of the PSM soils was similar to that of the FBM soils discussed in Chapter 4. As such no stress-strain, stress-path, or excess pore water pressure generation response curves are discussed in this section.

7.3.1. PSM1 steady state lines

The steady state line of the PSM1-0 sand is presented in Figure 7-4. This is the clean sand benchmark response used to define the expected steady state line ranges of all other PSM1 soils with f_C < 30%. Note that this steady state line is located very close to the maximum void ratio, e_{max}, suggesting that very few initial states could result in strain-softening during axial compression. This is also similar to the steady state line of the FBM-1 sand which was presented in Chapter 4, suggesting similarities in monotonic response between the two sands.

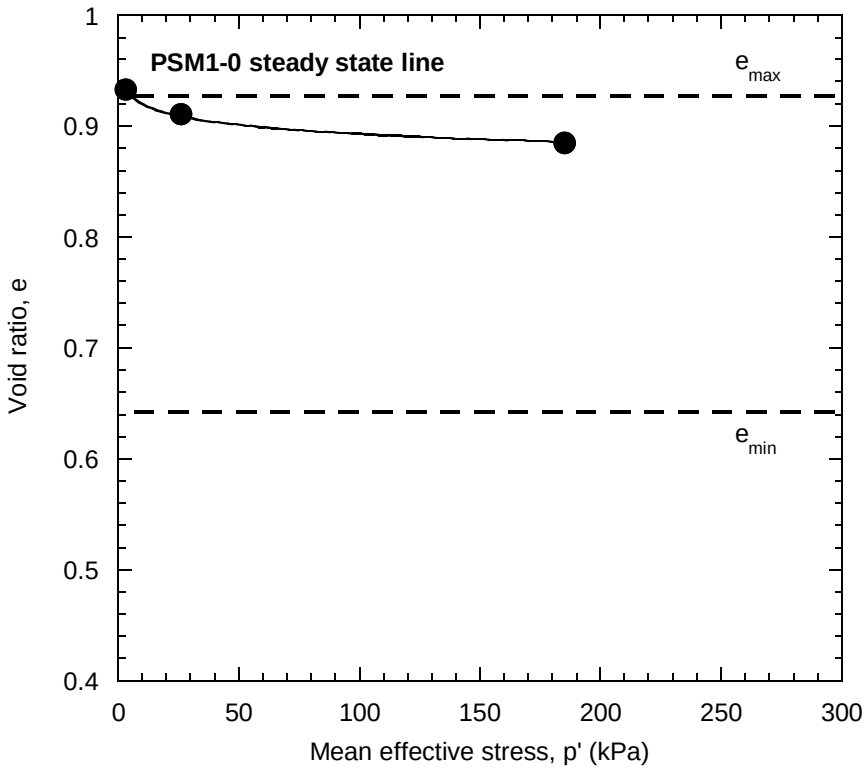

Figure 7-4 Observed steady state line of the PSM1-0 sand.

As displayed in Figure 7-4, a logarithmic curve was fitted to the PSM1-0 steady state data points to define the steady state line. This logarithmic curve is given by Equation (7-1):

$$e^* = 0.947 - 0.027 \log p' \qquad (\text{when } p' \geq 10\text{kPa}) \tag{7-1}$$

Note that in Equation (7-1) the steady state line is defined using the equivalent granular void ratio, e^*. This is because the clean sand steady state line of the PSM1-0 sand defines the expected steady state line location for all PSM1 soils in the $e^* - p'$ plane when $f_C < 30\%$. The b_{SSL} range, as printed in Section 7.2, was used in conjunction with Equation (7-1) and Equation (7-2) to predict the steady state line ranges in the $e - p'$ plane for the PSM1 soils with $f_C = 10\%$ and $f_C = 20\%$. These predicted ranges are presented in Figure 7-5 and Figure 7-6, along with the actual steady state data for the PSM1-10 and PSM1-20 soils obtained from subsequent undrained monotonic compression tests.

$$e = e^*[1 - (1 - b) f_C] - (1 - b) f_C \tag{7-2}$$

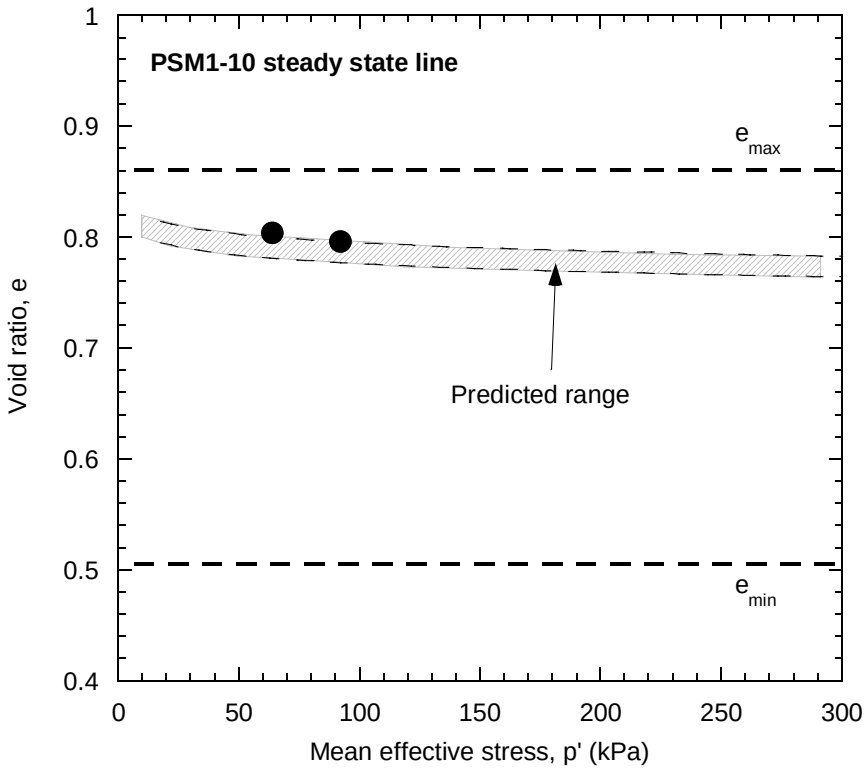

Figure 7-5 Predicted steady state line range of the PSM1-10 soil and observed steady state data points.

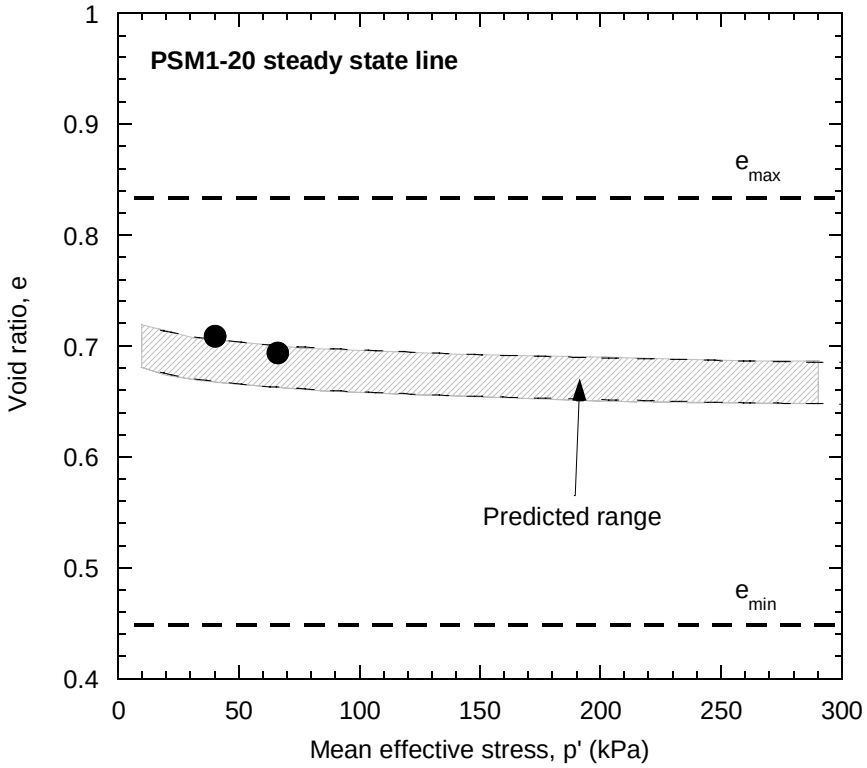

Figure 7-6 Predicted steady state line range of the PSM1-20 soil and observed steady state data points.

In Figure 7-5, the observed PSM1-10 steady state data sits on the upper limit of the predicted steady state line range obtained using the simplified estimation method. This is also the case for the PSM1-20 steady state data displayed in Figure 7-6. These plots suggest that the simplified method has effectively estimated the approximate response of the PSM1-10 and PSM1-20 soils at the steady state of deformation, using a range of $0.38 \leq b_{SSL} \leq 0.48$.

To confirm this conclusion, the actual individual best fit b_{SSL} values of the PSM1-10 and PSM1-20 soils were back-calculated using the obtained test data and the procedure outlined in Chapter 5. This produced a best fit $b_{SSL} = 0.49$ for the PSM1-10 soil, a best fit $b_{SSL} = 0.48$ for the PSM1-20 soil, and a best fit $b_{SSL} = 0.48$ when using the combined PSM1-10 and PSM1-20 data. Note that these values are on the upper limit of the estimated b_{SSL} range, suggesting that the simplified estimation method slightly underestimated the effect of additional fines on the PSM1 sand response at the steady state of deformation. This is also why the obtained test data sits on the upper limit of the predicted response ranges.

Based on the observed results in Figure 7-5 and Figure 7-6, the predicted steady state line ranges of the PSM1 soils could be used to predict the general expected response of the PSM1 soils with non-plastic fines of $f_C < 30\%$. Initial states above the steady state line ranges will exhibit contractive behaviour under monotonic loading. Initial states below the steady state line ranges will be associated with dilative response when large strains corresponding to the steady state of deformation are reached.

Therefore in summary, when interpreting the response of the PSM1 soils at the steady state of deformation using the simplified estimation method:

- The PSM1-10 and PSM1-20 observed steady state data points from monotonic compression tests sit within the steady state line ranges predicted using the simplified estimation method
- The back-calculated b_{SSL} values = 0.49 and 0.48 locate on the upper limit of the estimated b_{SSL} range obtained using the simplified estimation method
- This suggests the simplified method slightly underestimated the effect of fines on the response of the PSM1 sand at the steady state of deformation
- The predicted steady state lines ranges can be used to predict the general monotonic response of the PSM1 soils when $f_C < 30\%$ for non-plastic fines

7.3.2. PSM2 steady state lines

The steady state line of the PSM2-0 sand is presented in Figure 7-7. It is located at a similar position to that of the PSM1-0 sand, although it is located slightly below the maximum void ratio, e_{max}. This implies that there is a small difference in the undrained monotonic response between the PSM1 and PSM2 sands, even though they were sourced from the same field location and have similar particle size distributions, as shown in Section 7.2.

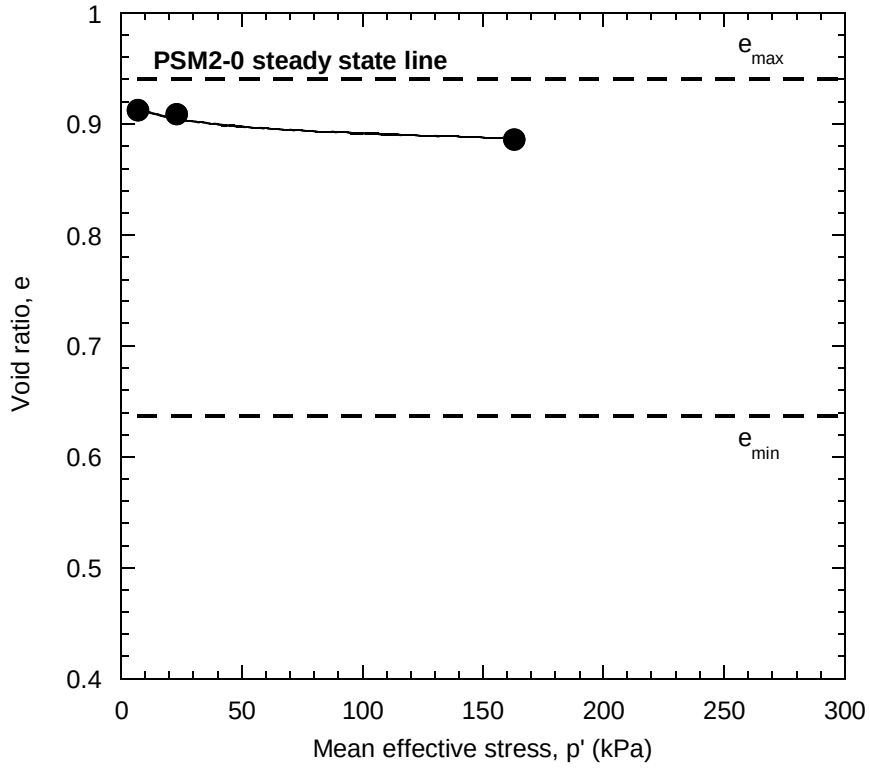

Figure 7-7 Observed steady state line of the PSM2-0 sand.

The steady state line of the PSM2-0 sand was used as the clean sand benchmark response to predict the steady state line ranges of the PSM2-10 and PSM2-25 soils. A logarithmic curve was again fitted to the PSM2-0 steady state data to define the steady state line. This logarithmic curve is given by Equation (7-3). The b_{SSL} range as calculated in Section 7.2 was used with Equation (7-3) and Equation (7-2) to predict the steady state line ranges in the $e - p'$ plane for the PSM2 soils with f_C = 10% and f_C = 25%. The predicted ranges are displayed in Figure Figure 7-8 and Figure 7-9 with the observed steady state data from testing.

$$e^* = 0.924 - 0.020 \log p' \qquad (\text{when } p' \geq 10\text{kPa}) \qquad (7\text{-}3)$$

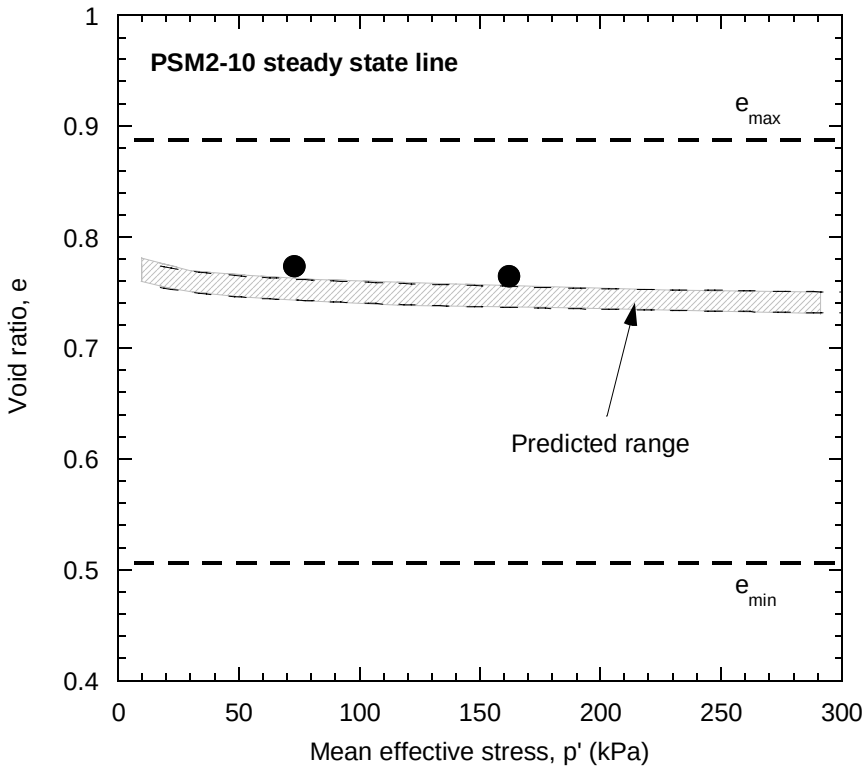

Figure 7-8 Predicted steady state line range of the PSM2-10 soil and observed steady state data points.

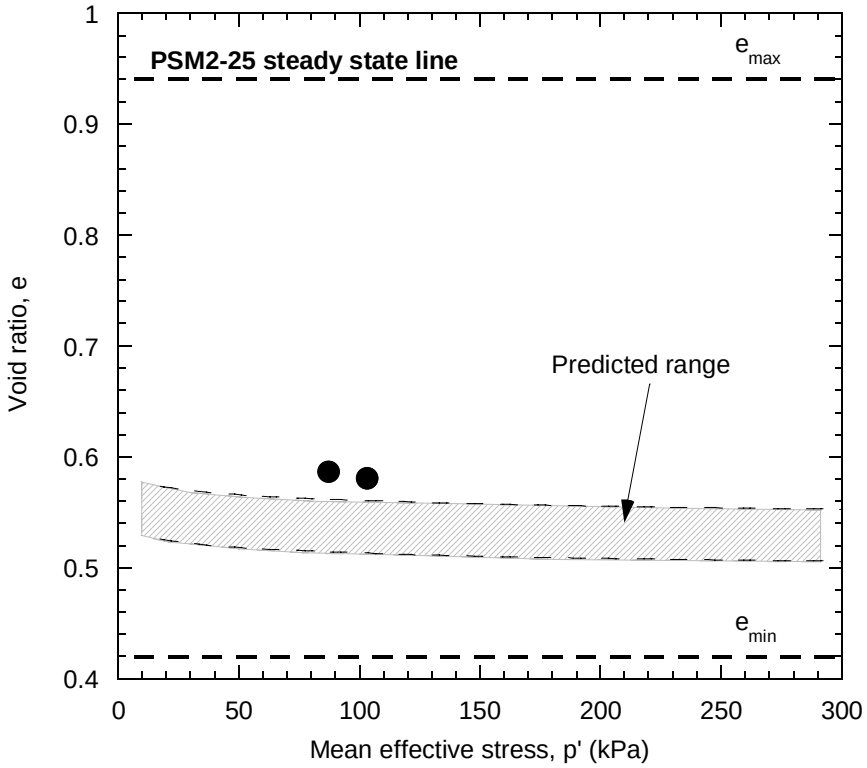

Figure 7-9 Predicted steady state line range of the PSM2-25 soil and observed steady state data points.

Figure 7-8 and Figure 7-9 present the predicted steady state line ranges for the PSM2-10 and PSM2-25 soils respectively, as well as the observed steady state data points for the soils obtained from monotonic compression tests. As can be seen, the observed data points sit outside of the predicted steady state line ranges. The fact that these actual data points are located at lower densities than the expected ranges suggests that the simplified estimation method underestimated the effect of fines on the response of the PSM2 sand at the steady state of deformation.

To confirm this, the actual best fit b_{SSL} values of the PSM2-10 and PSM2-25 soils were back-calculated. These were found to be $b_{SSL} = 0.36$ and $b_{SSL} = 0.35$ for the respective soils. Note that both of these values are higher than the estimated b_{SSL} range of $0.20 \leq b_{SSL} \leq 0.30$. This confirms that the influence of additional fines on the PSM2 sand response was higher in reality than approximated by the simplified method. It also suggests that the simplified estimation method was not as effective in estimating the monotonic response of the PSM2 soils as it was for the response of the PSM1 soils.

However, given that the actual steady state data points in Figure 7-8 and Figure 7-9 are located relatively close to the predicted steady state line ranges, these ranges could still be used to predict the response of the PSM2 soils when undergoing monotonic compression. It is likely that the actual response would be slightly more dilative than expected, due to the underestimation of the effect of fines. Practically this means that the approximated response will be slightly on the conservative side.

As such, the following points were concluded when interpreting the response of the PSM2 soils at the steady state of deformation using the simplified estimation method:

- The PSM2-10 and PSM2-25 observed steady state data points from monotonic compression tests sit outside of the steady state line ranges predicted using the simplified estimation method
- The back-calculated b_{SSL} values = 0.36 and 0.35 were higher than those obtained using the simplified estimation method ($0.20 \leq b_{SSL} \leq 0.30$)
- The simplified method therefore underestimated the effect of fines on the response of the PSM2 sand at the steady state of deformation
- The predicted steady state lines ranges could still be used to predict the general monotonic response of the PSM2 soils when $f_C < 30\%$, although the actual response will be slightly more dilative than the predicted one

7.4. Predicted and Observed Cyclic Resistance Curves

The validity of the simplified estimation method was also tested by comparing the cyclic resistance curves of the PSM soils with the predicted curve ranges. As for the monotonic steady state lines discussed in Section 7.3, the PSM clean sands were firstly tested to define the benchmark response. The expected cyclic resistance curve ranges were then predicted using the clean sand benchmark response and the fines influence factors, b_{CR}, derived in Section 7.2. Further cyclic tests were then carried out on the PSM sandy soils to obtain the actual liquefaction resistances when f_C = 10% and f_C = 20% for the PSM1 sand, and when f_C = 10% and f_C = 25% for the PSM2 sand.

The cyclic response of the PSM1 soils is firstly discussed, presenting both the liquefaction resistance curves obtained from cyclic testing, and the derived cyclic resistance curves at N_C = 15. Following this, the response of the PSM2 soils are discussed. Note that the general undrained cyclic response of the PSM soils was similar to that of the FBM soils discussed in Chapter 4, and hence no stress-strain, stress-path, or excess pore water pressure development responses are displayed in this section.

7.4.1. PSM1 cyclic resistance curves

The liquefaction resistance curves of the PSM1-0 sand are presented in Figure 7-10. Only curves for two different densities (D_r = 5% and 43%) were obtained as this was considered sufficient to define the location of the PSM1-0 cyclic resistance curve, which is displayed in Figure 7-11. Here the cyclic resistance curve has been defined at N_C = 15, with the maximum and minimum void ratios of the sand also shown to demonstrate the range of possible soil densities.

A power curve was fitted to the PSM1-0 cyclic data points in Figure 7-11 to define the cyclic resistance curve. This power curve is given by Equation (7-4), where CSR_{15} = the cyclic stress ratio at N_C = 15:

$$e^* = 0.546(CSR_{15})^{-0.273} \tag{7-4}$$

Note in Equation (7-4) the curve is defined using the equivalent granular void ratio, e^*. This is because the PSM1-0 sand cyclic resistance curve defines the expected cyclic resistance curve of all PSM1 soils in the $e^* - p'$ plane when f_C < 30%.

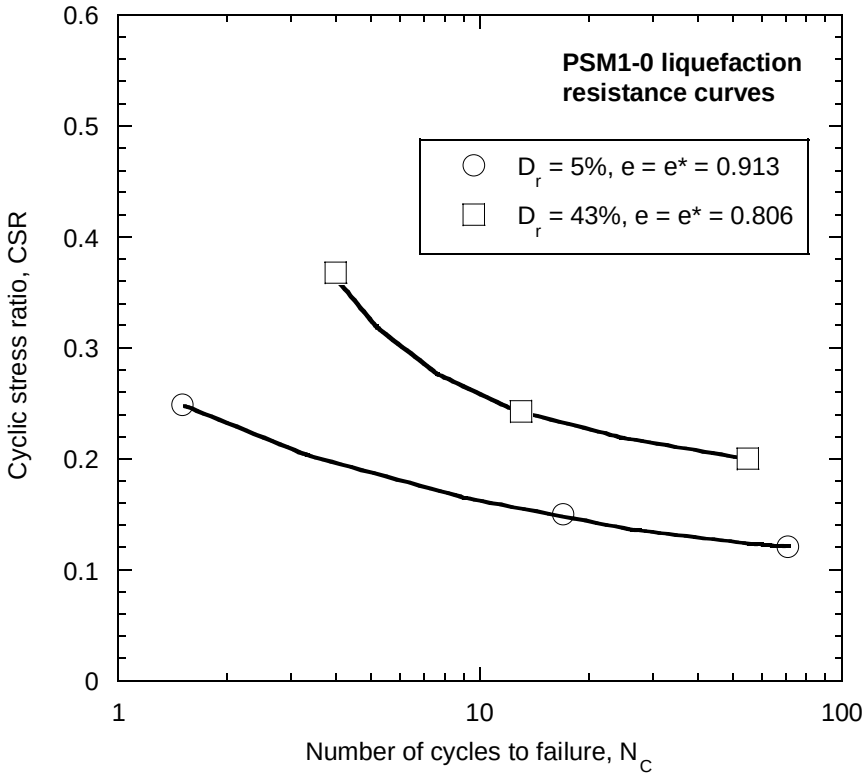

Figure 7-10 Observed liquefaction resistance curves of the PSM1-0 sand.

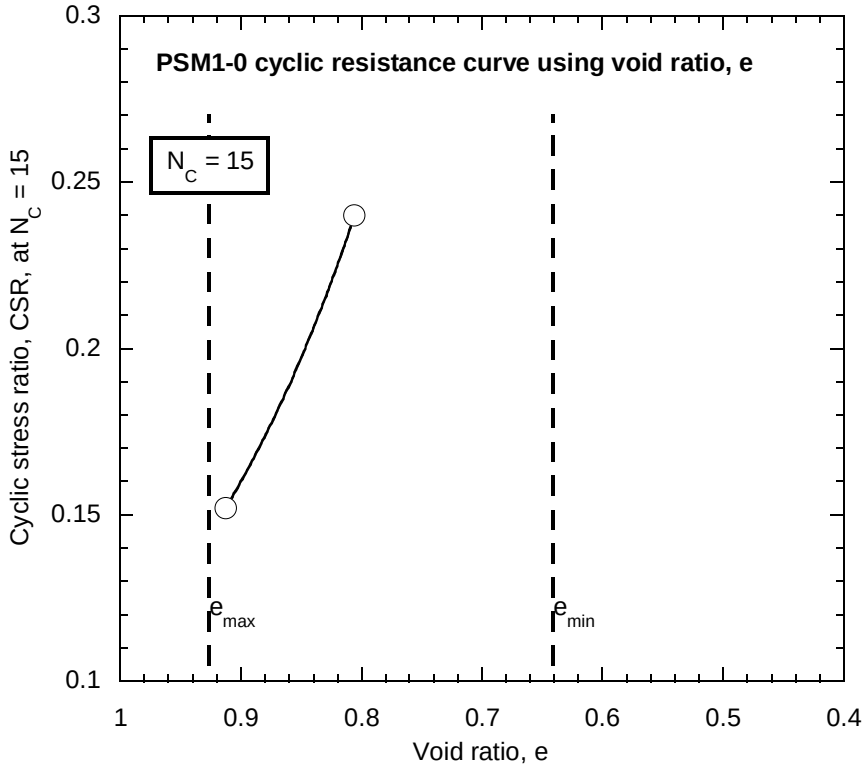

Figure 7-11 Observed cyclic resistance curve at N_C = 15 of the PSM1-0 sand using global void ratio, *e*.

The b_{CR} range calculated in Section 7.2 was used in conjunction with Equation (7-4) and Equation (7-2) to predict the expected cyclic resistance curve ranges for the PSM1 sandy soils with f_C = 10% and f_C = 20%. These ranges were then used to choose the specimen densities and cyclic stress ratios of the cyclically tested PSM1-10 and PSM1-20 soil specimens. The aim was to reach liquefaction in these tests after 15 load cycles, or as close to 15 cycles as possible, to test the accuracy of the simplified estimation method. If the first test on a specimen resulted in liquefaction being reached when N_C < 15, the cyclic stress ratio of the next test was reduced so that liquefaction was reached after N_C > 15. This method of testing resulted in the PSM1-10 and PSM1-20 liquefaction resistance curves covering a small range of N_C values, as can be observed in Figure 7-12 and Figure 7-13 respectively.

The observed cyclic resistance data points of the PSM1-10 and PSM1-20 soils are presented in Figure 7-14 and Figure 7-15, along with the predicted cyclic resistance curve ranges derived from the simplified estimation method, as well as the maximum and minimum void ratios of the respective soils.

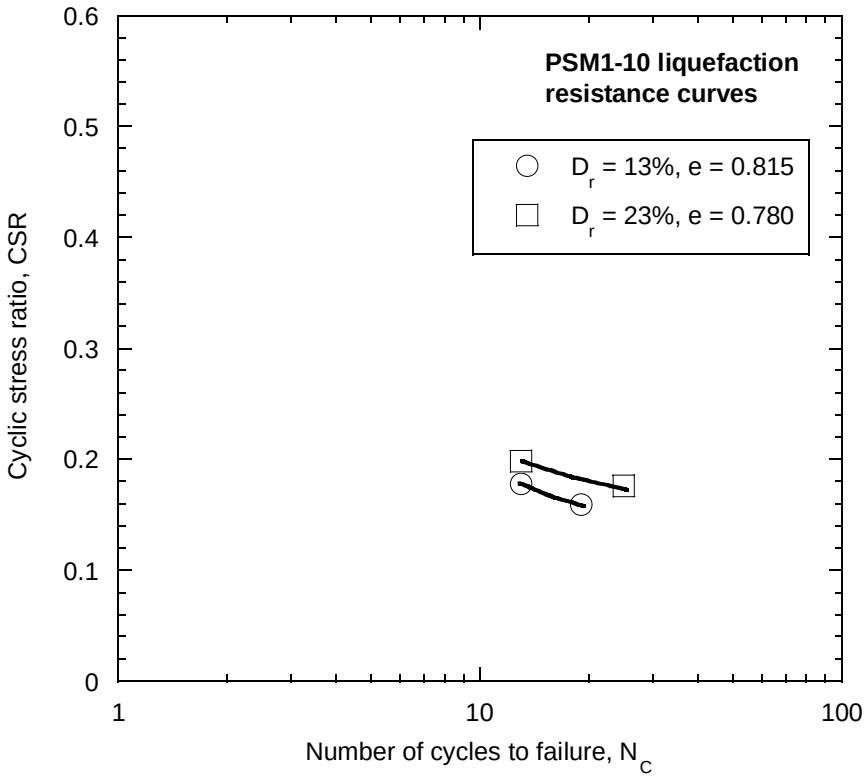

Figure 7-12 Observed liquefaction resistance curves of the PSM1-10 soil.

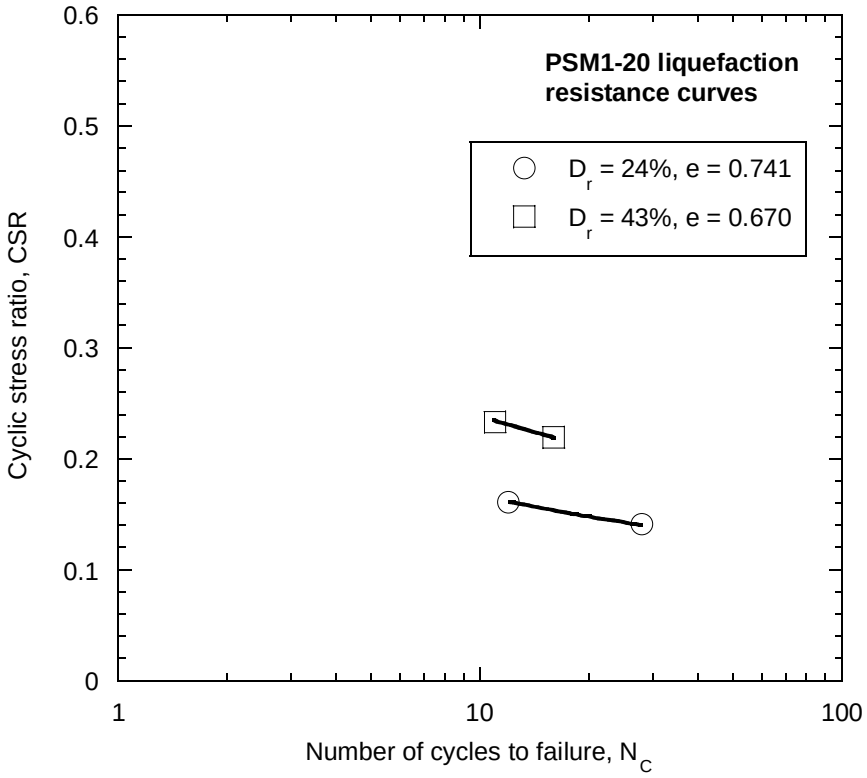

Figure 7-13 Observed liquefaction resistance curves of the PSM1-20 soil.

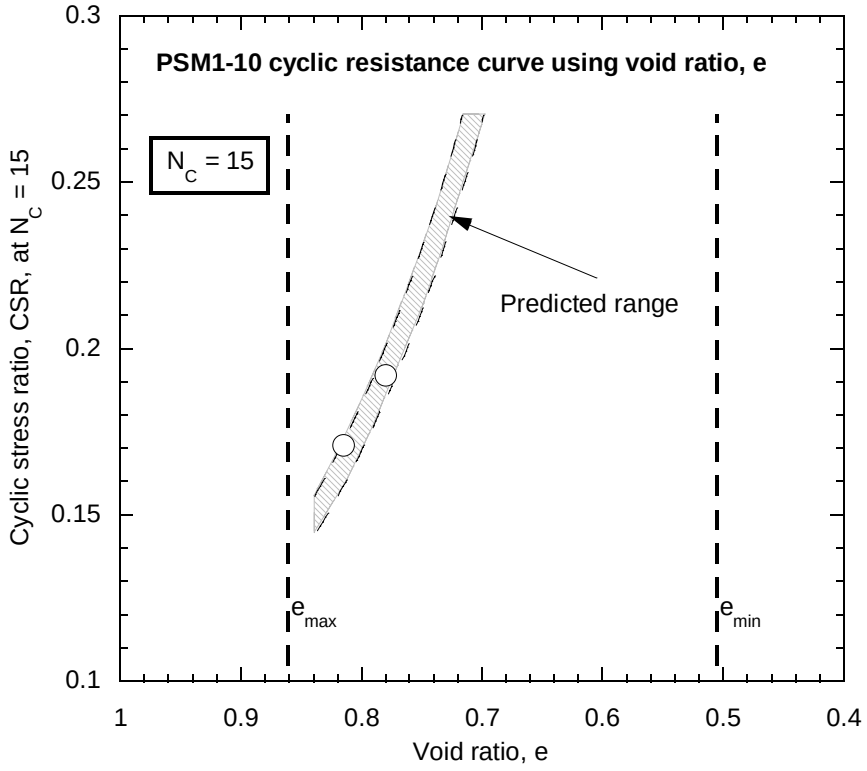

Figure 7-14 Comparison of the observed and predicted cyclic resistance of the PSM1-10 soil.

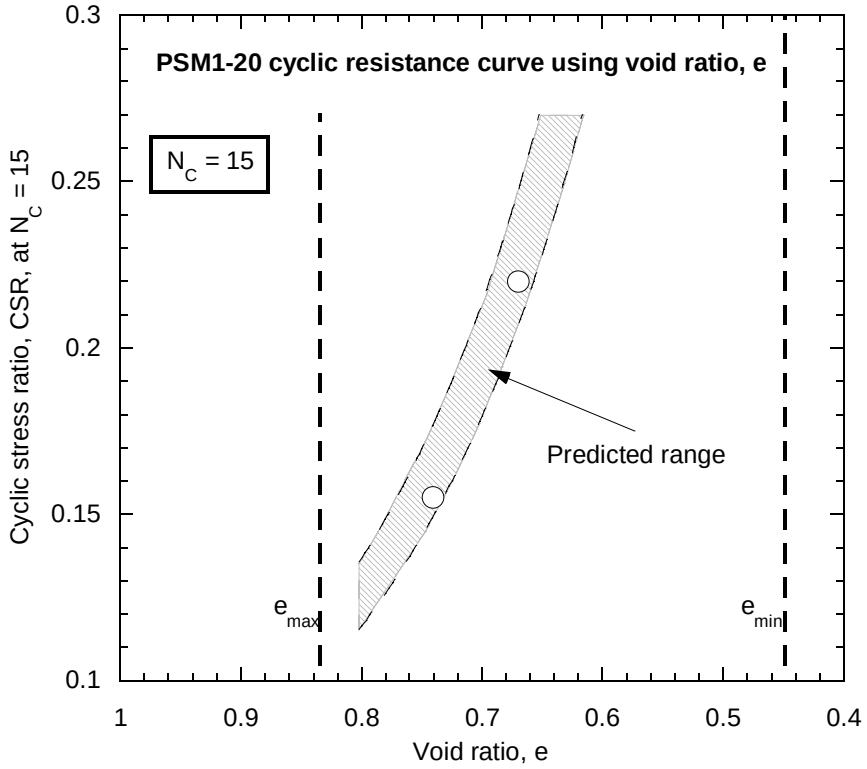

Figure 7-15 Comparison of the observed and predicted cyclic resistance of the PSM1-20 soil.

The PSM1-10 and PSM1-20 observed cyclic resistance data points obtained from cyclic testing sit within the predicted cyclic resistance ranges shown in Figure 7-14 and Figure 7-15. This suggests that the simplified method accurately estimated the cyclic response of the PSM1 soils with 10% - 20% fines when liquefaction is reached in 15 load cycles, using a fines influence factor range of $0.54 \leq b_{CR} \leq 0.64$.

The individual best fit b_{CR} values for PSM1-10 and PSM1-20 were also back-calculated using the observed test data to confirm the b_{CR} values of the sandy soils. A best fit $b_{CR} = 0.61$ was produced for the PSM1-10 soil, whilst a best fit $b_{CR} = 0.57$ was calculated for the PSM1-20 soil. Note that both of these back-calculated values are within the estimated b_{CR} range found using the simplified estimation method.

As such, the expected cyclic resistance curve ranges of the PSM1 soils could be used to predict the cyclic response of the PSM1 sand when $f_C < 30\%$ for non-plastic fines, but only when moist tamping is used to deposit the soil. Soil specimens with densities higher than the predicted ranges would reach liquefaction after $N_C > 15$ for a given cyclic stress ratio, showing a slower rate of pore water pressure buildup per loading cycle. Specimens with densities below the predicted ranges would conversely reach liquefaction in less than 15 load

cycles, whilst displaying more contractive response and a higher rate of increase in the pore water pressure.

So in summary, when interpreting the cyclic response of the PSM1 soils using the simplified estimation method:

- The PSM1-10 and PSM1-20 observed cyclic resistance data points from the cyclic tests sit within the cyclic resistance curve ranges predicted using the simplified estimation method
- The back-calculated b_{CR} values = 0.61 and 0.57 are within the b_{CR} range obtained using the simplified estimation method
- The predicted cyclic resistance curve ranges can therefore be used to predict the cyclic response of the PSM1 soils when f_C < 30% for non-plastic fines, and moist tamping is used to deposit the sandy soil

7.4.2. PSM2 cyclic resistance curves

The liquefaction resistance curves of the PSM2-0 sand are presented in Figure 7-16. These two curves were used to define the PSM2-0 cyclic resistance curve at N_C = 15, which is displayed in Figure 7-17. Note that a power curve was fitted to the PSM2-0 cyclic data points in Figure 7-17 to define the cyclic resistance curve. Equation (7-5) describes this power curve:

$$e = e^* = 0.584(CSR_{15})^{-0.223} \tag{7-5}$$

Equation (7-5) was used in conjunction with the b_{CR} range calculated in Section 7.2 and Equation (7-2) to predict the expected cyclic resistance curve ranges of the PSM2 sandy soils. As for the PSM1 soils, the predicted ranges were used to choose the specimen densities and cyclic stress ratios of the cyclically tested PSM2-10 and PSM2-25 soil specimens. Evidently the liquefaction resistance curves of these soils, presented in Figure 7-18 and Figure 7-19, are defined over a larger range of load cycles than for the PSM1 soils, as the observed cyclic response varied significantly from the predicted response, which was typically lower than the observed resistance. This led to larger values of N_C being reached during the first cyclic test at a particular soil density. The cyclic stress ratio was subsequently raised for the second cyclic test at that particular density, allowing liquefaction to be reached in N_C < 15, ensuring that the liquefaction resistance at N_C = 15 could be defined.

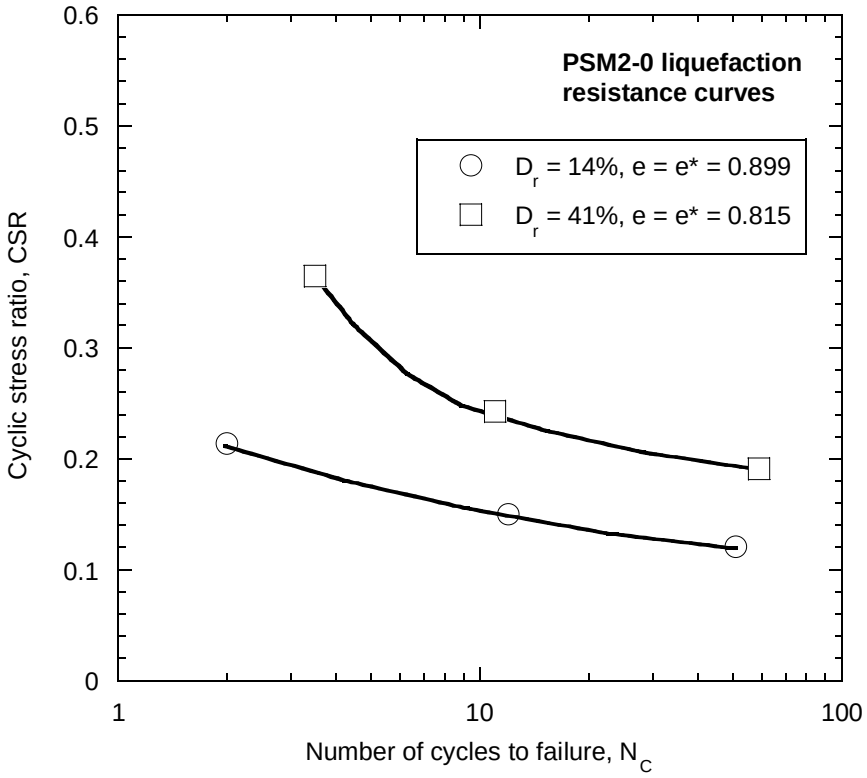

Figure 7-16 Observed liquefaction resistance curves of the PSM2-0 sand.

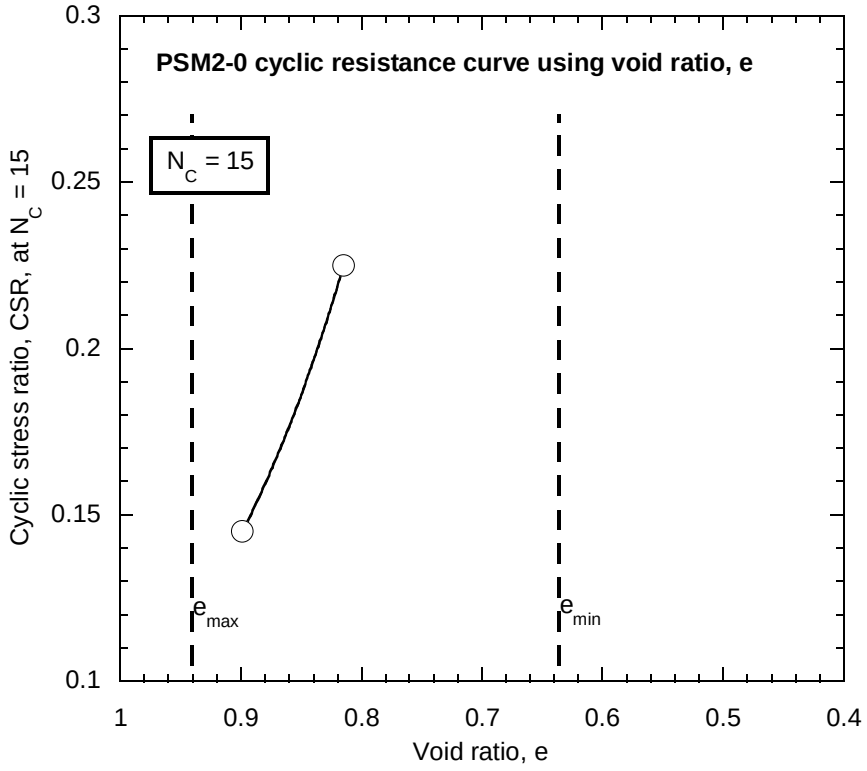

Figure 7-17 Observed cyclic resistance curve at N_C = 15 of the PSM2-0 sand using global void ratio, *e*.

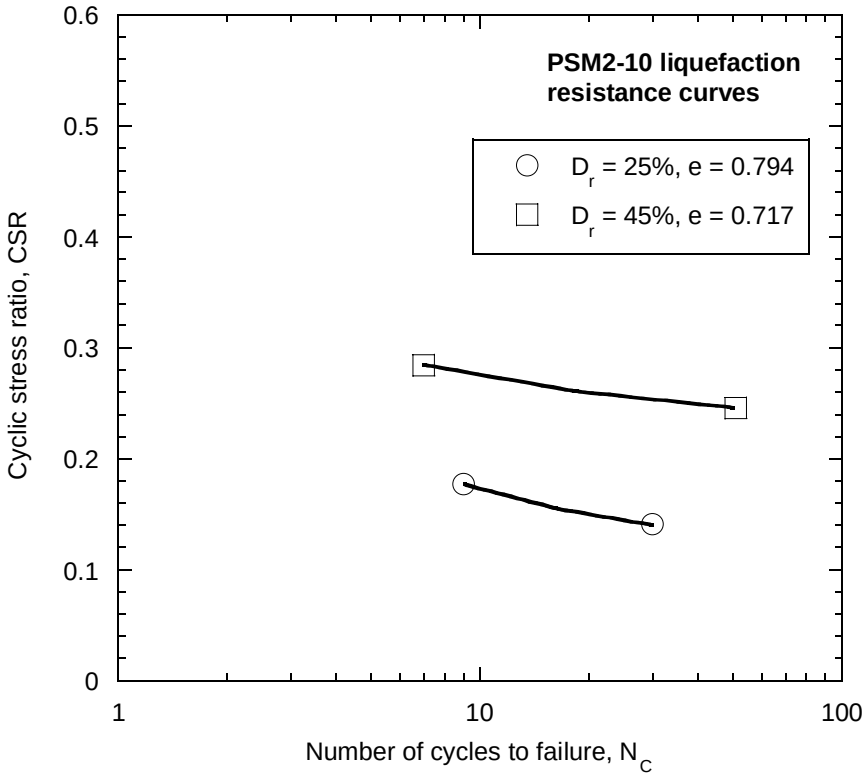

Figure 7-18 Observed liquefaction resistance curves of the PSM2-10 soil.

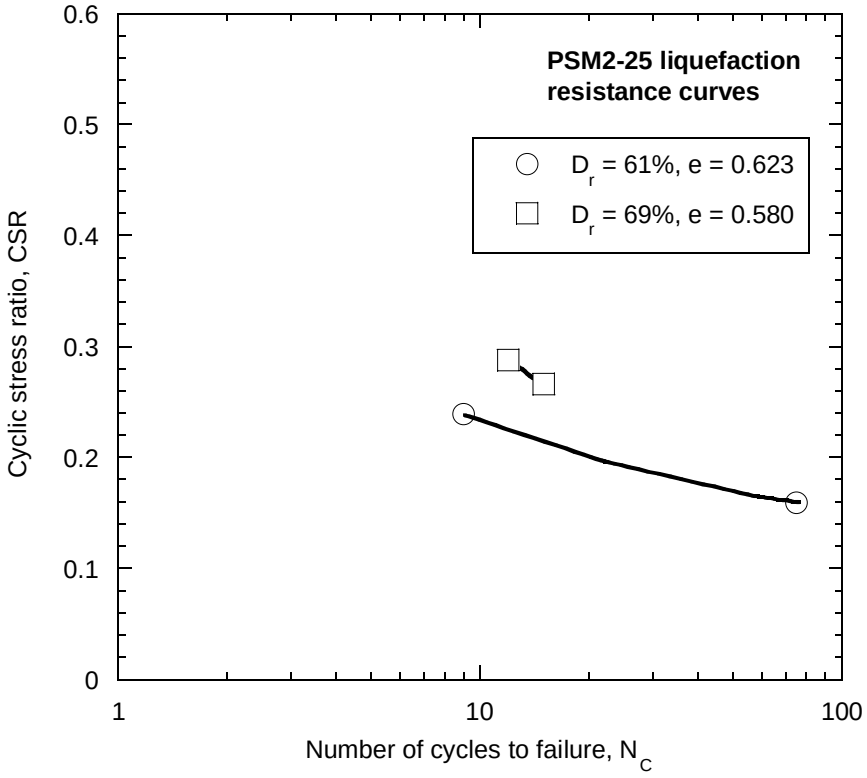

Figure 7-19 Observed liquefaction resistance curves of the PSM2-25 soil.

Figure 7-20 and Figure 7-21 present the predicted cyclic resistance curve ranges for the PSM2-10 and PSM2-25 sandy soils, along with the observed cyclic resistance data points obtained from cyclic testing. In both plots the observed data points are located outside of the predicted response ranges, at significantly lower soil densities. This suggests that the simplified estimation method underestimated the liquefaction resistance of the PSM2-10 and PSM2-25 soils, and that the estimated range of $0.24 \leq b_{CR} \leq 0.34$ is lower than the actual b_{CR} values of the PSM2 sandy soils.

Individual best fit b_{CR} values for PSM2-10 and PSM2-25 were subsequently back-calculated from the observed cyclic test data. A best fit $b_{CR} = 0.59$ was calculated for the PSM2-10 soil, and a best fit $b_{CR} = 0.55$ was calculated for the PSM2-25 soil. Note that these back-calculated b_{CR} values are much higher than those of the estimated b_{CR} range, being approximately double in value. This confirms that the actual effect of additional fines on the cyclic response of the PSM2 sand was larger than the one predicted using the simplified estimation method.

The fact that the predicted cyclic resistance ranges of the PSM2 soils underestimated the actual liquefaction resistance means the simplified method gave a conservative estimate of cyclic response. If the predicted resistance ranges were used again to predict the cyclic response of a PSM2 soil specimen, then liquefaction would be reached after a higher number of load cycles than predicted, due to a slower buildup in pore water pressure per load cycle. Note a conservative prediction of liquefaction resistance may not occur when considering the cyclic response of all sandy soils – it is specific to the mixture of PSM2 sand and fines.

Overall, when interpreting the cyclic response of the PSM2 soils using the simplified estimation method:

- The PSM2-10 and PSM2-25 observed cyclic resistance data points from the cyclic tests sit outside of the cyclic resistance curve ranges predicted using the simplified estimation method
- The back-calculated b_{CR} values = 0.59 and 0.55 were higher than the b_{CR} range obtained using the simplified estimation method, suggesting there was more effect from the fines on the cyclic response of the PSM2 sand than expected
- The predicted cyclic resistance curve ranges therefore underestimate the liquefaction resistance of the PSM2 soils when moist tamping is used to deposit the sandy soil, and $f_C < 30\%$ for non-plastic fines

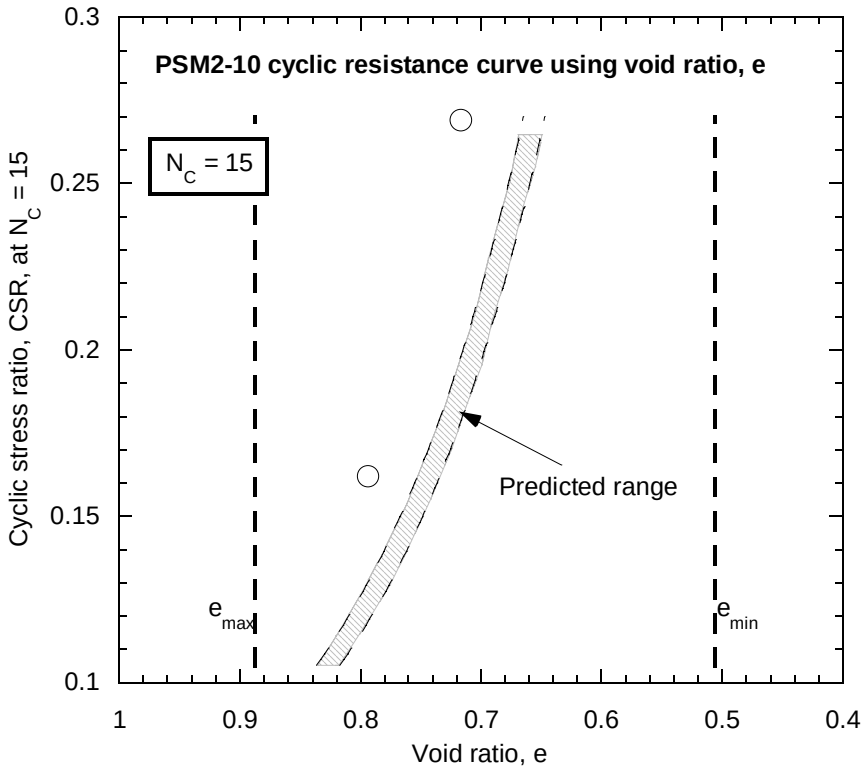

Figure 7-20 Comparison of the observed and predicted cyclic resistance of the PSM2-10 soil.

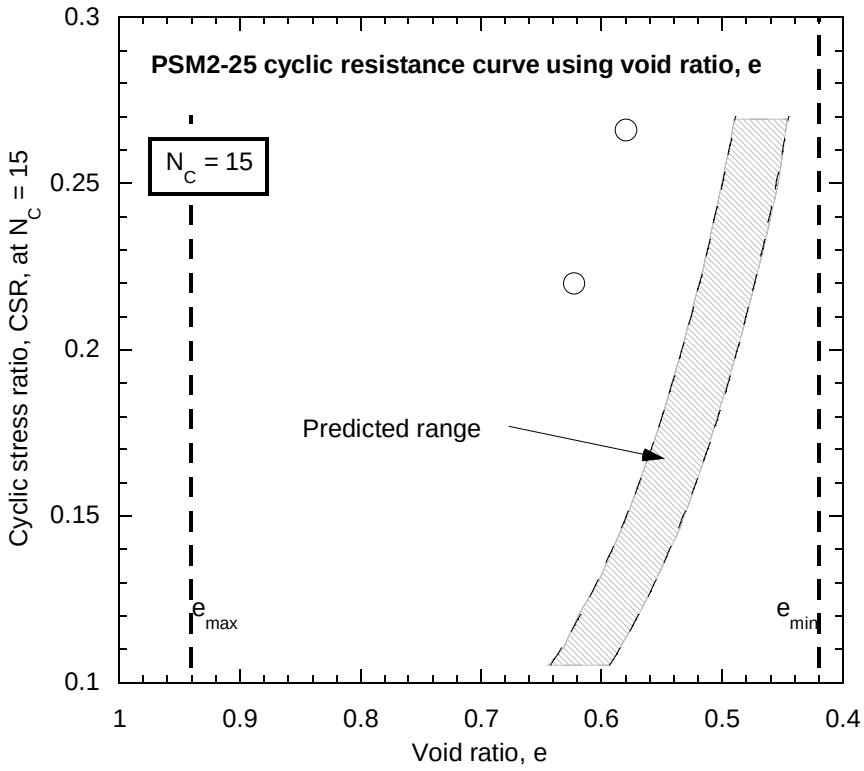

Figure 7-21 Comparison of the observed and predicted cyclic resistance of the PSM2-25 soil.

7.5. Critical Review of the Simplified Estimation Method

The simplified estimation method proposed in Chapter 6 was used in this chapter to predict the steady state lines and cyclic resistance curves of two sandy soils sourced from the Pinnacles site. It was also used to make a basic assessment of the liquefaction resistance of soil layers at that site to show potential practical application. This section critically reviews how the simplified estimation method performed within the context of the laboratory tests, highlighting the advantages, the limitations, and the areas of the method that require more research.

PSM1 soil tests – the simplified estimation method performed well when predicting the steady state lines and cyclic resistance curves of the PSM1 sandy soils. As discussed in Section 7.3.1, the observed steady state points of the PSM1-10 and PSM1-20 soils obtained from monotonic testing were located very close to, or within, the boundary of the predicted range. In terms of relative density, the predicted range for the f_C = 10% soil covered D_r = 17 - 24% at values of p' = 60 – 100kPa. Of the two tests performed, the specimen that reached a p'_{ss} = 64kPa had a D_r = 16% (e = 0.804), meaning the observed relative density was 1% below that predicted by the simplified estimation method for a p'_{ss} = 64kPa. The other test specimen reached a p'_{ss} = 92kPa with D_r = 18% (e = 0.796), which was within the predicted range. The predicted range for the f_C = 20% soil covered a ΔD_r = 10% for a given value of p'. For the two tests performed at this fines content, the maximum difference in relative density between the predicted range and observed result was less than 1%.

The observed cyclic resistances and predicted cyclic resistance curve ranges of the PSM1 soils were presented in Section 7.4.1. The performance of the simplified estimation method during these tests was quantitatively better than that for the monotonic tests, as all observed results were located within the predicted cyclic resistance ranges. Also note that, as for the monotonic tests, the predicted ranges covered a ΔD_r = 5% for the PSM1-10 soil and a ΔD_r = 10% for the PSM1-20 soil at a given value of CSR.

As such, it can be concluded that the simplified estimation method performed very well when predicting the steady state lines and cyclic resistances at N_C = 15 for the PSM1 soils as the fines content was raised up to f_C = 20%. This is because the observed test results varied from the predicted ranges by a maximum difference in relative density of 1%, which is considered to be relatively insignificant. It should however be recognized that the accuracy of the simplified method in this case may be helped by the similarities between the PSM1 and

FBM soils. Both mixtures of sand and fines had similar particle size distributions up to f_C = 20%, as well as similar particle angularities based on the SEM photos presented in Chapter 3. Such similarities in material properties are understandable as the soils were sourced from sites within 2km of each other in central Christchurch, which suggests similar geological processes are responsible for each deposit. As test data and material properties of the FBM soils were used in Chapter 6 to help define the simplified estimation method, it is not surprising that the undrained responses of a similar sandy soil, in terms of material properties and geographical source location, would be accurately predicted by the simplified method. Therefore to make a more informed conclusion as to the general performance of the simplified estimation method, it would be advantageous to perform further tests on sandy soils sourced from outside of the Christchurch region.

The results from the PSM1 soil tests do however demonstrate an advantage of using the simplified estimation method – the approximate locations of the steady state lines and cyclic resistance curves can be generated when f_C < 30% without performing numerous tests on the sand at different fines contents. Given that time required to prepare, saturate and consolidate a sand specimen increases with increasing fines content, the simplified estimation method can enable a major reduction in testing hours if only a reasonable approximation of the undrained response is needed.

PSM2 soil tests – the simplified estimation method did not perform as well when predicting the steady state lines and cyclic resistance curves of the PSM2 sandy soils, compared with the PSM1 soils. The observed steady state points of the PSM2-10 and PSM2-25 soils, presented in Section 7.3.2, were located outside of the predicted response ranges, at higher void ratio values. In relative density terms, the observed steady state points for the PSM2-10 soil were a maximum of 3% below the predicted range values, which occurred for the specimen that reached a p'_{ss} = 73kPa (D_r = 30%, e = 0.774). Note that the predicted range for this soil covered a ΔD_r = 5%. For the PSM2-25 soil, the observed steady state points were located at a maximum of 5% relative density below the predicted range, which occurred for the specimen that obtained a p'_{ss} = 87kPa (D_r = 68%, e = 0.587). The predicted range for the PSM2-25 soil covered a ΔD_r = 9%. Overall this still demonstrates reasonable performance of the simplified estimation method, as the observed steady state points were located outside of the predicted ranges by a difference in relative density less than that of the predicted range itself – for example, the PSM2-10 steady state points were a maximum of 3% out, yet the

predicted range covered a ΔD_r = 5%. It was therefore concluded that the method could be used to reasonably approximate the locations of the PSM2 steady state lines when f_C < 30%.

The observed cyclic resistances of the PSM2 soils however, as discussed in Section 7.4.2, were significantly different to those predicted by the simplified estimation method. For the PSM2-10 soil, the observed cyclic resistance points were located at relative densities a maximum of 11% below the predicted range. This difference increased when the PSM2-25 soil was considered, where the observed points were a maximum of 20% in relative density terms below the predicted range values. Such differences are clearly significant, and because of this it was concluded that the simplified estimation method did not approximate the actual cyclic response of the PSM2 soils as the fines content was increased up to 25%, indicating poor performance. It is also interesting that the performance of the method was poorer when considering cyclic resistance, as opposed to the response at the steady state of deformation.

It should be noted that the PSM2-25 soil was highly gap-graded with a large uniformity coefficient (C_u = 68.8) compared with the FBM-30 soil and PSM1-20 soil (both having C_u = 12.2 respectively). The large gap in the PSM2-25 gradation was caused by the fines-sized particles between 37 – 75μm being removed in order to create a sand-fines mixture different to that of the PSM1 soils in terms of particle size distribution. As such, the PSM2-25 soil in particular had significantly different grain distribution properties to all other sand-fines mixtures tested in this study. Whilst there is currently not enough data to make a definitive conclusion, the results may suggest that the undrained responses of highly non-uniform sandy soils are unable to be estimated accurately using the simplified estimation method. Further investigation into this issue is required to properly quantify any such effect on the simplified estimation method coming from highly non-uniform soils.

Figure 7-22 and Figure 7-23 present the locations of the observed b_{SSL} and Δb values for the PSM1 and PSM2 soils respectively relative to the correlations made with χ_e in Chapter 6.

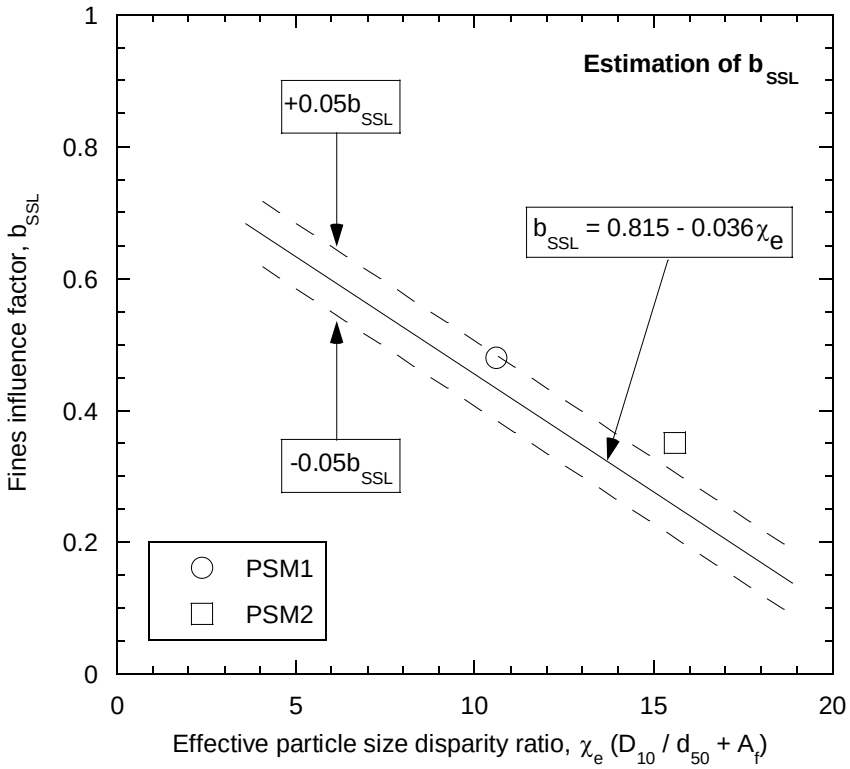

Figure 7-22 Location of the observed PSM1 and PSM2 b_{SSL} values relative to the simplified estimation method correlation with χ_e.

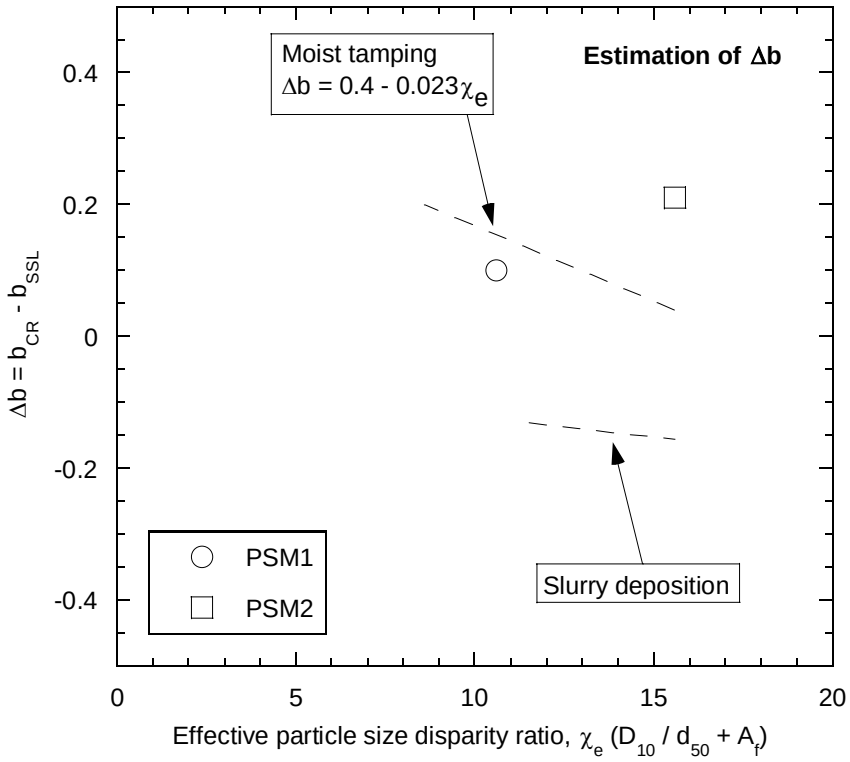

Figure 7-23 Location of the observed PSM1 and PSM2 Δb values relative to the simplified estimation method correlation with χ_e.

The results shown in Figure 7-22 and Figure 7-23 demonstrate (a) the accurate prediction of the effect of fines on the PSM1 sand by the simplified estimation method, and (b) the poor prediction of the effect of fines on the PSM2 sand. For the PSM1 soils, the slight underestimation of b_{SSL} combined with the slight overestimation of Δb led to the good fit between observed and predicted cyclic resistances shown in Section 7.4.1. The predictions made for the PSM2 soils however both underestimated the effects of fines, which led to a very poor fit between the observed and predicted cyclic resistances presented in Section 7.4.2. This highlights another important issue with the simplified estimation method – errors in the prediction of b_{SSL} carry through into the prediction of b_{CR}. It is therefore recommended that a higher priority be given to refining the correlation of soil material properties with b_{SSL}, as this is used as reference to determine the effect of fines on the cyclic response. However it is also necessary to further investigate the relationship between Δb and χ_e, as there was a minimal amount of available data that contained both steady state lines and cyclic resistance curves for given sand-fines mixtures – both of which are required to back-calculate Δb.

A number of other issues with the simplified estimation method were also identified during the review of the PSM1 and PSM2 test results. Firstly, no consideration is given to the angularity of the fines particles when quantifying their effect on the behaviour of sand. This was due to the difficulty in assessing the angularity of fines, which cannot be simply performed with a magnifying glass, and the lack of reported angularities in the literature. It is however thought that the effect of sand particle angularity has a greater bearing on the fines influence factor value, as sand is the dominant particle size when $f_C < f_{Cth}$.

Another limitation of the simplified method is the reliance on the choice of representative particle sizes for the sand and fines respectively. Although it appears that using a ratio of the sand D_{10} and the fines d_{50} gives a reasonable indication of the effects of fines on the sand response, other particle sizes within the soil gradation also dictate the undrained behaviour. This is best highlighted by the poor cyclic resistance prediction for the PSM2-25 soil, where a large gap in the particle size distribution curve (and high value of C_u) was clearly evident, and was not accounted for by the simplified estimation method.

7.6. Summary

This chapter firstly presented the results from a series of undrained monotonic and cyclic triaxial tests on the PSM1 and PSM2 sandy soils. The simplified estimation method, as outlined in Chapter 6, was used to estimate the fines influence factors for the sandy soils

based on material properties. These values of these estimated factors were b_{SSL} = 0.43, b_{CR} = 0.59 for the PSM1 soils, and b_{SSL} = 0.25, b_{CR} = 0.29 for the PSM2 soils. Initial undrained monotonic and cyclic tests were performed on the clean sand fractions of the PSM sands to define the benchmark response curves for the soil mixtures – steady state lines were defined from the monotonic response and cyclic resistance curves were defined from the cyclic response. These benchmark curves, in conjunction with the estimated fines influence factors, enabled the expected response ranges for the PSM1-10, PSM1-20, PSM2-10, and PSM2-25 soils to be defined before triaxial tests were carried out.

Comparisons between the predicted undrained response of the PSM soils and observed response differed between the two mixtures of sand and fines. The observed steady state and cyclic resistances of the PSM1 soils were accurately predicted by the simplified estimation method, with all data points sitting within, or very close to, the predicted response ranges. The observed responses of the PSM2 soils however were less accurately predicted, with all data points sitting outside of the predicted response ranges. This was due to a tendency for the simplified estimation method to underestimate the influence of additional fines on the response of the PSM2 clean sand. Practically this meant the test specimens displayed higher strengths than were predicted, which suggested the estimation method was conservative in this assessment.

Finally, a critical review of the simplified estimation method was made by discussing the performance during the PSM1 and PSM2 triaxial tests. It was concluded that the method performed well in predicting the steady state and cyclic resistance responses of the PSM1 soils, as the observed results only differed in terms of relative density by a maximum of 1%. It was however noted that the accurate prediction may have been helped by the similarities in particle size distributions between the FBM and PSM1 soils.

Conversely, it was concluded that the simplified estimation method did not perform well when predicting the responses of the PSM2 sandy soils. It was discussed that the observed cyclic resistance data points for the PSM2-25 soil had relative densities approximately 20% below those predicted by the simplified method for a given level of *CSR*. This may have been caused however by the highly non-uniform nature of the PSM2-25 soil compared with all other soils tested in this study, although this is difficult to confirm and quantify at this stage. It was also discussed that the simplified estimation method causes errors in b_{SSL} prediction to be continued through into the prediction of b_{CR}, whilst a lack of consideration for the angularity of fines particles was also highlighted.

8. Conclusions and Future Research

8.1. Conclusions

This study presented an investigation on the effects of fines on the undrained behaviour of sand under both monotonic and cyclic loadings. Such effects were assessed using undrained response data derived from laboratory triaxial testing performed as part of this study, and with triaxial test data sourced from the literature. A number of different measures of initial state were used to characterize the behaviour of these soils. The following sections summarize the main conclusions drawn, and significant contributions made, by this study.

8.1.1. Summary of the Experimental Study

The experimental study was carried out by performing monotonic and cyclic triaxial tests on three different mixtures of sand and fines. The host sand of each mixture had different amounts of fines systematically added to them, allowing the effect of fines on the undrained behaviour of the sand to be investigated. Note that other such studies have been carried out in previous experimental studies. The names of each sand-fines mixture and the various fines contents the host sands were tested in this study at are listed in the following:

- Fitzgerald Bridge Mixture (FBM)
  - FBM-1 (f_C = 1%)
  - FBM-10 (f_C = 10%)
  - FBM-20 (f_C = 20%)
  - FBM-30 (f_C = 30%)
- Pinnacles Sand Mixture 1 (PSM1)
  - PSM1-0 (f_C = 0%)
  - PSM1-10 (f_C = 10%)
  - PSM2-20 (f_C = 20%)
- Pinnacles Sand Mixture 2 (PSM2)
  - PSM2-0 (f_C = 0%)
  - PSM2-10 (f_C = 10%)
  - PSM2-25 (f_C = 25%)

The monotonic tests were performed on the sandy soils to identify what effect the addition of fines had on the stress-strain, stress-path, and excess pore water pressure responses of the host sand. They were also used to define the steady state lines of each of the soils, as the state concept was used as a reference for soil response when interpreting the behaviour using a range of initial state measures.

The cyclic tests were performed on the soils to observe the effect of additional fines on the undrained response of sand leading up to a double amplitude axial strain of 5%, which was considered to be cyclic liquefaction in this study. This enabled the liquefaction resistance curves ($CSR - N_C$) of the soils to be defined, as well as the cyclic resistance curves (CSR – state measure) at $N_C = 5$ and $N_C = 15$. It was the cyclic resistance curves that were used as a response reference when interpreting the effects of fines with different measures of initial soil state.

The data gained from the experimental tests was supported by data sourced from the literature. This support data was used to extrapolate the findings about the effect of fines gained from the FBM and PSM tests to soils with differing material properties.

8.1.2. Effects of Fines based on the FBM Test Results

The effects of fines on the undrained behaviour of FBM sand were interpreted using a range of different initial state measures. In particular, the effects observed on the undrained cyclic response when using the state parameter and state index as state measures were unique to this study. All effects are summarized in the following:

(1) When using void ratio, e, or relative density, D_r:

– The addition of fines to FBM sand resulted in more contractive behaviour both under monotonic and cyclic loadings.

– For monotonic loading, this resulted in the steady state lines being located at lower void ratios / higher relative densities, suggesting there were more initial $e - p'$ states that would cause fully contractive behaviour and the sandy soils to undergo flow liquefaction.

– For cyclic loading, the cyclic resistance curves showed a decrease in the liquefaction resistance of the soils with increasing fines content. This meant that, for a given cyclic stress ratio and void ratio / relative density, the number of load cycles required to cause cyclic liquefaction reduced with the addition of fines.

(2) When using the intergranular void ratio, e_g:

– The addition of fines to FBM sand resulted in less contractive behaviour both under monotonic and cyclic loadings.

– For monotonic loading, this resulted in the steady state lines being located at higher intergranular void ratio values, suggesting there were fewer initial $e_g - p'$ states that would cause fully contractive behaviour and the sandy soils to undergo flow liquefaction.

– For cyclic loading, the cyclic resistance curves showed an increase in the liquefaction resistance of the soils with increasing fines content. This meant that, for a given cyclic stress ratio and intergranular void ratio value, the number of load cycles required to cause cyclic liquefaction increased with the addition of fines.

Note that the interpretations made using these three parameters (e, D_r, e_g) showed similar trends when considering both monotonic and cyclic loadings. For example, if a decrease in the potential for fully contractive behaviour with the addition of fines was observed for monotonic loading, then an increase in liquefaction resistance was observed for cyclic loading. It was however determined that none of these measures were useful for quantifying the effects of fines, as none were able to normalize the undrained response of the soils to account for variations in the fines content.

(3) When using the state parameter, ψ, and state index, I_s:

– The addition of fines to FBM sand resulted in less contractive behaviour under cyclic loading.

– This meant the cyclic resistance curves showed an increase in the liquefaction resistance of the soils with increasing fines content. As such, for a given cyclic stress ratio and state parameter / state index value, the number of load cycles required to cause cyclic liquefaction increased with the addition of fines.

Note that only an interpretation of the cyclic response was made using ψ and I_s. This was because both measures include a reference to the steady state of deformation as parameters in their definitions, making comparisons of the steady state lines redundant. The interpretation did however clearly show that the effects of fines are dependent on the parameter chosen as a basis for the response comparison. This was because the effects of fines on the cyclic response of the FBM sand were reversed when ψ and I_s were used instead of e and D_r, pointing out the need to identify a measure that normalizes the effects of fines.

8.1.3. Effects of Fines using the Equivalent Granular Void Ratio

The equivalent granular void ratio, e^*, was identified from the literature as a measure of initial soil state that normalizes the effects of fines on the undrained behaviour of sand. It is based on the concept that only a certain fraction of the fines-sized particles mixed within sand participate in the internal soil force-chain during loading (Thevanayagam, Fiorillo et al. 2000). By knowing this fraction, e^* can interpret the undrained response of sandy soil independent of the fines content, for soils below the threshold fines content, f_{Cth}, which in this study was adopted to be 30%.

The fraction of participating fines is given by the parameter b, termed the fines influence factor in the equivalent granular void ratio definition. This definition is presented in Equation (8-1):

$$e^* = \frac{e + (1-b) f_C}{1 - (1-b) f_C} \tag{8-1}$$

Note that the value of the fines influence factor quantifies the effects of fines on the undrained behaviour of sand. A value of b = 1.0 represents participation of all fines in the internal soil force-chain during loading, whilst a value of b = 0 represents no fines participation. In the literature the value of the fines influence factor has been assumed to be both constant with variation in fines content, and a function of the fines content itself.

The undrained responses of the FBM soils were normalized using the equivalent granular void ratio. This required back-calculation of the fines influence factor, which was determined to have different values when interpreting the steady state lines (b_{SSL}) and the cyclic resistance curves (b_{CR}). This difference was suggested to be due to the different effects of fines on soil dilatancy at the different levels of strain corresponding to cyclic liquefaction (ε_a < 5%) and the steady state of deformation (ε_a > 20%), and had yet to be identified in previous literature. Using a constant value for each fines influence factor was also confirmed to be a reasonable approximation for a given mixture of sand and fines. As such, the values of the fines influence factors for the FBM sand-fines mixtures were:

- b_{SSL} = 0.49 for the FBM steady state lines
- b_{CR} = 0.65 for the FBM cyclic resistance curves

The laboratory test data reported in the literature was also interpreted using the equivalent granular void ratio as a measure of initial soil state. This was one significant contribution made by this study, as the interpretation and quantification of a large data set including both monotonic and cyclic responses using the equivalent granular void ratio had yet to be achieved. The interpretations required back-calculation of all fines influence factor values, which ranged from b_{SSL} = 0.12 – 0.69 for the steady state line data and b_{CR} = 0.11 – 0.81 for the cyclic resistance curve data. This quantitatively highlighted the variability in the effect of fines on the undrained sand response.

When back-calculating the fines influence factor values for each of the sand-fines mixtures, the response of the clean sand was used a benchmark for all soil response as the fines content was increased. As the normalizations were not exact, the error between the e^* value of the clean sand and the e^* value of the sand with fines at a given level of response (p'_{ss} or *CSR* at N_C = 15) was investigated. It was found that, when using the back-calculated values of b, these differences were no more than ± 0.05 e^*. Based on these interpretations, the equivalent granular void ratio was considered conceptually to be a good parameter for characterizing and quantifying the effects of fines on the undrained behaviour of sand, assuming the fines influence factor value could be derived.

8.1.4. Correlation of *b* with Material Properties

An investigation was made into how the values of the fines influence factors, b_{SSL} and b_{CR}, vary with changing material and depositional properties of sand-fines mixtures, using the FBM test data and supporting data from the literature. This is considered to be the major contribution of this thesis, as no previous correlations had been made in the literature considering the relationships between the fines influence factor, sand particle angularity, and initial soil fabric. The correlations were made to allow prediction of the value of e^* without the need to back-calculate b from test data. The three specific properties correlated with b_{SSL} and b_{CR} were:

- Particle sizes of the sand and fines
- Angularity of the sand particles
- Depositional method / soil fabric of the test specimens

(1) Correlation of b_{SSL} with sand particle size, D_{10}, and fines particle size, d_{50},:

– The ratio of D_{10} of sand with d_{50} of fines was defined as the particle size disparity ratio, χ. This parameter was chosen to correlate with b_{SSL} based on binary particle packing theory from the literature, which suggested a lower influence of fines on the sand as the relative size of the fines became smaller.

– A general trend of decreasing b_{SSL} values with increasing χ values was observed for the range of sandy soils presented in this study. There was however a large amount of scatter between the $b_{SSL} - \chi$ data points.

(2) Correlation of b_{SSL} with sand particle angularity:

– The scatter observed when correlating b_{SSL} with χ led to the realization that the angularity of the sand particles had a significant effect on the value of b_{SSL}. It was concluded that an increase in sand particle angularity corresponded to a decrease in the value of b_{SSL}.

– To account for the effects of angularity, a new parameter was defined: the effective particle size disparity ratio, χ_e. This was proposed to be equal to the particle size disparity ratio, χ, plus an angularity effect factor, A_f. A linear correlation between b_{SSL} and χ for rounded sand particles was used as a reference, leading to rounded sand particles having an $A_f = 0$ and very angular sand particles having an $A_f \approx 11$.

– The angularity effect factor values of sand were related with the particle regularity values, ρ, through a correlation of ρ with the maximum void ratio, e_{max}. It was found that as e_{max} increased, the sand particle regularity ρ decreased, and hence the value of the angularity effect factor A_f increased. It was also suggested that $A_f = 0$ when $\rho > 0.76$, and that $A_f = 11$ when $\rho < 0.60$.

(3) Dependency of b_{CR} with deposition method / soil fabric:

– It was determined that the value of b_{CR} was dependent on the method of soil deposition, due to the sensitivity of cyclic resistance to the initial soil fabric. Given that the steady state of deformation is independent of initial soil fabric, it was proposed that the value of b_{SSL} be used as a reference for determining the value of b_{CR}. As such, the parameter Δb was defined as the difference between b_{CR} and b_{SSL}.

– Δb was correlated with the effective particle size disparity ratio, χ_e, showing that for moist-tamped soils the value of Δb was positive, indicating that $b_{CR} > b_{SSL}$ for a given mixture of sand and fines. For slurry deposition, it was concluded from a limited amount of data that Δb appears to be negative, indicating $b_{CR} < b_{SSL}$.

It was also noted that the definition of the fines influence factor based on the theory of binary particle packing should be considered only as one rough approximation for actual sandy soils. As such, the definition of the fines influence factor was redefined for use in this study as "*a factor that accounts for all the combined effects of different parameters on the undrained response of sand due to the addition of fines below the threshold fines content*".

8.1.5. Review of the Proposed Simplified Estimation Method

A simplified estimation method was proposed to allow the prediction of the steady state lines and cyclic resistances curves of sandy soils as the fines content was increased up to 30%, and is considered to be the other main contribution made by this study. The proposed method uses the correlations of the fines influence factor with material and depositional properties, the equivalent granular void ratio concept, and the known undrained response of the clean sand to perform the response predictions.

The PSM1 and PSM2 soils were tested to allow a critical review the proposed method. The following conclusions were drawn from the triaxial tests:

(1) Advantage of the simplified estimation method:

– The locations of the steady state lines and cyclic resistance curves can be accurately predicted for fines contents up to 30% without the need for numerous tests to be performed. This was based on the accurate prediction of the PSM1-10 and PSM1-20 responses, which varied by a maximum of 1% relative density from the predicted response ranges.

– It incorporates effects on the value of the fines influence factor coming from differences in sand particle angularity and initial soil fabric.

(2) Issues with the simplified estimation method:

– The predicted cyclic resistance responses for the PSM2-10 and PSM2-25 soils varied significantly from the actual test responses, with a maximum difference in relative density of 20% being observed. It was concluded from these results that the simplified estimation method may not be applicable to highly gap-graded soils.

– The PSM2 test results highlighted the fact that an error in the prediction of b_{SSL} carries through into the prediction of b_{CR}.

– The angularity of the fines particles is not considered in the estimation of the fines influence factor, even though the angularity will have an effect on the influence of fines.

– The simplified estimation method does not consider the whole gradation of a soil when making a prediction of the fines influence factor, but rather relies only on D_{10} of sand and d_{50} of fines to represent the particle size distributions. This can lead to poor performance of the method in predicting response, as shown by the PSM2 test results.

(3) Further investigation required for the simplified estimation method:

– The good prediction of the PSM1-10 and PSM1-20 soil responses may have been helped by the similarities between the PSM1 soils and the FBM soils, in terms of particle size distributions and the geographical proximity of site locations. It would therefore be advantageous to perform response predictions and tests for other sand-fines mixtures sourced from outside the Christchurch region.

– Further testing is required to determine the relationship of Δb with χ_e for a range of soil depositional methods. Thus far only data is available for specimens prepared by moist-tamping and slurry deposition.

– The relationship between particle angularity and the angularity effect factor, A_f, can be significantly refined through better quantification of particle angularity. This could be carried out using numerical shape analyses of scanning electron microscope images of sand-fines particles.

8.2. Recommendations for Future Research

Whilst this study has made a number of contributions to the knowledge about the effects of fines on the undrained behaviour of sand through the testing of soils sourced from Christchurch, there exists much more research to be performed on both of these topics. Some suggestions for future studies are presented in the following:

- Conduct tests on a range of sands mixed with plastic fines to determine how plasticity affects the value of the fines influence factor. This would enable the effects of plastic fines on the undrained behaviour of sand to be quantified.

- Continue verification / improvement of the simplified estimation method by (a) testing soil samples from a range of different sites; (b) determining the effect of different depositional methods / soil fabrics on the value of b_{CR}; (c) improving the quantification of the soil particle angularities using numerical shape analyses.

- Perform a liquefaction assessment at a site using the simplified procedure of Seed and Idriss, the simplified estimation method presented in this study, and the results from tests performed on undisturbed specimens. This would allow comparison between the two methods based on the actual cyclic resistance ratios of the in-situ soil.

- Investigate the use of discrete element modeling to better understand the undrained response of sand and fines. This would allow a high degree of control over the soils being modeled, which could enable parameters such as particle size, angularity, and fabric to be systematically varied. In doing this, the effect of such parameters on the undrained response may be able to be better understood and quantified.

References

ABERG, B. (1992) Void ratio of noncohesive soils and similar materials. *Journal of geotechnical engineering,* 118**,** 1315 - 1334.

AMINI, F. & QI, G. Z. (2000) Liquefaction Testing of Stratified Silty Sands. *Journal of Geotechnical and Geoenvironmental Engineering,* 126**,** 208 - 217.

ANDERSON, C. & MCMORRAN, T. (2003) An application of liquefaction hazard evaluation in urban planning. *2003 Pacific Conference on Earthquake Engineering.* Christchurch, New Zealand, New Zealand Society for Earthquake Engineering.

BAZIAR, M. H. (2009) Query about the plasticity of Ardebil fines. IN REES, S.

BAZIAR, M. H. & DOBRY, R. (1995) Residual strength and large-deformation potential of loose silty sands. *Journal of Geotechnical Engineering - ASCE,* 121**,** 896 - 906.

BECA CARTER HOLLINGS & FERNER LTD (2004) Christchurch Liquefaction Study - Stage IV. Christchurch, Beca Carter Hollings & Ferner Ltd.

BERRILL, J. B., MULQUEEN, P. C., OII, E. & PAUTRE, J.-L. (1994) Liquefaction at Kaiapoi in the 1901 Cheviot, New Zealand Earthquake. Christchurch, University of Canterbury.

BOULANGER, R. W. & IDRISS, I. M. (2006) Liquefaction susceptibility criteria for silts and clays. *Journal of Geotechnical and Geoenvironmental Engineering,* 132**,** 1413 - 1426.

BOULANGER, R. W., MEJIA, L. H. & IDRISS, I. M. (1997) Liquefaction at moss landing during loma prieta earthquake. *Journal of Geotechnical and Geoenvironmental Engineering,* 123**,** 453 - 467.

BRAY, J. D. & SANCIO, R. B. (2006) Assessment of the Liquefaction Susceptibility of Fine-grained Soils. *Journal of Geotechnical and Geoenvironmental Engineering,* 132**,** 1165 - 1177.

BROWN, L. J. & WEEBER, J. H. (1992) *Geology of the Christchurch Urban Area,* Lower Hutt, Institute of Geological and Nuclear Sciences Ltd.

BSI (2002) BS 1377-4:1990 Methods of tests for soils for civil engineering purposes. *Part 4: Compaction-related tests.* .

CARRARO, J. A. H., BANDINI, P. & SALGADO, R. (2003) Liquefaction Resistance of Clean and Nonplastic Silty Sands based on Cone Penetration Resistance. *Journal of Geotechnical and Geoenvironmental Engineering,* 129**,** 965 - 976.

CASAGRANDE, A. (1976) Liquefaction and Cyclic Deformation of Sands, A Critical Review. *Harvard Soil Mechanics Series,* 88.

CASTRO, G. & POULOS, S. J. (1977) Factors Affecting Liquefaction and Cyclic Mobility. *ASCE J Geotech Eng Div,* 103**,** 501 - 516.

CHANG, N. Y., YEH, S. T. & KAUFMAN, L. P. (1982) Liquefaction Potential of Clean and Silty Sands. *3rd International Earthquake Microzonation Conference.*

CHEN, Y.-C. & LIAO, T.-S. (1999) Dynamic Properties and State Parameter of Sand. *International Offshore and Polar Engineering Conference 1.*

CHIEN, L. K., OH, Y. N. & CHANG, C. H. (2002) Effects of Fines Content on Liquefaction Strength and Dynamic Settlement of Reclaimed Soil. *Canadian Geotechnical Journal,* 39**,** 254 - 265.

CHO, G. C., DODDS, J. & SANTAMARINA, J. C. (2006) Particle shape effects on packing density, stiffness, and strength: Natural and crushed sands. *Journal of Geotechnical and Geoenvironmental Engineering,* 132**,** 591 - 602.

CHRISTENSEN, S. A. (2001) Regional Liquefaction Study for Waimakariri District. *NZSEE 2001 Conference.* Taupo, New Zealand, New Zealand Society for Earthquake Engineering.

CUBRINOVSKI, M. & ISHIHARA, K. (1998) Modelling of sand behaviour based on state concept. *Soils and Foundations,* 38**,** 115 - 127.

CUBRINOVSKI, M. & ISHIHARA, K. (2000) Flow potential of sandy soils with different grain compositions. *Soils and Foundations,* 40**,** 103 - 119.

CUBRINOVSKI, M. & ISHIHARA, K. (2002) Maximum and Minimum Void Ratio Characteristics of Sands. *Soils and Foundations,* 42**,** 65 - 78.

CUBRINOVSKI, M. & REES, S. (2008) Effects of Fines on Undrained Behaviour of Sands. *Geotechnical Earthquake Engineering and Soil Dynamics IV.* Sacremento.

DEZFULIAN, H. (1984) Effects of Silt Content on Dynamic Properties of Sandy Soils. *8th World Conference on Earthquake Engineering.*

ERTEN, D. & MAHER, M. H. (1995a) Cyclic Undrained Behaviour of Silty Sand. *Soil Dynamics and Earthquake Engineering,* 14**,** 115 - 123.

ERTEN, D. & MAHER, M. H. (1995b) Liquefaction Potential of Silty Soils. *Soil Dynamics and Earthquake Engineering VII.*

FINN, W. D. L., LEDBETTER, R. H. & WU, G. (1994) Liquefaction in silty soils: design and analysis. *Geotechnical Special Publication***,** 51 - 76.

GDS INSTRUMENTS LTD (2000) *GDS Advanced Digital Controller,* GDS Instruments Ltd.

GDS INSTRUMENTS LTD (2002a) *GDS 8 Channel Serial Data Acquisition Pad,* GDS Instruments Ltd.

GDS INSTRUMENTS LTD (2002b) *GDS Motorised Triaxial Cell Handbook,* GDS Instruments Ltd.

GDS INSTRUMENTS LTD (2005) *GDS Laboratory Users Handbook,* GDS Instruments Ltd.

GEOKON, INC. (2002) *Instruction Manual Model 2100 The Nold DeAerator,* Geokon, Inc.

GUILHEM, O. & BERRILL, J. (1993) Cone Penetrometer Results and Estimates of Liquefaction Potential at some Key Christchurch Lifeline Sites. Christchurch, University of Canterbury.

HUANG, Y. T., HUANG, A. B., KUO, Y. C. & TSAI, M. D. (2004) A Laboratory Study on the Undrained Strength of a Silty Sand from Central Western Taiwan. *Soil Dynamics and Earthquake Engineering,* 24**,** 733 - 743.

HYODO, M., ISHIKAWA, S. & ORENSE, R. P. (2008) Undrained Cyclic Shear Characteristics of Silt and Sand Mixtures *18th NZGS Geotechnical Symposium on Soil-Structure Interaction.* Auckland.

HYODO, M., ORENSE, R. P., ISHIKAWA, S., YAMADA, S., KIM, U. G. & KIM, J. (2006) Effects of Fines Content on Cyclic Shear Characteristics of Sand-clay Mixtures. *New Zealand Workshop on Geotechnical Earthquake Engineering 2006.* Christchurch.

ISHIHARA, K. (1993) Liquefaction and Flow Failure during Earthquakes. *Geotechnique,* 43**,** 351 - 415.

ISHIHARA, K. & KOSEKI, J. (1989) Discussion on the cyclic shear strength of fines-containing sands. *Eleventh International Conference on Soil Mechanics and Foundation Engineering.* Rio de Janiero, Brazil.

ISHIHARA, K., SODEKAWA, M. & TANAKA, Y. (1978) Effects of Overconsolidation on Liquefaction Characteristics of Sands Containing Fines. *Dynamic Geotechnical Testing***,** 246 - 264.

ISHIKAWA, S., HYODO, M., SADAHIRO, Y., ORENSE, R. P., NAKATA, Y. & YOSHIMOTO, N. (2007) Cyclic Shear Characteristics of Plastic and Non-plastic Fines and Sand Mixtures. *42nd National Conference on Geotechnical Engineering.* Nagoya.

KENNY, T. C. (1977) Residual strength of mineral mixtures. *ICSMFE 9.* Tokyo.

KRUMBEIN, W. C. & SLOSS, L. L. (1963) *Stratigraphy and Sedimentation,* San Francisco, W. H. Freeman and Company.

KUERBIS, R., NEGUSSEY, D. & VAID, Y. P. (1988) Effect of gradation and fines content on the undrained response of sand. *Geotechnical Special Publication.* 21 ed. Fort Collins, CO, USA, Publ by ASCE.

LADD, R. S. (1978) Preparing Test Specimens Using Undercompaction. *Geotechnical Testing Journal,* 1**,** 16 - 23.

LADE, P. V., LIGGIO JR, C. D. & YAMAMURO, J. A. (1998) Effects of Non-Plastic Fines on Minimum and Maximum Void Ratios of Sand. *Geotechnical Testing Journal,* 21**,** 336 - 347.

LADE, P. V. & YAMAMURO, J. A. (1997) Effects of Nonplastic Fines on Static Liquefaction of Sands. *Canadian Geotechnical Journal,* 34**,** 918 - 928.

LAW, K. T. & LING, Y. H. (1992) Liquefaction of Granular Soils with Non-Cohesive and Cohesive Fines. *10th World Conference on Earthquake Engineering.* Balkema, Rotterdam.

LEE, K. M., SHEN, C. K., LEUNG, D. H. K., MITCHELL, J. K. & MEMBER, H. (1999) Effects of Placement Method on Geotechnical Behavior of Hydraulic Fill Sands. *Journal of Geotechnical and Geoenvironmental Engineering,* 125**,** 832 - 846.

LEES, G. (1964) A New Method for Determining the Angularity of Particles. *Sedimentology,* 3**,** 2 - 21.

MITCHELL, J. K. (1976) *Fundamentals of Soil Behavior,* New York, John Wiley & Sons.

MITCHELL, J. K. (1993) *Fundamentals of Soil Behavior,* New York, John Wiley & Sons.

MIURA, K., MAEDA, K., FURUKAWA, M. & TOKI, S. (1997) Physical Characteristics of Sands with Different Primary Properties. *Soils and Foundations,* 37**,** 53 - 64.

MULILIS, J. P., SEED, H. B., CHAN, C. K., MITCHELL, J. K. & ARULANANDAN, K. (1977) Effects of Sample Preparation on Sand Liquefaction. *ASCE J Geotech Eng Div,* 103**,** 91 - 108.

MURTHY, T. G., LOUKIDIS, D., CARRARO, J. A. H., PREZZI, M. & SALGADO, R. (2007) Undrained Monotonic Response of Clean and Silty Sands. *Geotechnique,* 57**,** 273 - 288.

NAEINI, S. A. & BAZIAR, M. H. (2004) Effect of Fines Content on Steady-state Strength of Mixed and Layered Samples of a Sand. *Soil Dynamics and Earthquake Engineering,* 24**,** 181 - 187.

NI, Q., DASARI, G. R. & TAN, T. S. (2006) Equivalent Granular Void Ratio for Characterization of Singapore's Old Alluvium. *Canadian Geotechnical Journal,* 43**,** 563 - 573.

NI, Q., TAN, T. S., DASARI, G. R. & HIGHT, D. W. (2004) Contribution of Fines to the Compressive Strength of Mixed Soils. *Geotechnique,* 54**,** 561 - 569.

PAPADOPOULOU, A. & TIKA, T. (2008) The Effect of Fines on Critical State and Liquefaction Resistance Characteristics of Non-plastic Silty Sands. *Soils and Foundations,* 48**,** 713 - 725.

PITMAN, T. D., ROBERTSON, P. K. & SEGO, D. C. (1994) Influence of Fines on the Collapse of Loose Sands. *Canadian Geotechnical Journal,* 31**,** 728 - 739.

POLITO, C. P. (1999) The Effects of Non-Plastic and Plastic Fines on the Liquefaction of Sandy Soils. *Faculty of the Virginia Polytechnic Institute and State University.* Virginia Polytechnic Institute and State University.

POLITO, C. P. & MARTIN II, J. R. (2001) Effects of Nonplastic Fines on the Liquefaction Resistance of Sands. *Journal of Geotechnical and Geoenvironmental Engineering,* 127**,** 408 - 415.

POLITO, C. P. & MARTIN II, J. R. (2003) A Reconciliation of the Effects of Non-Plastic Fines on the Liquefaction Resistance of Sands Reported in the Literature. *Earthquake Spectra,* 19**,** 635 - 651.

RAHMAN, M. M. & LO, S.-C. R. (2007) Equivalent Granular Void Ratio and State Parameters for Loose Clean Sand with Small Amount of Fines. *10th Australia New Zealand Conference on Geomechanics.* Brisbane.

RAHMAN, M. M., LO, S. R. & GNANENDRAN, C. T. (2008) On Equivalent Granular Void Ratio and Steady State Behaviour of Loose Sand with Fines. *Canadian Geotechnical Journal,* 45**,** 1439 - 1456.

ROPER, M. (2006) Applications and Procedures of Triaxial Tests. Christchurch, University of Canterbury.

SEED, H. B. (1979) Soil Liquefaction and Cyclic Mobility Evaluation for Level Ground during Earthquakes. *ASCE J Geotech Eng Div,* 105**,** 201 - 255.

SEED, H. B. & IDRISS, I. M. (1971) Simplified procedure for evaluating soil liquefaction potential. *ASCE J Geotech Eng Div,* 97**,** 1249 - 1273.

SEED, H. B., IDRISS, I. M. & ARANGO, I. (1983) Evaluation of liquefaction potential using field performance data. *Journal of Geotechnical Engineering - ASCE,* 109**,** 458 - 482.

SHEN, C. K., VRYMOED, J. L. & UYENO, C. K. (1977) The Effect of Fines on Liquefaction of Sands. *9th International Conference on Soil Mechanics and Foundation Engineering.*

SINGH, S. (1995) Re-examination of the Effects of Fine Contents on the Liquefaction Characteristics of Sands. *Earthquake Geotechnical Engineering (Ishihara Edition)***,** 829 - 831.

SLADEN, J. A. & HANDFORD, G. (1987) A Potential Systematic Error in Laboratory Testing of Very Loose Sands. *Canadian Geotechnical Journal,* 24**,** 462 - 466.

STANDARDS ASSOCIATION OF NEW ZEALAND (1986) NZS 4402: 1986 Methods of Testing Soils for Civil Engineering Purposes Wellington, New Zealand, Standards Association of New Zealand.

STARK, T. D. & OLSON, S. M. (1995) Liquefaction resistance using CPT and field case histories. *Journal of Geotechnical Engineering - ASCE,* 121**,** 856 - 869.

STIRLING, M., GERSTENBERGER, M., LITCHFIELD, N., MCVERRY, G., SMITH, W., PETTINGA, J. & BARNES, P. (2008) Seismic hazard of the Canterbury Region, New Zealand: New earthquake source model and methodology. *Bulletin of the New Zealand Society for Earthquake Engineering,* 41**,** 51 - 67.

STIRLING, M., PETTINGA, J., BERRYMAN, K. & YETTON, M. (2001) Probabilistic Seismic Hazard Assessment of the Canterbury Region, New Zealand. *Bulletin of the New Zealand Society for Earthquake Engineering,* 34**,** 318 - 334.

TATSUOKA, F. & HAIBARA, O. (1985) Shear Resistance Between Sand and Smooth or Lubricated Surfaces. *Soils and Foundations,* 25**,** 89 - 98.

THEVANAYAGAM, S. (1998) Effects of Fines and Confining Stress on Undrained Shear Strength of Silty Sands. *Journal of Geotechnical and Geoenvironmental Engineering,* 124**,** 479 - 491.

THEVANAYAGAM, S. (1999) Role of Intergrain Contacts, Friction, and Interactions on Undrained Response of Granular Mixes. *International workshop on Physics and Mechanics of Soil Liquefaction, September 1998.* Baltimore.

THEVANAYAGAM, S. (2007) Intergrain Contact Density Indices for Granular Mixes-I: Framework. *Earthquake Engineering and Engineering Vibration,* 6**,** 123 - 134.

THEVANAYAGAM, S., FIORILLO, M. & LIANG, J. (2000) Effect of Non-plastic Fines on Undrained Cyclic Strength of Silty Sands. *Geo-Denver 2000 - Soil Dynamics and Liquefaction 2000.* Denver.

THEVANAYAGAM, S. & MARTIN, G. R. (2002) Liquefaction in Silty Soils - Screening and Remediation Issues. *Soil Dynamics and Earthquake Engineering,* 22**,** 1035 - 1042.

THEVANAYAGAM, S. & MOHAN, S. (2000) Intergranular State Variables and Stress-strain Behaviour of Silty Sands. *Geotechnique,* 50**,** 1 - 23.

THEVANAYAGAM, S., SHENTHAN, T. & KANAGALINGAM, T. (2003) Role of Intergranular contacts on Mechanisms causing Liquefaction and Slope Failures in Silty Sands. Buffalo, University of Buffalo.

THEVANAYAGAM, S., SHENTHAN, T., MOHAN, S. & LIANG, J. (2002) Undrained Fragility of Clean Sands, Silty Sands, and Sandy Silts. *Journal of Geotechnical and Geoenvironmental Engineering,* 128**,** 849 - 859.

TOKIMATSU, K. & YOSHIMI, Y. (1983) Empirical Correlation of Soil Liquefaction based on SPT N-value and Fines Content. *Soils and Foundations,* 23**,** 56 - 74.

TRONCOSO, J. H. & VERDUGO, R. (1985) Silt Content and Dynamic Behaviour of Tailing Sands. *12th International Conference on Soil Mechanics and Foundation Engineering.*

TSUKAMOTO, Y., ISHIHARA, K. & NONAKA, T. (1998) Undrained Deformation and Strength Characteristics of Soils from Reclaimed Deposits in Kobe. *Special Issue of Soils and Foundations***,** 47 - 55.

U.S. GEOLOGICAL SURVEY (2009) Historic earthquakes: Niigata, Japan. U.S. Geological Survey.

URS NEW ZEALAND LTD (2006) Geotechnical and Hazard Issues related to a review of Residential Density in New Brighton. Christchurch.

VAID, Y. P. (1994) Liquefaction of Silty Soils. *Geotechnical Special Publication***,** 1 - 16.

VAID, Y. P. & SIVATHAYALAN, S. (2000) Fundamental factors affecting liquefaction susceptibility of sands. *Canadian Geotechnical Journal,* 37**,** 592 - 606.

VERDUGO, R. (1992) Characterization of Sandy Soil Behaviour Under Large Deformation. *Department of Civil Engineering.* Tokyo, University of Tokyo.

VERDUGO, R. & ISHIHARA, K. (1996) The Steady State of Sandy Soils. *Soils and Foundations,* 36**,** 81 - 91.

WADELL, H. (1932) Volume, shape and roundness of rock particles. *Journal of Geology,* 40**,** 443 - 451.

XENAKI, V. C. & ATHANASOPOULOS, G. A. (2003) Liquefaction resistance of sand-silt mixtures: An experimental investigation of the effect of fines. *Soil Dynamics and Earthquake Engineering,* 23**,** 183 - 194.

YAMAMURO, J. A. & COVERT, K. M. (2001) Monotonic and Cyclic Liquefaction of Very Loose Sands with High Silt Content. *Journal of Geotechnical and Geoenvironmental Engineering,* 127**,** 314 - 324.

YAMAMURO, J. A. & LADE, P. V. (1997) Static Liquefaction of Very Loose Sands. *Canadian Geotechnical Journal,* 34**,** 905 - 917.

YANG, S., LACASSE, S. & SANDVEN, R. (2006a) Determination of the Transitional Fines Content of Mixtures of Sand and Non-plastic Fines. *Geotechnical Testing Journal,* 29**,** 102 - 107.

YANG, S. L., SANDVEN, R. & GRANDE, L. (2006b) Steady-state Lines of Sand-silt Mixtures. *Canadian Geotechnical Journal,* 43**,** 1213 - 1219.

YOUD, T. L. & IDRISS, I. M. (2001) Liquefaction resistance of soils: Summary report from the 1996 NCEER and 1998 NCEER/NSF workshops on evaluation of liquefaction resistance of soils. *Journal of Geotechnical and Geoenvironmental Engineering,* 127**,** 297 - 313.

ZLATOVIC, S. (1994) Residual Strength of Silty Soils. *Department of Civil Engineering.* Tokyo, University of Tokyo.

ZLATOVIC, S. & ISHIHARA, K. (1997) Normalized Behavior of Very Loose Non-plastic Soils: Effects of Fabric. *Soils and Foundations*, 37**,** 47 - 56.